BEHAVIOUR OF ELASTOHYDRODYNAMIC FILMS SUBJECTED TO OSCILLATORY MOTION

-by-

KONSTANTINOS KALOGIANNIS

A Thesis submitted to

The University of Sussex

for the Degree of

DOCTOR OF PHILOSOPHY

FEBRUARY 2013

CONFERENCE PROCEEDINGS AND PUBLICATIONS

Kalogiannis, K., Mares, C., Glovnea, R.P. and Ioannides, E.: Elastohydrodynamic Film Thickness Response to Harmonic Vibrations. *Proceedings of the International Multi-Conference on Engineering and Technological Innovation (IMETI),* Orlando , Florida , USA , June 29th -July 2nd , 2008

Kalogiannis, K., Glovnea, R.P. and Ioannides, E.: The Response of EHD Films to Lateral Oscillations. *Proceedings of the 4th World Tribology Congress (WTC IV),* Kyoto, Japan, 6th - 11th September, 2009

Kalogiannis, K., Glovnea, R.P., Morales, G. and Ioannides, E.: Behaviour of EHD Films under Oscillatory Conditions. *Proceedings of the 11th International Conference on Tribology*, IASI, Romania 4th - 6th November, 2010

Nagata, Y., **Kalogiannis**, **K.** and Glovnea, R.P.: The effect of Lateral Vibrations upon Track Replenishment in Grease – Lubricated EHD Contacts. *66th STLE Annual Meeting & Exhibition, Atlanta*, Georgia, USA, 15th – 19th May, 2011

Kalogiannis, K., Mares, C., Glovnea, R.P. and Ioannides, E.: Experimental investigation into the Response of Elastohydrodynamic Films to Harmonic Vibrations. *International Journal of Mechatronics and Manufacturing Systems (IJMMS) , Vol. 4 , No. 1 , pp. 61-73 , 2011*

Kalogiannis, K., Glovnea, R.P., Morales, G. and Ioannides, E.: Behaviour of EHD Films subjected to Lateral Oscillations. *Bulletin of the Polytechnic Institute of Iasi, Machine Construction, Tome* 52 (1), 2011

Nagata, Y., **Kalogiannis, K.**, Glovnea, R.P.: Track Replenishment by Lateral Vibrations in Grease-Lubricated EHD Contacts. *STLE Tribology Transactions, Vol. 55, Issue 1, pp. 91-98, 2012*

AWARDS

Session's Best Paper Award at the *International Multi- Conference on Engineering and Technological Innovation* for the paper entitled: ***"Elastohydrodynamic Film Thickness Response to Harmonic Vibrations"***

ABSTRACT

The main aim of this research was to understand the influence of vibration of machine components on lubricating films formed in high-pressure contacts.

In the current investigation Spacer Layer Imaging Method has been used to monitor the response of elastohydrodynamic films subjected to lateral and vertical vibrations. For both cases the EHL contact was produced by steel or tungsten carbide ball and a transparent disc which was made of glass or sapphire, loaded against each other. The contacting side of the disc was sputtered with a thin chromium layer and a silica spacer layer. White light was shown onto the contact through a specially built microscope. The interferometric fringes formed by the rays reflected by the chromium layer and by the ball's surface are captured by a high speed CCD camera. The images were subsequently analyzed and converted to film thickness maps according to calibration curves.

During the tests conducted under lateral vibrations the effect of several parameters including the frequency of lateral motion, Hertzian pressure, temperature variation and the main entrain speed were investigated. Results have shown that lateral oscillations create ripples through the lubricant film only at highest lateral frequency and low entraining speeds. The parameter which influences the formation of the perturbations in the film is the ratio between the main rolling speed and the lateral speed of the contact. The smaller the ratio the larger the transient phenomena can be identified. It has also been found that temperature change has no significant influence upon the film behaviour.

The effect of vertical vibrations on the film thickness was also investigated. The analysis of the film thickness has shown that a sudden increase of load had an effect of increasing the contact diameter and at the same time modified the convergence in the inlet, an enhanced

film thickness was produced at the inlet periphery of the initial contact zone and travel through the contact at a velocity equal to the average speed of the contacting surfaces.

“Dedicated to my parents Grigoris and Athena”

ACKNOWLEDGEMENTS

First and foremost, the author would like to give special thanks to his supervisor Dr. Romeo Glovnea for his kindness, encouragement, support and also for his helpful comments and proposals during this project.

Funding by the Engineering and Physical Science Research Council and support by industrial partner SKF is gratefully acknowledged.

Last but not least, I would like to express my gratitude to my parents for their immense support, patience and encouragement not only during the PhD study but throughout my life.

TABLE OF CONTENTS

LIST OF ILLUSTRATIONS

LIST OF TABLES

LIST OF SYMBOLS

Chapters	Symbols	Description
2	S	Contact area (equation 2.20)
2	$h(x, y)$	Gap between two solids (equation 2.21)
2	δ	Mutual approach of two remote points in the solids
2	W	Load between two solid surfaces (equation 2.22)
2	η_0	Dynamic viscosity at ambient pressure (equation 2.23)
2	α	Pressure-viscosity coefficient (equation 2.23)
2	p_r	Pressure at reference point (equation 2.24)
2	Z_r	Pressure viscosity index (equation 2.24)
2	ρ_0	Density of the fluid at ambient pressure (equation 2.25)
2	$\overline{U}$	Dimensionless speed parameter (equation 2.26)
2	$\overline{G}$	Dimensionless materials parameter (equation 2.26)
2	$\overline{W_L}$	Dimensionless load parameter (equation 2.26)
2	$H_{\min}$	Dimensionless minimum film thickness
2	k	Ellipticity parameter
2	$h_{\min}$	Minimum film thickness (equation 2.27)
2	h_c	Central film thickness (equation 2.28)
2	U	Mean velocity of the contacting surfaces (equation 2.29)
2	h	Film thickness (equation 2.29)
2	h_c	Film thickness at maximum pressure (equation 2.29)
2	g_V	Dimensionless viscosity parameter (equation 2.34)
2	g_E	Dimensionless elasticity parameter (equation 2.35)
2	$\hat{H}_{\min}$	Dimensionless film thickness parameter (equation 2.36)

3	h_s	Steady state film thickness (equation 3.1)
3	u_ξ	Velocity where the fluid element travelled at a speed u (equation 3.1)
3	a	Constant acceleration (equation 3.1)
3	u	Average velocity of two surfaces (equation 3.2)
3	K	Constant incorporating other factors involved (equation 3.4)
3	h_i	Initial film thickness at time t=0 (equation 3.9)
4	I_R	Resultant Intensity of interference to optical path difference (equation 4.1)
4	λ	Wavelength of the light (equation 4.1)
4	I_1 , I_2	Intensities of the initial rays (equation 4.1)
4	δ	Phase difference (equation 4.1)
4	h_{opt}	Optical path difference (equation 4.2)
4	ϕ	Net phase change (equation 4.2)

Chapters	Symbols	Description
4	N	Order of interference (equation 4.3)
4	n_{silica}	Refractive index of the film (silica) (equation 4.5)
4	n_{lub}	Refractive index of the lubricant film (equation 4.5)
4	h_{silica}	Thickness of the silica spacer layer (equation 4.5)
4	h_{lub}	Thickness of the lubricant film (equation 4.5)
5	h_{exp}	Experimental film thickness
5	h_p	Predicted film thickness
5	$V_{lateral}$	Theoretical lateral speed
5	$V_{resultant}$	Theoretical resultant speed
5	U_{main}	Theoretical main entrainment speed
5	t_r	Replenishment time (equation 5.1)
5	η_0	Viscosity of the base oil (equation 5.1)
5	a	Width of the track (equation 5.1)
5	σ_s	Surface tension of the oil (equation 5.1)

CHAPTER 1: Introduction

1.1 Overall Scope and Objectives

The research presented in this dissertation consists of two topics. The first part introduces an initial stage of a study based on the effects of lateral oscillations upon elastohydrodynamic films. Results obtained show the effect of various conditions and parameters upon film thickness. The parameters varied during this analysis are the frequency and amplitude of the lateral oscillations and the main entrainment speed. The second part of this research focused on behaviour of EHD films under normal vibrations. These vibrations caused by changing the load leading to different surface geometry of point contacts. Both experimental studies were conducted on a dynamic test rig which was purposely designed and built for this research.

The overall scope of this research was to understand the influence of vibration of machine components on lubricating films and vice versa. Therefore, the questions that arise are what is the effect of these vibrations upon the behaviour of the film in point contacts and what is the influence of working parameters and lubricant properties on this behaviour. In more detail, the main objectives of this study were to:

a) observe the behaviour of EHD films during well controlled, oscillatory, lateral motion.
b) measure the film thickness during lateral oscillations over-imposed on a rolling contact.
c) quantify the influence of frequency and amplitude of harmonic, lateral vibrations upon EHD film thickness.
d) evaluate the effect of vibrations normal to the contact upon film thickness in EHD lubrication.

1.2 Structure of the Thesis

The structure of this thesis is organised as follows:

Chapter 2: Elastohydrodynamic Lubrication

In this section, Governing equations including Reynolds, Film Thickness and Force Balance equation are presented. Also, the theory of Elastohydrodynamic (EHD) Lubrication is described in some detail.

Chapter 3: Transient Phenomena in EHD Lubrication

A review of studies concerning different aspects on transient events such as variation of surface velocity including squeeze, entrainment and a combination of the two, variation of load and surface geometry is presented in this chapter.

Chapter 4: Experimental Methods

In chapter 4, the methods associated with the investigation of EHD films are discussed. The optical interferometry principle is depicted. Furthermore, the experimental test rigs for both lateral and normal vibration studies are described. The experimental procedure and working parameters are also presented.

Chapter 5: Lateral Oscillations in EHD Films

In this chapter, systematic tests carried out in order to assess the effect of the main rolling speed, the frequency of the oscillations and the Hertzian pressure upon the behaviour of the EHD film under lateral oscillations are described. The effect of the lubricant viscosity was tested by running tests different temperatures.

Chapter 6: EHD Films subjected to Vertical Vibrations

The behaviour of EHD films subjected to vibrations taking place on a direction perpendicular to the contact has been examined. The EHD film studied was established under a constant load and thereafter this load was varied in a controlled, sinusoidal fashion. A forced vibration system was therefore obtained.

Chapter 7: Conclusions and Recommendations for Future Research

The conclusions of the study are discussed and the potential areas for further work are highlighted.

CHAPTER 2: Elastohydrodynamic Lubrication

2.1 Introduction

Elastohydrodynamic lubrication is a regime which occurs in machine elements and is associated with non-conformal or counter-formal contacts (Figure 2.1). It is characterized by a small contact area and a film thickness of about 1 micron or less. In addition, the contact pressures can reach up to 3 GPa or more which cause the solid surfaces to distort elastically and the lubricant viscosity to increase many orders of magnitude. EHL phenomena also occur in some low elastic modulus contacts of high geometrical conformity such as lip seals, conventional journal and thrust bearings with soft liners.

Figure 2.1: Examples of non-conformal contacts

2.2 Non – Conformal contact of smooth surfaces

The theory of contact mechanics is concerned with the stresses and deformations which arise when the surfaces of two solid bodies are brought into contact.

In 1880, geometrical effects on local elastic deformation have been considered in the Hertz's theory of elastic deformation [1]. Hertz's model of contact analysis is based on the following simplifying assumptions [2]:

- The size of the contact area is small compared with the dimensions of the curved bodies
- Both contacting surfaces are smooth and frictionless
- The two surfaces in contact are non-conformal
- There are no tangential forces acting between the contacting bodies

The shape of the contact area relies on the shape (curvature) of the contacting bodies. When two solid surfaces are in contact under zero – load condition, one of two types of contact occurs:

- **Point Contacts**: two solid surfaces are brought into contact at a single point such as in ball bearings
- **Line Contacts**: two solid surfaces touch along a line , as in roller bearings

The shape of the contact region depends on the ratio of the radii of curvature in the x and y directions of the two bodies as a result the point expands to an ellipse and the line to a rectangle. The point contact refers to a contact between two parabolically surfaces with the radii of curvature r_{ax}, r_{bx} in the x-direction and r_{ay}, r_{by} in the y-direction (Figure 2.2).

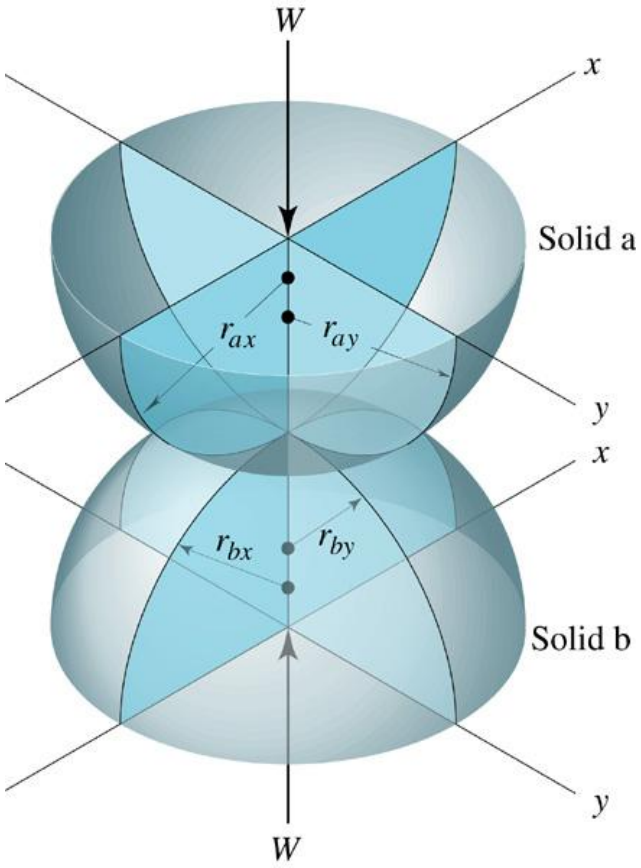

Figure 2.2: Geometry of contacting solids [3]

The reduced radii of curvature in x and y directions are defined by:

$$\frac{1}{r_x} = \frac{1}{r_{ax}} + \frac{1}{r_{bx}} \qquad \text{and} \qquad \frac{1}{r_y} = \frac{1}{r_{ay}} + \frac{1}{r_{by}} \tag{2.1}$$

Where: r_X , r_y represent the reduced radius of curvature in the x and y direction

r_{ax} , r_{ay} refer to the radii of curvature of solid A in the x and y direction.

r_{bx} , r_{by} correspond to the radii of curvature of solid B in the x and y direction.

In the most general case r_x and r_y are finite and non-zero thus the area of contact is an ellipse. In this case an equivalent radius of curvature is defined as the geometric mean of the two: $R = \sqrt{r_x\, r_y}$. The dimensions of the contact and the maximum pressure are given by:

$$c = \sqrt{ab} = \left(\frac{3}{4}\frac{PR}{E*}\right)^{1/3} F_1 \tag{2.2}$$

$$p_0 = \left(\frac{1}{\pi}\right)\left(\frac{6PE*^2}{R^2}\right)^{1/3} F_1^{-2} \tag{2.3}$$

Function F_1 as well as the ratio b/a are given as functions of the square root of the radii ratio $\sqrt{r_x / r_y}$.

In these relationships the reduced Young's modulus is defined by the relation:

$$\frac{1}{E'} = \left[\frac{1-\nu_A{}^2}{E_A} + \frac{1-\nu_B{}^2}{E_B}\right] \tag{2.4}$$

where:

ν_A and ν_B : are the Poisson's ratios of the contacting bodies 'A' and 'B' , respectively

E_A and E_B: are the Young's modulus of the contacting bodies 'A' and 'B', respectively

Particular cases are: when r_x or $r_y = \infty$ the contact becomes rectangular. Alternatively when $r_x = r_y$ the contact is circular. In the later situation the radius of the contact can be defined as:

$$a = \left(\frac{3}{4}\frac{PR}{E*}\right)^{1/3} \tag{2.5}$$

The Hertzian pressure is:

$$p_0 = \left(\frac{6PE*^2}{\pi^3 R^2}\right)^{1/3} \tag{2.6}$$

The maximum deflection of the surface is given:

$$\delta = 1.0397\left(\frac{W^2}{E'R'}\right) \tag{2.7}$$

2.3 Governing Equations of EHL

To describe the fully flooded EHL contact, three equations need to be simultaneously satisfied: Reynolds equation, describing the flow in the gap, the *film thickness equation* gives the shape of the lubricant film including the elastic deformation and finally the *force balance equation* which describes the fact that the lubricant's pressure should balance the applied load. Each of these equations are analysed below.

2.3.1 Reynolds Equation

The differential equation governing pressure distribution in a Newtonian lubricant film was first obtained by Reynolds [4] and it can be derived from the Navier-Stokes equations by taking into account some simplifying assumptions at appropriate points in the analysis. These are [5]:

1. Body forces are negligible
2. Pressure is constant through the film in z direction
3. No slip at the boundary surfaces
4. Lubricant flow is laminar
5. Inertia and surface tension forces are negligible compared with viscous forces
6. Shear stress and velocity gradients are only significant across the lubricant film (z direction)
7. Lubricant is Newtonian
8. The lubricant viscosity and the fluid density are constant across the film (z direction)
9. The lubricant boundary surfaces are parallel or at small angle with respect to each other

Consider a fluid between two parallel plates where h is the surface separation, p = f(x, y, h, η, u_1, u_2, v_1, v_2, w_1, w_2) is the fluid pressure, η is the dynamic viscosity of the lubricant film and u, v , w are the velocities of the surfaces in the x, y and z-directions. Figure 2.3 illustrates two generalized surfaces in relative motion.

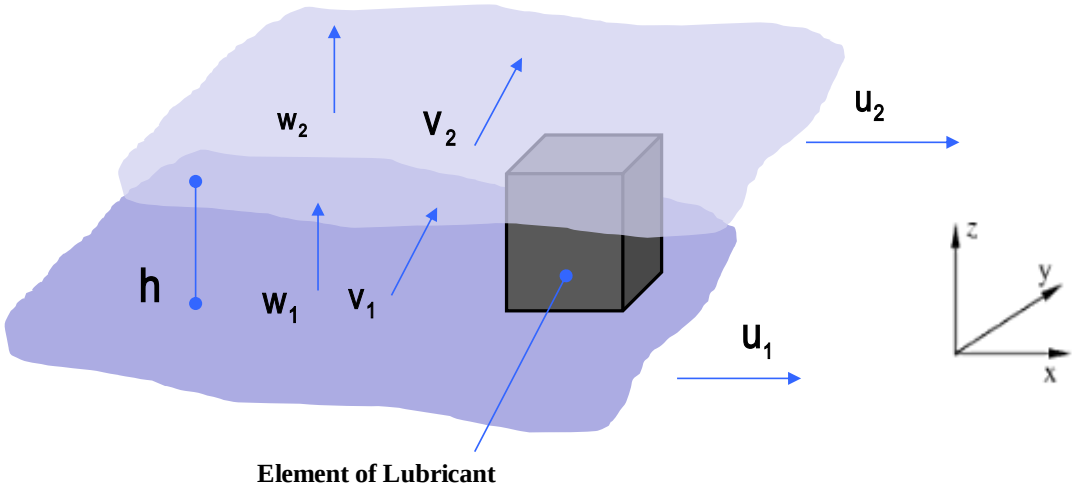

Figure 2.3: Two surfaces in relative motion

The derivations of Reynolds equation can start either by applying the above stated simplifying assumptions to Navier-Stokes equations, or by writing the dynamic equilibrium of an element of volume from the fluid.

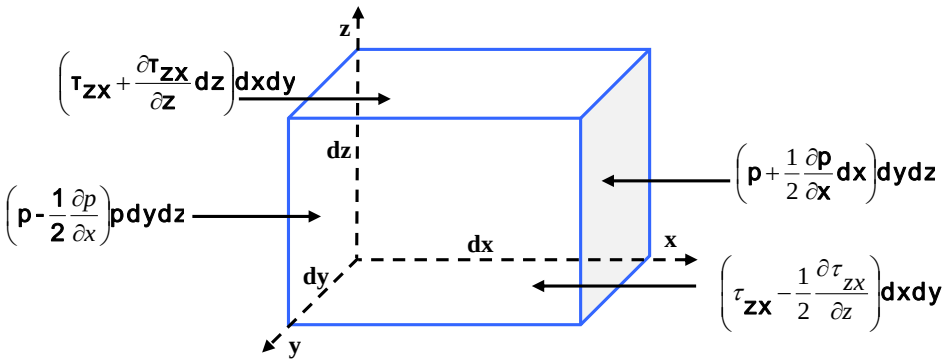

Figure 2.4: Forces on an element

Consider a small element of fluid from a hydrodynamic film (Figure 2.4). In this case the forces of the element are acting only in the x direction. The balance of forces in x direction yields:

$$\frac{\partial \tau_{zx}}{\partial z} = \frac{\partial p}{\partial x} \tag{2.8}$$

Similarly in the y direction,

$$\frac{\partial \tau_{zy}}{\partial z} = \frac{\partial p}{\partial y} \tag{2.9}$$

According to the second assumption, since the pressure is constant through the film in the z direction the pressure gradient is equal to zero

$$\frac{\partial p}{\partial z} = 0 \tag{2.10}$$

Considering the fluid as Newton's the shear stress is directly proportional to the shear strain with the factor of proportionality the viscosity η:

$$\tau_{zx} = \eta \frac{u}{h} = \eta \frac{\partial u}{\partial z} \tag{2.11}$$

where: τ_{zx} is the shear stress acting in the 'x' direction [Pa]

Furthermore the velocity in the y direction is different and consequently the shear stress is different:

$$\tau_{zy} = \eta \frac{v}{h} = \eta \frac{\partial v}{\partial z} \tag{2.12}$$

where: τ_{zy} : is the shear stress acting in the 'y' direction [Pa]

v : is the sliding velocity in the 'y' direction [m/s]

Combine equations (2.8) and (2.11) and equations (2.9) and (2.12), the equilibrium conditions for the forces acting in the 'x' and 'y' directions can be obtained:

$$\frac{\partial p}{\partial x} = \frac{\partial}{\partial z}\left(\eta \frac{\partial u}{\partial z}\right) \tag{2.13}$$

$$\frac{\partial p}{\partial y} = \frac{\partial}{\partial z}\left(\eta \frac{\partial v}{\partial z}\right) \tag{2.14}$$

Now by integrating the above formulas (2.13) and (2.14) twice and taking into account assumption 3, the velocities through the film thickness, for both x and y direction become:

$$u = \left(\frac{z^2 - zh}{2\eta}\right)\frac{\partial p}{\partial x} + (U_1 - U_2)\frac{z}{h} + U_2 \tag{2.15}$$

$$v = \left(\frac{z^2 - zh}{2\eta}\right)\frac{\partial p}{\partial y} + (V_1 - V_2)\frac{z}{h} + V_2 \tag{2.16}$$

If we apply the condition of continuity of flow to a column h and following assumption 3, the volume flow rates per unit width in the x and y direction can be defined as:

$$q_x = \rho\int_0^h u\,dz \qquad \text{and} \qquad q_y = \rho\int_0^h v\,dz \tag{2.17}$$

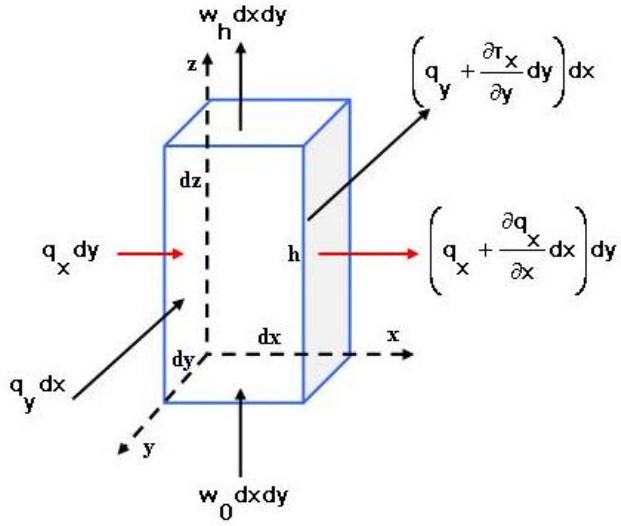

Figure 2.5: Flow through a column

Where: ρ denotes the density

Substituting the velocity components (2.15) and (2.16) in the above equations, the full Reynolds equation becomes:

$$\frac{\partial}{\partial x}\left[\frac{\rho h^3}{\eta}\frac{\partial p}{\partial x}\right]+\frac{\partial}{\partial y}\left[\frac{\rho h^3}{\eta}\frac{\partial p}{\partial y}\right]=6\left\{\frac{\partial}{\partial x}\left[\rho h\left(U_1+U_2\right)\right]+\frac{\partial}{\partial y}\left[\rho h\left(V_1+V_2\right)\right]+2\frac{d}{dt}\left(\rho h\right)\right\} \qquad (2.18)$$

where: p = p (x, y, t) = is the hydrostatic pressure above ambient pressure

h = h (x, y, t) = is the gap between contacting surfaces

η = η (x ,y, t) = viscosity

The terms on the left hand side represent the flow due to pressure gradients across the domain while the terms on the right hand side represent the flow induced by motions of the bounding surfaces and shear induced flow by the sliding velocities U and V. At the edges of the domain, the pressure equals the ambient pressure level. Hence the pressure in the Reynolds equation has to be understood as the rise from ambient pressure level. In the outlet region, where the gap is widening, the Reynolds equation in general predicts negative pressures leading to cavitation [6].

2.3.2 Film Thickness equation

Film thickness equation describes the gap between the undeformed surfaces. As the contact area dimensions are smaller than the reduced radii of curvature, the undistorted surfaces can be estimated by paraboloids. The elastic deformations of two solid bodies can be determined

by neglecting the tangential stresses on the surfaces. Therefore the normal displacement of the surface of a semi-infinite solid caused by the distributed load *p* is [6]:

$$\upsilon(x,y)=\frac{1-\nu^2}{\pi E}\times\frac{p}{\sqrt{x^2+y^2}} \tag{2.19}$$

Where: E: is the Young's modulus

ν : is the Poisson's ratio

The deformation caused by a distributed load p(*x, y*) on the surface can therefore be obtained by integration:

$$\upsilon(x,y)=\frac{1-\nu^2}{\pi E}\iint_s\frac{p(x'y')dx'}{\sqrt{(x-x')^2+(y-y')^2}} \tag{2.20}$$

Where: S denotes the contact area.

Finally by adding the elastic deformation of both solids to the parabolic approximation of the undeformed gap the actual gap *h*(*x, y*) between the two solids is now obtained:

$$h(x,y)=-\delta+\frac{x^2}{2r_x}+\frac{y^2}{2r_y}+\frac{2}{\pi E'}\iint_s\frac{p(x'y')dx'}{\sqrt{(x-x')^2+(y-y)^2}} \tag{2.21}$$

δ represents the mutual approach of two remote points in the solids. The expression remote is used to specify that the elastic deformation is negligible at these points. The different terms in equation (2.21) are depicted in the Figure below.

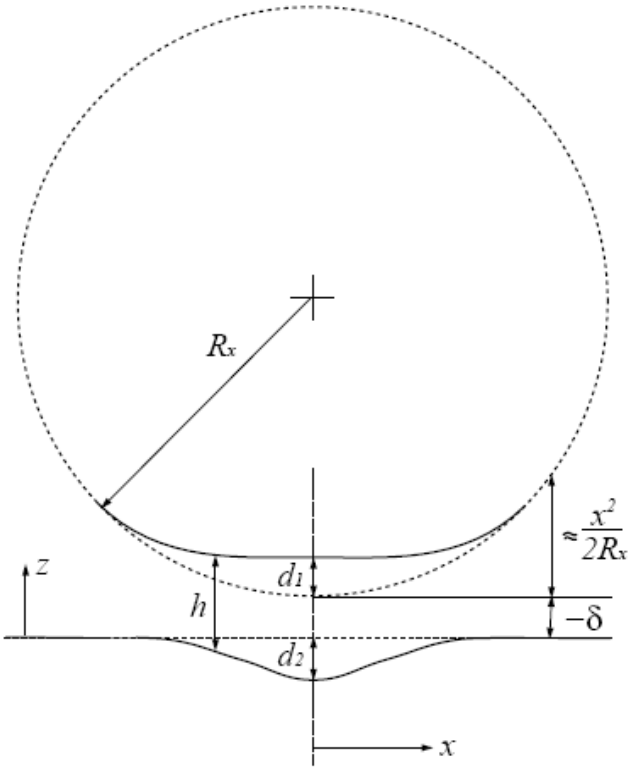

Figure 2.6: Geometry of the gap in an EHL point contact for *y=0* [7]

2.3.3 Force Balance equation

Since the load W, pressing the two solids together, is transmitted by the EHD film, the integral of the pressure distribution should balance with the applied load.

$$W = \int_A \int p dx dy \tag{2.22}$$

2.3.4 Viscosity – Pressure Variation

Both viscosity and density of the lubricant are pressure dependent. Especially in EHL contacts this dependence cannot be neglected as high pressures are occurring.

The increase of the viscosity with pressure can be described with Barus equation [8], which was proposed as early as 1893, provided a very simple exponential relationship with pressure.

$$\eta = \eta_0 e^{\alpha p} \tag{2.23}$$

where: η_0: is the dynamic viscosity at ambient pressure [Pas]

α: is the pressure-viscosity coefficient in Pa^{-1}

If the ambient temperature is high, the equation becomes inaccurate above 0.5 GPa. However, this equation is adequate when solving the Reynolds equation for film thickness, but not when estimating the friction.

Other equations have been proposed, but Roeland [10] introduced an equation which more accurately the lubricant viscosity, however it only applies in a limited range of pressure and is more complex and describes. It is widely applied in EHL problems nowadays, as most of them fall into the range Roeland's equation can produce accurate results.

Roeland's equation is presented below:

$$\eta = \eta_0 \exp\left(\left\{\ln(\eta_0) + 9.67\left[\left(1 + \frac{p_e}{p_r}\right)^{Z_r} - 1\right]\right\}\right) \tag{2.24}$$

Where $p_r = 1.96 \times 10^8$ and Z_r is the pressure viscosity index.

2.3.5 Density– Pressure Variation

In this section, the density variation with pressure is considered based on Dowson and Higginson model [11]. This model is the most used density variation relationship in EHL. It can be stated as follows:

$$\rho = \rho_o \frac{0.59 \times 10^9 + 1.34p}{0.59 \times 10^9 + p} \tag{2.25}$$

Where ρ_0: denotes the density at ambient pressure

2.3.6 Non-Dimensional Equations and Parameters

The physical parameters which are required in order to characterize the EHL problem can be combined into independent dimensionless groups. Dowson and Higginson [12] introduced the following set of dimensionless parameters to describe a typical linear EHL contact. Those are the speed parameter $\overline{U}$, materials parameter $\overline{G}$ and load parameter $\overline{W_L}$ expressed as:

$$U^* = \frac{U\eta_0}{E'R'_x} \qquad G^* = \alpha E' \qquad W_L{}^* = \frac{W}{E'R'_X L} \tag{2.26}$$

Therefore, the dimensionless minimum film thickness can be expressed as,

$$H_{\min} = f(W, U, G, k)$$

The minimum and the central film thickness formulas which were obtained by Hamrock and Dowson [13], [14] for an elastohydrodynamic elliptical conjunction are as follows,

$$\frac{h_m}{R_x'} = 3.63U^{*0.68}G^{*0.49}W^{*-0.073}\left(1-e^{-0.68}\right) \tag{2.27}$$

$$\frac{h_c}{R_x'} = 2.69U^{*0.67}G^{*0.53}W^{*-0.067}\left(1-e^{-0.75}\right) \tag{2.28}$$

2.4 Grubin's Theory

The first theoretical solution to account for the effects of both elastic deformation and pressure dependence of viscosity was published in 1949 by Grubin and Vinogradova [15], for linear contacts, and two years later by Petrushevish [16] for point contacts. Their work established most of the critical properties of EHL in concentrated contacts:

- The Hertzian contact zone is presumed to form a parallel film region as seen in Figure 2.7.

- In static condition the pressure distribution curve follows the Hertzian ellipse over most of the contact area (Figure 2.8).
- Near the exit of the high-pressure region a constriction is formed which is often correlated with a sharp second maximum pressure so called Petrushevish spike (Figure 2.8).

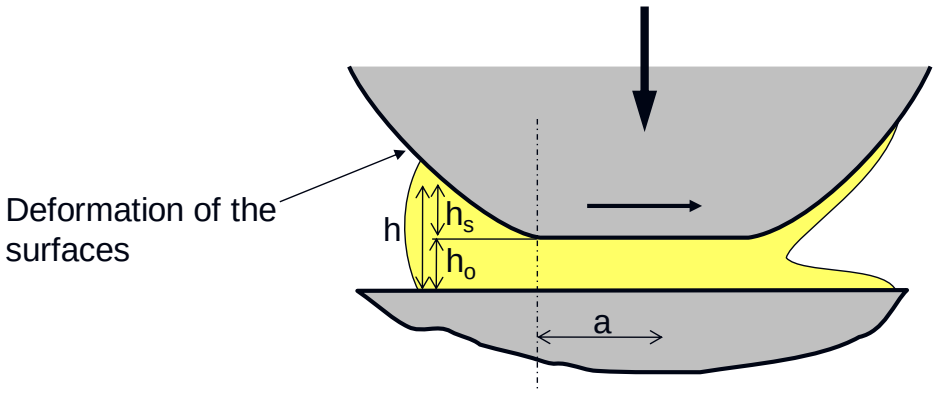

Figure 2.7: Grubin's film approximation

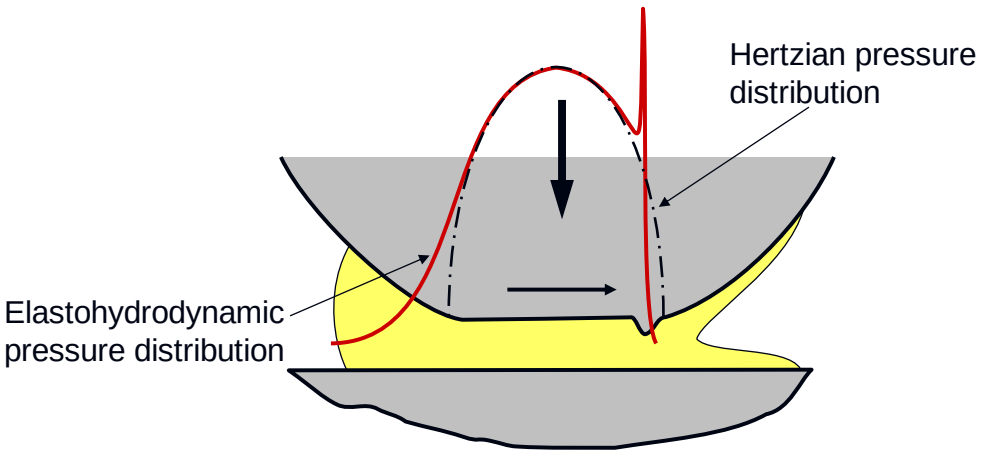

Figure 2.8: Exit constriction and pressure distribution

Referring to Figure 2.7 Grubin's method can be explained as follows. He derived an approximation to the minimum film thickness by assuming that the solid surfaces are distorted elastically and are separated by a constant lubricant film at the centre line as well as at the position where the maximum pressure occurs. Firstly, he used the one-dimensional Reynolds equation,

$$\frac{dp}{dx} = 6U\eta_0\left(\frac{h-h_c}{h^3}\right) \tag{2.29}$$

where: U: denotes the mean velocity of the contacting surfaces

h: is the film thickness

$h_c = h_o$ indicates the film thickness at maximum pressure

Taking into account the Barus exponential law, the above equation becomes:

$$e^{-\alpha p}\frac{dp}{dx} = 6U\eta_0\left(\frac{h-h_c}{h^3}\right) \tag{2.30}$$

A reduced pressure can be defined by the expression:

$$q = \frac{1}{\alpha}\left(1-e^{-\alpha p}\right) \tag{2.31}$$

The gap in the inlet is given by Hertz's theory to which the constant lubricant film thickness is added:

$$h = h_0 + \frac{2W}{LE'}\left\{|\bar{x}|\sqrt{\bar{x}^2 - 1} - \ln\left(|\bar{x}| + \sqrt{\bar{x}^2 - 1}\right)\right\} \tag{2.32}$$

where: $|\bar{x}| = \frac{x}{a}$ and $\frac{W}{L}$ is the load per unit length

Substituting Equations (2.31), (2.32) into (2.30), the pressure profile in the EHD contact is given by the relation:

$$\frac{h_c}{R} = 1.93\left(\overline{U}\right)^{3/4}\left(\overline{G}\right)^{3/4}\left(\overline{W}_L\right)^{-1/8} \tag{2.33}$$

The dimensionless parameters $\overline{U}$, $\overline{G}$ and $\overline{W}_L$ have been described in section 2.1.6.

2.5 EHD Features

It is well known that the elastohydrodynamic film thickness is established in the inlet of the contact and is influenced by:

- the viscosity of the lubricant
- the entrainment speed (e.g. double speed increases the film thickness with a factor of 1.6)
- the temperature due to large effect on oil viscosity
- only slightly by load

In reality the film is not completely constant across the whole contact. In order to accommodate the sudden drop of pressure at the sides of the contact, the separation between surfaces is reduced in these areas. Thus, the minimum film thickness can be found at the sides and at the exit of the contact region giving the contact the distinctive a horseshoe shape. Figure 2.9 shows typical coloured fringes of an EHD contact visualized by optical interferometry method.

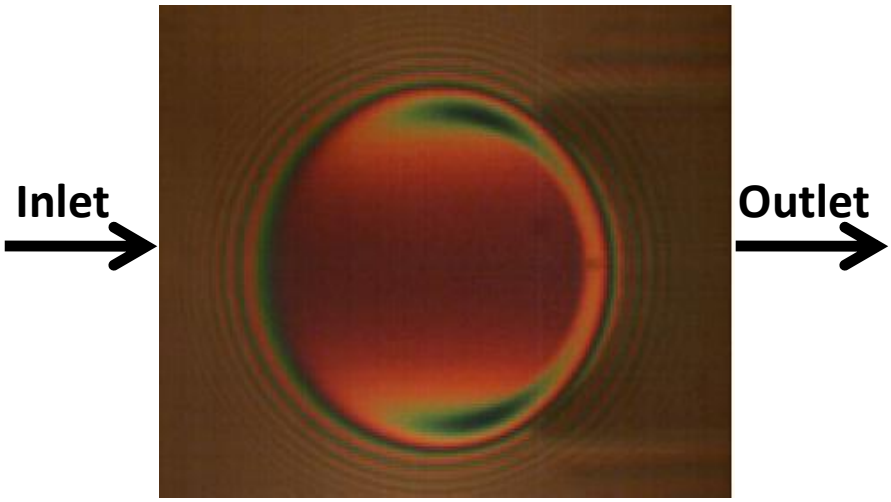

Figure 2.9: Typical image of an EHD contact using optical interferometry

2.6 Fluid Film lubrication Regimes

As discussed in section 2.1, the type of lubrication of a particular contact is influenced by the elastic deformation of the solid surfaces under an applied load and by the increase in fluid-viscosity with pressure. So, it is possible to have four fluid- film lubrication regimes, depending on the magnitude of these effects and on their importance [17]. These are:

Rigid Isoviscous Regime: In this lubrication regime the elastic deformations are small compared with lubricant film thickness and can be ignored. Also the maximum pressure in the contact is low so that the effect of pressure on viscosity can be neglected. This form of lubrication is typically found in circular –arc thrust bearing pads and in lightly loaded counter – formal contacts. This regime refers to the classical hydrodynamic lubrication.

Rigid Piezo-viscous Regime: In this regime, the contact pressures are high enough to increase the lubricant's viscosity within the conjunction significantly, yet not so high as to initiate significant elastic deformation in the bearing material. This form of lubrication may be encountered on roller end-guide flanges, in contacts of moderately loaded cylindrical tapered rollers and between some piston rings and cylinder liners.

Elastic Piezo-viscous Regime: In fully developed EHL, the elastic deformation of the solids can be larger than the film thickness and the contact pressure is high enough to cause a significant increase in the viscosity of the lubricant. Examples include: rolling bearings, gears, cams and followers.

Elastic Iso-viscous Regime: This lubrication regime, is characterized by a significant elastic deformation, however the pressure within the conjunction is quite low and insufficient to cause any substantial increase in viscosity. This situation arises with materials of low elastic modulus such as tires, seals, human joints and elastomeric – material machine elements.

2.6.1 Dimensionless Groups

In 1970 Johnson [18] has pointed out that the behaviour which distinguishes the four lubrication regimes, including point contacts, can be considered by three dimensionless parameters:

- The reduced pressure parameter p , is a measure of the fluid pressure generated by an iso-viscous lubricant when elastic deformation is neglected
- The inverse pressure viscosity coefficient , is a measure of viscosity change with pressure
- The maximum Hertzian pressure Ph , is the maximum pressure of a dry elastic contact

The dimensionless parameters are given below,

Dimensionless viscosity parameter: $$g_V = \frac{G^* W^{*3}}{U^{*2}} \tag{2.34}$$

Dimensionless elasticity parameter: $$g_E = \frac{W^{*8/3}}{U^{*2}} \tag{2.35}$$

Dimensionless film thickness parameter: $$\hat{H}_{\min} = H_e \left(\frac{W}{U} \right)^2 \tag{2.36}$$

The film thickness contours for the four fluid film lubrication regimes can be illustrated graphically in Figure 2.10 by taking into account the physical parameters stated above.

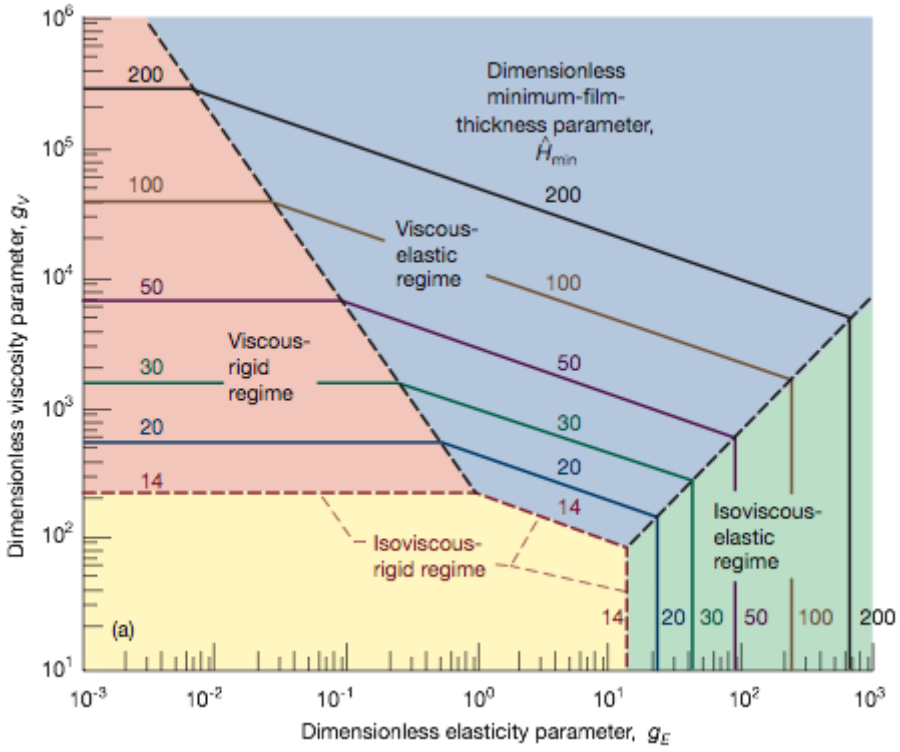

Figure 2.10: Map of lubrication regimes [19]

CHAPTER 3: Transient Phenomena in EHD lubrication

3.1 Literature Review

The effect of transient phenomena on the lubricant film behaviour in EHD contacts has received a merited attention during the past two-three decades from both theoretical and experimental point of view. Transient events in elastohydrodynamic lubrication can be grouped into three main categories such as variation of surface velocity including squeeze, entrainment and a combination of the two, variation of load and surface geometry [20].

3.1.1 Phenomena associated with variation of speed

The velocity of the contacting bodies which form a contact can vary on a direction normal to the surfaces (squeeze) and on a direction contained in the tangent plane (variable entrainment).

a) Squeeze films

The squeeze effect occurs when one solid surface drops or rebounds on a lubricated surface and secondly when the two solid surfaces approach or separate rapidly due to a variation of entrainment speed.

Christensen [21] was the one who first considered squeeze action in a theoretical EHL analysis. His study was based on the motion of two infinitely long cylinders in normal approach by solving Reynolds equation in order to obtain pressure distributions and load carrying capacity. The author showed that very high pressures developed in the central region of the contact that could exceed the corresponding maximum Hertzian pressure.

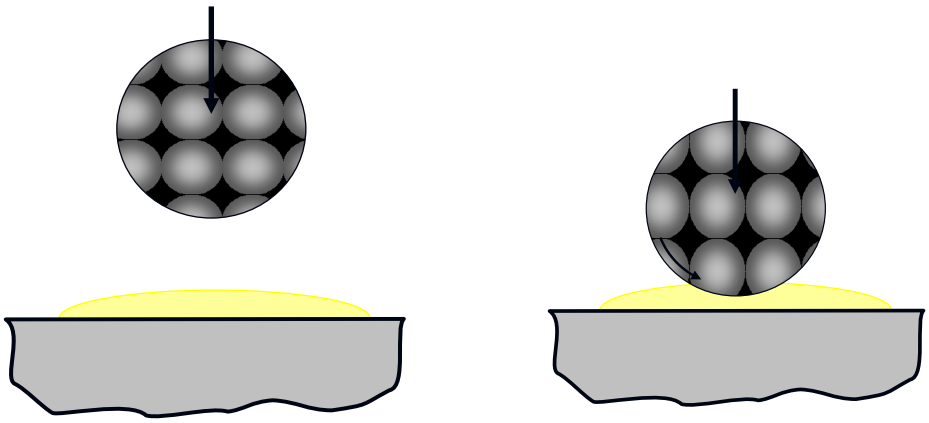

Figure 3.1: Squeeze action

Vichard [22] carried out theoretical and experimental studies into the effect of load variation upon EHD film thickness. He developed a Grubin type approximation and was able to calculate the minimum film thickness under a sinusoidal load. The electrical capacitance method was used in order to measure film thickness between a rotating eccentric disc and a flat surface and then compared with theoretical predictions. He realized that the squeeze effect contributes to the stability of lubricating thin films and that this phenomenon takes place in various situations when sudden variations of the parameters of the contact occur. In general his study agreed with the classical knowledge of the lubrication of machines and mechanisms which work under severe conditions. Finally from the experimental point of view, it was concluded that, as shown by the theoretical results, for moderate variations of the parameters of the contact, the flow was not disturbed and the squeeze effect really corresponds to a viscous damping phenomena.

Wang and Cheng [23] applied Vichard's analysis on gears and their work gave a comprehensive investigation of film thickness, temperature and load in spur gear transmissions.

After the 1980's more experimental investigations on transient phenomena, involving film squeeze, using optical interferometry technique have been carried out by various researchers such as Honglund and Jacobson [24], Wada and Tsukijihara, [25], Yang and Wen [26], Wong et al. [27], and others [28-31]. Larsson and Lundberg [32] performed an experimental study of lubricated impacts between a steel ball of 70 mm diameter mounted on a pendulum and a flat glass disc of 100 mm diameter. Optical interferometry has been used with a monochromatic light source, a microscope and high speed video system. In this investigation the authors have used PAO lubricant of five different viscosities (ν). The following table shows the experimental parameters of this work.

Table 3.1: Impact velocities and viscosities used in the experiments [32]

$V_m(ms^{-1})$	$\nu(mm^2s^{-1})$ at 23±0.6 ^oC
0.078±0.004 (A)	27±3 (VG15)
0.160±0.004 (B)	94±5 (VG46)
0.14±0.02 (C)	350±10 (VG150)
0.174±0.003 (D)	850±15 (VG320)
0.290±0.003 (E)	2600±50 (VG1000)

Their results showed that:

- In the case of low lubricant (VG 15 and VG46), the maximum dimple depth occurred at the beginning of the impact. Later on, the dimple depth decreased more or less to a constant level.
- At low viscosities, by increasing the impact velocity the dimple became deeper. This happened for high viscosities as well. Moreover, it can be noted that by increasing the impact velocity, the time for the entrapped lubricant to flow out from the contact region became shorter.
- The viscosity of the lubricant has an influence on dimple diameter
- Cavitation took place just outside the edges of the dimple and at the end of the impact time

b) Variation of entrainment

The variation of the entrainment speed, which usually is accompanied by squeeze due to rapid variation of film thickness, has also been investigated from both theoretical [e.g. 38-41] and experimental point of view. Experimental studies in this aspect of EHD lubrication have been carried out many researchers and groups such as: Kaneta and co-authors [33-34], Rutlin et al. [35], Scales et al [36], Ohno and Yamada [37] and others.

Research studies on the effect of entrainment speed variation have addressed five particular types of motion. These are:

- Start-up of motion
- Start-stop of motion
- Step of entraining speed
- Reversal of entraining speed

A number of studies focused on non-steady state conditions were conducted by Sugimura and co-authors [42, 43]. They have used optical interferometry for measuring EHD film under various speed conditions.

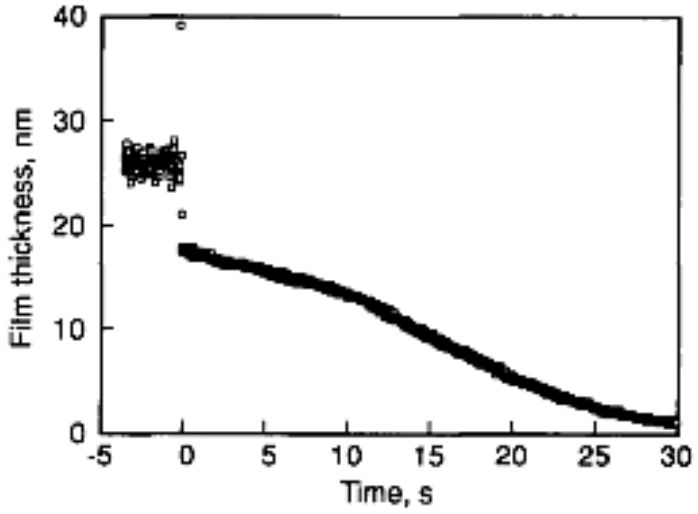

Figure 3.2: Film profiles at start-up for HVI650 at 80 ˚C and 50 m/s^2 acceleration [42]

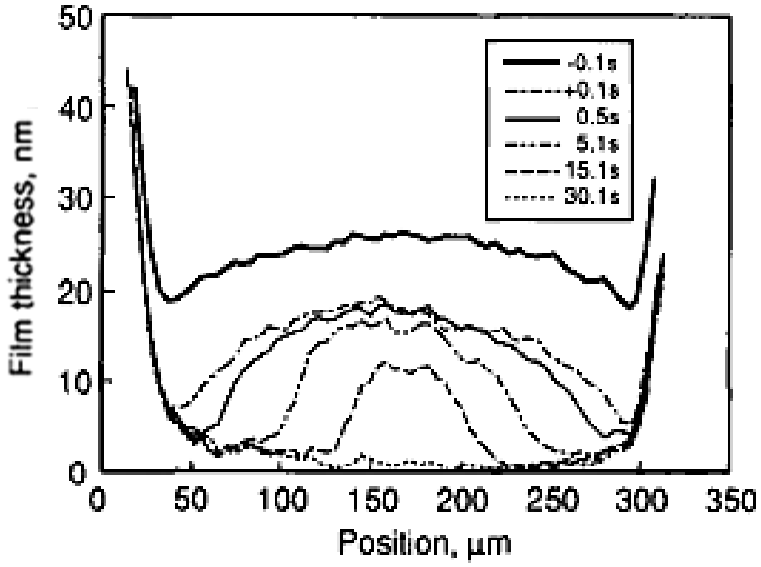

Figure 3.3: Film profiles at start-up for HVI650 at 80 ˚C and 50 m/s^2 acceleration [42]

The contacts worked in pure rolling conditions, with the disc driving the ball. Various types of motion were produced using a function generator in order to control the DC motor of the disc. The monochromatic images obtained were recorded by a conventional S-VHS video recorder. From the analysis of the results it was found that, during halting of motion the central and the minimum film thickness collapsed very rapidly within a period of less than 0.1 seconds .This can be observed in Figures 3.2 and 3.3.

In addition, results obtained in accelerating and decelerating tests have shown that the values of the film thickness differ with those formed at steady state conditions. In the case of accelerating motion the film thickness being thinner while during decelerating motion the film found to be thicker than expected. Figures 3.4 (a) to (c) illustrate the variation of the central film thickness during accelerating / decelerating motion performed at 3 different frequencies.

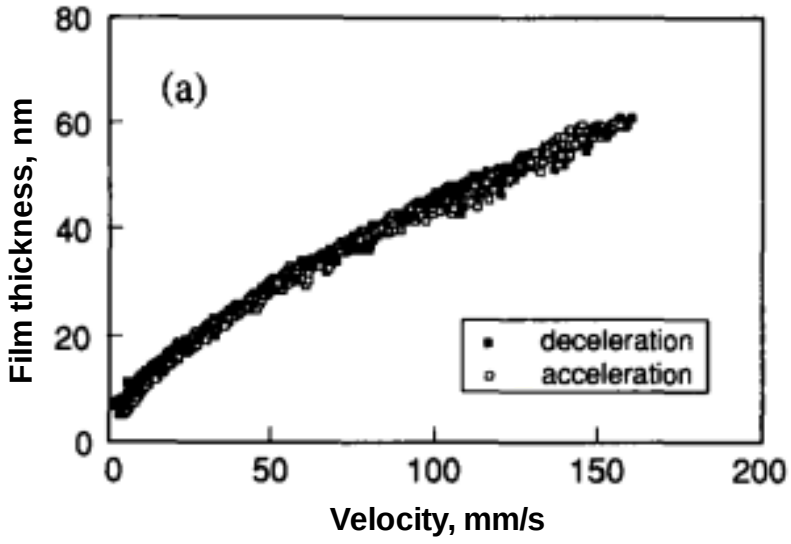

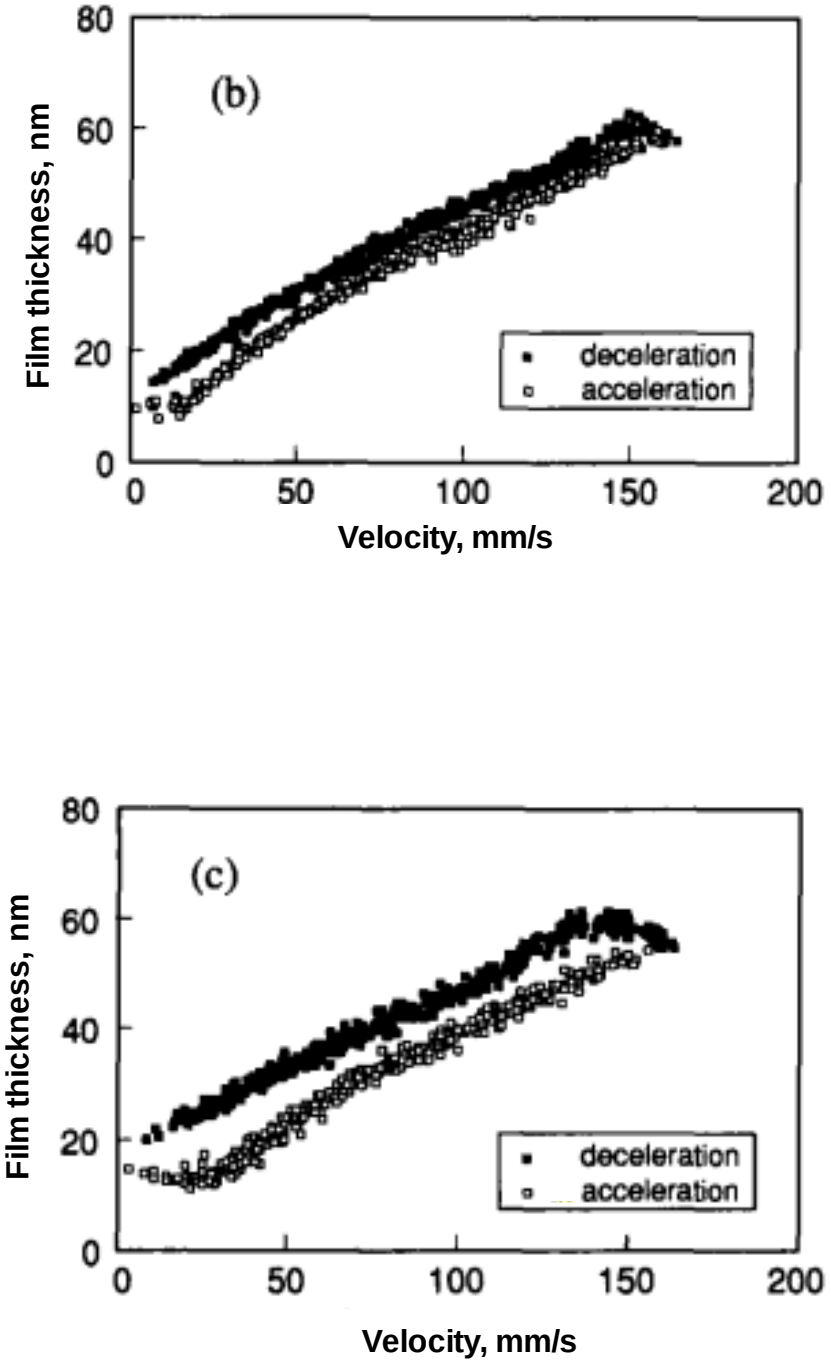

Figure 3.4: Variation of the EHD central film thickness with velocity (a) at 0.1 Hz, (b) at 1 Hz and (c) at 2 Hz [42]

A theoretical study based on the above experimental results has been reported in [39]. A simple approximation of EHD film thickness under speed variation conditions was proposed and the equation was based on continuity of flow. In that study it was assumed that the central film thickness was related to the velocity of the boundaries when the fluid flowed into the conjunction at the upstream of the Hertzian edge. In addition, it was also assumed that the film thickness could be approximated using the conventional steady-state EHD formula but with the upstream velocity. The formula below corresponded to the central film thickness at the velocity u and under acceleration a,

$$h(u,a) = h_s\left(u_\xi\right) \tag{3.1}$$

where h_s : defines the steady state central film thickness

u_ξ : is the velocity where the fluid element travelled at a speed u

In the case of constant acceleration a , the velocities u and u_ξ are related by,

$$u^2 - u_\xi{}^2 = 2a\xi b \tag{3.2}$$

Where,

$$u_\xi = u\left(1 - a\xi b / u^2\right)^{1/2} \tag{3.3}$$

In addition, the steady state film thickness h_s , was assumed to be given from the following formula

$$h_s(u) = Ku^{0.67} \tag{3.4}$$

where u : is the average velocity of the two surfaces and

K : is a constant incorporating other factors involved

By combining Equations (3.1), (3.3) and (3.4) gives

$$h(u,a) = Ku^{0.67}\left(1 - 2a\xi b/u^2\right)^{0.67/2} \tag{3.5}$$

Finally, after neglecting the higher order terms then have

$$h(u,a) = Ku^{0.67}\left(1 - 0.67a\xi b/u^2\right) \tag{3.6}$$

This theoretical analysis has shown that the EHD film thickness under constant acceleration can be predicted by a simple model based on the Equation (3.6). The model stated above assumed that the film which formed in the inlet region moved downstream with little subsequent change in its thickness even though the surfaces velocities were varying. It can be also stated that, the approximation model was supported by experimental results of non-steady state film thickness measurements using ultra-thin film interferometry method.

The results of an experimental investigation carried out by the Glovnea and co-authors [30] focused on the elastohydrodynamic film formation at start-up of motion were published in 2011. They also have used ultra-thin film interferometry method to measure film thickness. In this study, two set of experiments were performed under pure rolling and pure sliding conditions at a temperatures of 40 ˚C and 80 ˚C respectively. The lubricants used in this study were a mineral oil HVI650, a polyalphaolefin (PAO) and a polyphenylether (5P4E).

The applied load was 20 N which produced a Hertzian pressure of about 0.5 GPa and a contact diameter of 0.27 mm. In pure sliding conditions, the disc was kept stationary whilst the ball was accelerating at a constant rate from rest until the ball surface at the contact point reached at a speed of 0.4 m/s. At high accelerations it was found that, the passage of the lubricant was slightly delayed at the start-up of motion. This feature is seen in Figure 3.5. At

this very high acceleration a complete film was formed within one frame even at the high frame rate speed camera of 1000 frames per second. At lower accelerations, as seen in Figures 3.6 (a) and 3.6 (b) the film forms as a plug of lubricant which passes through the conjunction from the inlet to the exit, approximately at the average speeds of the surfaces.

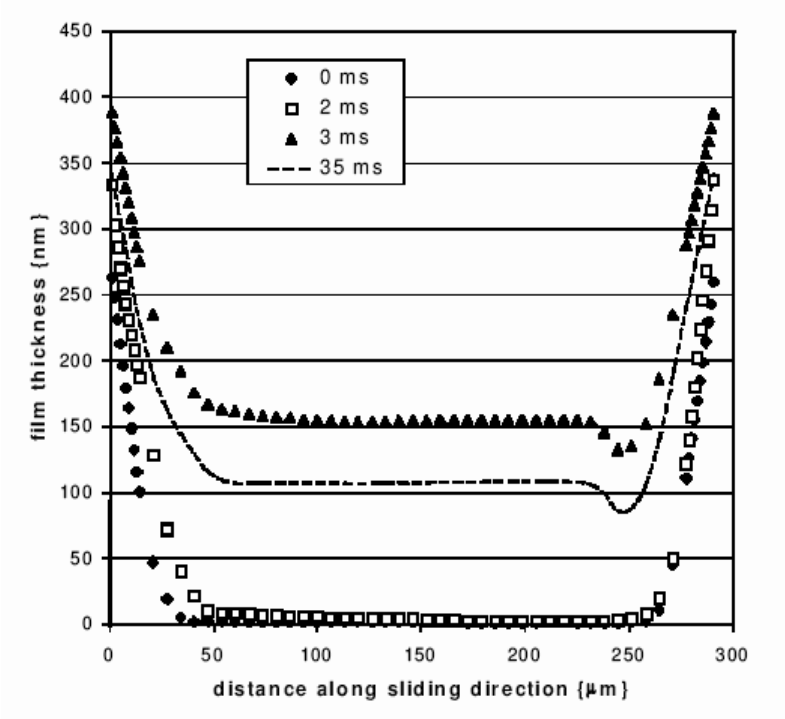

Figure 3.5: Film profiles at start-up for HVI650 at 80 ˚C and 50 m/s^2 acceleration [44]

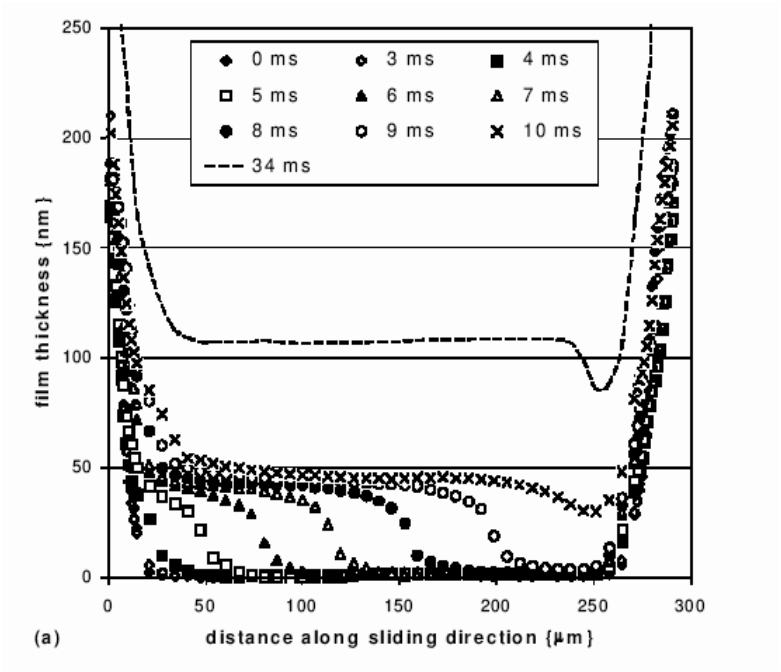

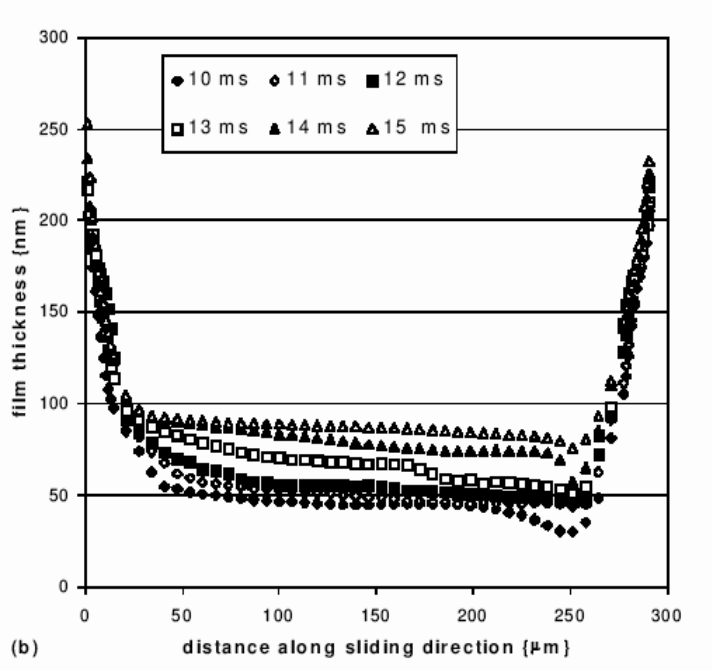

Figure 3.6: (a) Film profiles for HVI650 at 80 ˚C and 50 m/s^2 acceleration, (b) Profiles of the second front of lubricant for HVI650 in pure sliding at 80 ˚C and at 5 m/s^2 acceleration [30]

The most notable feature of the EHD film behaviour observed were the film thickness fluctuations which once formed in the inlet, travel through the EHL conjunction unchanged. This can be seen in Figure 3.7 where a series of images were taken at 5 m/s^2 and at 60 ˚C. The analysis of the results showed that these perturbations occurred when the time needed for the entrainment speed to reach its final value is close to the time needed by the first front of lubricant to travel along the EHL conjunction.

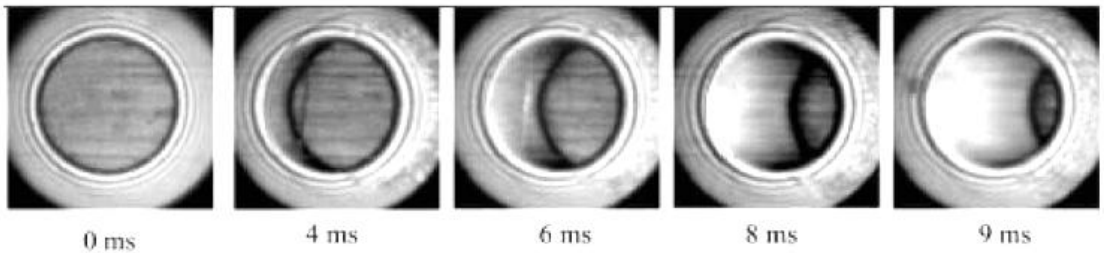

Figure 3.7: Images of the contact at start-up for at 5 m/s^2 acceleration [44]

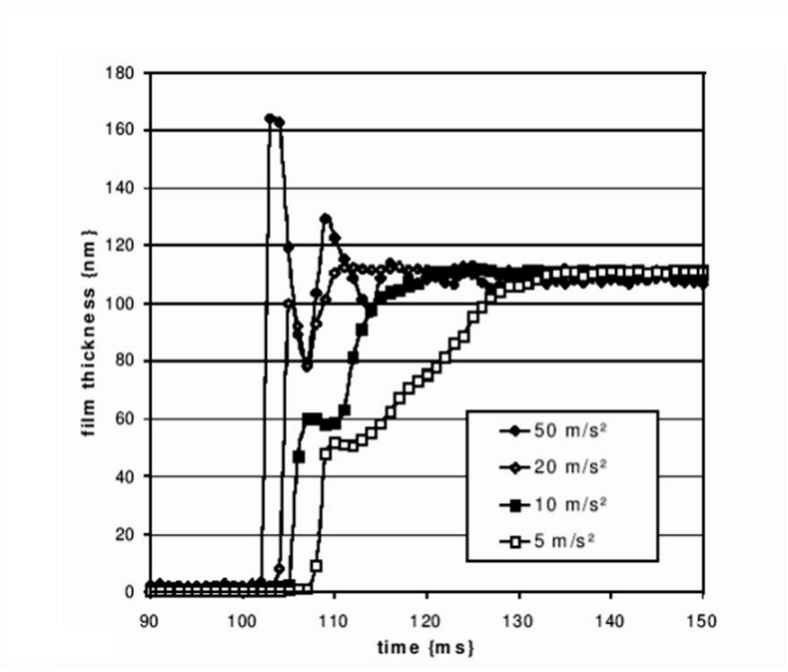

Figure 3.8: Central film thickness at different accelerations for HVI650 at 80 ˚C [44]

The central film thickness at different accelerations for HVI650 at 80 ˚C is depicted in Figure 3.8. As it can be observed from the graph at the highest acceleration applied, the central film thickness values were greater compared with those obtained at steady state condition, followed by a short period of damped oscillation, to level out at the steady state value of 108 nm at a period of 30 ms.

In the case of PAO and 5P4E oils, the film behaviour was similar to that observed for HVI650. The differences observed was attributed to different values of the viscosity and in the pressure viscosity coefficient which different values of film thickness.

There have also been reported experimental and theoretical studies on the EHD film behaviour under controlled deceleration. An experimental investigation has been conducted by the same authors [45, 46] on the elastohydrodynamic film collapse during rapid deceleration. The Ultrathin interferometry technique coupled to a high speed camera have been used to measure the film thickness and film geometry during fast, controlled deceleration under pure rolling and sliding conditions. In pure sliding conditions, the disk was kept stationary during the tests while the ball was rotating at different rolling speeds and then halted. During pure rolling conditions, the disc and ball were driven by independent motors with the same speed and then were halted at the same time. The load of 20 N has been kept constant in all tests. The lubricant used in these experiments was a polyalphaolefin (PAO). The pure rolling tests were performed at a controlled temperature of 50 ˚C while the pure sliding tests were conducted at 70 ˚C. Results showed that during decelerating motion the EHD film experiences two distinct stages; a first stage when the film thickness drops

rapidly, without significant change of geometry and the second stage when the central film thickness remains almost constant while the overall shape changes in order to entrap a plug of lubricant in the middle. It was also observed that during pure sliding the values of the measured central film thickness were higher than the predicted values based on the steady state theory. Figures 3.9 and 3.10 illustrate the measured as well as the theoretical film at two different halting times.

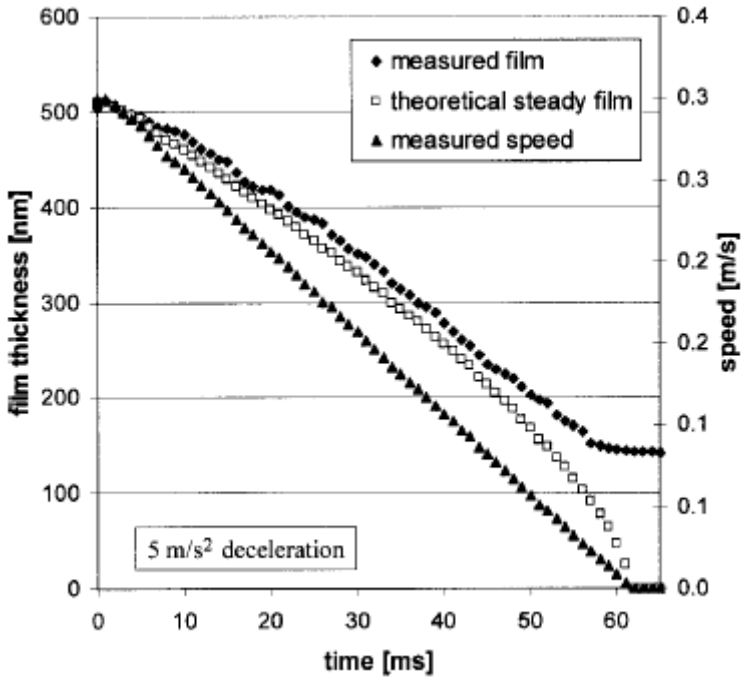

Figure 3.9: Comparison of measured film thickness collapse with steady-state prediction at 60 ms halting time (10 m/s^2 deceleration rate) [45]

Finally, it was found that the lower the halting time thus the slower deceleration rates the thinner the film. The central film thickness evolution from an initial entrainment speed of 0.3 m/s over six different halting times can be observed in Figure 3.11.

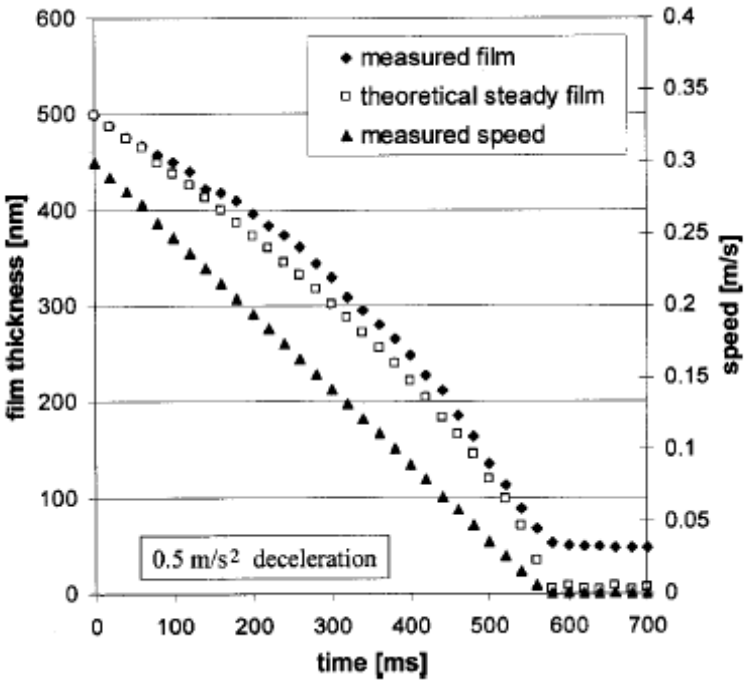

Figure 3.10: Comparison of measured film thickness collapse with steady-state prediction at 0.6 s halting time (1 m/s^2 deceleration rate) [45]

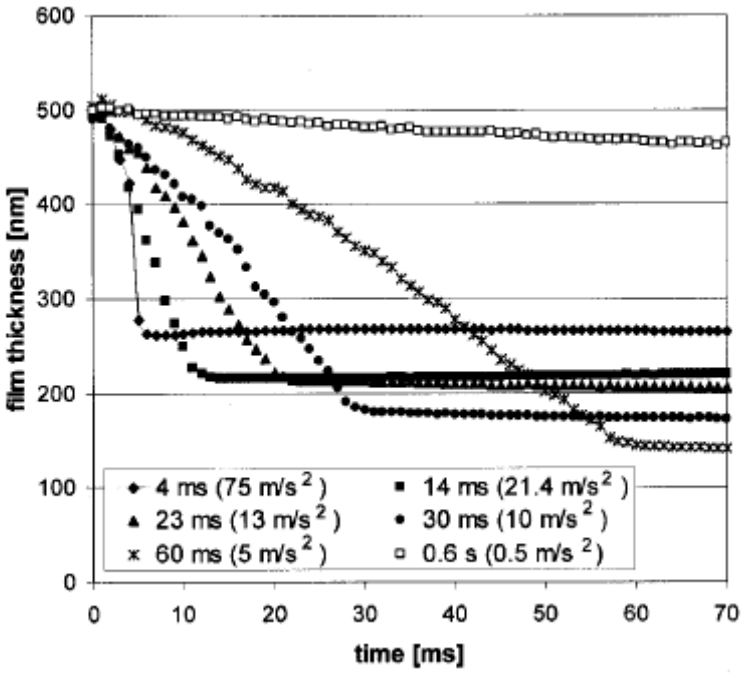

Figure 3.11: Central film thickness collapse at six different halting times [45]

A theoretical analysis [46] was carried out in order to compare it with the experimental findings. A theoretical model was used for the determination of film thickness in high decelerating motions based on Grubin's analytical solution of the elastohydrodynamic lubrication. This analytical solution followed the assumption that the inlet geometry does not change considerably during the first stage of the deceleration time. Therefore based on Reynolds' equation, the pressure gradient includes the time variable term:

$$\frac{\partial p}{\partial x} = 6\eta U \frac{h - h_0}{h^3} + 12\eta \dot{h}_0 \frac{x - x_0}{h^3} \tag{3.7}$$

Performing a semi-analytical analysis similar to Grubin's solution the central film thickness can be written as:

$$h_0 = h_s \left(1 - 6.522 \frac{b}{h_0} \frac{\dot{h}_0}{U} \right) \tag{3.8}$$

Furthermore it was observed that this equation is a Bernoulli's - type differential equation which can be solved analytically to give the central film thickness as follows:

$$h_0(t) = \frac{h_s}{e^{\left(-\frac{1}{6.522b} \int_0^t U dt \right)} \left\{ \frac{h_s}{h_i} + \frac{U^{8/11}}{6.522b} \int_0^t \left[U^{3/11} e^{\left(\frac{1}{6.522b} \int_0^t U dt \right)} \right] dt \right\}} \tag{3.9}$$

Where h_i denotes the initial film thickness at time t = 0.

The theoretical model based on Equation (3.9) showed a good agreement over about 80-85 percent of the halting time with the experimental results. Figures 3.12 to 3.13 illustrate the comparison between the theoretical and experimental predictions during different deceleration phases under pure sliding and pure rolling conditions.

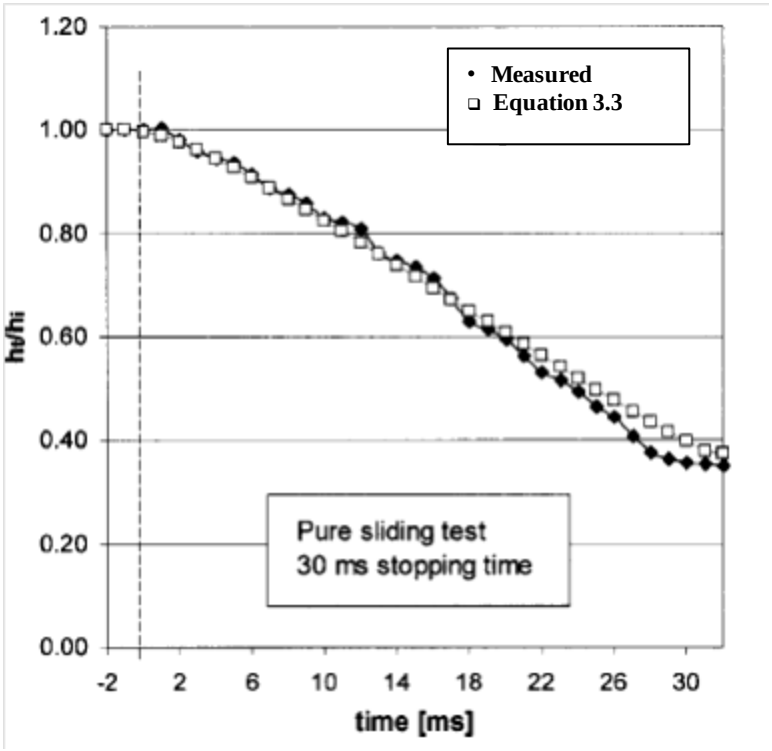

Figure 3.12: Comparison of measured film thickness collapse with prediction of Eq. (3.3) (deceleration 10 m/s^2 in pure sliding) [46]

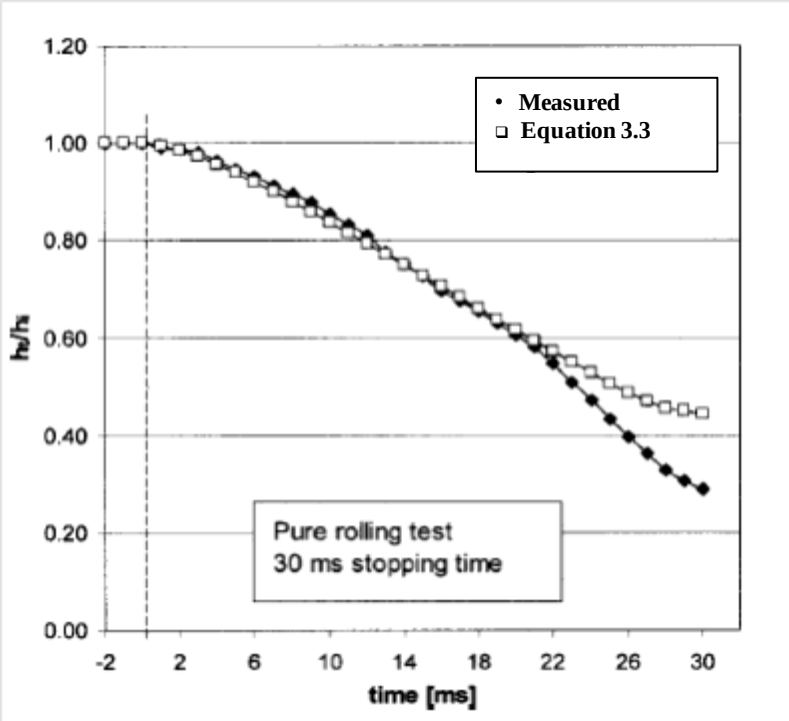

Figure 3.13: Comparison of measured film thickness collapse with prediction of Eq. (3.3) (deceleration 13.3 m/s^2 in pure rolling) [46]

A year later an experimental investigation was presented by Glovnea and co-workers [47] based on the behaviour of EHD films under start-stop conditions with applications to stepper motors used in space applications. In all experiments the start-stop motion was produced by keeping the disc stationary and switching the ball speed between 0 and 0.1 m/s. Tests were carried out at two different frequencies (2 Hz and 50 Hz) and two temperatures (25 $^{\circ}$C and 80 $^{\circ}$C) . Furthermore, four different lubricants were tested. The properties of the lubricants are shown in the table below.

Table3.2: Lubricant properties [47]

Lubricant	Temperature (^{o}C)	Viscosity (Pa.s)	Pressure-viscosity coefficient (GPa^{-1})
Penzane 2000	25	0.183	15.9
	80	0.017	13.1
Krytox 143 AC	25	0.92	24
	80	0.075	15.6
PAO	25	0.106	9.7
	80	0.012	5.8
BXL 413	25	0.422	5.2
	80	0.12	10.1

It can be stated that, the overall features of the EHD films were similar for all four lubricants tested. The film collapsed in two different cases. At 2 Hz during the stationary periods the film thickness collapsed but none significant change on the shape could be observed. Initially at the sides of the contact the film thickness was decreasing quicker than in the centre and then an entrapment was formed inside the contact region depending on the lubricant properties. Also, at higher frequency (50 Hz) employed in these tests, because of the short stationary period, the film thickness didn't have time to collapse completely. Additionally, during start –up conditions the central film thickness showed an overshoot, followed by a number of oscillations in both frequencies. As a result a series waves of enhanced film thickness were separated by constriction travelled through the contact. Figure 3.14 shows images of the contact recorded during alternative start –stop of motion.

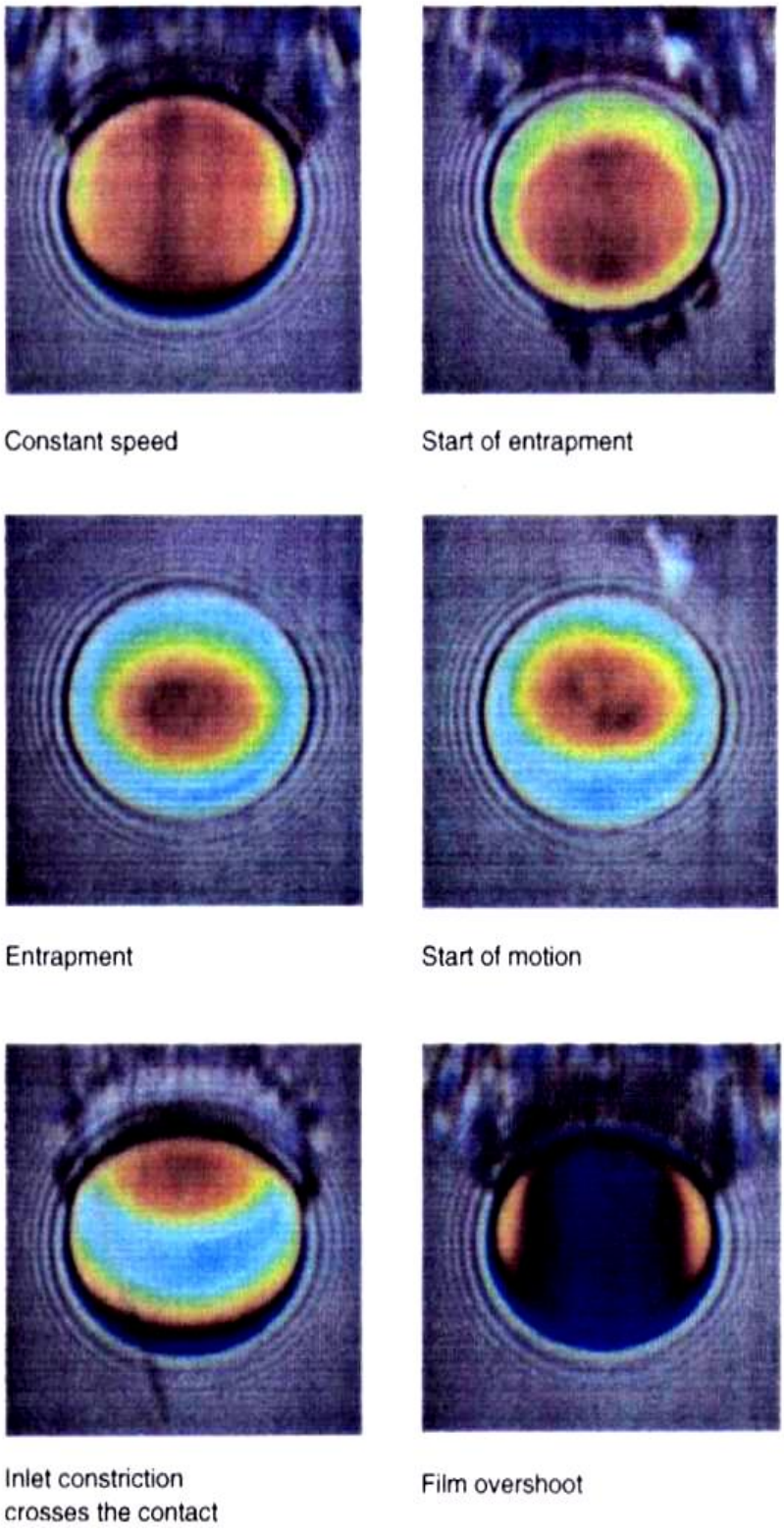

Figure 3.14: Coloured interferometric images during start-stop motion [47]

3.2 Non-Steady State Phenomena involving Transient Loading and Vibrations

In the beginning of ‘70s, Carson and Johnson [48] carried out an experimental work focused on the dynamic effects generated by surface corrugations in a rolling contact disc machine. They’ve used a twin disc machine and have found that vibrations caused by irregularities of the contacting surfaces in a rolling motion could be so severe that the dynamic forces in the contact could exceed the elastic limit of one or both bodies. The preliminary tests showed that corrugations were generated spontaneously in two different cases:

- Brass discs rolling , with or without sliding , in contact with a hard steel disc developed corrugations by plastic indentation, which spread progressively from an irregularity on the surface
- Duralumin discs, rolling with sliding in the absence of a lubricant , developed severe corrugations by a ‘stick-slip process’

A year later, Gray and Johnson [49] extended this approach and showed that the response of the rough surface system was dominated by the contact resonance and that system damping played a predominant role in determining whether contact force exceeded a critical level. The same year, Sanborn and Winer [50] studied the effect of transient loading upon the film thickness in pure sliding EHD contacts. The intefrerometric fridges were captured using high speed video during rapid change of the applied load. The authors concluded that the film thickness during rapid loading in sliding and rolling conditions could be predicted from the steady state behaviour. It should however be noted that the speed of load variation was limited by the acquisition speed of the camera.

An experimental work was performed by Dareing and Johnson [51] focused on the fluid film damping of rolling contact vibrations. The contact was formed between two rotating discs. The experiments were conducted with and without lubricant film and at various rotational speeds for contacting forces of 75, 180 and 310 lbf. As it was deducted from the results, the squeeze film properties of the lubricant film made a major contribution to the total damping of the system. It was also observed that fluid film damping may be more important under light loading conditions where Hertz compression is small.

In 1983 Smith and Cameron [52], showed experimentally that the elastohydrodynamic contacts under vibrations could experience sudden scuffing at a critical frequency and also a dramatic loss in fatigue life at other frequencies. Both responses suggested a severely diminished lubricant film thickness. Ren et al. [53] performed an experimental investigation which provided various types of EHL with dynamic load under point and line contacts. They used a high-speed camera to study the contact between a rolling ball and a lubricated glass, while the ball was subjected to a harmonically varying load. The dynamic load and the varying rolling speed were measured by fast frequency response transducer. The results showed that, for point contacts the dynamic film thickness and shape were consistently different from that predicted by the steady EHL theory. Also, a deep central dimple and outlet film thickness constriction appeared as sheen in Figure 3.15 and thus the film thickness profile showed combined features of squeeze and steady EHL condition.

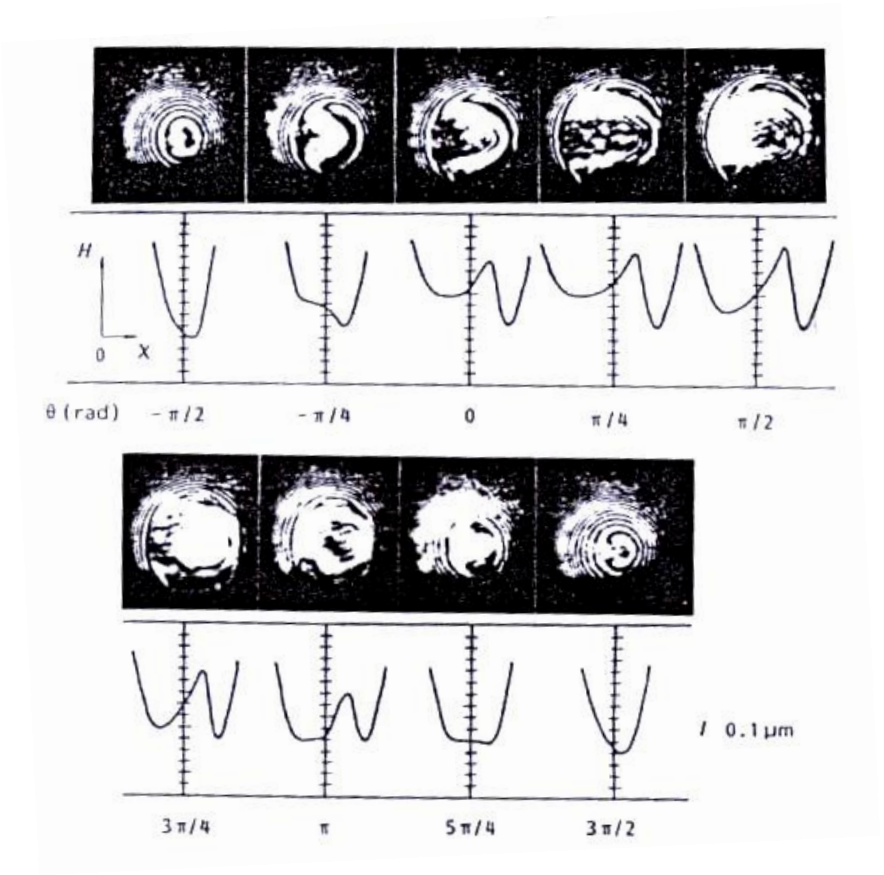

Figure 3.15: Dynamic film thickness of point contacts [53]

Sabot and co-authors [54] studied experimentally and numerically the effect of non-linear vibrations of sphere-plane contact excited by a normal load. Two sets of experiments were conducted based on non-linear free vibrations and forced contact vibrations. The latter was performed for the study of the dynamic contact load during the non-linear resonance phenomenon. The experimental apparatus consisted of two external amplifiers connected to an impedance head thus allowing the exciting force to be produced by the vibration exciter. Additionally, a three-orthogonal-component piezoelectric transducer was used to measure the contact dynamic load which was transmitted to the lower plane of the test apparatus. For free vibration tests, it can be observed from Figure 3.16 that there was a good agreement between the experimental values of the measured natural frequency and the natural frequency which

was predicted theoretically. That comparison showed less than 2.5 % difference. Furthermore, in dry contacts, the contact damping was small and therefore can be expressed as hysteretic damping. On the other hand, in lubricated contacts a fluid-pumping mechanism could be also added to the existing damping of the materials.

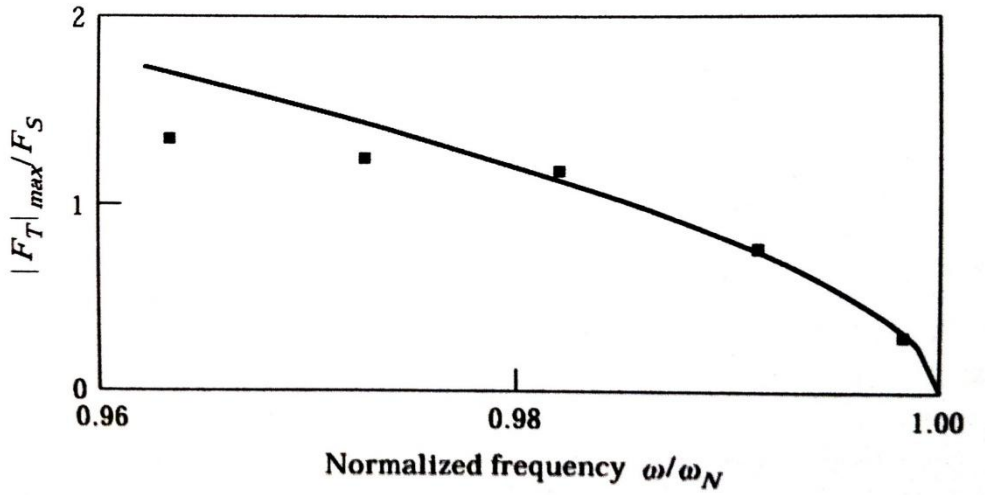

Figure 3.16: Normalized largest amplitude $|F_T|max/F_S$ of the normal contact load Vs normalized frequency ω/ω_N during free vibrations of the moving cylinder [54]

Referring to the forced vibration experiments a softening behaviour was observed. At the same time the level of the dynamic contact load was found to be twice as large as the static load just before the jump observed during a scan of decreasing frequency, as illustrated in Figure 3.17.

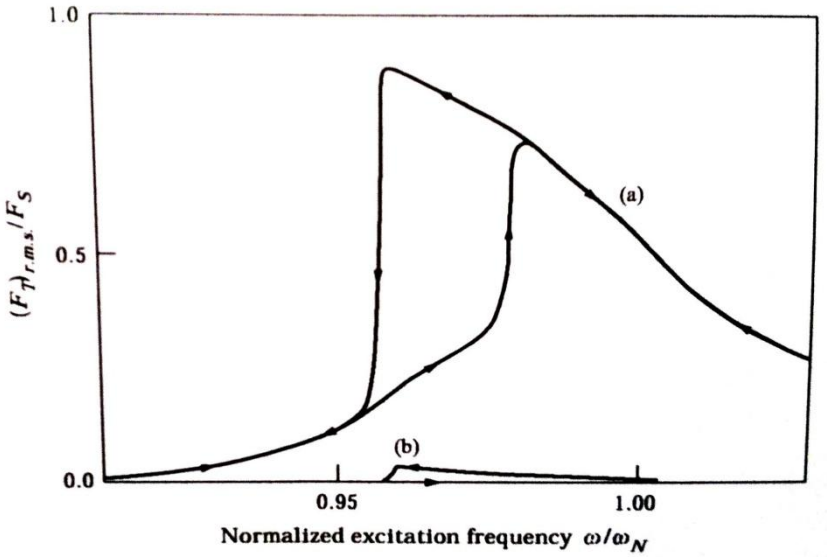

Figure 3.17: Measurements of the normalized r.m.s. value (F_T)r.m.s./FS of the contact load Vs normalized excitation frequency ω/ω_N for a harmonic excitation force (F_e)r.m.s./F_s =0.018 and a sphere diameter 2R= 18 mm, (a) Normal component; (b) ten times the tangential component [54]

In 1999 Wijnant et al. [55], used numerical methods in order to study the influence of lubrication on the dynamic behaviour of ball bearings. The main focus was on the stiffness and damping of EHL contacts. In this investigation both dry and lubricated contacts have been examined. The stiffness was presented for different values of load parameters M and lubricant parameters L for ellipticity parameter κ=1.0, 0.22 and 0.05 using efficient numerical solutions for circular and elliptical contact. Stiffness was determined precisely from steady state numerical solutions. For circular contact, results showed that when Δ_∞ (mutual approach) decreases with M and becomes negative for larger values of L, then the stiffness of the lubricant cannot be neglected. These results were obtained for κ=0.22 and 0.05.

Alternatively the damping values have been presented for one value of the dimensionless frequency Ω = 5.13 by fitting numerical solutions of the full EHL problem to the solution of a

simplified spring-damper model for circular contacts only. Due to absence of pressure-induced flow in the high pressure region, fluctuations can be observed in film thickness and pressure for the transient simulation.

This study also includes a non-linear dynamic model that has been developed in order to explain the relations between the different structural components of a ball bearing. This dynamic model incorporates a flexible outer ring. In the case of a non-rotating speed, the EHL contacts act as dry contacts. When the bearing rotates, entrainment is created therefore a fluid film builds up between the rolling elements and a raceway. This film influences the stiffness and the eigenfrequencies of the bearing. It was found that this influence, compared to the dry contact, was reasonable for medium loads and low rotational speeds but increases for high speeds and low loads.

Wijnant et al. [56] performed an investigation which focused on the effect of the vibrations on the film thickness and pressure. In this paper, a comparison of results between experiments that were carried out on a ball and disc apparatus with results obtained with the EHL contact model was investigated. The experimental apparatus used in this study consisted mainly of a polished steel ball of 50 mm diameter mounted on a shaft which was driven by an electric motor. The ball was loaded against a 104 mm diameter circular glass disc. When the ball was driven by the friction in the contact thus nominally pure rolling conditions were achieved. The lubricant used in this investigation was a fully formulated polyalphaolefin oil viscosity grade and it was applied in a small reservoir in which the ball on its shaft was mounted. The lubricant temperature was held at a room temperature of 23˚C. A static load was applied by a pneumatic cylinder placed between the ball shaft holder and the base of the

apparatus. The load was rapidly increased by impacting a wedge between the base and the ball holder. The initial load was 45N and was rapidly increased to 165N. Optical interferometry was used with a white light source, a microscope and high speed video system.

A series of interferograms showing the film thickness at the initial load are observed in Figure 3.18. For this particular case, the measured central film thickness was h_c= 0.34μm and the minimum film thickness was h_m=0.15μm. It can be seen that, when the load increases, it leads to a larger contact area. The fifth frame corresponded to the final load.

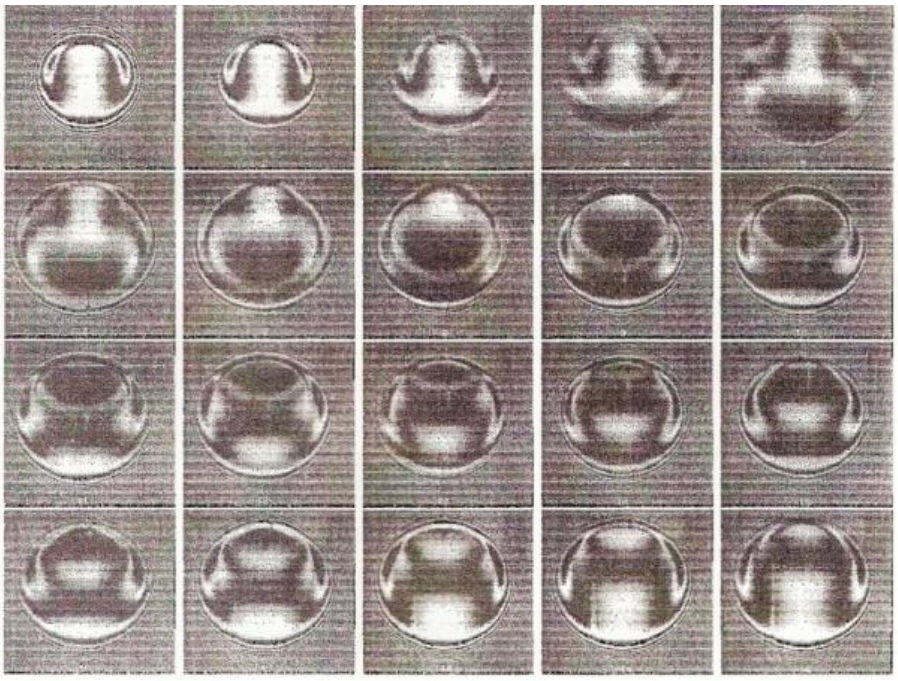

Figure 3.18: Interferograms of film thickness for 0<t≤4.22ms [56]

In addition an EHL model for constant loads was presented in the theoretical part of this investigation which described the entire dynamic interaction between the ball and the glass

disc. The model assumed a raceway of infinite mass and the only "vibrating mass'' was the ball. In order to facilitate a comparison with the experimental results pseudo interferograms were generated from the computed film thickness by using the wavelength of the light. The calculated central film thickness was h_c=0.32μm and the calculated minimum film thickness was h_m=0.18μm. The difference between the calculated value of central film thickness and the experimental value it was found to be 5.9 percent. For the minimum film thickness a 20 percent difference it was found.

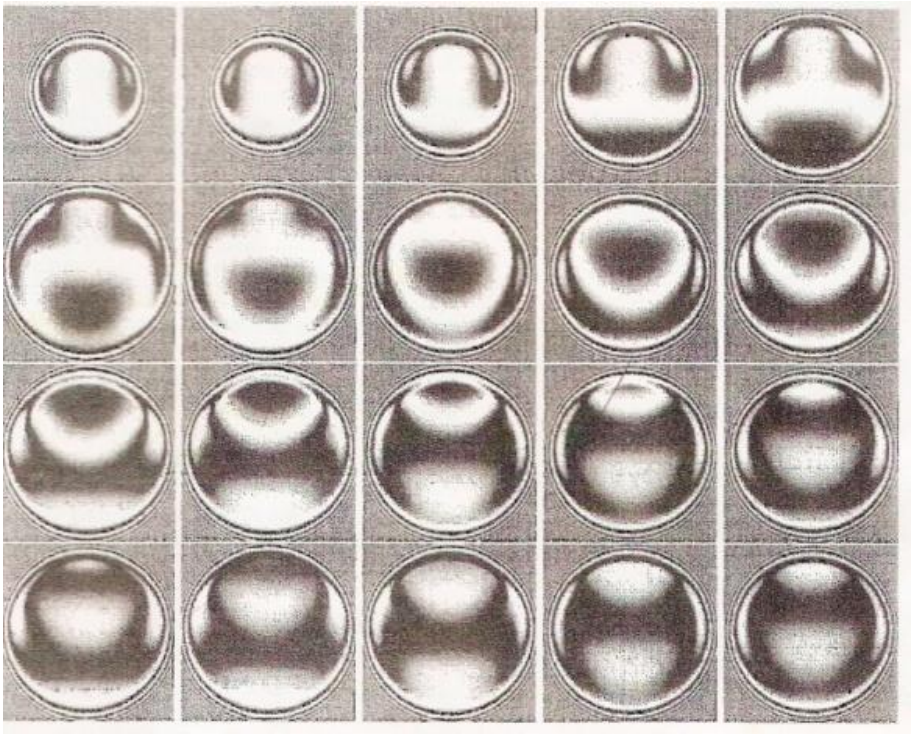

Figure 3.19: Computed pseudo interferograms of film thickness for $0<t\leq4.22$ms [56]

After the load increased similarities of film thickness and pressure with experimental ones can be observed, hence a good agreement between the theoretical results and the experimental results can be found. This agreement shows that the effects on the film

thickness of the dynamic behavior of structural elements other than the ball and glass disc must be small.

In 2003 Rigaud and Liaudet [57] carried out an experimental and numerical investigation on the dynamic responses of a preloaded vibro-impacting Hertzian contact subjected to sinusoidal excitation. The experimental test rig used for this study is illustrated in Figure 3.20. A steel ball with a diameter of 15 mm was placed between two steel discs which were fixed to a rigid frame.

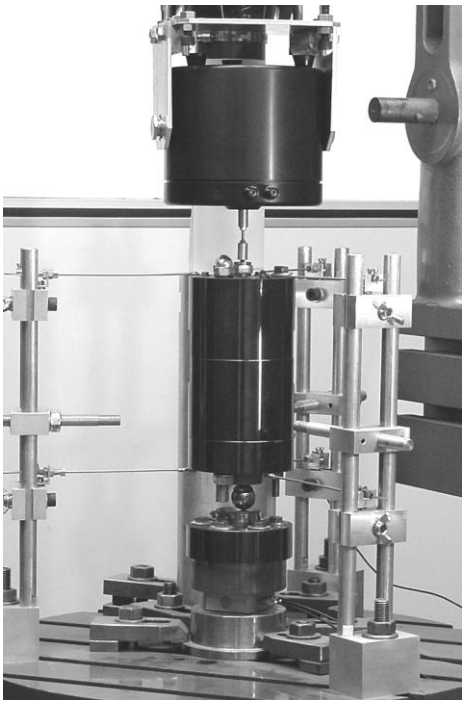

Figure 3.20: Experimental apparatus [57]

A moving cylinder was held by six titanium stems connected to the rigid frame in order to avoid lateral displacements and rotations. The contact was excited with the help of a vibration exciter connected to the moving cylinder. A piezoelectric transducer was placed between the

vibration exciter and the moving cylinder in order to measure the excitation force. Finally, the input force and the dynamic responses were displayed on a four-channel oscilloscope as well as the harmonic signal and were analyzed using a lock-in amplifier.

The results showed that, when the level of the sinusoidal force was small, the contact dynamic behaviour was almost linear and no loss of contact can be found. For higher external input amplitudes, the dynamic system revealed a non-linear softening behaviour when the frequency response curve was bent to frequencies lower than the linearized contact frequency, leading to jump discontinuities. Finally computational methods applied to non-linear problems were also used in order to perform a theoretical investigation based on the dynamic response of the Hertzian contact. They observed that, there was a good agreement between experimental and theoretical results.

Sakamoto et al. [58] performed an investigation of the effects of cyclic pulsating loads on point contact EHL film under sliding and rolling conditions by direct observations using optical interferometry technique. For pure rolling conditions, the entrainment speed was 12mm/s and the load varied between 5 and 55 N. A series of interferograms taken at different time intervals can be observed in Figure 3.21. Results showed that, for the loading process, the effect of sudden increase of the load was an enlarged contact region, therefore a thick film was created in the inlet region. On the other hand, in the unloading process, the maximum film thickness was preserved, but the film thickness is reduced at the inlet region which subsequently travelled through the contact.

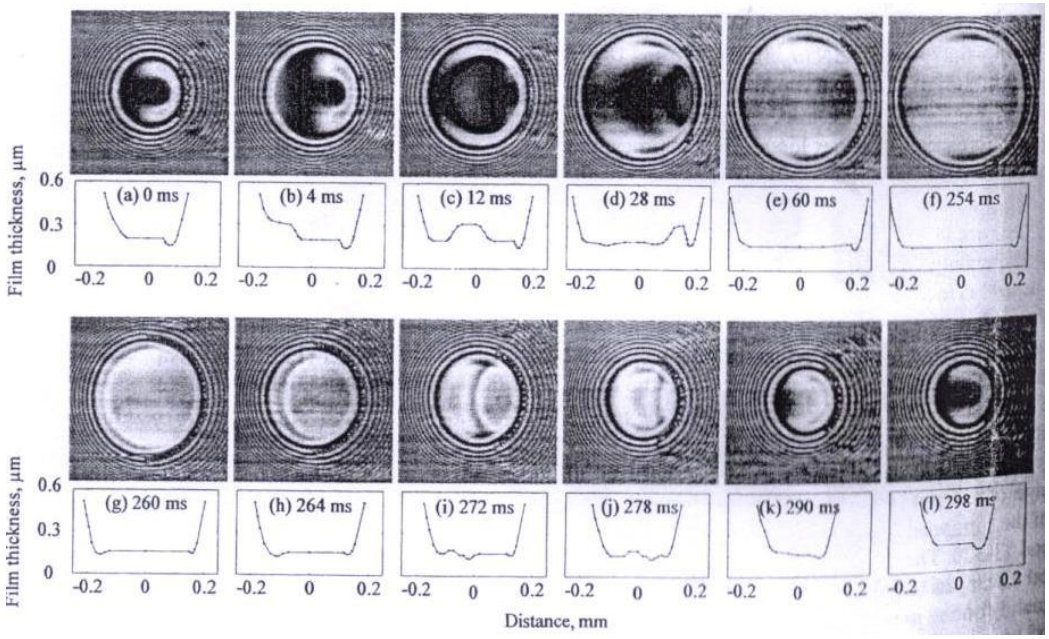

Figure 3.21: Effect of pulsating load on pure rolling EHL films [58]

Similar work was carried out by Kaneta and co-authors [59]. Their study was focused on the effect of impact loads on EHL point contacts. The contact was formed between a steel ball of 25 mm diameter and a glass disc of 180 mm diameter. The steel ball was supported by four taper rollers which were fixed on a lever arm. The impact load was applied by pushing up the lever with the help of a piezo actuator. Strain gauges were attached to a holder of the piezo actuator in order to measure the contact load between the two surfaces. Duochromatic optical interferometry was used to determine the shape and the thickness of the film.

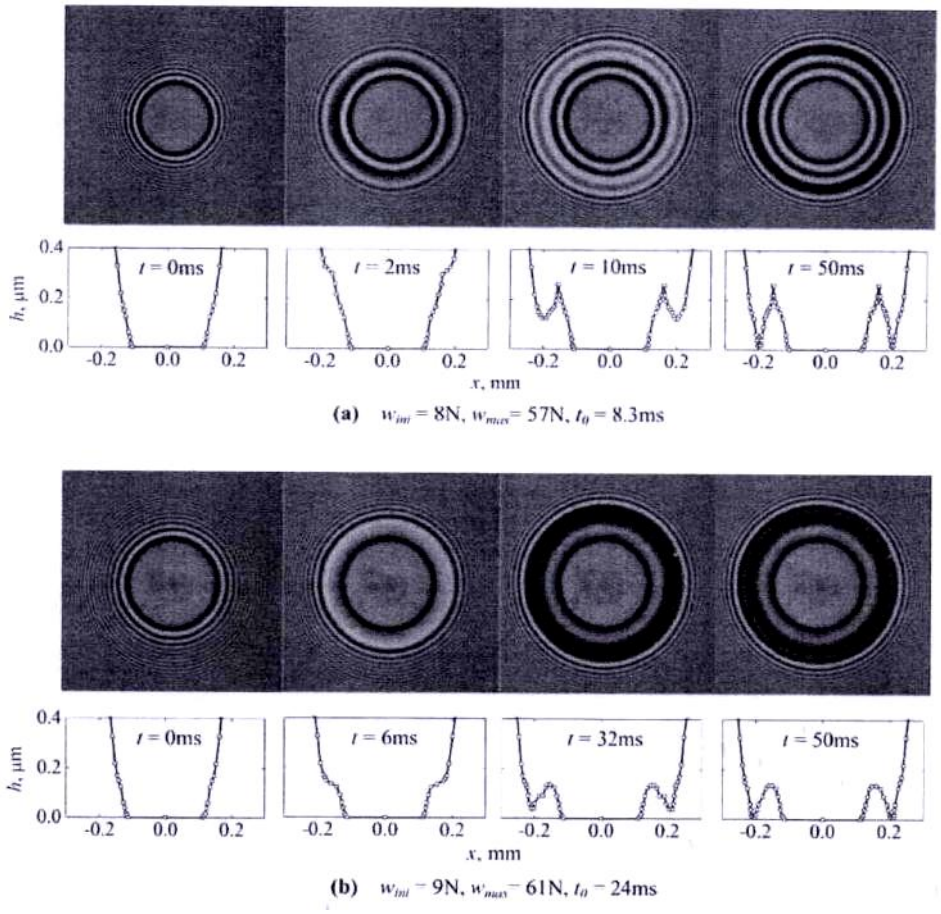

Figure 3.22: Time variations of the interferograms and mid-plane film profiles for an impact on an oily Hertzian contact [59]

From the results it can be concluded that:

- When impact load was applied to a lubricated Hertzian contact, entrapped oil was found just outside the initial Hertzian contact as seen in Figure 3.22. The maximum entrapped film thickness was determined by the average increasing rate of the Hertzian contact radius.

- Under rolling / sliding conditions, the impact load caused a crescent shaped oil entrapment (Figure 3.23), which was produced at the inlet of the EHL contact and travelled along the contact region.

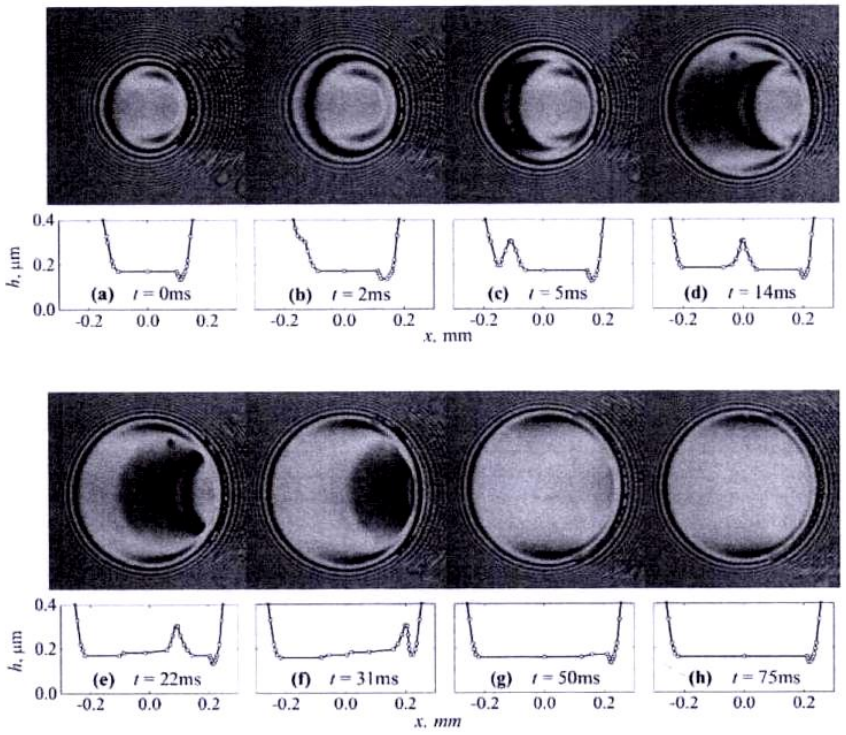

Figure 3.23: Interferograms and mid-plane film profiles [59]

El Kilali and co-authors [60] studied the behaviour of lubricated contacts subjected to dynamic normal excitation forces applied to double sphere-plane Hertzian contacts. Modal properties were also investigated experimentally and numerically. The numerical dynamic model was based on the finite element method. From the experimental point of view, first tests were carried out under static conditions. The lubricant used in this study was a 400 NS mineral oil with a dynamic viscosity of 153 mPa.s at 26.8 $^{\circ}$C. The impact loading was obtained using a hammer. A set of interference fringe patterns and the relative film thickness

are present in Figure 3.24. In this situation the lubricant was squeezed out of the contact area at the periphery, and the pressure at the centre became larger.

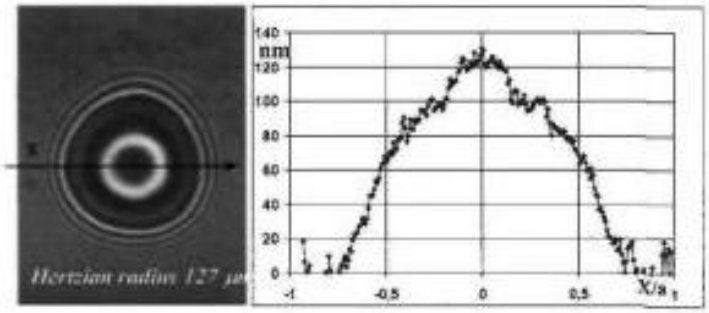

Figure 3.24: Set of interference fringe patterns and the relative film thickness [60]

These results also showed that, a dimple was formed in the middle of the contact during the free shock response. Additional experiments were conducted under pure rolling conditions with the main rolling speed set at 0.3 m/s. Figure 3.25 shows the film thickness along the rolling direction. The measured central film thickness was h_c = 324 nm and the minimum film thickness was h_m = 250 nm.

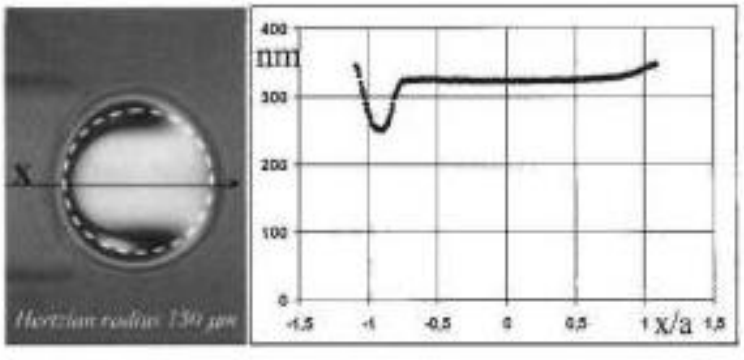

Figure 3.25: Lubricant film thickness along the rolling direction inside the contact [60]

When stationary lubrication regime was obtained, a free dynamic shock was applied at a constant speed. It was found that an increase of load had an effect of increasing the contact diameter from 150 μm to 203 μm. Therefore, an enhanced film thickness was generated which in turn travelled across the contact generating ripples in the film thickness (Figure 3.26). In this case the film thickness variation was about 138 nm.

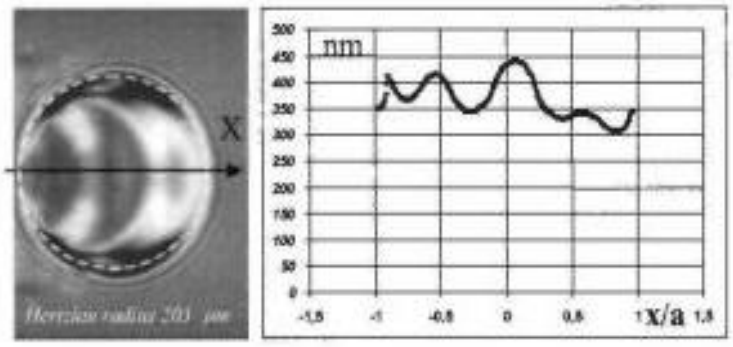

Figure 3.26: Free dynamic response of lubricant film thickness along the rolling direction inside the contact [60]

Ciulli and Bassani [61] carried out an experimental investigation which focused on the vibrations and their effects on EHL non-conformal point contacts. Experiments were carried out using a test rig able to identify the friction force by using a load cell and the film thickness as well as shape using the optical interferometry method. A high-speed camera was used for recording the interferometric images. The lubricated contact was formed between a glass discs and spherical specimens with a diameter of 25 mm and 41 mm respectively. The load (20N) and the oil temperature were kept constant during all tests. The load was applied with weights via a lever mechanism with a radial gas bearing as fulcrum. Results showed that, there was a connection between the variation detected of the friction force and the fluctuations of the film thickness. It was difficult to extract any quantitative relations between

vibrations and the behaviour of the film, as those vibrations were randomly created by inaccuracies of the experimental apparatus, and thus impossible to control.

Recent studies focused on the behaviour of EHD films under lateral vibrations. Glovnea and Spikes [62] and Kalogiannis et al. [63] have shown that oscillations transverse to the main rolling motion create ripples through the lubricant film thickness which propagate along the instantaneous entrainment direction. These two studies have pioneered the research into the effect of lateral oscillatory motion upon the behaviour of EHD films, but they were limited by either the performance of the experimental rig or by the values of the parameters investigated.

3.3 Micro-geometry effects in EHD films

Roughness and surface features become very important when compared with the lubricant film thickness, which can induce wear. Furthermore, local pressure variations increasingly cause surface-induced fatigue. Therefore, the understanding of roughness behaviour in EHL contact performance has become important [64].

Early measurements of film thickness aimed at the geometry variation such as found in cams and gears have been investigated using electrical methods [65, 22]. The transient effect of micro-geometry on the behaviour of EHD films has been intensely studied both numerically and experimentally. Other experimental investigations which considered the effect of surface

roughness on lubricant film thickness and fatigue life have been carried out by Dawson [66] and Tallian and Mccool [67].

Choo and co-authors [68] studied the effects of three-dimensional model surface roughness features on lubricant film thickness in EHL contacts. The Spacer Layer Imaging method was used for the investigation of the influence of the surface roughness features on the thickness and shape of elastohydrodynamic films. At first, the aim of this work was to compare the experimental behaviour of 3-D roughness in mixed lubrication with previous studies at various working parameters. Secondly, the experimental measurements on 3-D roughness behaviour were compared with the predictions of modelling work at different film thickness conditions and finally the similarities and differences between 2-D and 3-D roughness features in thin film, rough surface lubricated contact were identified. The test apparatus consisted of a glass disc pressed against a steel ball under a consistent load of 20 N which produced a maximum Hertzian pressure of 0.527 GPa and a Hertzian contact diameter of 0.27 mm. The disc and ball were driven by independent motors thus allowing various rolling and sliding conditions to be set. In that investigation two types of lubricants (HVI650, PAO) were used at a constant temperature of 40 $^{\circ}$C. The artifial features (roughness) consisted of bumps sputtered on smooth steel balls with a diameter of 19.05 mm. The geometry of sputtered bumps as well as the surface roughness parameters of the smooth balls are listed in the table below.

Table 3.3: Geometry of sputtered bumps and surface roughness parameters of the three smooth balls [68]

Ball Name	Peak to Base Height (nm)	Diameter at Base (μm)	Distance between Bump Peaks (μm)	CLA(nm)	RMS (nm)
MRB1	260	38.5	75	94.5	112.3
MRB2	129	40.0	75	47.0	55.0
MRB3	65	42.0	75	24.1	28.5

At first, the tests were carried out in pure rolling condition with a main entrainment speed varying from 26 to 210 mms^{-1}. In the second part of this experimental study the tests were conducted under mixed sliding-rolling at slide roll ratios, SRR of ± 10 percent, ± 30 percent, ± 70 percent and ± 100 percent at a constant rolling speed of 99 mms^{-1}. Under pure rolling conditions, results have shown that micro-EHL films were formed at all bump heights. Figure 3.27 shows a series of film profiles for both test lubricants taken across a bump along the entrainment direction. From the analysis it was clearly observed that the film thickness at the bumps as well as at the regions between the bumps increasing with the speed.

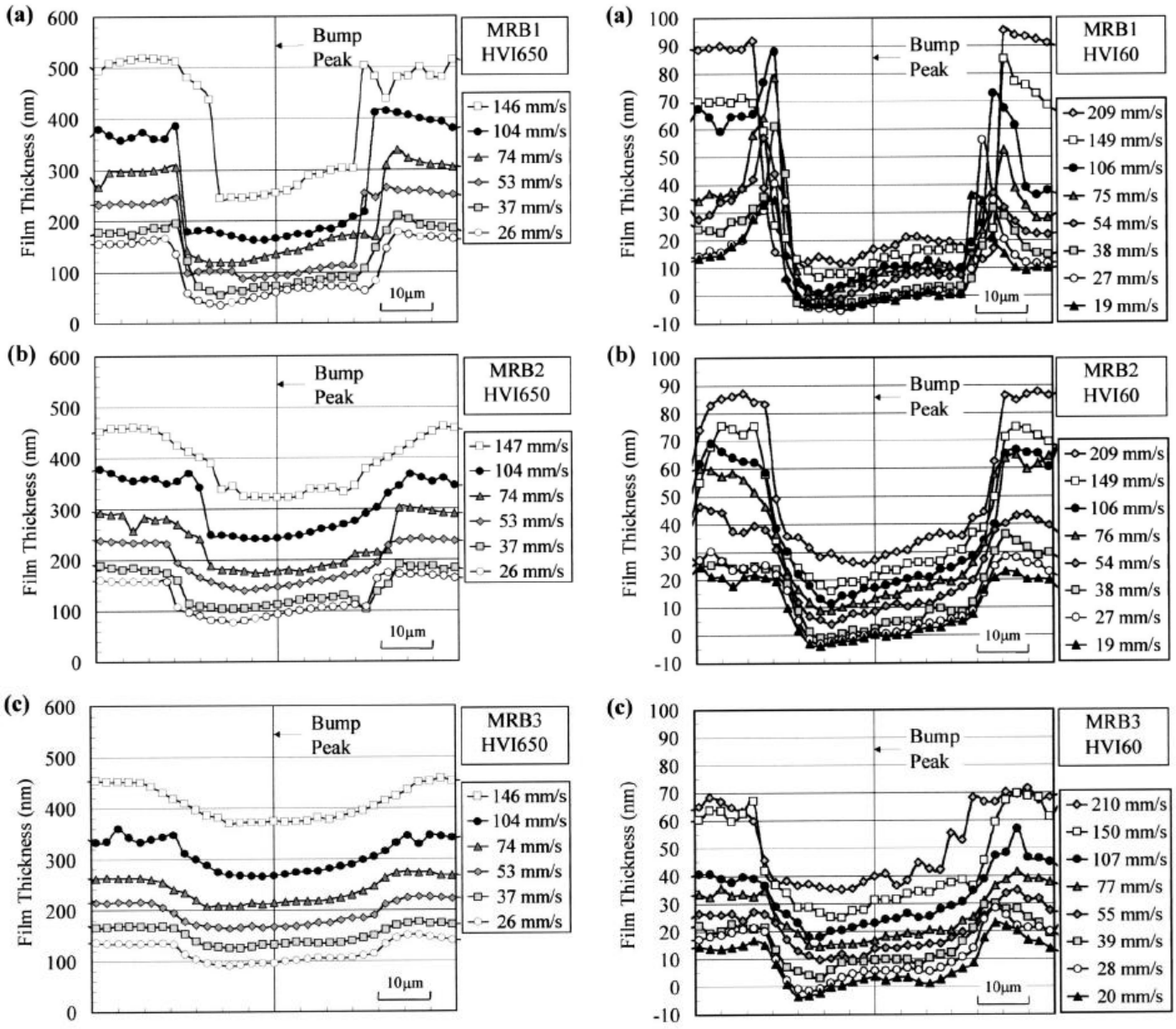

Figure 3.27: Profiles along the entrainment direction across a bump in thick film [on left column] and thin film conditions [on right column].Pure rolling, inlet on left.(a) large bump height, (b) intermediate bump height, (c) small bump height [68]

Under thick film conditions and in the case of the highest bump (MRB1) it was observed that the bump shape evolved as the speed increases. In the case of MRB2 the bump shape changes at the highest speed employed (147 mm/s) while for MRB3 it happens at a speed of 104

mm/s. For the low viscosity tests it was shown that the micro-EHL film appeared to be a wedge-like shape for all bump heights. In addition, for all bump heights, as the main entrainment speed increases the slope of the wedge-like film is also increased. Figure 3.28 shows an interferometric image captured at pure rolling conditions where an array of bump was sputtered on the steel ball.

As seen from this Figure, a micro-constriction was formed at the leading edge of the bump. This characteristic becomes more obvious at thicker films. Another observation was that, the small local constriction in the micro- EHL film was noticeable at a position opposite the crescent. So it can be stated that, the orientation of micro-EHL films formed at the bumps does not depend only on the entrainment direction but also on the inlet location as the bump enters the contact.

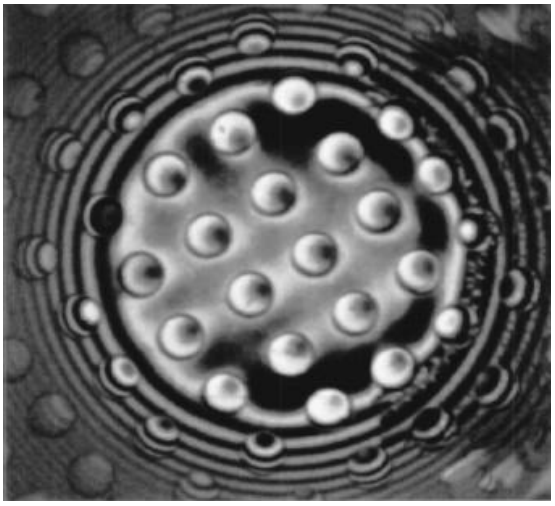

Figure 3.28: Interferogram of a circular EHL contact under pure rolling conditions where an array of near-hemispherical bumps was sputtered on a steel ball. Inlet is on left [68]

Figure 3.29 shows interferograms under mixed sliding-rolling conditions at the lowest bump height (MRB3) and the lowest oil viscosity.

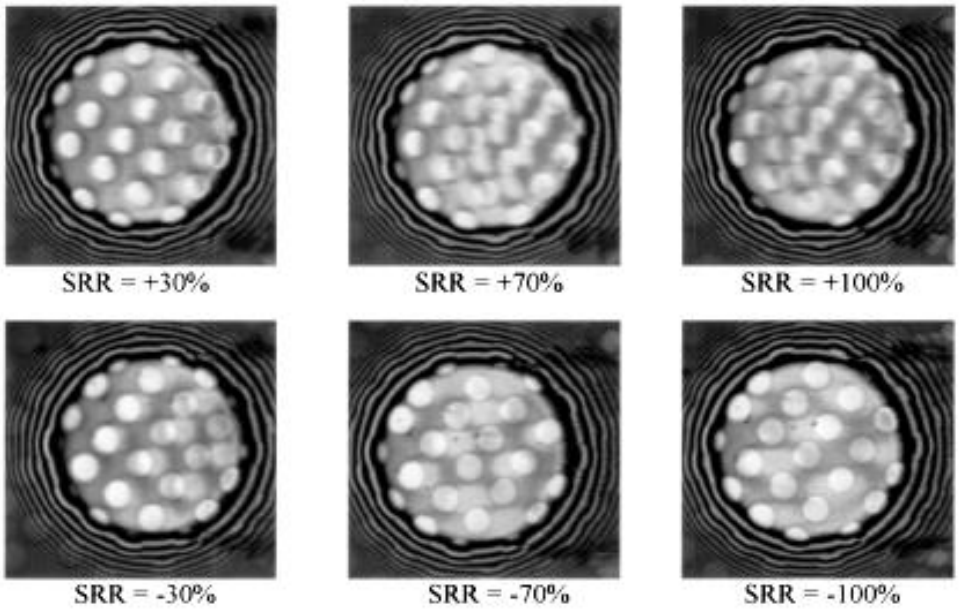

Figure 3.29: Interferograms showing convection of micro-EHL film in rolling-sliding, thin film conditions. + SRR on top row, - SRR on bottom row, MRB3, U = 99 mms^{-1}, inlet is on left [68]

The analysis of the results showed that, in the case of low SRR values of ± 10 percent, ± 30 percent the bumps within the inlet of the contact formed a wedge-like micro-EHL film shape. At a SSR ± 70 percent, the micro –EHL film developed at the bumps were convected away at the mean velocity of the surfaces. Finally in thick film conditions as illustrated in Figure 3.30 it was found that the lubrication of the bumps switched from that of a micro-EHL film developed at the inlet of the contact to a classical horseshoe shape.

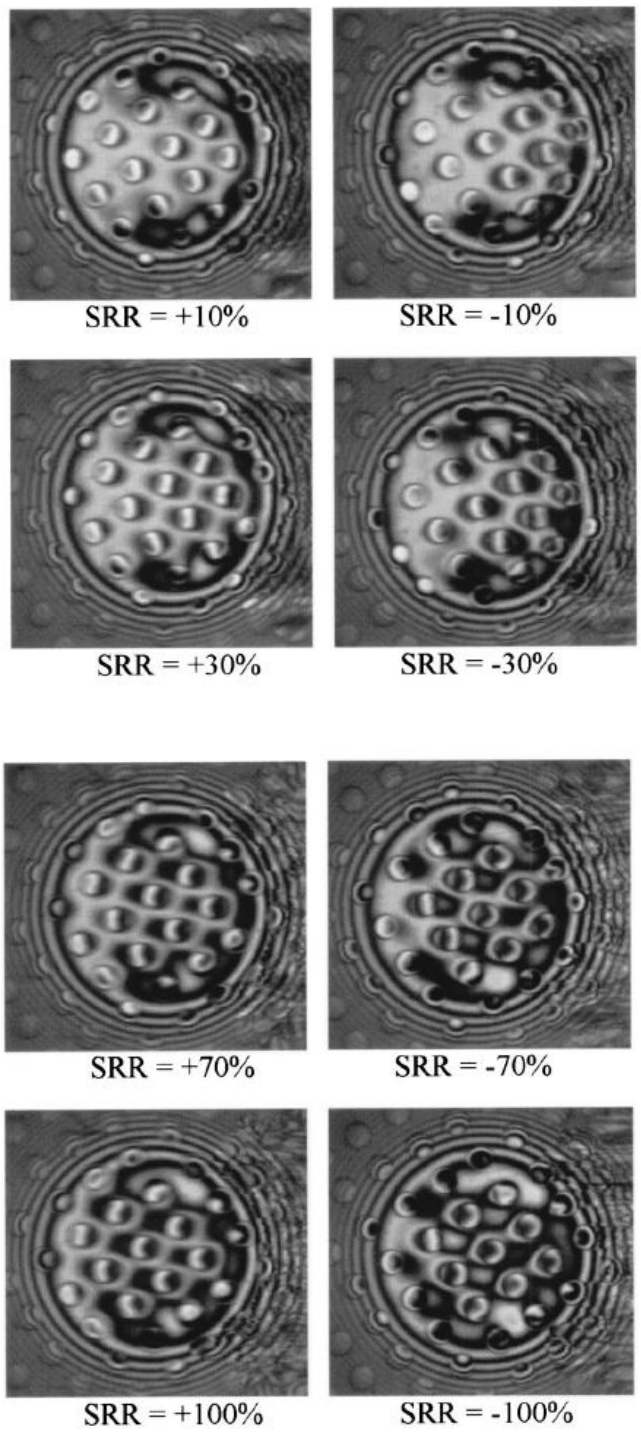

Figure 3.30: Interferograms showing the development of a steady-state micro-EHL film in rolling –sliding, thick film conditions. + SRR on left column, - SRR on right, MRB1, U = 99 mms^{-1}, inlet is on left [68]

An investigation on a single transverse ridge in a circular EHD contact using ultra-thin interferometry technique was conducted by Glovnea et al. [69]. This technique was applied for the first time to the study of rough surface in EHD lubrication. In the current investigation, the EHD contact was formed between a transparent disc coated on the underside surface with chromium and silica spacer layer pressed against a steel ball. An artificial ridge-shaped asperity was deposited on the ball surface, transversely oriented on the rolling direction which had a height of 100 nm , a width of approximately 40 µm and a length of 2mm. Figure 3.31 illustrates the measured profile of the ridge which was obtained using a stylus profilometer .

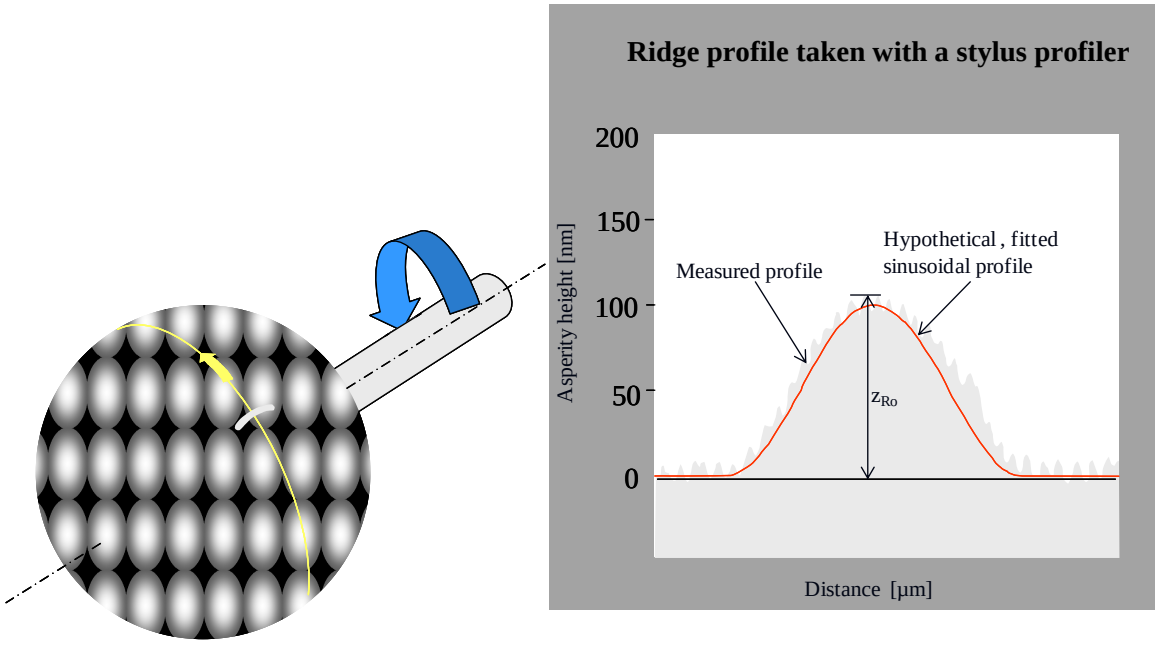

Figure 3.31: Measured profile of the ridge obtained with a stylus profilometer [69]

The majority of the experiments were conducted under pure rolling conditions with a speed of 0.025 m/s. Also, three different lubricants were used at different temperatures. The lubricant properties as well as the working temperatures are listed in Table 3.4.

Table 3.4: Lubricant properties [69]

Lubricant	***Temperature [^oC]***	***Viscosity [Pa.s]***	***Pressure/Viscosity coefficient [GPa^{-1}]***
PAO 1	40	0.0137	15
	25	0.0253	15.1
PAO 2	80	0.055	18.2
	60	0.123	22.4
PAO 3	80	0.165	20.6
	60	0.38	21.1
	40	1.03	27.3
	25	2.61	31.5

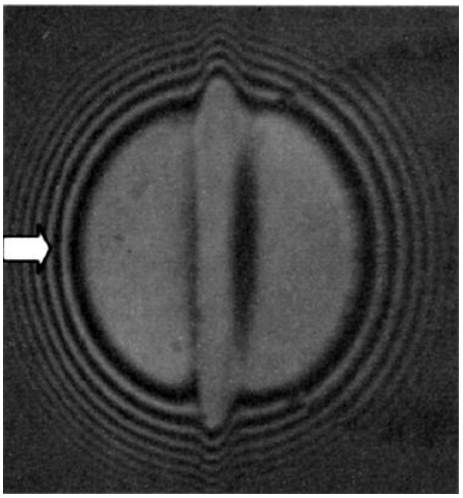

Figure 3.32: Interferometric image of the contact [69]

Figure 3.32 shows a typical interferometric image of the ridge passing through the contact obtained using a high speed video camera.

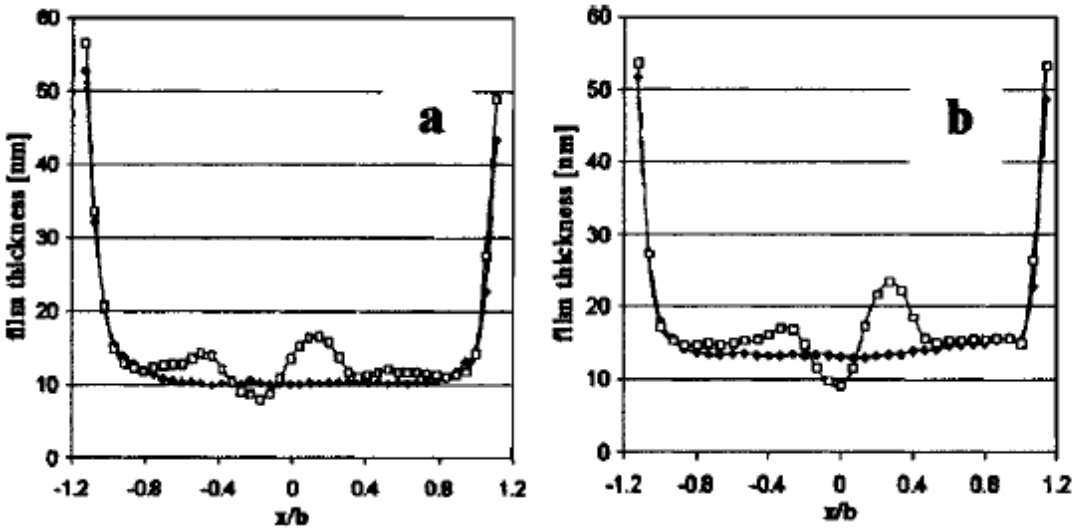

Figure 3.33: Film thickness profiles at different viscosities [69]

Figures 3.33 (a) to 3.33 (b) show film thickness profiles taken at moment when the ridge was in the middle of the contact under pure rolling conditions for different oil viscosities. As can be seen the rear entrapment occurred when the average film thickness was lower than the height of the ridge. It was also showed the deformed ridge and the film perturbations travelled at the same speed during pure rolling conditions. The film thickness profiles were used to calculate the pressure in the contact.

Several other experimental studies on the effect of model of real roughness on the EHD film have been carried out by Kaneta and co-workers [70-73], Guanteng et al. [74-75], Felix-Quinonez et al [76- 77] and Ehret et al [78], Krupka and Hartl [79, 81], to name only some of them.

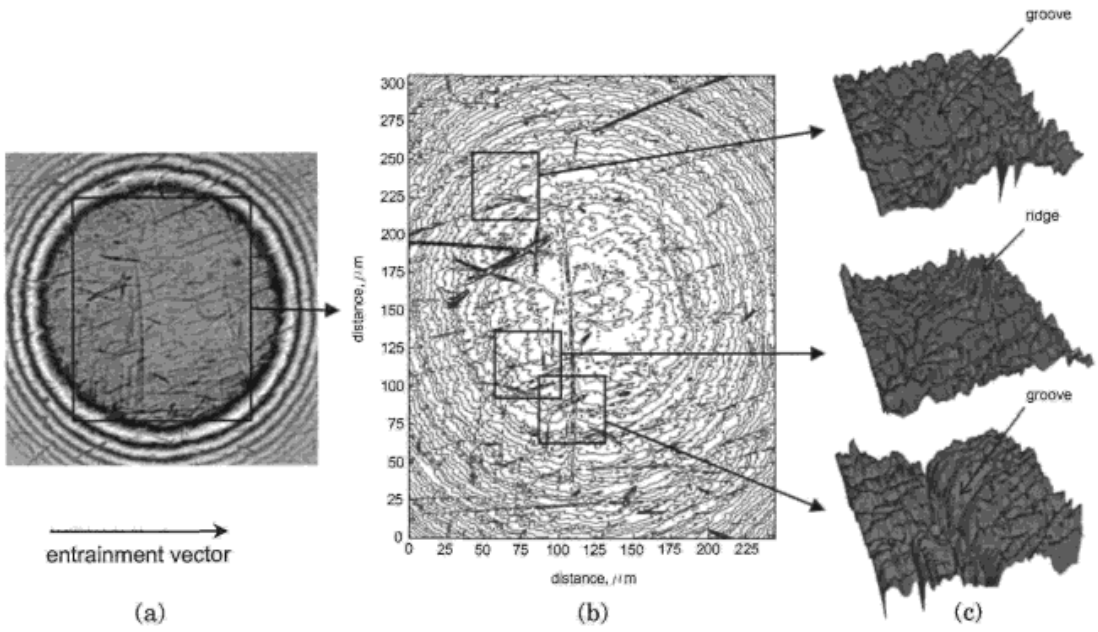

Figure 3.34: Real surface roughness features shapes and their position within lubricated contact [79]

Hartl et al. [79] performed an experimental study of the transient effects of real isotropic moving asperities on lubricant film thickness in EHD point contact formed between a real, random, rough surface, steel ball and smooth glass. For the first detail experimental investigation of changes in real surface micro-geometry passing through EHD conjunction, the authors used two different methods: Thin Film Colorimetric Interferometry (TFCI) was used in order to assess the film thickness from chromatic interferogram taken at the same ball position while the Phase Shifting Interferometry (PSI) was used for measuring the surface topography. From the surface roughness, conveniently oriented features such as transverse ridges and groove have been identified, in order to compare their behaviour with the one that which was observed with artificial asperities. Figure 3.34 presents an intimate view on both these features.

An important research effort concerned the theoretical modelling of the phenomena associated with the passage of surface asperities through elastohydrodynamic contacts. Greenwood and co-workers [82, 83], Hooke [84], Hooke and Venner [85-86], Venner and Lubrecht [87-89] Kweh et al [90] and many others. Holmes et al. [91] carried out a transient analysis on the effect of transverse roughness in elliptical EHL, with application to gear contacts. They have shown that the materials experience cyclical stress variation due to asperities passing through the EHD contact. Significant edge effects have been predicted, as the film thickness decreases at the periphery of the contact, due to the leakage of the lubricant through the valleys of the asperities.

Almqvist and Larsson [92] used the same coupled differential method for Reynolds and film thickness equations and multilevel technique to accelerate convergence of the solution. They investigated the influence of elementary surfaces features such as dents and ridges on the film thickness and pressure using transient non-Newtonian simulations of an EHL line contact. From their work, it can be concluded that, certain effect in transient EHL must take into account two-sided treatment of roughness especially when sliding is present in the contact.

3.4 Dynamic Behaviour of Rolling Element Bearings

The rolling element bearing is a complex system where the rolling elements, inner raceway, outer raceway and cage often experience noise and vibrations. Vibrations are very common to all kinds of machinery running at high speeds. Most of these applications involve combined vibrations in both vertical and longitudinal directions. For example, in gears and rolling element bearings, vertical vibrations are caused by changes in load, speed or geometry at the contact point, while longitudinal vibration is often a direct result of the torsional vibration of the shaft due to changes from either machine elements or motors. The level of vibrations depend upon many aspects including the energy of impact, the point at which the vibration is measured and the construction of the bearing. The design of the bearing can be changed by altering the geometrical and material properties. Important parameters for the internal design of the ball bearing are the number of rolling elements, the *osculation* and the radial *clearance*. The *osculation* is the ratio between the curvatures of the contacting bodies. The stiffness in the contacts can be controlled by the osculation and clearance [93].

3.4.1 Sources of Vibrations

The bearings themselves can be sources of vibrations due to several mechanisms. These are:

- Variable compliance
- geometrical imperfections (waviness)
- Surface roughness
- Other vibration sources (micro-pitting occurring, environmental impact, etc.)

In the first case, the time dependency of the bearing stiffness as a result of the rotation of the loaded rolling elements causes a so-called parametric excitation. Even if the bearings are geometrically perfect, they are still subjected to bearing vibrations under radial and misaligned loads. Figures 3.35(a) and 3.35(b) show normal path pattern under various rotational and loading conditions.

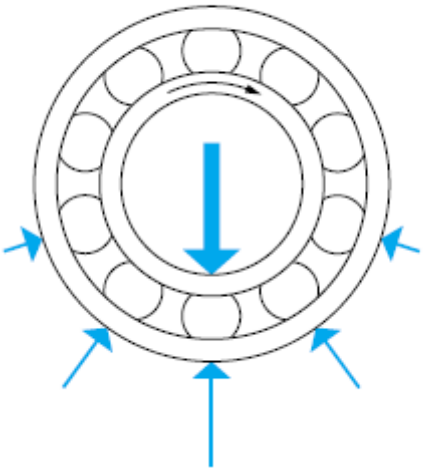

Figure 3.35(a): Uni-directional radial load, rotating inner ring- fixed outer ring [94]

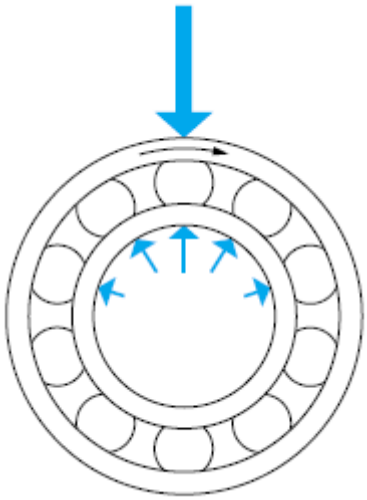

Figure 3.35(b): Uni-directional radial load, fixed inner ring- rotating outer [94]

Variable compliance vibration is strongly dependent on the number of the rolling elements supporting the external load, therefore the greater the number of loaded rolling elements, the less the vibration.

Other important sources of vibrations are small geometrical imperfections of the raceways (waviness). A wavy feature of a rolling element bearing is shown in Figure 3.36. Waviness is caused by the irregularities in manufacturing process, for instance during grinding or honing. Waviness can cause variations in the contact loads when the bearing is running. The magnitude of the variation depends on the amplitude of the imperfection, the stiffness and damping in the contact [94], therefore, it's crucial for controlling component waviness and surface finish during the manufacturing process as it may not only have a negative effect on vibration but also in bearing life.

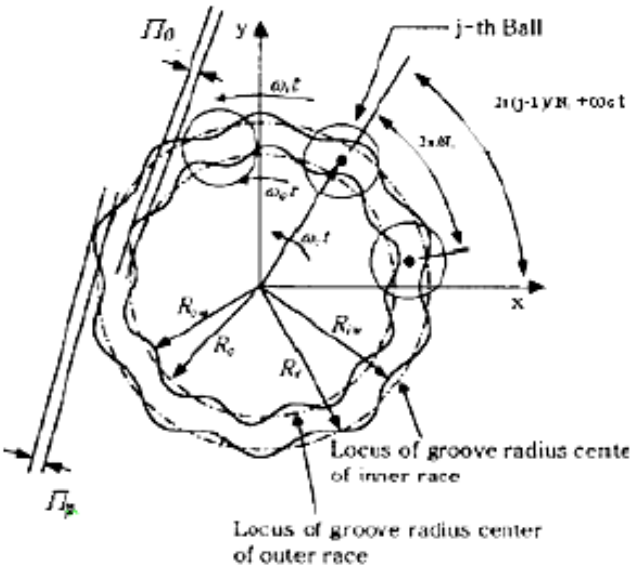

Figure 3.36: Waviness excitation in a rolling ball bearing [94]

In addition, surface roughness also produces vibrations when the level of the surface roughness is high in comparison with lubricant film thickness between the contacts of the rolling element raceway.

Finally other important factors which contribute to the generation of vibrations in rolling bearings are

- Contamination - causes wear and damage to the rolling contacts which in turn will generate vibrations across a wide range of frequencies.
- Cage defects – excessive clearance cause vibrations when the rolling elements are under acceleration and deceleration conditions through the contact zone which in turn results large impact forces between the rolling elements and the cage pockets.
- Grease – the level of vibration is initially high as the rolling elements distributes the grease but with running time it will be irregular and therefore doesn't have any negative effect in rolling bearings
- Micro-pitting – is a type of fatigue failure occurring in gears and rolling element bearings that operate in the mixed or micro EHL lubrication regime. It can be observed in many different cases depending on the loads, speeds, rolling and sliding velocities, lubricant properties.

3.4.2 Sources of Damping in Bearings

It is already known that vibrations are excited by the dynamic forces and mechanisms which can be found in many rotating machines. The method by which vibration gradually diminishes in amplitude is called damping. In damping, the energy of the vibrating system is dissipated as friction or heat, or transmitted as sound. The fluid damping can be either viscous or turbulent. Regarding viscous damping, the damping force is proportional to the velocity while in turbulent damping the force is proportional to velocity squared [95].

Damping of bearing vibrations is enhanced due to

- the EHD film within the Hertzian contact zone between the rolling elements and the raceway of the bearing.
- the Hertzian deformation of the rolling elements and the raceway.
- the squeezed film within the inlet region
- the bearing interface damping between the bearing rings and housings

Figure 3.37 illustrates damping sources in rolling element bearings.

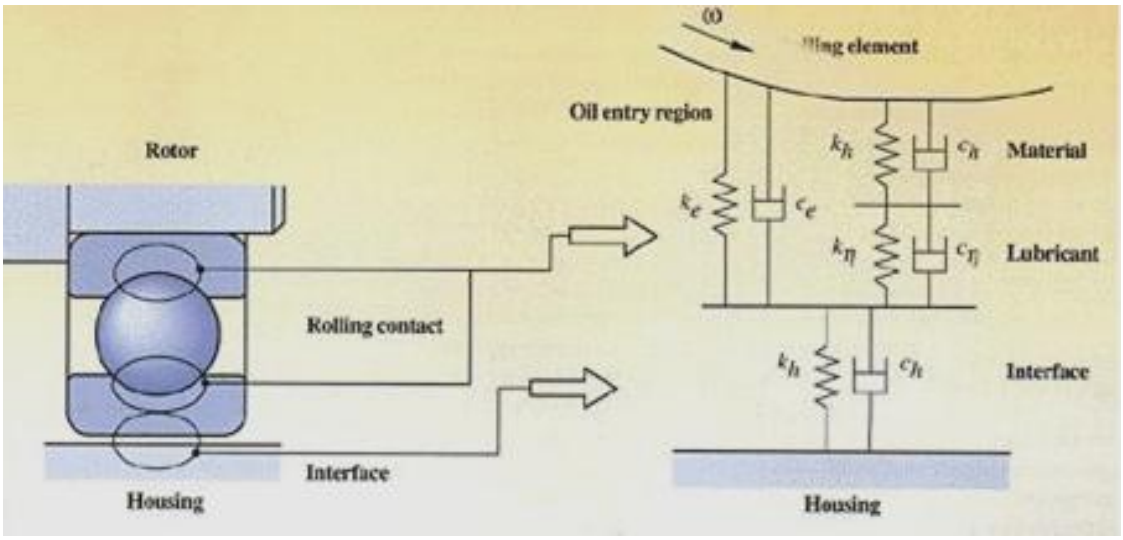

Figure 3.37: Damping sources in rolling element bearings [96]

CHAPTER 4: Experimental Methods

4.1 Methods of investigating EHD films

Various elastohydrodynamic film thickness measurement techniques have been developed over the years. The two main methods can be generally classified as electrical and optical (interferometric) methods.

First experimental methods used for the study of the formation of the elastohydrodynamic films were based on electrical measurement of the contact. Usually the electrical circuit was used to measure both resistance and capacitance, the former used to detect full film conditions (complete separation between the contacting bodies) and the latter to measure the thickness of film [97-99]. The electrical resistance method was also used relatively extensive for the study of the mixed lubrication regime, where the load is carried by both, hydrodynamic effect in the fluid and asperity contacts [100-102]. The electrical methods are relatively simple to devise and their main advantage is the fact that the elastohydrodynamic contact is formed between two bodies made out of steel (or other metals), which is similar to the contacts found in the machine components that work in the elastohydrodynamic regime. There are however some disadvantages to the electrical methods too: they are difficult to calibrate, and therefore can only be used for qualitative and not quantitative studies, they give, in general average quantities and are not as precise of optical methods.

The capacitance method involves the measurement of the electrical capacity of the lubricating film. The major problem associated with this method is that the dielectric constant of the lubricating film varies with temperature and pressure therefore, the constant must be determined before the evaluation of film can be performed.

Progressively the electrical methods of measuring film thickness in EHD contacts have been replaced with the optical interferometry methods such as Ultra –Thin Interferometry, Spacer Layer Imaging Method, Differential colorimetry or Relative optical interferometry intensity.

4.2 The principle of Optical Interferometry

The optical interferometry method is at the moment the most popular techniques for studying film thickness and shape of Elastohydrodynamic –lubricated contacts. This method uses interference of light, which results from the wave characteristic of light. This physical phenomenon was first used to measure thin lubricant films in EHD contacts in the mid 1960s [103]. It utilizes a flat transparent disc (usually glass or sapphire), loaded against a shiny steel ball or roller. The contacting side of the disc is sputter coated with an approximately 10-20 [nm] thick semi-reflecting layer of chromium. When a monochromatic light is shone through the glass, a division of amplitude of the incoming ray occurs where this is partially reflected by the glass-metal layer interface and the other passes through the lubricant film before being reflected from the steel ball surface. The two reflected rays are coherent but, because they have travelled different distances they undergo optical interference upon recombination [104]. This process produces an interference fringe pattern, which is recorded and analyzed in order to extract film thickness. The later is found from the fact that two adjacent dark fringes correspond to a variation of the separation between surfaces of one quarter of the wavelength of the light used. The optical interferometry principle is illustrated in the Figure 4.1.

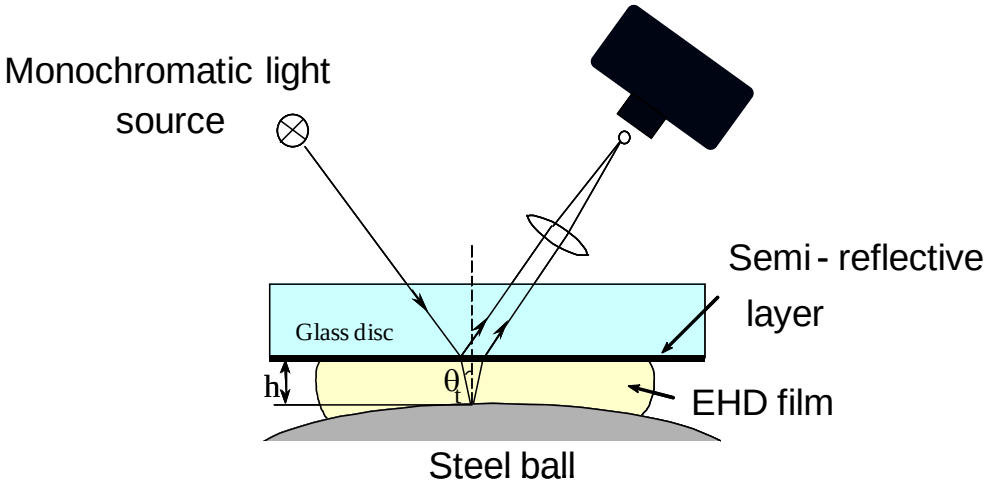

Figure 4.1: Schematic diagram of optical interferometry principle

For the two-beam interferometry, the equation regarding intensity of interference to optical path difference is given by the relationship:

$$I_R = I_1 + I_2 + 2\sqrt{I_1 I_2}\cos\left(\frac{2\pi\delta}{\lambda}\right) \tag{4.1}$$

where λ is the wavelength, I_1 and I_2 are the intensities of the initial rays and δ is the phase difference. The latter can be expressed in terms of the optical path difference, h_{opt} and the net phase change at reflection ϕ:

$$\delta = 2h_{opt} + \lambda\phi \tag{4.2}$$

Full constructive interference occurs when,

$$(N-\phi)\lambda_{max} = 2h_{opt} \tag{4.3}$$

Where: *N:1,2,3...* is an integer and represents the order of interference. The complete destructive interference is given by:

$$\left(N-\frac{1}{2}-\phi\right)\lambda_{min} = 2h_{opt} \tag{4.4}$$

4.2.1 Earlier studies based on optical interferometry

The application of optical interferometry to the measurement of film thickness in elastohydrodynamic contacts was developed in the mid 1960's by Cameron and his research group at Imperial College London. They have confirmed previous theoretical approaches and also have revealed the typical horse shoe shape of the film thickness contour.

In [105] Gohar's and Cameron's described results from two sets of experiments: sphere on a plane and roller on plane. The experimental apparatus consisted mainly of an one inch steel ball of one μinch diameter CLA surface finish 40 μinches sphericity, loaded against a conical surface which was rotated by a flexible 1/8 inch diameter shaft. A glass disc was mounted on a plate which could be loaded against the ball. On top of the contact a microscope with 4x objective and 10x eyepiece was mounted and a side illuminator placed between the objective and the eyepiece in order to provide a colliminated light. For this investigation three sources

were used, white, sodium yellow and mercury green. The reason for using diamond (2 mm thick with polished faces 1mm diameter) for this investigation was because it has good thermal properties. For the point contact experiments, base stock has been used as a lubricant with viscosity of 40 cP at 22˚C and for the line contact work on oil 32 cP at 22˚C. In the first set of experiment (sphere on plane) three loads (W = 2, 8, 16 lb) and three speeds (U=0, 2, 7 cm/sec) were employed. The midplane film thickness in the direction of motion, obtained from these experiments, is illustrated below.

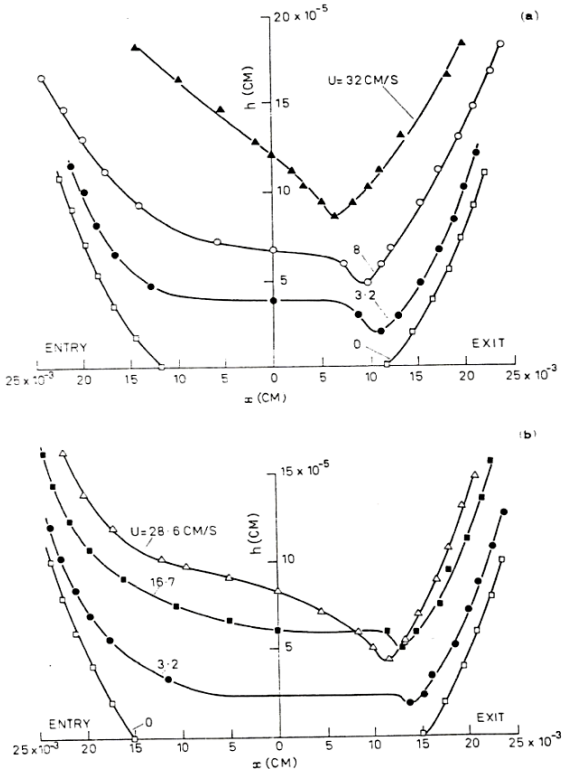

Figure 4.2: Mid-plane film thickness in the direction of motion [105]

It was found that, in both transverse and longitudinal directions, the minimum clearance is inside the Hertzian zone, and it moves towards the centre line as the speed increases. This was is visible at all speeds and loads.

The work done by Cameron and his team proved an important step forward in the understanding of the mechanisms which govern elastohydrodynamic lubrication, but also the role of lubricant's chemistry, study of starvation and the impact of surface alignment and roughness features on film shape [106-112]. One of the most notable improvement to the technique was the introduction of a "spacer layer" which eliminated the disadvantage of the minimum films thicker than a quarter of wavelength to be measured, Westlake and Cameron [113]. Eventually optical interferometry became widely used throughout the 1970's to study EHL and finally it became a common experimental research tool.

4.2.2 Further developments of optical interferometry

The main limitation of conventional optical interferometry applied to the measurement of film thickness in lubricated contacts is that it cannot distinguish films less than a quarter of the wavelength of the light employed This drawback can be overcome by adding another layer on top of the chromium layer which is known as spacer layer. This layer is usually made out of silica which has a refractive index close to that of mineral oils which makes it act as a 'solid lubricant'. As a result the separation between the surfaces of the contact increases and therefore allows film thicknesses smaller than a quarter of the wavelength of light to be measured. The second limitation of this method, in its classical form is the relative poor resolution, as it relies on the evaluation of the distance between fringes or on the perception of the operation of various colours. These two limitations of the optical interferometry have been largely eliminated in the co-called Ultra –Thin Film Interferometry, (UTFI) which

combines a spacer layer technique with spectral analysis of the reflected beam [114]. The principle of this method is shown Figure 4.3.

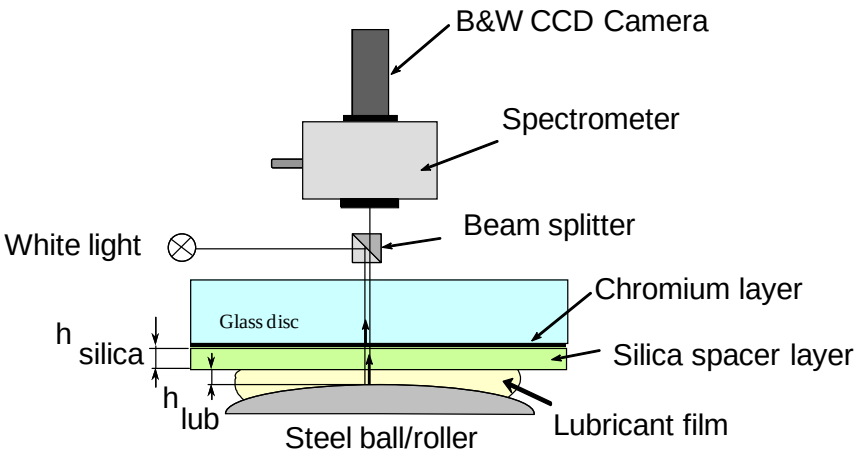

Figure 4.3: Schematic diagram of ultra - thin interferometry principle

When white light passes through a microscope towards the contact, the reflected beam is directed, by a beam splitter, to the entry slit of a spectrometer, where is dispersed by wavelength. Subsequently the spectra image is recorded by a black and white CCD camera and finally the band spectrum is analysed to find the wavelength corresponding to maximum intensity. A typical spectrometer image is illustrated in Figure 4.4. The lighter regions of the spectrum indicate the constructive interference at a specific wavelength while the dark regions refer to destructive (or partially constructive) interference.

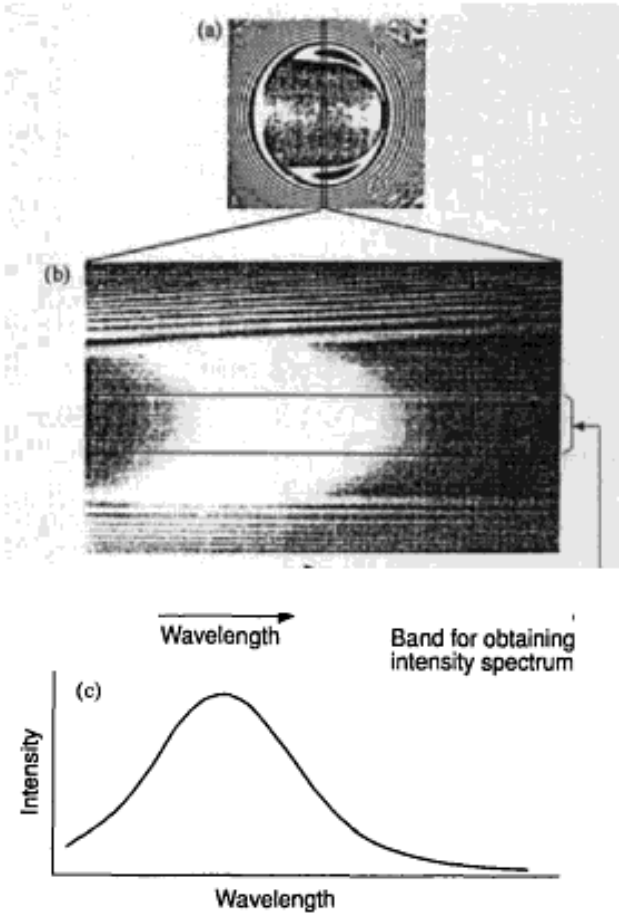

Figure 4.4: (a) An interference image of an EHD contact, (b) a spectrum image, (c) light intensity spectrum at the central band in (b) [115]

In this case the sum of the optical lubricant film thickness and the silica spacer layer thickness is given by:

$$h_{opt} = n_{silica} h_{silica} + n_{\text{lub}} h_{\text{lub}} \tag{4.5}$$

where *n* is the refractive index of the film (silica or oil). Thus by measuring the spacer layer thickness, in dry conditions, and then the spacer layer plus oil thickness, the oil only film thickness can be readily obtain by subtracting the two values. It has also been established that, this technique is capable of measuring lubricant films between 1 and 500 nm thicknesses in EHD contacts, with an accuracy of ± 0.5 below 20nm and ± 0.2 percent above that.

The main limitation of UTFI is that it cannot produce a full two dimensional map of the film thickness across a contact but only one-dimensional film profile [104]. To overcome this, in 1994 Gustafson et al. have proposed a method of film thickness evaluation based on image analysis [116]. A similar method named Spacer Layer Imaging Method was introduced by Cann et al. two years later [117].

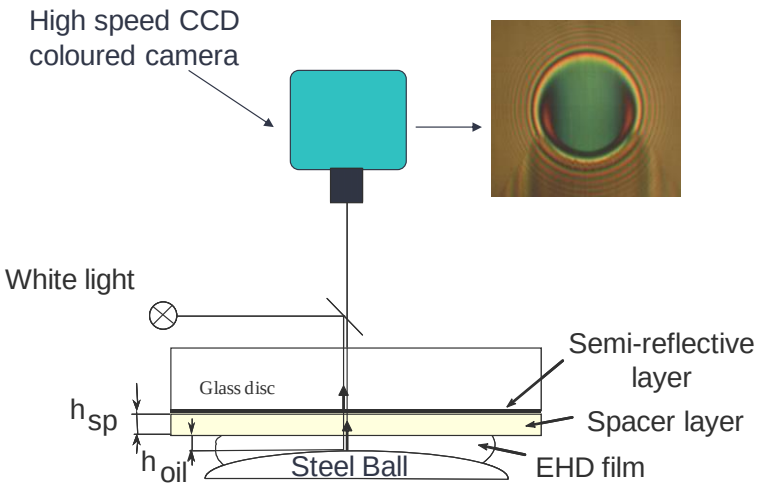

Figure 4.5: Schematic diagram of spacer layer imaging method principle

This technique is a development of Ultra – Thin Interferometry in that it relies on the later to calibrate the RGB content in an image versus film thickness. It is known that certain wavelengths will interfere in a larger or lesser extent at different separations, thus in this case the interfered image is captured by a CCD coloured camera rather being passed to a spectrometer. In addition, the analysis of each pixel is based on RGB calibration curves to

produce a measure of the separation at that point and afterwards by subtracting the thickness of the spacer layer the actual film thickness can be obtained. Figure 4.5 illustrates a schematic diagram of the Spacer Layer Imaging Method. This technique can produce maps of film thickness in the contact down to about 2-3 nm ± 1 nm, the main limitations lying in the accuracy of the calibration used and variations of the light source and camera detector used.

Other techniques for measuring film thickness, based on optical interferometry, are relative optical interferometry intensity (ROII), developed by Wen and co-workers [118], and differential colorimetry due to Hartl and Krupka [119].

4.3 Experimental Test rig

Although the application of the research described in this thesis is the lubrication of rolling element bearings, the focus is on a simple, fundamental contact between a sphere and a flat. This approach allowed the employment of the optical interferometry technique described above to evaluate lubricant film thickness under vibrations. The experiments were carried out on a ball-on disc apparatus using spacer layer imaging technique (SLIM) [117] for film thickness evaluation under vibrations. Detailed descriptions and schematic diagrams of the experimental apparatus for both lateral and normal vibration are presented in the next sections.

4.3.1 Lateral Oscillations Tests

An EHL contact was produced by steel or tungsten carbide ball (4.6(a).1) and a transparent disc (4.6(a).2), which was made out of glass or sapphire, loaded against each other. The disc was driven by an DC motor through a gear box and a shaft, not figured in the photo, while the

ball was driven by a separate DC motor (4.6(a).3) attached to pot. The angular position and the velocity of the disc were monitored via a position encoder and a simple Visual Basic code, which interfaced between a PC computer and the encoder.

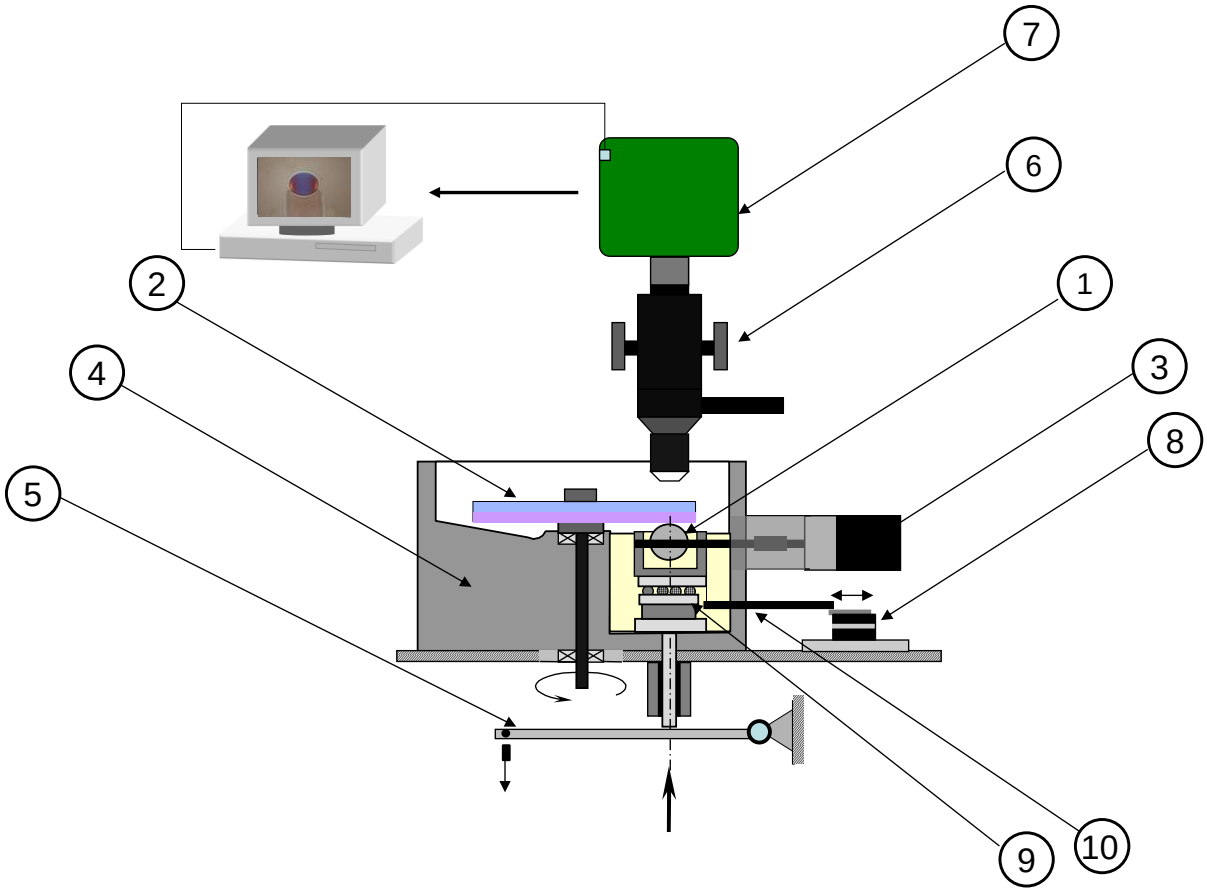

Figure 4.6(a): Experimental setup for lateral oscillation studies

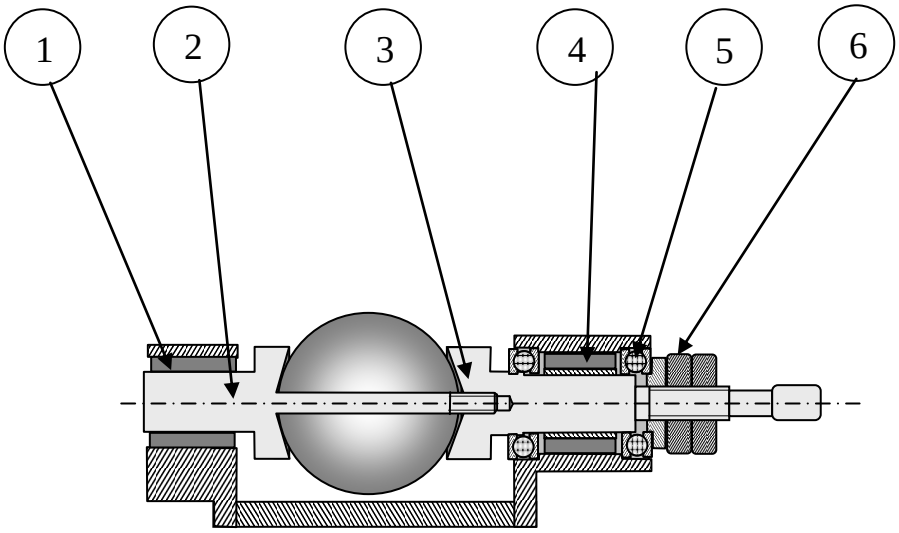

Figure 4.6(b): Experimental setup for lateral oscillation studies

The contacting side of the disc was coated with a thin chromium layer and a silica spacer layer about 130 nanometers thick. The ball was half immersed in a lubricant thermal chamber (4.6(a).4) such that full film conditions were achieved throughout the tests. A constant load was provided by a lever-dead weights system (4.6(a).5). Schematic of the test rig and a detail of the ball holder and actuation system is seen in Figures 4.6(a) and 4.6(b). The working chamber was heated with the help of a cartridge heater and the temperature was set by using a temperature controller .White light was directed through a microscope (4.6(a).6) towards the contact and the interferometric images were captured by a coloured high speed CCD camera (4.6(a).7). The lateral motion of the ball was imposed by a piezo actuator (4.6(a).8). A linear stage (4.6(a).9) was driven directly by the piezo actuator, on which the ball carriage was mounted thus allowing mobility in a direction perpendicular to the main rolling speed.

The stage (a precision linear bearing) was pushed-pulled by a rod (4.6(a).10), which was attached to a linear piezo actuator. In addition, a detailed view of the ball carriage system is illustrated in Figure 4.6(b). The primary half-shaft (4.6(b).3) received the motion from the electrical dc motor, through a special coupling, thus allowing axial motion for the carriage/ball. This shaft was supported by a needle bearing (4.6(b).4). The backlash of the lateral oscillations was cancelled by two thrust bearings (4.6(b).5), which were compressed by a spacer and nuts (4.6(b).6). There was a secondary shaft (4.6(b).2) which was connected to the primary shaft through a thread coupling. This shaft was supported to the carriage via another needle bearing (4.6(b).1). The fact that the primary and secondary shafts are supported by needle bearings makes the stiffness of contacts of the shafts and bearings much larger that of the contact between the EHD contact itself, even in the case of tungsten carbide (WC) ball and sapphire disc. This is important in the case of normal vibrations. Figure 4.7 presents a picture of the whole experimental set-up, including details of the working chamber and piezo actuator.

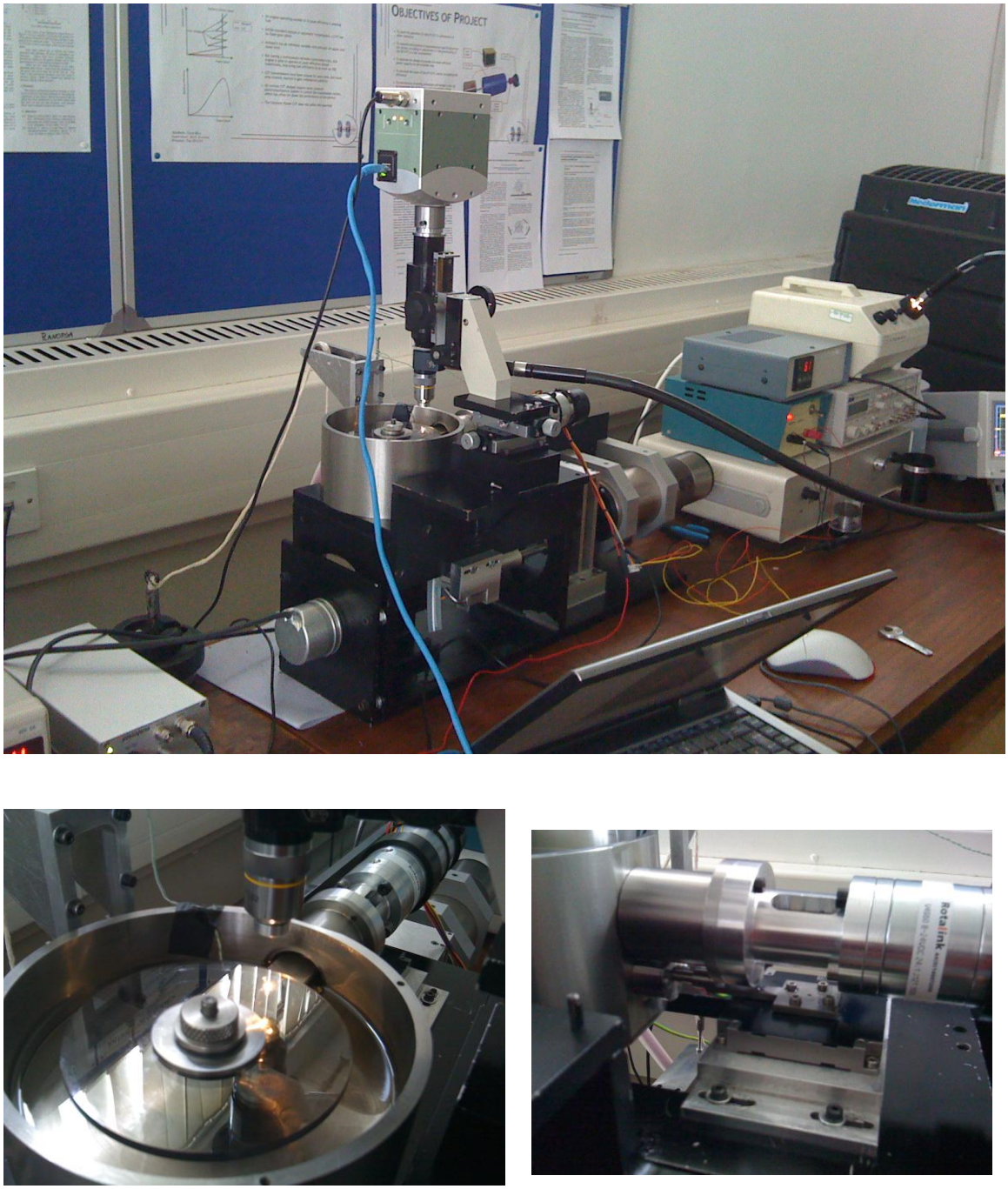

Figure 4.7: Experimental setup for lateral oscillation studies

4.3.2 Normal Vibrations Tests

The same contact between a ball and the flat of a glass disc was used in these experiments, the difference coming from the direction of the oscillatory motion of the ball, which in this case was perpendicular to the plane of the contact. The normal vibrations were created by a dynamic shaker (4.8.1) which was placed at the end and underneath of the lever arm (4.8.2). The frequency and amplitude were controlled by a power amplifier. The ball was firstly brought in contact with the disc by tightening the screw 3 in the diagram. Obviously the screw can achieve any desired pre-load of the contact.

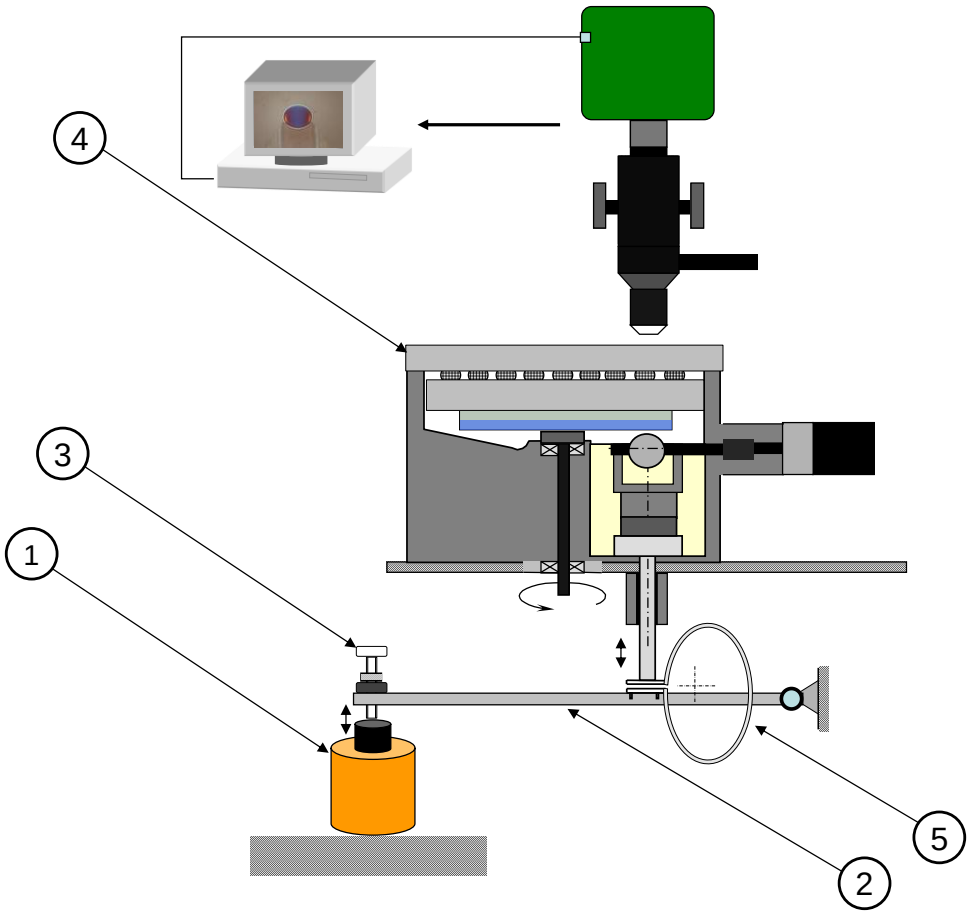

Figure 4.8: Schematic diagram of the experimental set up for normal vibration

In order to avoid excessive bending of the disc shaft, a thrust ball bearing (4.8.4) was placed on top of the disc and fixed to the pot.

Figure 4.9: Experimental setup for normal vibration studies

In addition, a ring type load cell (4.8.5) was placed between a lever and the plunger which actuated the ball carriage. In order to minimise friction the plunger was passed through a precision rolling-ball bush. The ring element acting as a force transducer by placing conveniently strain gauges on it. The strain gauges were bonded two on each side of the elastic surface of the ring element corresponding to a complete Wheatstone bridge (four active strain gauges) temperature compensated. Figure 4.9 shows a picture of the whole experimental set-up, including details of the force transducer and dynamic shaker.

More than one ring was designed, in such a way that it could give a wide range of loads by varying the outside diameter, or the thickness of it. Under loading condition, pure tensile and compressive forces were assumed on the outer fibres of the ring. The bridge was supplied with an excitation voltage of 5V. Also, a differential amplifier was used in order to increase the output signal as well as to filter any undesired noise. The differential amplifier consisted of an operational amplifier, a capacitor and four precision resistors. The circuit was connected then to an oscilloscope for recording the output readings. Figures 4.10, 4.11 show the completed strain gauge interface as well as the differential amplifier.

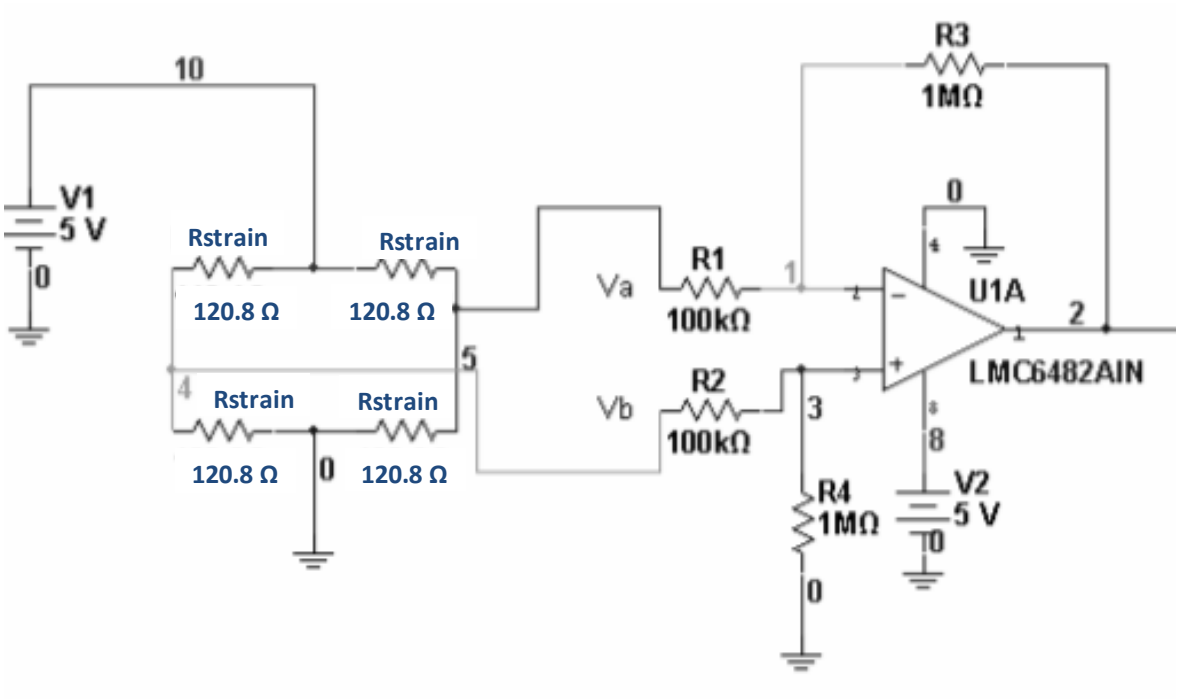

Figure 4.10: Completed Strain Gauge interface

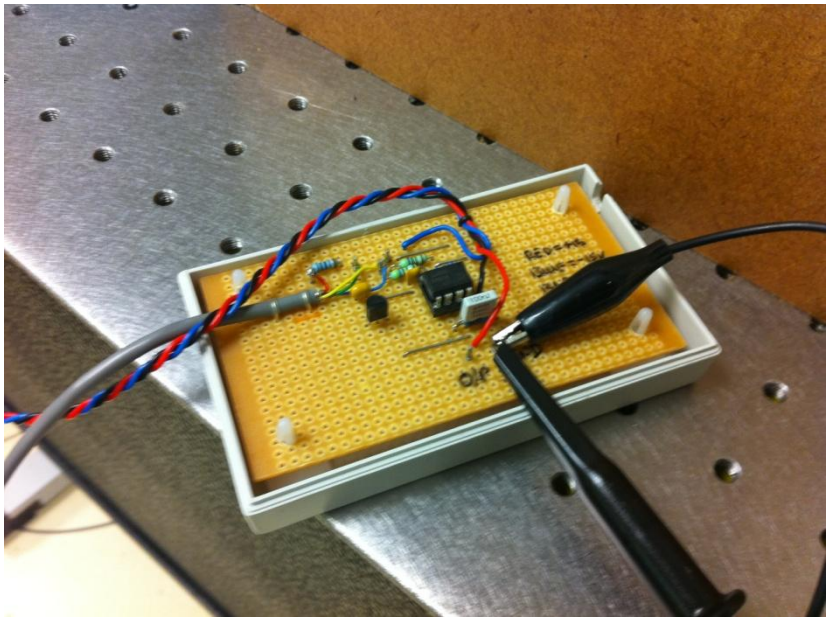

Figure 4.11: Differential amplifier

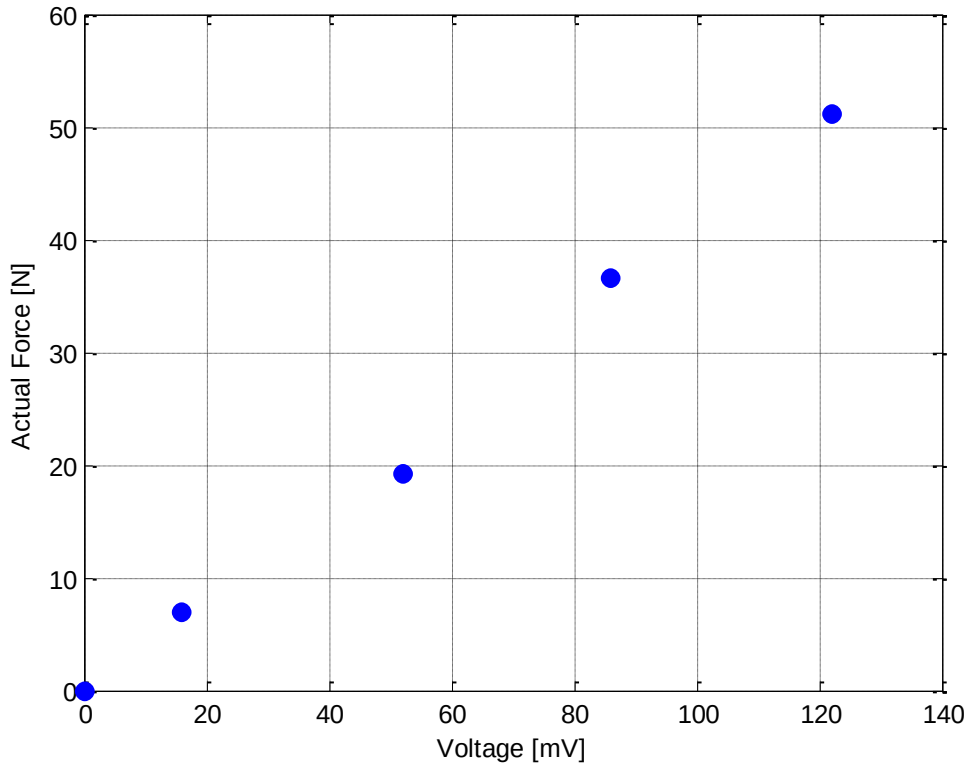

Figure 4.12: Actual Forces versus Voltage

In order to calibrate the load versus the voltage signal from the gauges, different loads starting from 0 up to 5 Kg, were applied to the ring element using a lever-dead weights system. Subsequently a linear interpolation as illustrated in Figure 4.12 was plotted between voltage and the known calibration loads in order to get a function used to evaluate the force applied to the contact.

4.3.3 Camera

In this investigation, a high speed camera was mounted on top of the microscope for capturing images of the contact area under lateral and normal vibrations. This camera has a maximum resolution of 512x512 pixels and a speed of 2503 frames per second at this resolution. The speed increases to up to 100,000 fps for lower resolutions. In the present study the coloured images were captured at 2503 fps with a shutter speed at 86 and 92 micro seconds. The objective lens fitted to the microscope was fitted had a X10 magnification and white light was used.

4.3.4 Piezo Actuator

The lateral oscillations were controlled by a piezo actuator. This nanoX400 stage is capable of generating a maximum push-pull force of 100N, has resonant frequency up to 3 KHz (with no additional mass) and a maximum stroke length of 400 microns.

4.3.5 Dynamic Shaker

The vertical vibrations were created by a dynamic shaker. This shaker is a wide range frequency band electro-dynamic actuator capable of producing a sine vector force of 196 N when force cooled and it has a resonant frequency up to 15 KHz.

4.4 Testing Material parameters and Experimental Procedure

4.4.1 Lateral Oscillation Tests

During the lateral oscillation experiments, a contact load of 45N was employed, which produced a Hertzian pressure between 0.69 GPa for steel ball glass disc and 1.78 GPa for tungsten carbide ball sapphire disc combindation.

The entrainment speed was set at given values between 0.05 up to 3 m/s in pure rolling conditions. Both discs had a diameter of 100 mm and the thickness of 12 mm for the glass disc and 4 mm for the sapphire one. The working parameters are summarized in the Table below.

Load	**45 N**
Hertzian Pressure	0.67 GPa for steel/glass ,1.78 GPa for tungsten carbide/sapphire
Ball Materials	Steel Ball , Tungsten carbide
Disc Materials	Glass , Sapphire
Entrainment Speed (Um)	0.05 m/s , 0.065 m/s , 0.08 m/s, 0.1m/s , 0.3 m/s , 0.5 m/s , 1 m/s , 2 m/s , 3 m/s

Table 4.1: Materials and working parameters

The lubricant used in these tests was a poly-alpha-olefin base oil (PAO4) with a dynamic viscosity of 0.027 Pa.s at 30ºC, which was the temperature of the tests. The reason for choosing this low viscosity oil, was to obtain thin EHD films, which are rather typical to rolling element bearings. This lubricant and the working conditions were agreed with the industrial sponsor, SKF, Engineering and Research Center. The frequency of the lateral oscillations of the ball was set at 10, 50 and 100 Hz for every speed, while the amplitude was equal to at least the contact diameter for each test. The lateral speed variation over one stroke length at a frequency of 100 Hz is illustrated in Figure 4.13. The speed of the lateral motion was calculated from the displacement of the contact between two consecutive images.

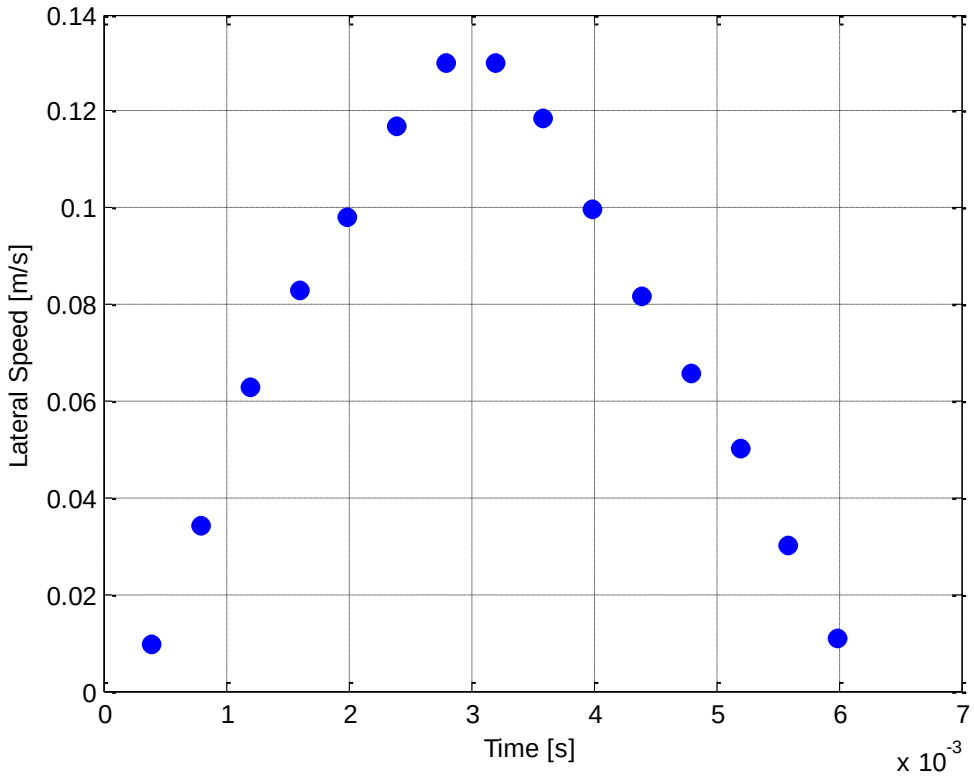

Figure 4.13: Variation of lateral speed over one stroke for 100 Hz

Additional tests were conducted using glass and steel ball combination but with a mixture of base oil and a viscosity index (VI) improver additive.

Table 4.2: Physical properties of viscosity index improver Viscoplex 0-101

Visual Appearance	**Clear**
Colour (ASTM D1500)	1
Viscosity at100 $^{\circ}$C, mm^2/s (ASTM D445)	750
Density at 15 $^{\circ}$C, g/cm^3 (ASTM D4052)	0.94
Flash Point, $^{\circ}$C (ASTM D3278)	150
Shear Stability Index (PSSI) KRL, 20 hour (CEC L-45-A-99)	25

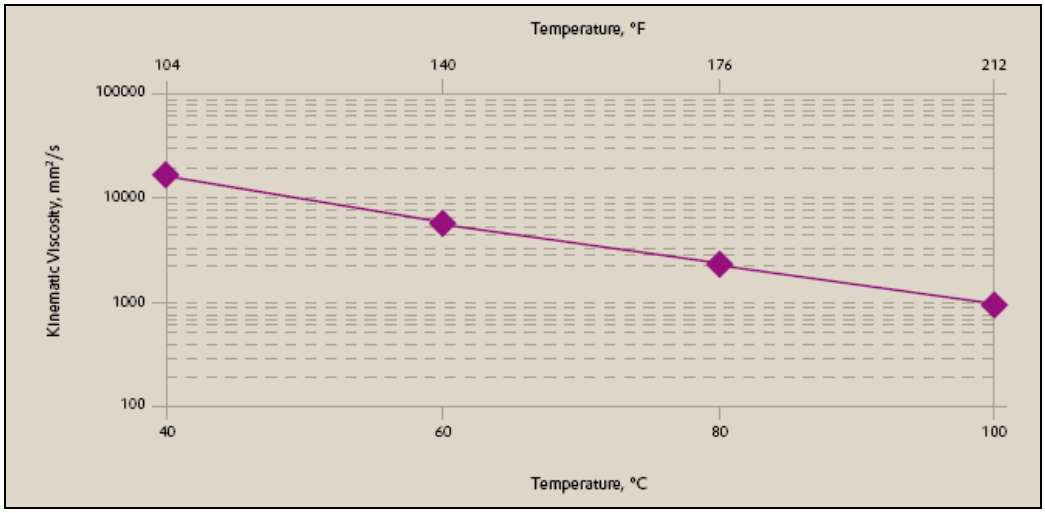

Figure 4.14: Kinematic viscosity versus Temperature (Viscoplex 0-101)

The mass concentration of the additive was 10.7 %. In this case the temperature were set to 30^{o}C and 80^{o}C as it is known that the VI improvers are effective in thin film conditions [120]. The physical properties of the VI improver are seen in Table 4.2. Also the plot of the kinematic viscosity versus temperature is shown in Figure 4.14.

Before each test the disc and ball were thoroughly cleaned with analar toluene and iso-propanol, dried and then assembled onto the rig. The same cleaning procedure was applied to the test chamber of the rig. The ball was loaded in static conditions to a load of 45N and images were captured, which were subsequently used to estimate the thickness of the silica spacer layer. A trigger point was set before each test such that images were recorded at known locations around the disc. In the next step, lubricant was added in the test chamber and the disc was set in motion, and the contact was loaded with a constant load, after which the amplifier of the piezo-actuator was switched on. The interferometric images of the contact were recorded for frequencies of 10, 50 and 100 Hz. These coloured images were captured by the high speed CCD camera and transferred to a PC for analysis. The CCD camera was

externally triggered during the experiments connected to an interface card using a custom-written code whenever the trigger position given by the position encoder was reached.

Lateral oscillations tests were also performed with grease as lubricant, as it is known that grease are very often used in rolling bearings' lubrication. The main purpose of this part of the research was to evaluate the effect of lateral oscillatory motion upon the track replenishment. The experiments were conducted using grease, supplied by the Japanese manufacturer Kyodo Yuishi, made of a synthetic hydrocarbon base oil and urea thickener. The concentration of the thickener was 10-20 percent while the base oil kinematic viscosity was 45mm^2/s at 40 P^{oP}C and 7.7mm^2/s at 100 ^{o}C . The experimental test apparatus is illustrated in Section 4.3.1. After following the cleaning procedure, a small amount of grease was uniformly spread on the contacting side of the disc and then both disc and ball were attached on to the rig. At first, the tests were carried out in steady state conditions such that a drop in film thickness was observed, sign that starvation of the contact settled in. Then, the lateral motion was exerted and images were recorded for about 10 minutes at 1 minute intervals. The stroke length of the lateral motion was 355 μm at frequency of 10 Hz while the main rolling speed was set at 0.5 m/s.

4.4.2 Normal Vibration studies

Experiments were conducted at a constant temperature of at 30ºC using a PAO 4. All tests were carried out at pure rolling conditions. The experimental procedure was similar with that in pure rolling conditions. The lubricant was purred into the thermal working chamber. Before switching on the power amplifier of the dynamic shaker, the ball and the disc were

slowly brought into contact such that a pulsating load was obtained after the shaker was powered up (variation between zero and a given value). Thereafter the captured images were transferred to a PC for film thickness analysis.

The moment in time the voltage from the amplifier was recorded and the moment when the camera was triggered were synchronised, such that a correlation between the load variation and the contact variation can be made. This can be seen in Figure 4.15.

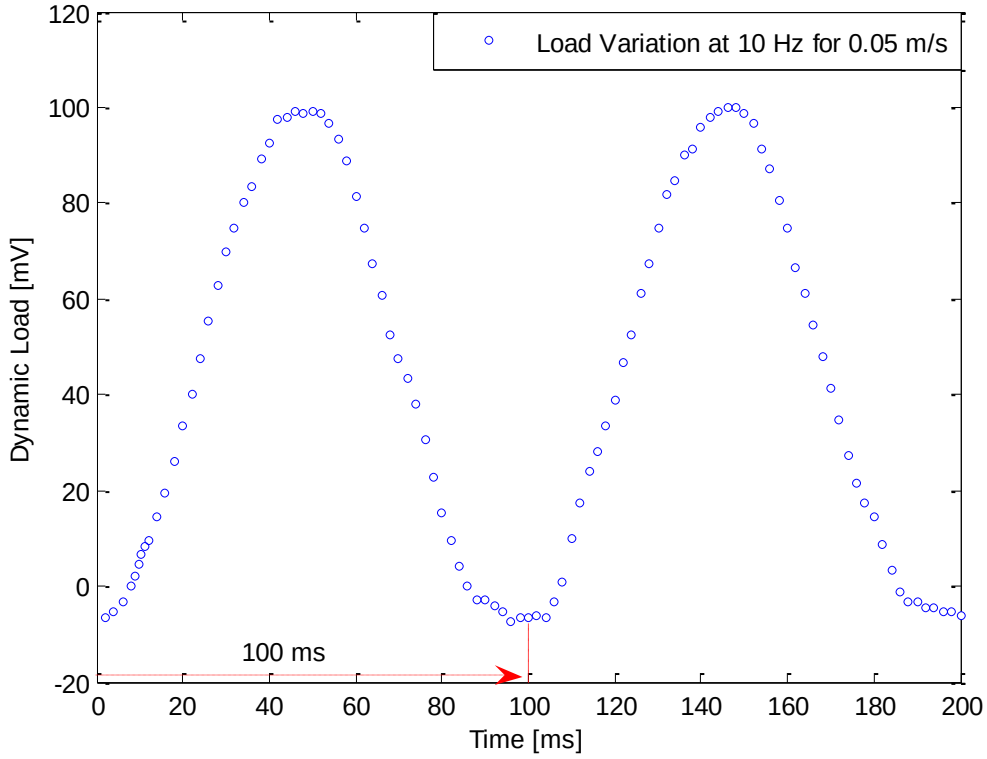

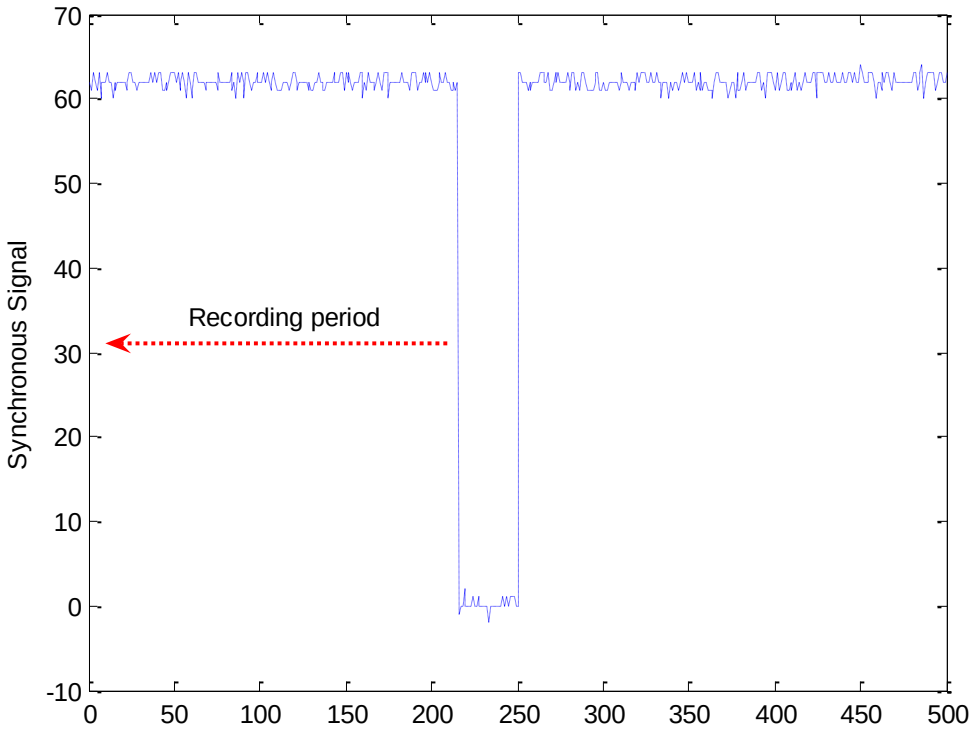

Figure 4.15: Synchronous signal measurement

4.5 Calibration of Colour versus Film Thickness

In order to find the correspondence between film thickness and a certain colour on the image, the central film thickness versus entrainment speed has first been obtained, using the UTFI method and a commercial test rig made by PCS Instruments. In this case, steady state, pure rolling conditions were used, with the temperature, load and speed accurately controlled. Two calibrations were performed using steel and tungsten carbide balls. The disc was made out of glass coated with chromium layer and an approximately 500nm thick silica spacer layer. Figure 4.16 shows the variation of the films thickness versus entrainment speed. Due to the fact that the dependency of the EHD film thickness on entrainment speed, follows a power law, the graph as appears as a straight line in log-log format.

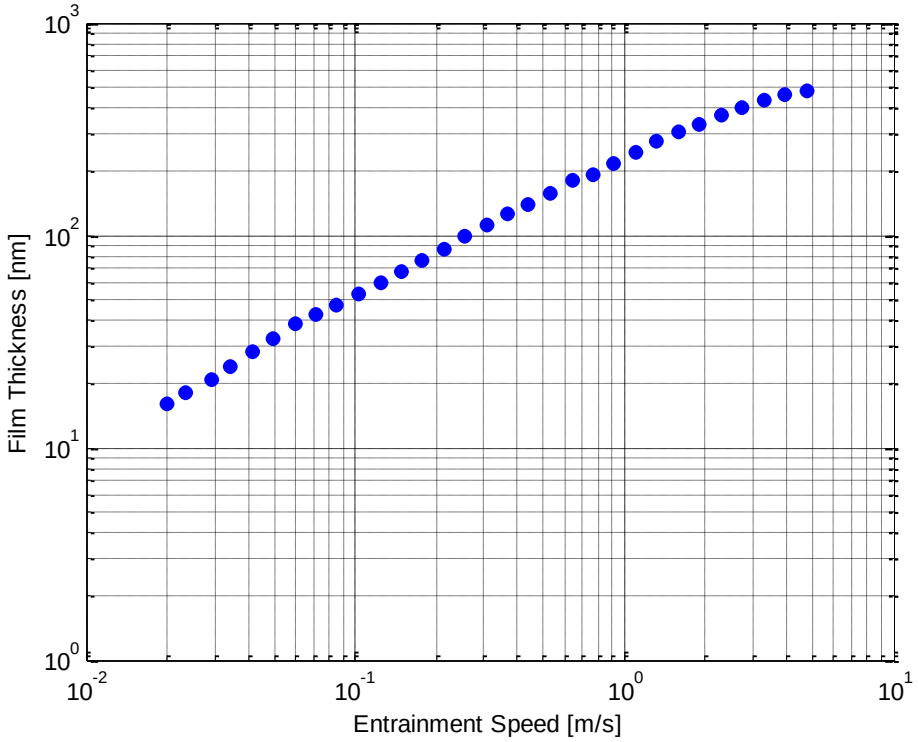

Figure 4.16: EHD film thickness versus entrainment speed

4.5.1 Analysis of RGB Values

In the next step of the calibration procedure, the double-layered disc was replaced with one coated with only a semi-transparent chromium layer. Images of the contact were recorded at exactly the same speeds for which the steady film thickness was measured, in the previous step.

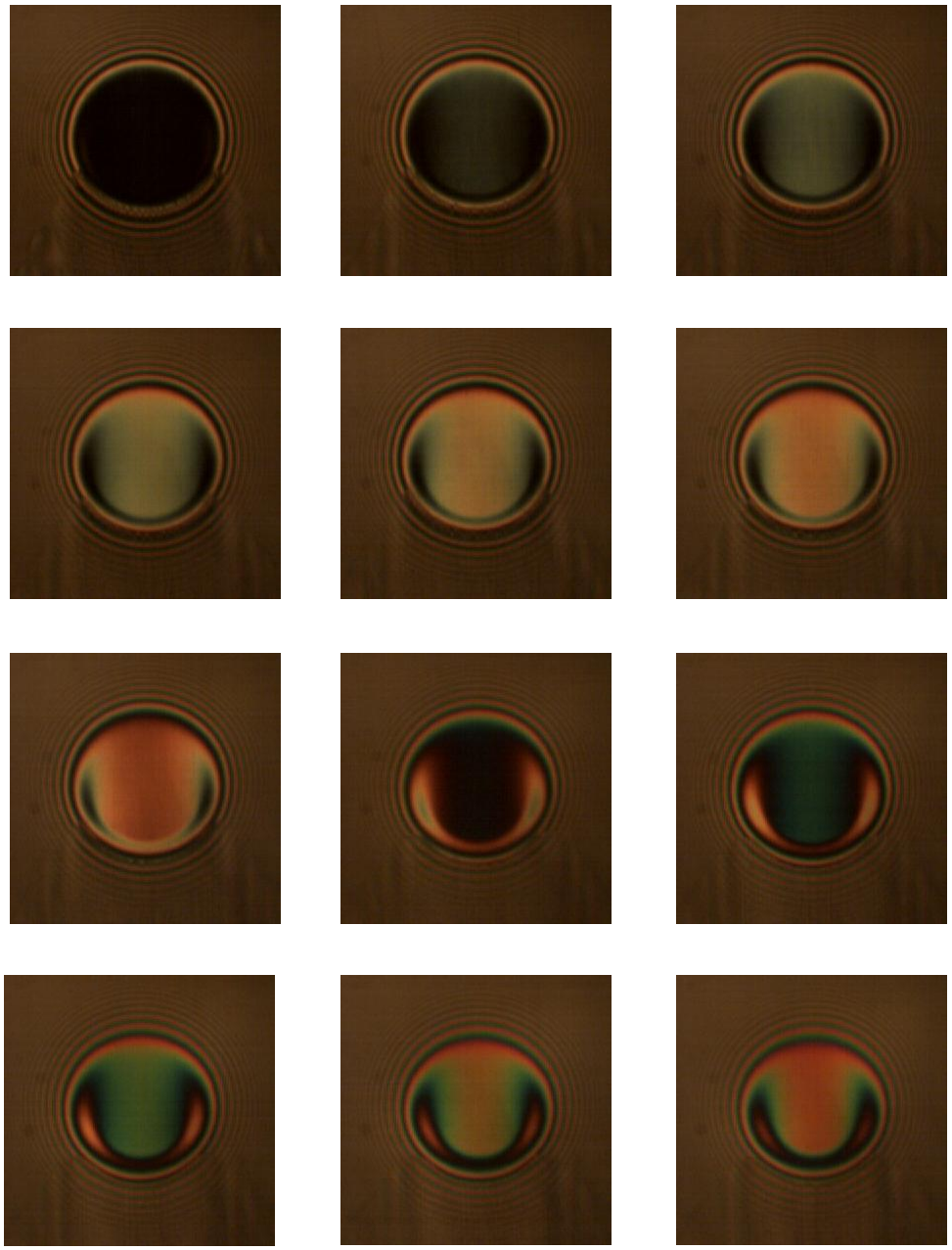

Figure 4.17: Interference fringe patterns of film thickness for various speeds

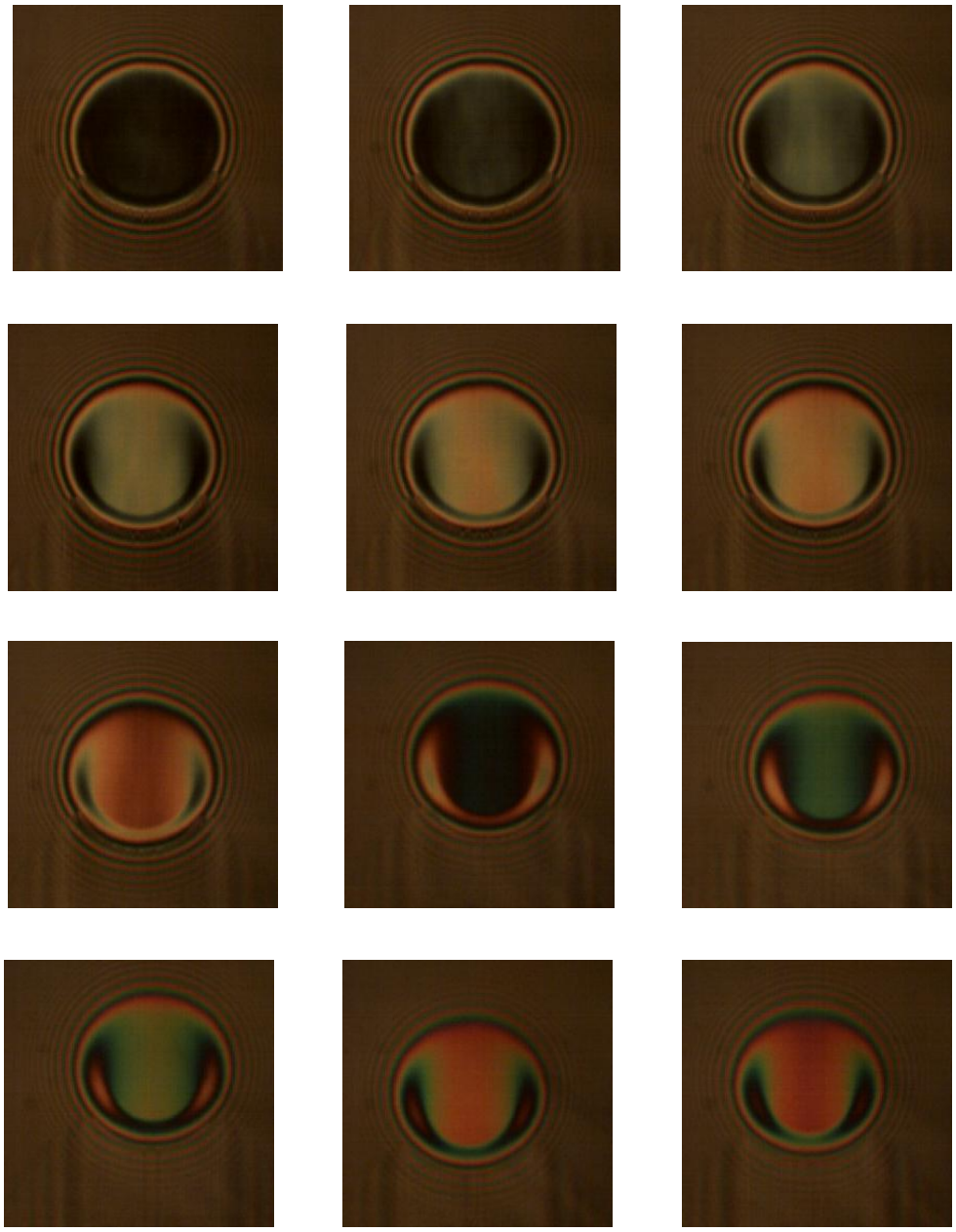

Figure 4.18: Interference fringe patterns of film thickness for various speeds (TCarbide – glass contacts) at 92 μsec shutter speed

Colour interferometric images for the two ball materials are shown in Figures 4.17, 4.18. In the final step of the calibration procedure, the averaged red-green-blues values were extracted from a rectangle in the central region of the contact, where it is known that the film thickness is almost constant. The dependence of the RGB content on the speed is obtained in this way. The reason for doing the calibration for both steel and tungsten carbide ball is that the phase shift at the reflection of the ball surface might be different for the two materials, thus the wavelength of constructive interference would also be different.

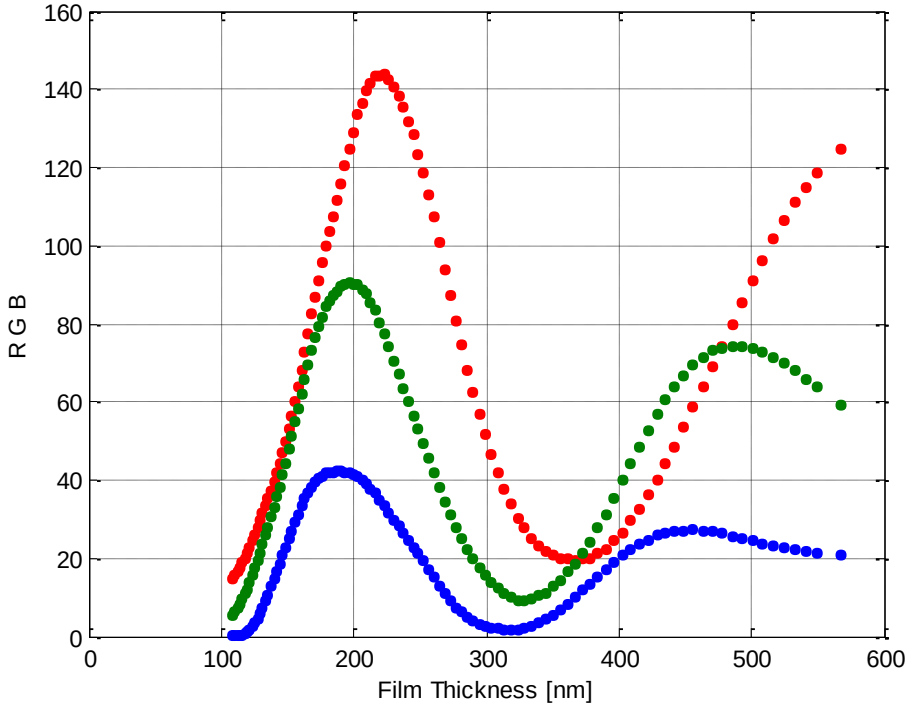

Figure 4.19: RGB versus Film thickness – Steel ball

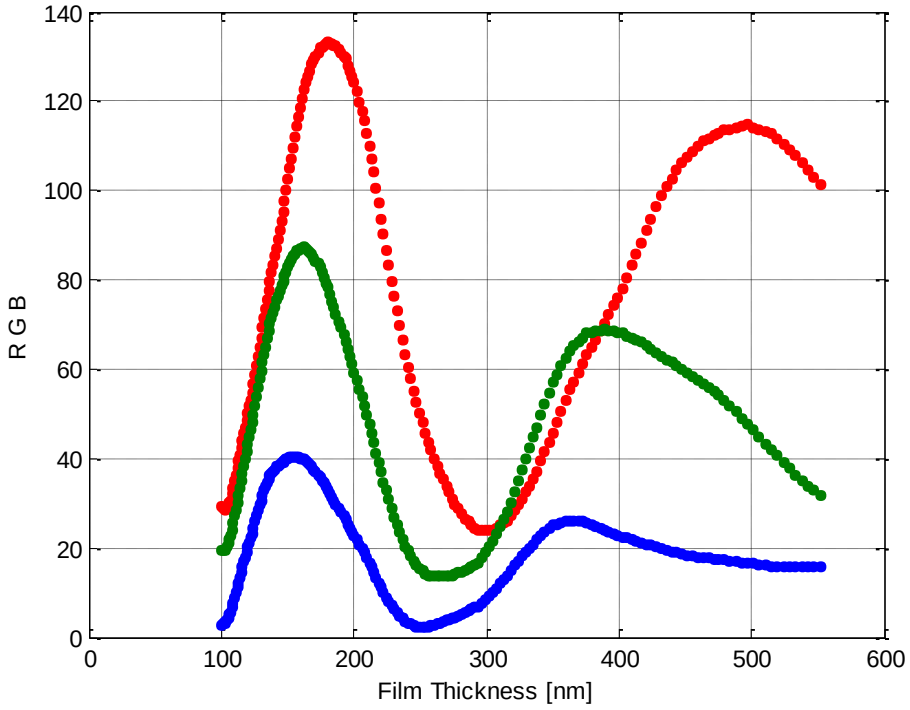

Figure 4.20: RGB versus Film thickness – TC ball

Subsequently, by eliminating the speed between the two sets of data, the film thickness versus RGB values is obtained. The curves for both tests are shown in Figures 4.19 and 4.20.

During the processing of variable-film thickness data, the RGB for each pixel is extracted and the corresponding film thickness is yielded by minimising the difference between the calibration and the actual RGB values.

CHAPTER 5: Lateral Oscillations in EHD films

In this chapter, systematic tests carried out in order to assess the effect of the main rolling speed, the frequency of the oscillations and the Hertzian pressure upon the behaviour of the EHD film under lateral oscillations are described. The effect of the lubricant viscosity was tested by running tests different temperatures. The actual film thickness was calculated using the RGB method which was described earlier in Chapter 4.

5.1 Results of Film Thickness under lateral oscillations (Glass on Steel contact)

The frequencies of the lateral oscillations at which the experiments were conducted were 10 Hz, 50 Hz and 100 Hz. The main lubricant used was polyalphaolefin, PAO 4 under pure rolling conditions at a main entrainment speed of 0.05 m/s. Figures 5.1(a) to (c) show the typical behaviour of an EHD contact subjected to lateral oscillatory motion at all working frequencies. In the case of 10 Hz, 250 images were captured corresponding to a complete lateral cycle. Only one out of every ten images was analyzed at 25 different points for one period of oscillation. The maximum lateral speed was 0.017 m/s. This estimated by measuring the distance travelled between consecutive positions of the contact and diving this by the time elapsed between two successive captured images of the contact (399 μs). For the 50 Hz tests, 50 images were captured for a complete lateral cycle and as seen in Figure 5.2 one image out of every two was analyzed at 25 different stroke positions during one period of lateral motion. In this case the maximum lateral speed was about 0.08 m/s. Finally for 100 Hz tests, 25 images were captured. The maximum lateral speed in this case was 0.13 m/s.

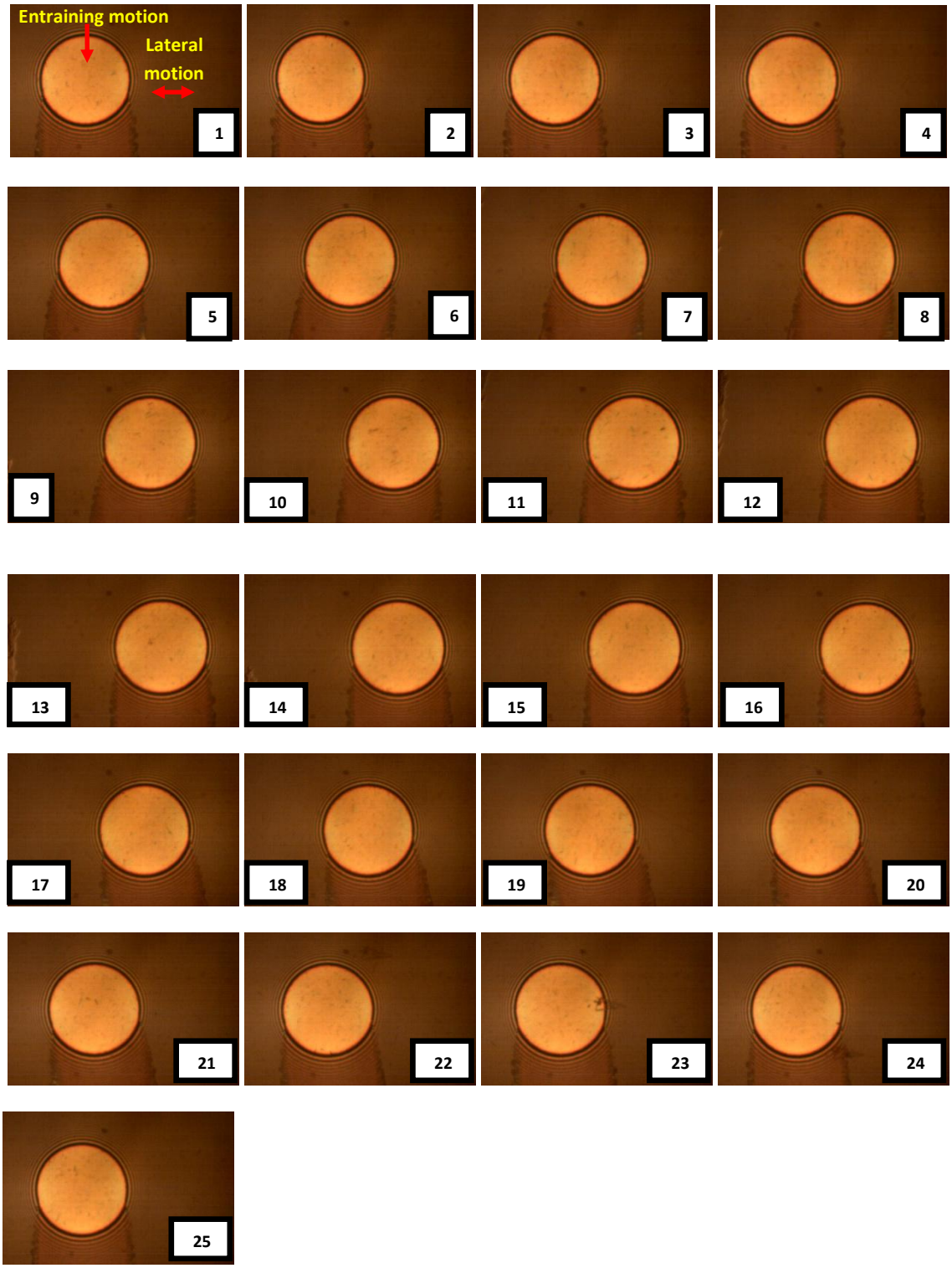

Figure 5.1(a): Typical Behaviour of an EHD contact subjected to lateral oscillatory motion at 10 Hz (Glass on Steel)

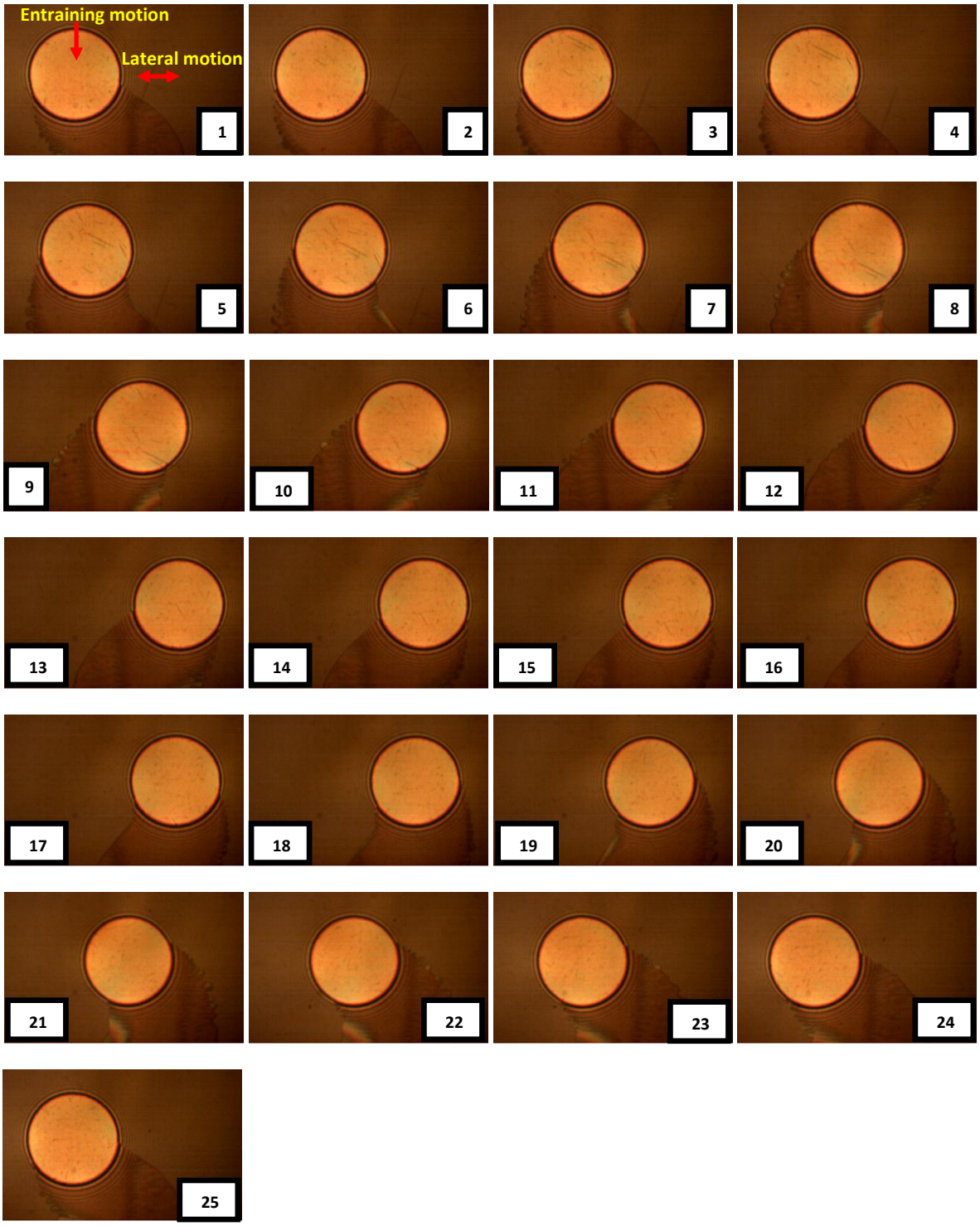

Figure 5.1(b): Typical Behaviour of an EHD contact subjected to lateral oscillatory motion at 50 Hz (Glass on Steel)

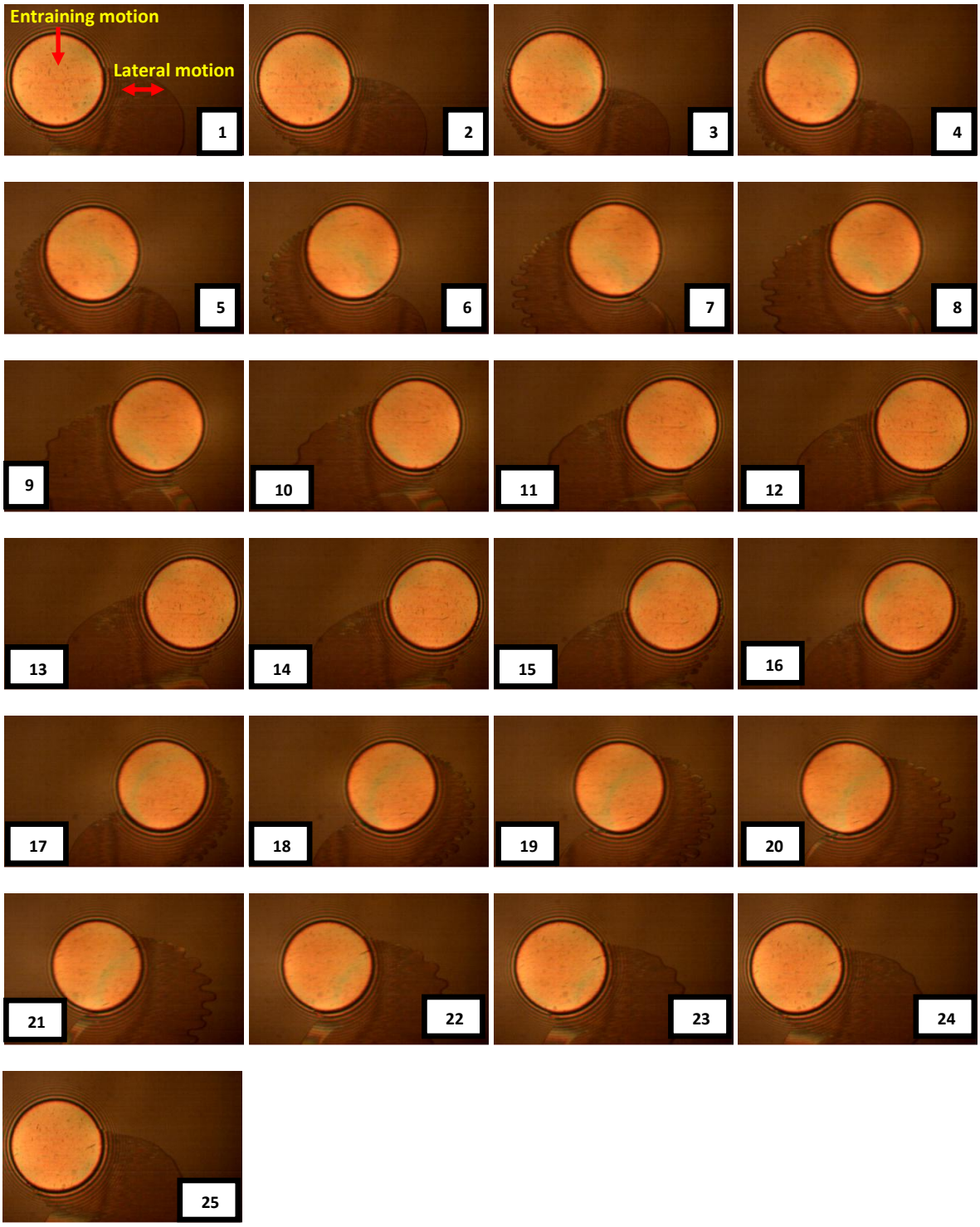

Figure 5.1(c): Typical Behaviour of an EHD contact subjected to lateral oscillatory motion at 100 Hz (Glass on Steel)

As seen from the images shown above, the lateral oscillations do not have a visible effect upon the film thickness, for the two lower frequencies. However at highest frequency used in these tests, that is 100 Hz, the lateral oscillations induced perturbations into the film thickness. These perturbations, generated at the end of the strokes (left to right and right to left) propagated along the contact at approximately the average speed of the surfaces. At the largest frequency the maximum lateral speed is 0.13 m/s, which is more than double the main rolling speed. The velocity of the ball surface is the vectorial sum between the main rolling speed (0.05 m.s) and the lateral speed. Obviously this varies between 0.05 m/s and 0.139 m/s. The net entrainment is on a direction formed by the vector sum of the velocities of the ball and disc surfaces. The maximum entrainment speed thus becomes 0.082 m/s.

Figures 5.2 (a) to 5.2 (c) illustrate snapshots of representative interferograms and the corresponding mid-plane profiles at all three frequencies and at a main entraining speed of 0.05 m/s. In the case of 100 Hz, the film thickness was calculated diagonally (i.e. top left to bottom right) while for the other two frequencies was taken along the entraining direction. The line indicates the direction from which the film profile is been taken from. The main entraining direction is shown by the large vertical arrows while the lateral motion is indicated by the small horizontal arrows.

From these graphs it is obvious that, for the lower frequencies of the lateral motion applied in this experiment, that is 10 Hz and 50 Hz, no film fluctuations has been detected. In the case of 100 Hz test, the height of the film thickness perturbation was about 13 nm. As the contact velocity in lateral direction becomes zero at the end of the stroke, a thinner film is formed at the inlet and subsequently travels across the contact.

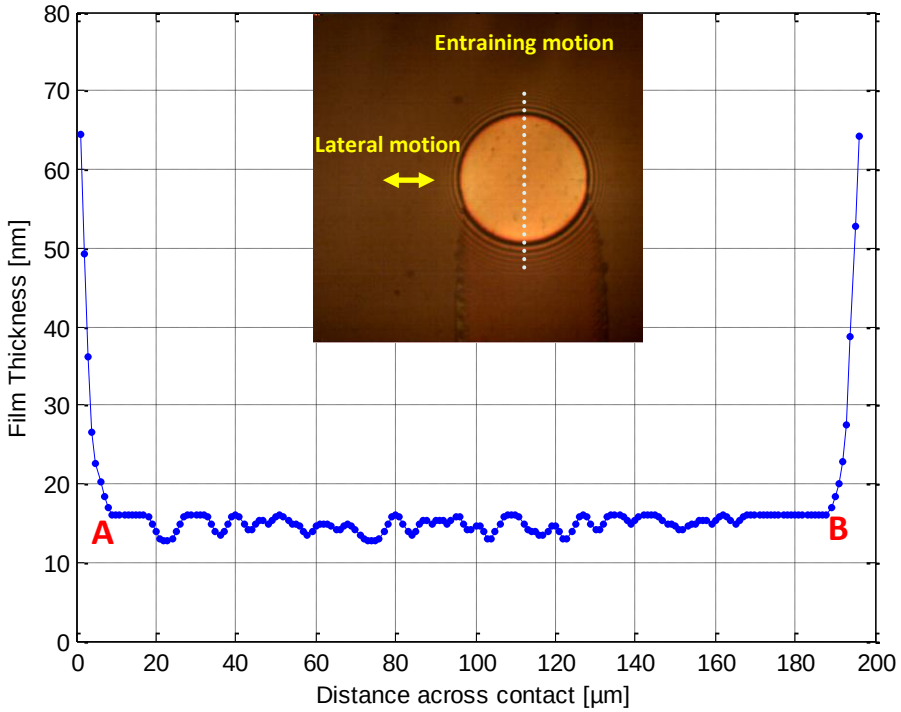

Figure 5.2 (a): Coloured interferogram and Film Thickness profile at 10 Hz

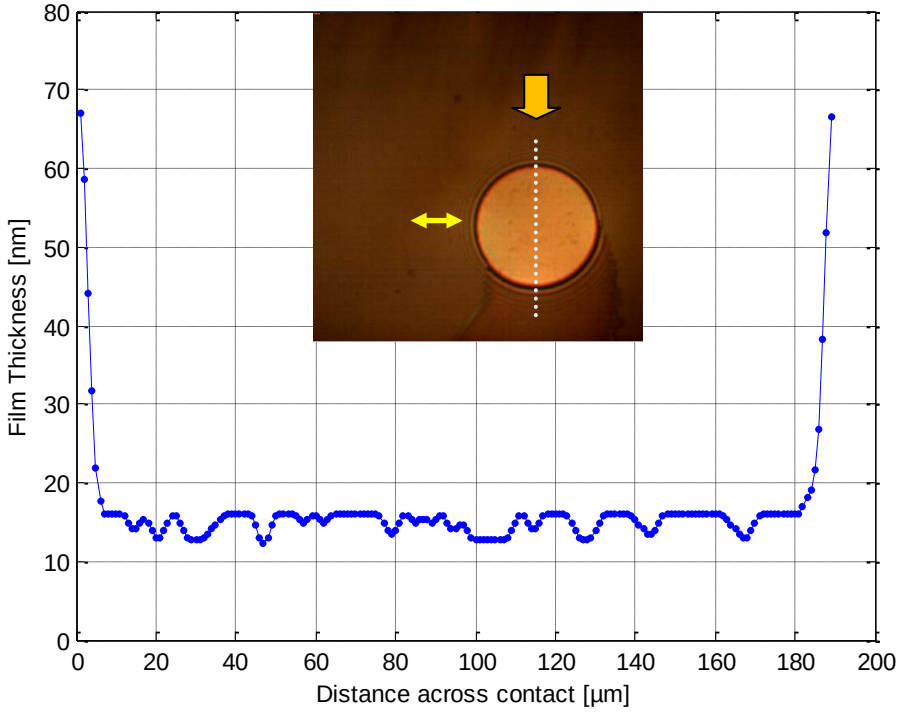

Figure 5.2 (b): Coloured interferogram and Film Thickness profile at 50 Hz

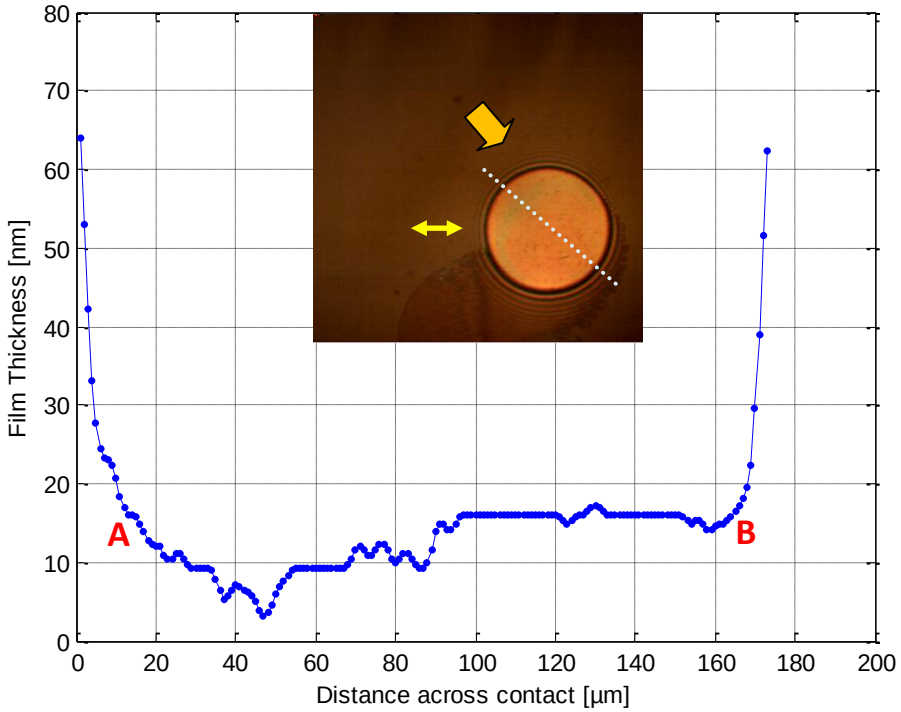

Figure 5.2 (c): Coloured interferogram and Film Thickness profile at 100 Hz

The wave of the thinner film propagates with the instantaneous entrainment speed, which, at that particular stroke position was 0.06 m/s which is larger than the entraining speed.

In order to examine the effect of the main entrainment speed and implicitly of the overall film thickness upon the behaviour of the EHD film subjected to lateral oscillations, film thickness has been measured over a range speeds, at a constant frequency of 100 Hz. The results are presented in Figure 5.3 (a) to 5.3 (d). In the case of low rolling speeds the film thickness was calculated diagonally (i.e. top left to bottom right). At higher speeds no visible effect of the lateral motion can be seen, thus the contact shows the characteristic horse-shoe pattern. For this reason the film thickness was calculated transverse to the entraining direction, in order to show the minimum film thickness, at the side lobes. The small horizontal arrows indicate the direction of lateral motion while the large arrows show the direction of the entraining motion.

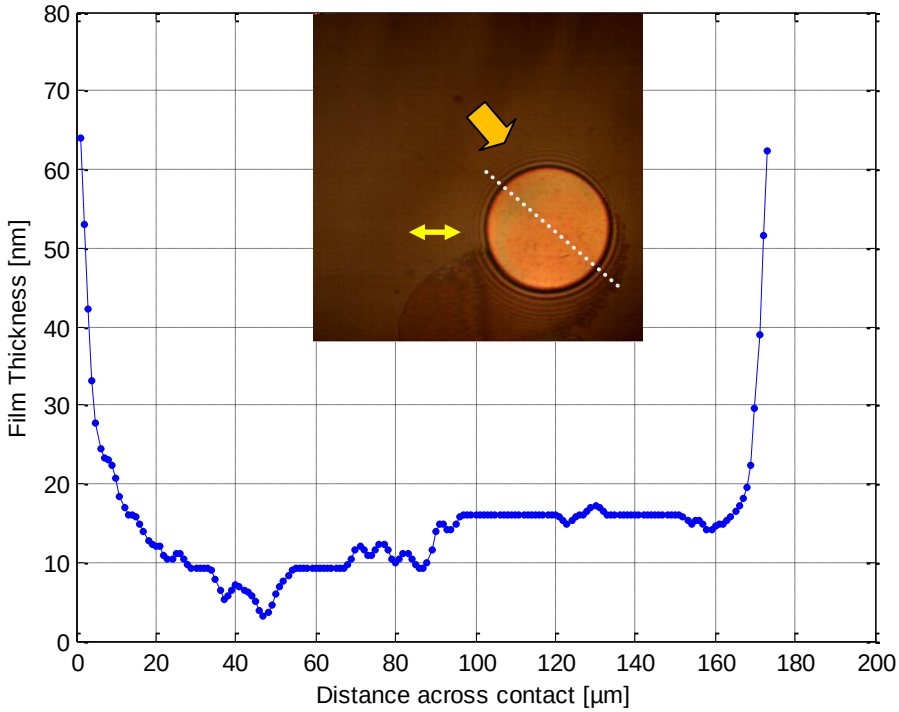

Figure 5.3 (a): Film Thickness profile at 100 Hz for 0.05 m/s

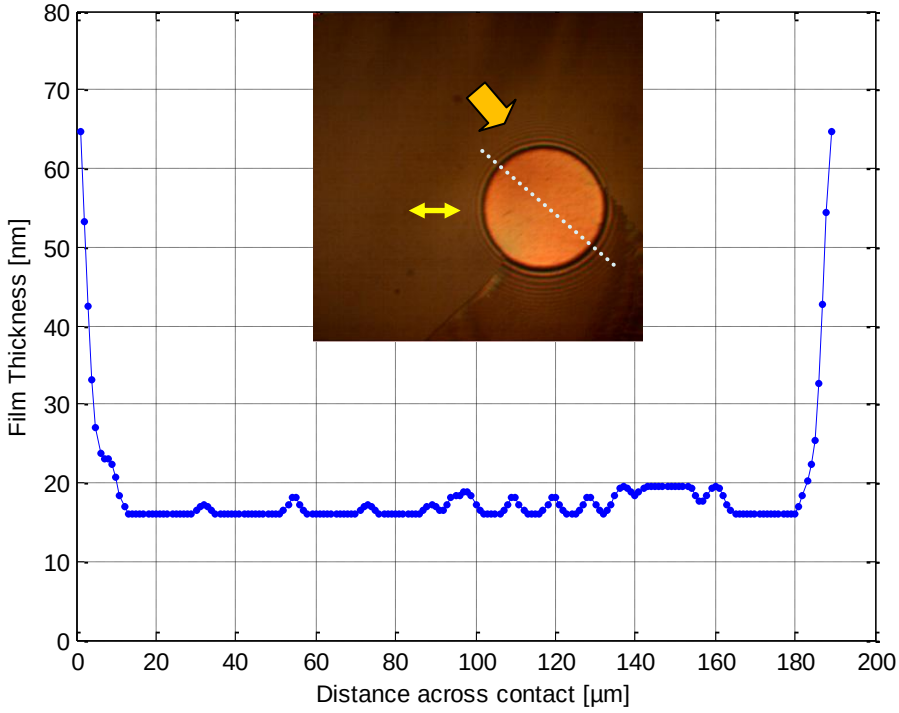

Figure 5.3 (b): Film Thickness profile at 100 Hz for 0.1 m/s

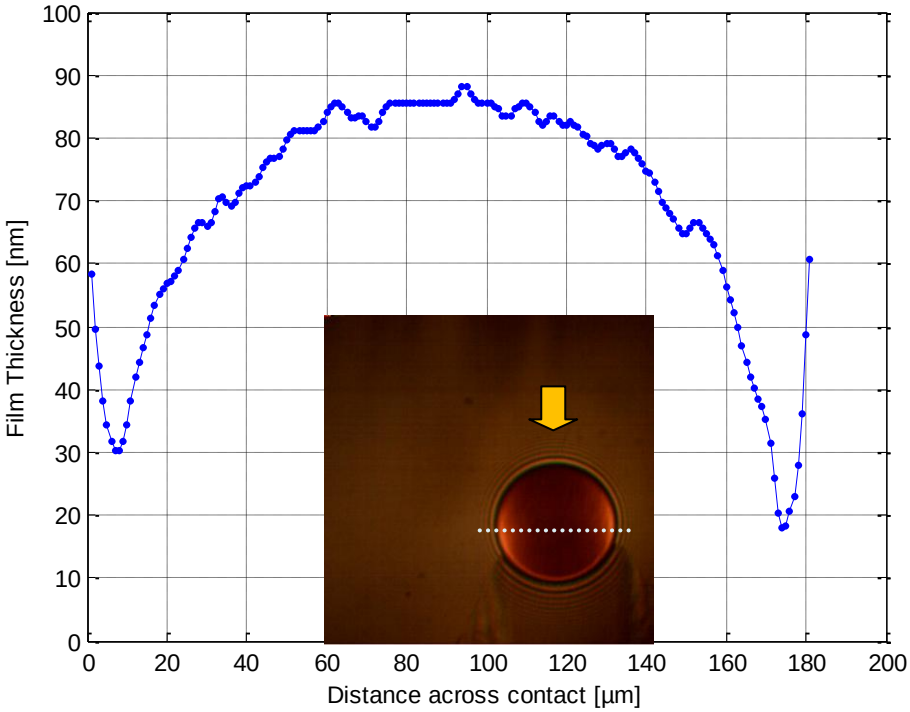

Figure 5.3 (c): Film Thickness profile at 100 Hz for 0.5 m/s

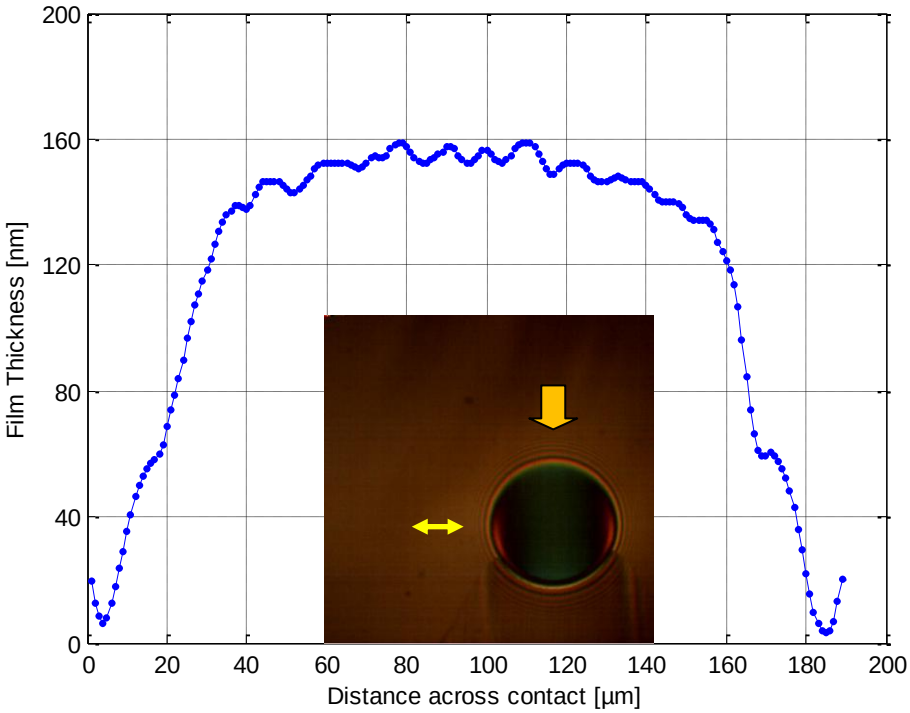

Figure 5.3 (d): Film Thickness profile at 100 Hz for 1 m/s

As the graphs show, perturbations in the film can be observed only at lowest entraining speed employed in these tests. For rolling speeds higher than 0.05 m/s no fluctuations in the film have been detected even by applying the largest frequency of the lateral oscillations. This can be explained by the fact that, as the main entrainment speed increases, the lateral speed becomes proportionally smaller thus the influence of the lateral variable speed decreases. At thicker overall films, the squeeze effect due to the variation of the lateral speed becomes less and less important, as also Sakamoto and co-authors [121] have found.

5.2 Results of Film Thickness under lateral oscillations (Sapphire – Tungsten Carbide)

Tests similar to those presented in section 5.1 have been carried out with the combination of a sapphire disc and tungsten carbide ball, in order to evaluate the effect of the Hertzian pressure upon the behaviour of EHD films subjected to lateral vibrations. In this case the Hertzian pressure is 1.78 GPa in comparison to 0.69 GPa for the glass/steel combination.

Figure 5.4 shows snapshots of the coloured interferograms from the tests conducted at a frequency of 100 Hz and at a rolling speed of 0.05 m/s. The stroke length was the same as in previous tests for glass-steel combination, thus, due to the smaller contact diameter the stroke length in this case is nearly three times the contact diameter. As the images show, at the end of a stroke, crescent-like film perturbations are formed then travel across the contact on a direction inclined to the main rolling direction. This is more obvious in diagrams 14 to 20.

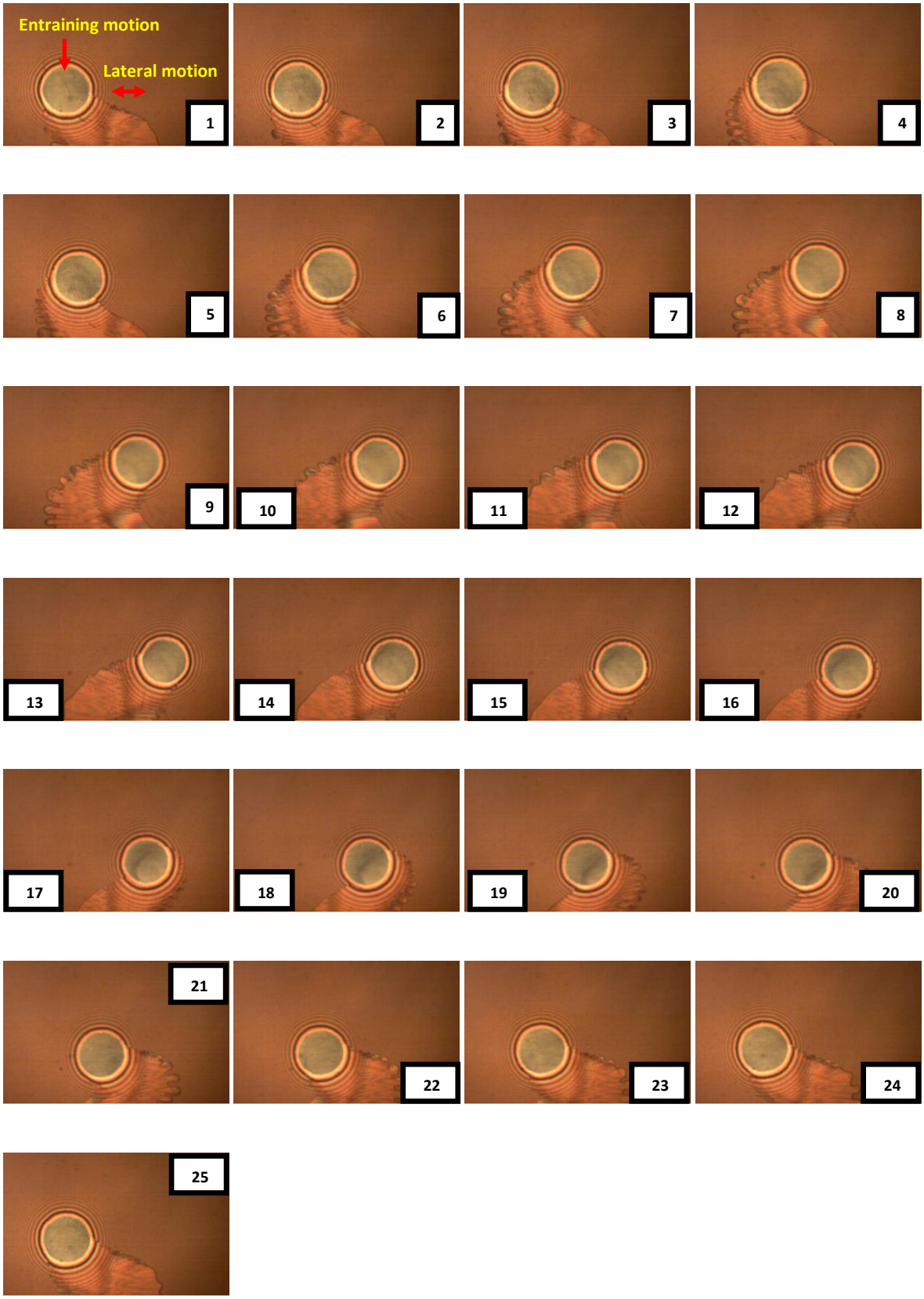

Figure 5.4: Behaviour of an EHD contact subjected to lateral oscillatory motion at 100 Hz (tungsten carbide – sapphire combination)

Typical images of the interferometric fringes, at different positions on the oscillatory cycle, together with the corresponded mid-plane film thickness profiles three frequencies of 10 Hz, 50 Hz and 100 Hz at a constant speed of 0.05 m/s are shown in Figures 5.5 (a) to (c). In the case of low frequencies i.e. 10 Hz and 50 Hz, the film thickness was measured along the entraining direction while for 100 Hz test the film thickness was calculated diagonally (i.e. top left to bottom right).

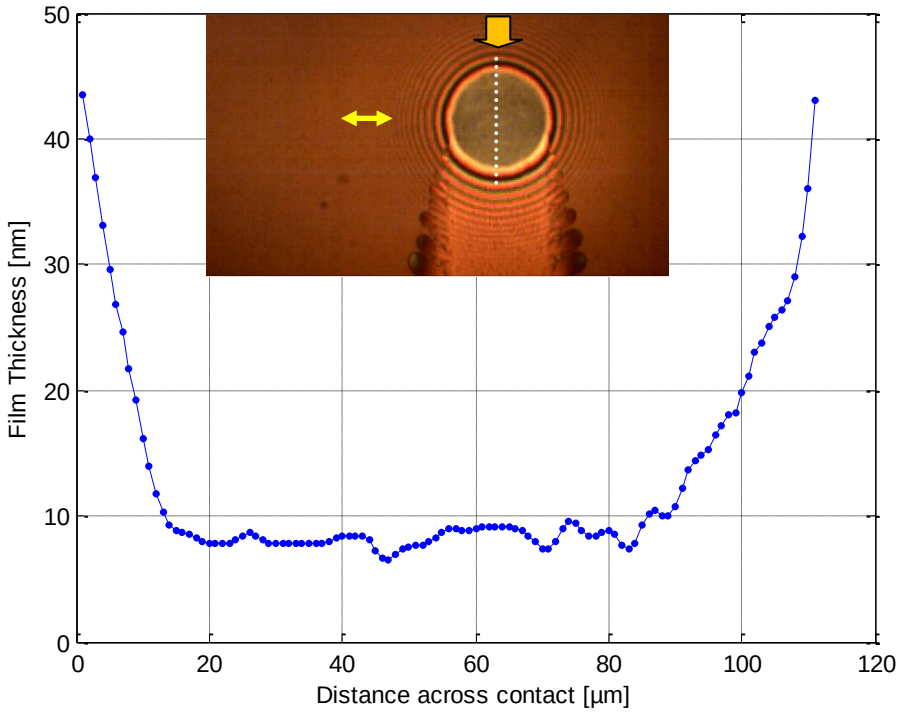

Figure 5.5 (a): Coloured interferogram and Film Thickness profile at 10 Hz for 0.05 m/s (tungsten carbide – sapphire combination)

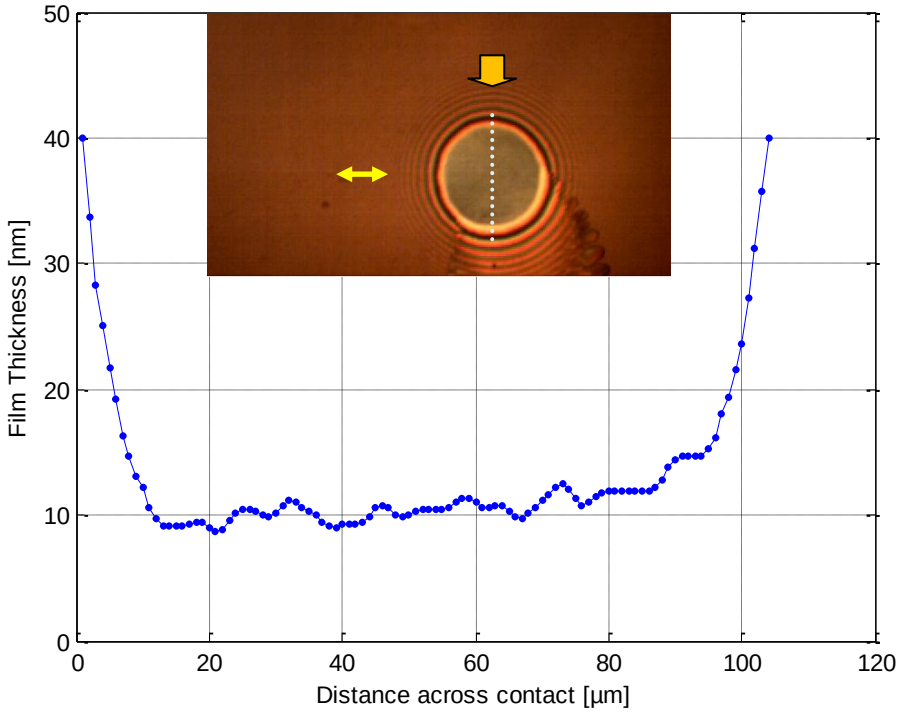

Figure 5.5 (b): Coloured interferogram and Film Thickness profile at 50 Hz for 0.05 m/s (tungsten carbide – sapphire combination)

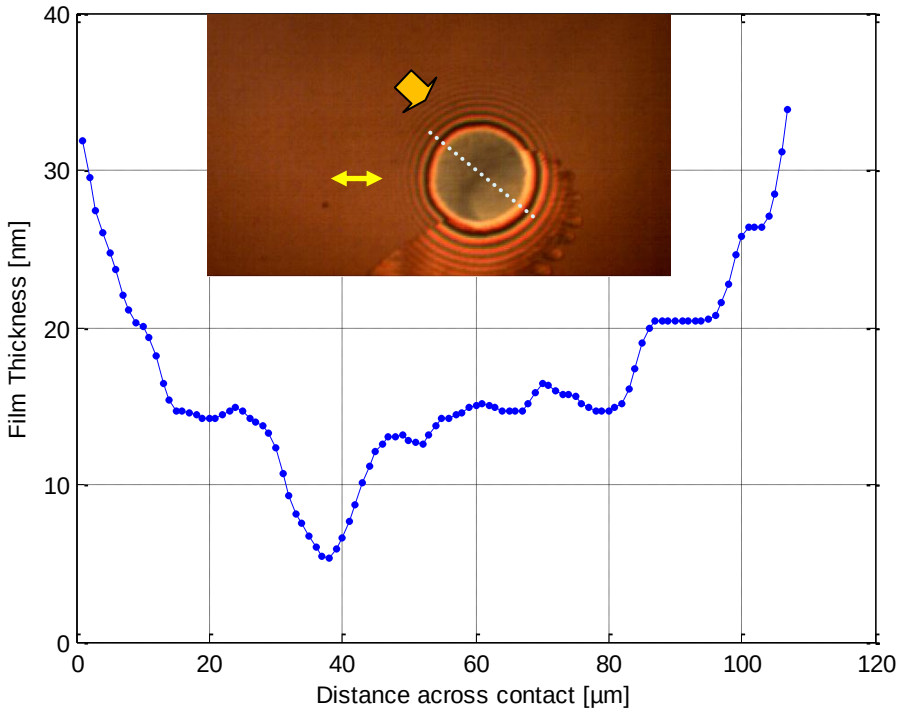

Figure 5.5 (c): Coloured interferogram and Film Thickness profile at 100 Hz for 0.05 m/s (tungsten carbide – sapphire combination)

Analyzing the results for different frequencies it can be clearly observed that, as it was the case for the glass steel contact, only at the highest frequency perturbations in the film have been detected.

The effect of the overall film thickness upon the response of the EHD film to lateral oscillations was examined by varying the main rolling speed in a range from 0.05 m/s to 1 m/s at a constant frequency of 100 Hz and the results are presented in Figures 5.6 (a) to (d). In the case of low speeds i.e. 0.05 m/s and 0.1 m/s the film thickness was calculated diagonally (i.e. top right to bottom left) while for larger speeds the film thickness was taken transverse to the entraining direction.

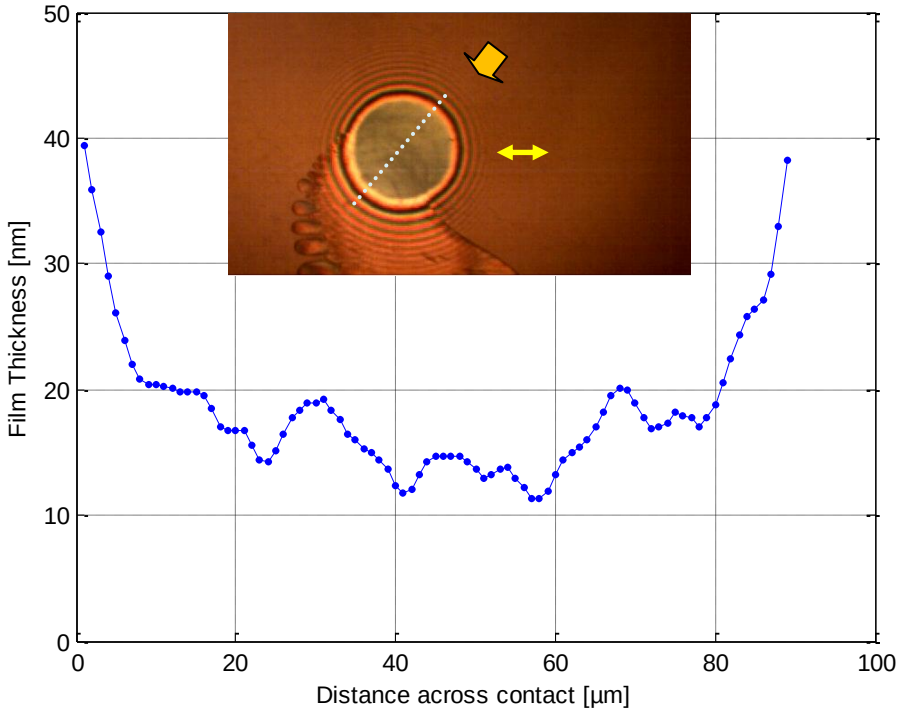

Figure 5.6 (a): Coloured interferogram and Film Thickness profile at 100 Hz for 0.05 m/s (tungsten carbide – sapphire combination)

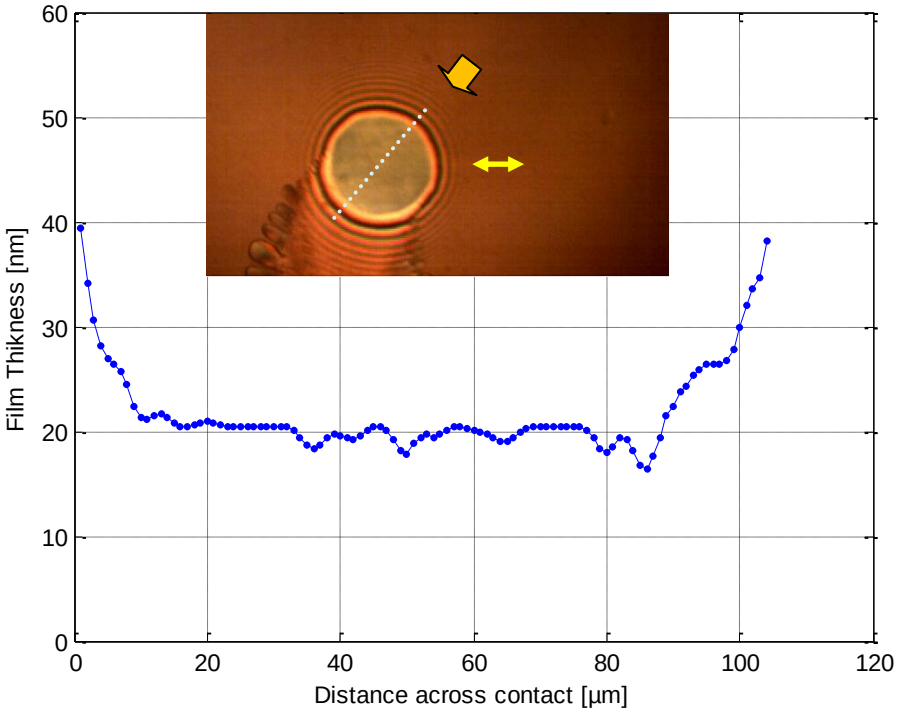

Figure 5.6 (b): Coloured interferogram and Film Thickness profile at 100 Hz for 0.1 m/s (tungsten carbide – sapphire combination)

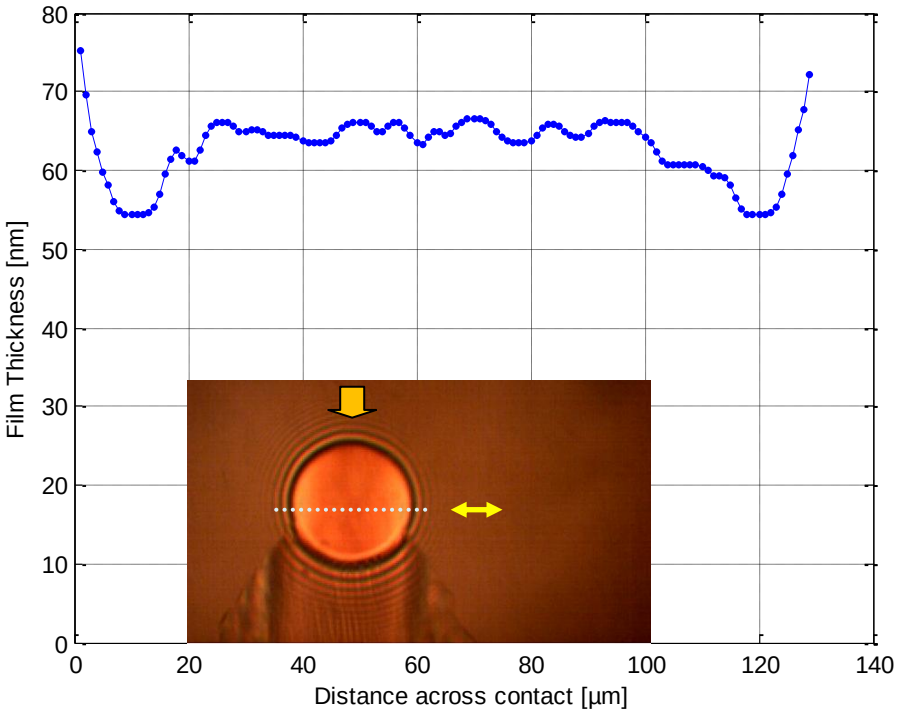

Figure 5.6 (c): Coloured interferogram and Film Thickness profile at 100 Hz for 0.5 m/s (tungsten carbide – sapphire combination)

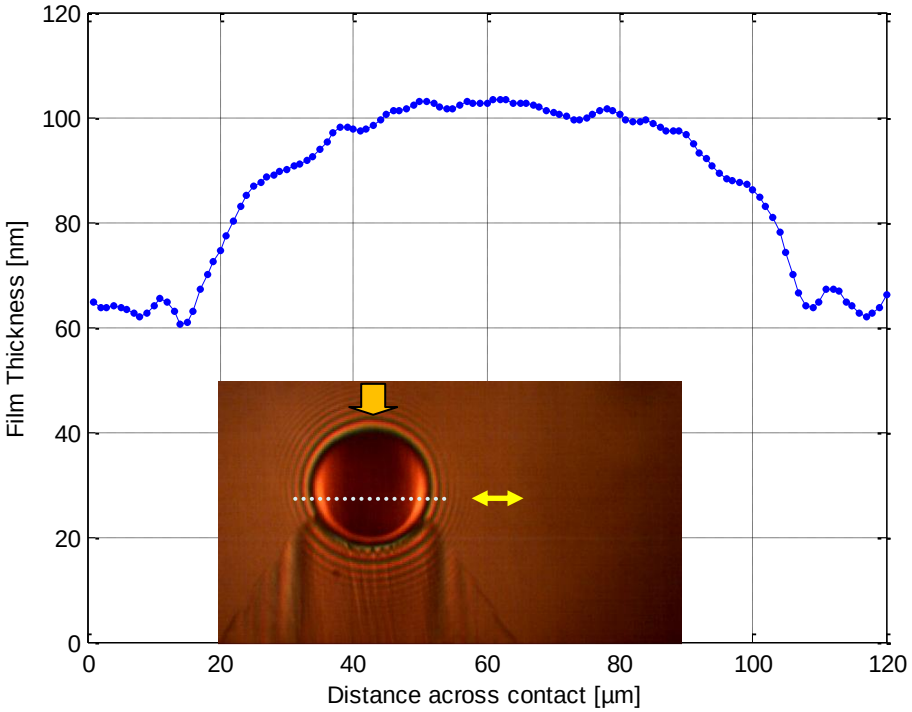

Figure 5.6 (d): Coloured interferogram and Film Thickness profile at 100 Hz for 1 m/s (tungsten carbide – sapphire combination)

Analysis of the above graphs shows that perturbations in the film were not observed at higher speeds. At lower speeds, the perturbation in the film formed during rapid deceleration, at the end of the stroke, travels along the direction of the instantaneous entrainment speed of the contact.

5.2.1 Comparison of Glass/Steel and Sapphire on Tungsten Carbide Results

The analysis of the results based on tungsten carbide / sapphire combination have shown the same trend with those results obtained for steel on glass contact. Since the contact stiffness of the material produced by sapphire/tungsten carbide combination is much higher than that in

the case of glass-steel contact, the fluctuations in the film thickness can give large pressure fluctuations in the contact. These in turn, if repeated at a regular interval can influence the fatigue life of the materials.

Figures 5.7 (a) to (c) shows, in comparison, a sequence of coloured interferograms during the lateral cycle for steel – glass and sapphire-tungsten carbide carried out at the lowest entraining speed of 0.05 m/s and at a frequency of 100 Hz. The vertical arrow indicates the direction of the rolling speed while the broken arrow represents the direction of the lateral motion.

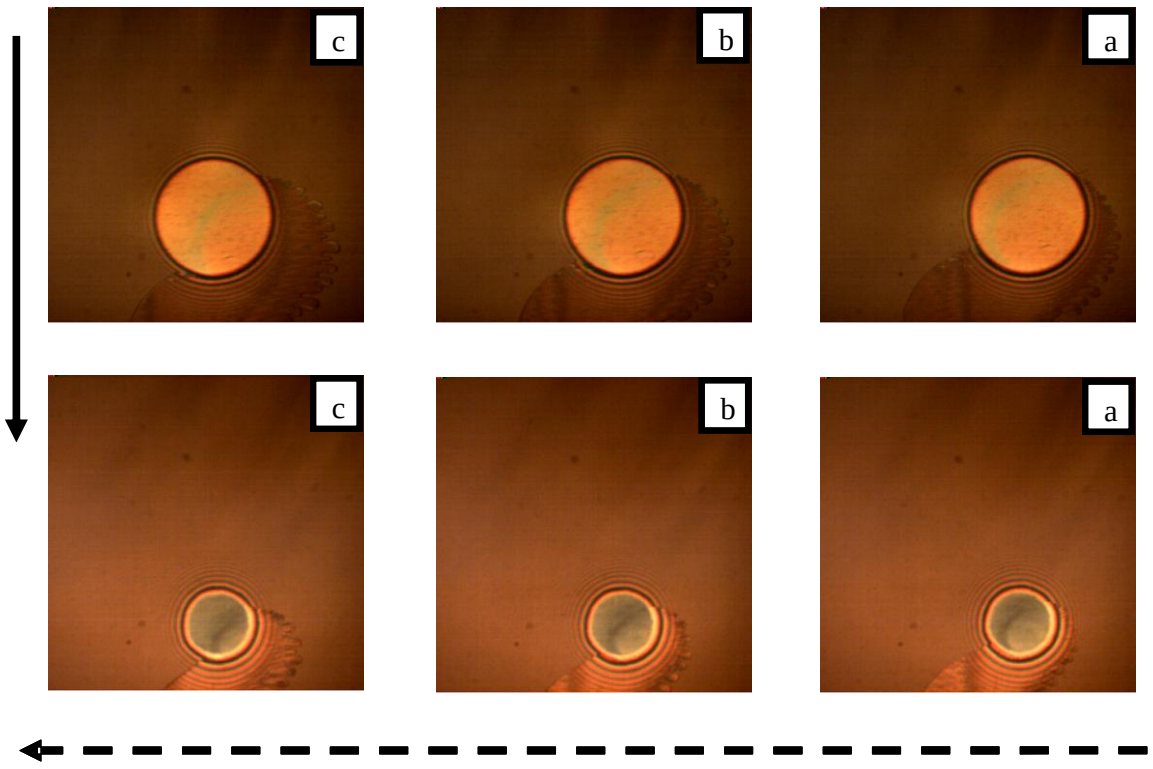

Figure 5.7: Coloured Interferograms: Steel / Glass and Sapphire / Tungsten Carbide contacts at 100 Hz and 0.05 m/s main entrainment speed

As seen from the images shown above, the film perturbation forms in a similar fashion for the two different pressures. The different colour of the tungsten carbide images indicates a slightly smaller film thickness due to different reduced elastic modulus of the two combinations of materials.

The following diagrams present a comparison of film thickness profiles between the tests obtained for glass on steel combination and those carried out with sapphire –tungsten carbide combination.

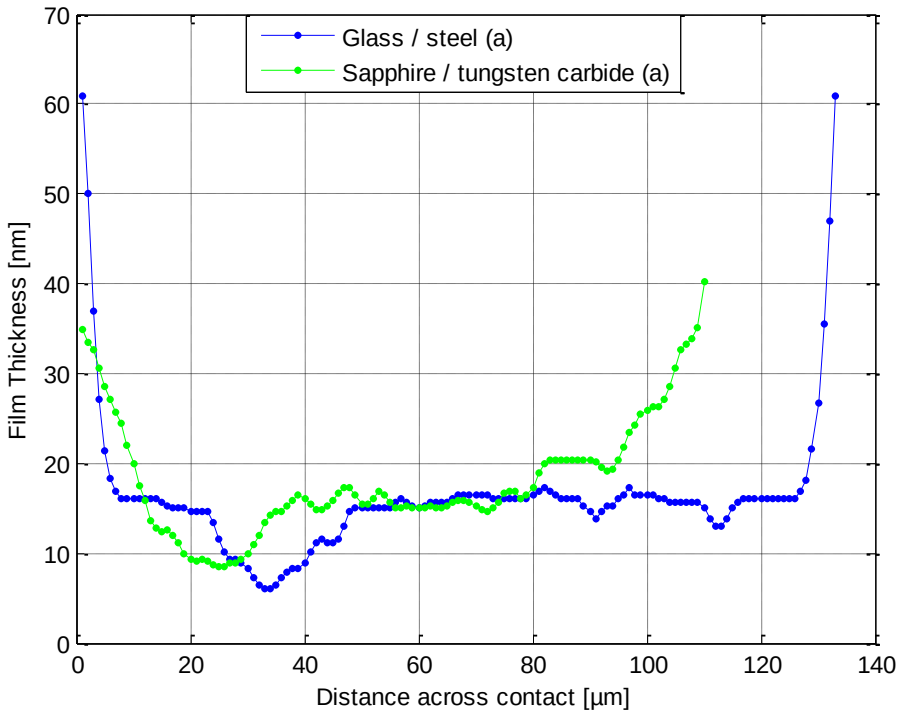

Figure 5.8 (a) : Film Thickness profile at 100 Hz and 0.05 m/s main entrainment speed for steel glass and WC / sapphire combination

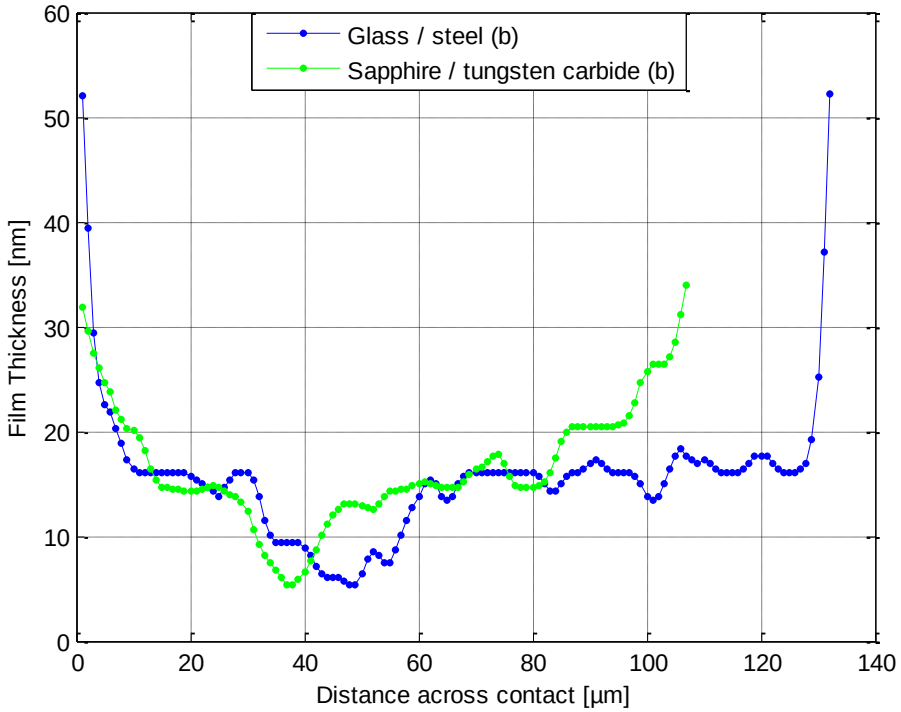

Figure 5.8 (b) : Film Thickness profile at 100 Hz and 0.05 m/s main entrainment speed for steel glass and WC / sapphire combination

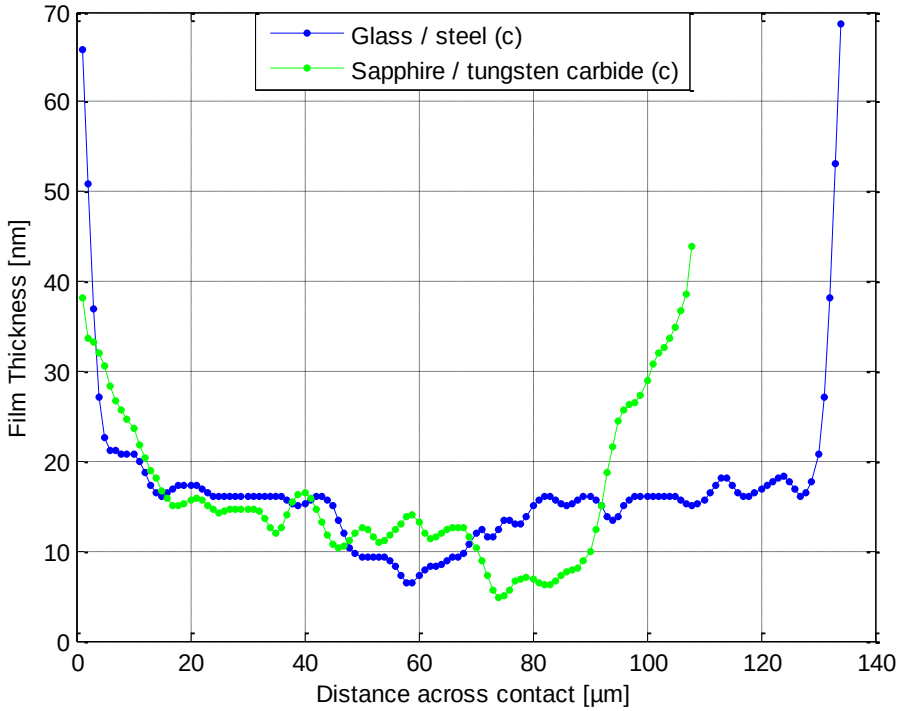

Figure 5.8 (c) : Film Thickness profile at 100 Hz and 0.05 m/s main entrainment speed for steel glass and WC / sapphire combination

By looking at the graphs, it can be seen that ripples were found inside the contact area even for larger Hertzian pressures. It has to be mentioned that, the amplitude of the film perturbation has similar values for both test arrangements, i.e. 10 – 12 nm for glass/steel contact and between 11 nm to 15 nm for the tungsten carbide / sapphire pair.

5.3 Simple Theoretical Analysis

In this section, the experimental film thickness, h_{exp}, has been compared with the predicted film thickness, h_p at pure rolling conditions and two Hertzian pressures. It has to be noted that is a simplified analysis, based on steady state film thickness calculations and taking into account only the time of passage of the fluid through the contact, but ignoring the squeeze effects.

5.3.1 Steel on Glass contact

Figure 5.9 show the distribution of velocities over the contact area. The net entrainment speed at any moment has the direction of the vector sum between the instantaneous ball surface velocity and the disc surface velocity.

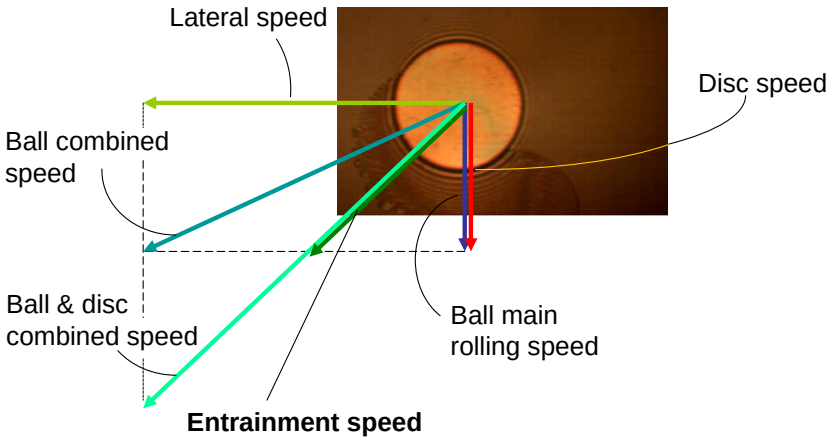

Figure 5.9: Instantaneous entrainment velocity during lateral oscillations

In Figure 5.10, a comparison of the theoretical film thickness obtained at 50 Hz and 100Hz at a main rolling speed of 0.05 m/s can be observed. This calculation is done at the centre of the contact and is based on the time of passage of the lubricant through the contact. Due to the thinner film generated at the end of the strokes, thinner film passes through the contact regular intervals.

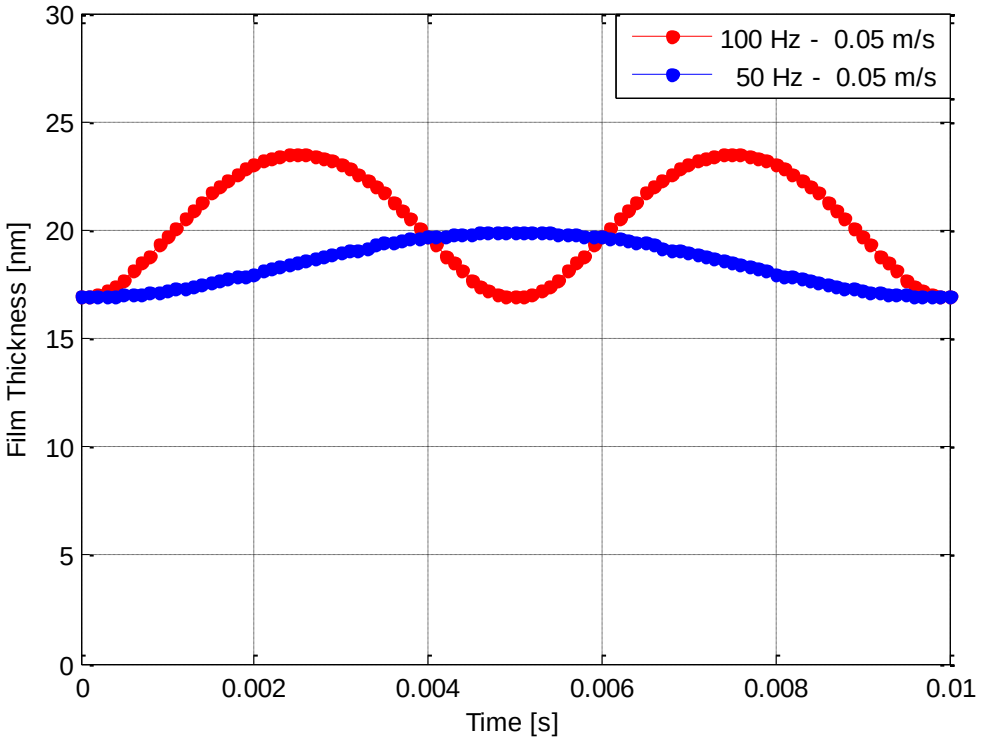

Figure 5.10: Theoretical Film Thickness variations across the contact at frequencies of 50 Hz and 100 Hz VS Time

Figure 5.11 presents the estimated variation of the lateral speed for all working frequencies. The maximum lateral speed was first estimated by two consecutive images then a sinusoidal function was assumed to calculate the instantaneous lateral speed of the ball.

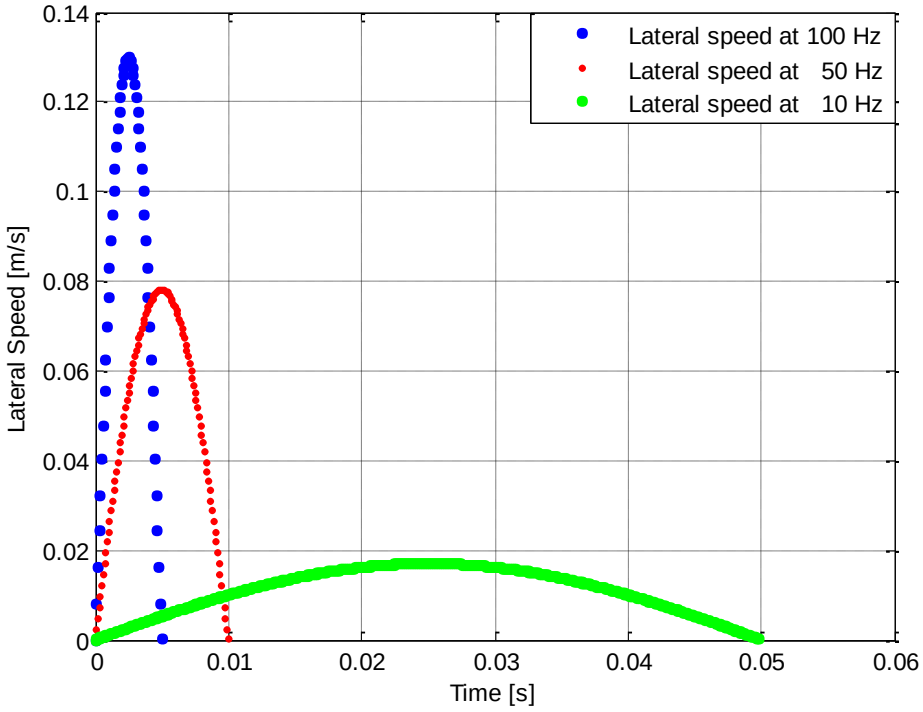

Figure 5.11: Maximum Lateral speeds at frequencies of 10 Hz, 50 Hz and 100 Hz

Another important factor which influences the film thickness is the ratio between the lateral speed and the main entraining speed, as seen from the experimental results. Figures 5.12 to 5.15 present the lateral speed, over half cycle, at 100Hz, at different main rolling speeds ranging from 0.05 m/s to 1 m/s. The common feature in theses graphs is that the resultant speed is always higher than the other two. In the first two graphs as shown in Figure 5.12 and Figure 5.13, the lateral speed is larger than the main entrainment speed which is the reason of the film fluctuations observed in experiments. At larger speeds, as seen in Figures 5.14 and 5.15 the greater main rolling speeds makes the lateral speed have no real influence upon the net entrainment, thus as a result no big variation in the film were detected.

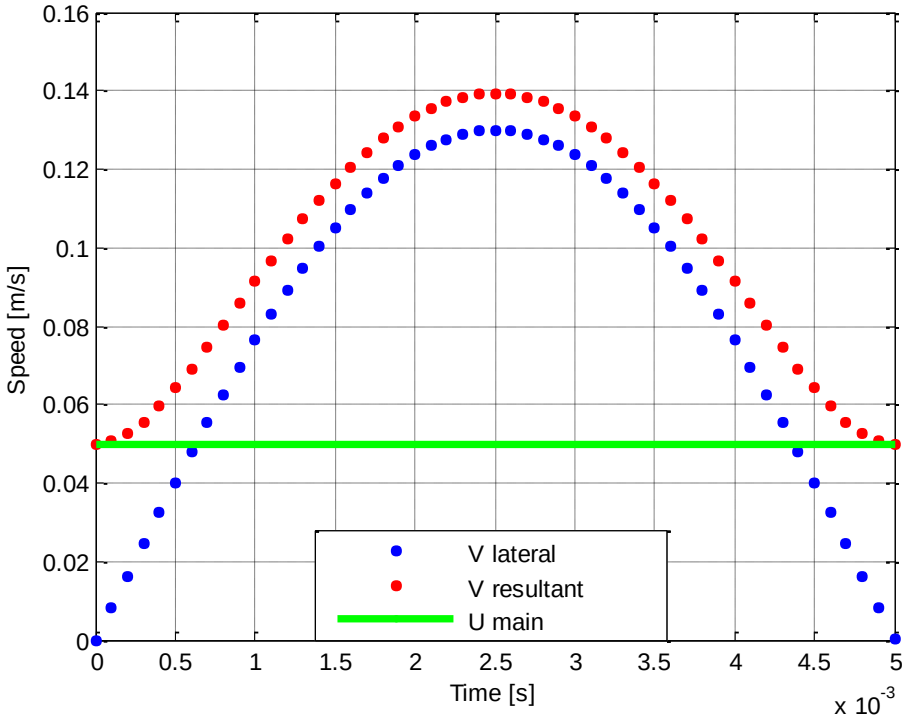

Figure 5.12: Theoretical speed variations at a main entrainment speed of 0.05 m/s

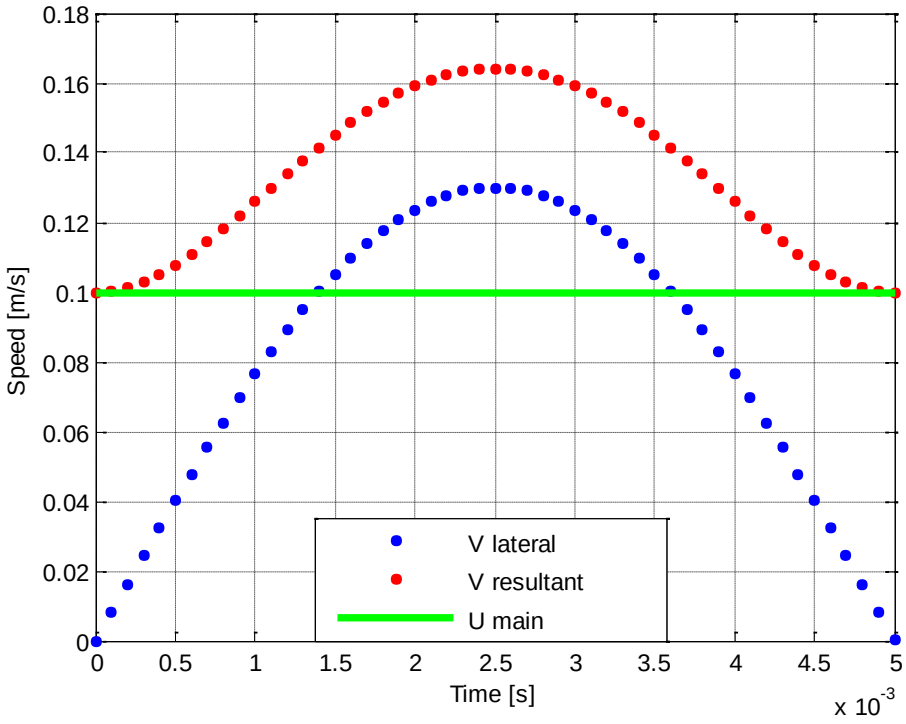

Figure 5.13: Theoretical speed variations at a main entrainment speed of 0.1 m/s

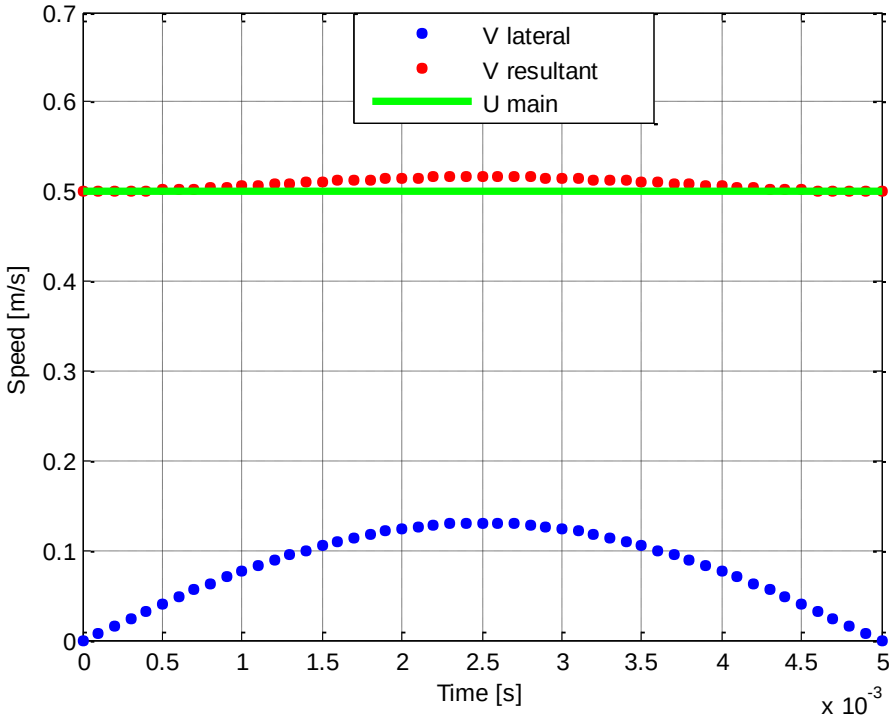

Figure 5.14: Theoretical speed variations at a main entrainment speed of 0.5 m/s

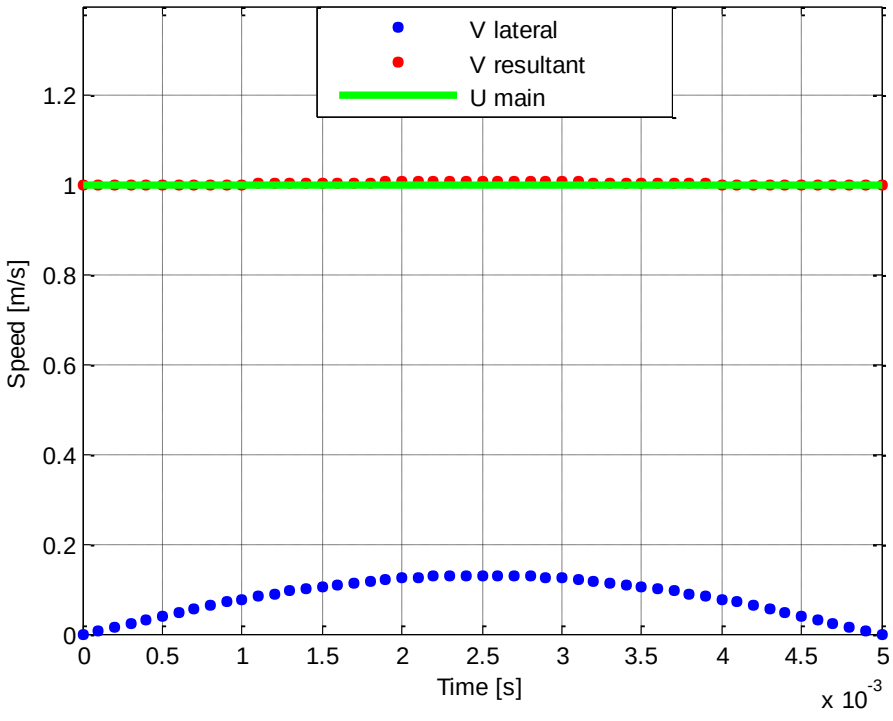

Figure 5.15: Theoretical speed variations at a main entrainment speed of 1 m/s

Based on the graphs stated above, the central film thickness was estimated at different stroke positions, Figure 5.16. The broken arrow indicates the direction of lateral motion. At the beginning of the stroke length, the film thickness gradually increases until it reaches the maximum value where can be found in the centre of the stroke position. Then as the contact moves towards the end of one half-cycle of oscillation the film thickness decreases. In addition, the film thickness was estimated along a diameter of the contact, as seen in Figure 5.17. In this case the film thickness variation was about 7 nm which was close to the experimental value of 13 nm. The difference may be due to neglecting the squeeze effects in this simple theoretical analysis.

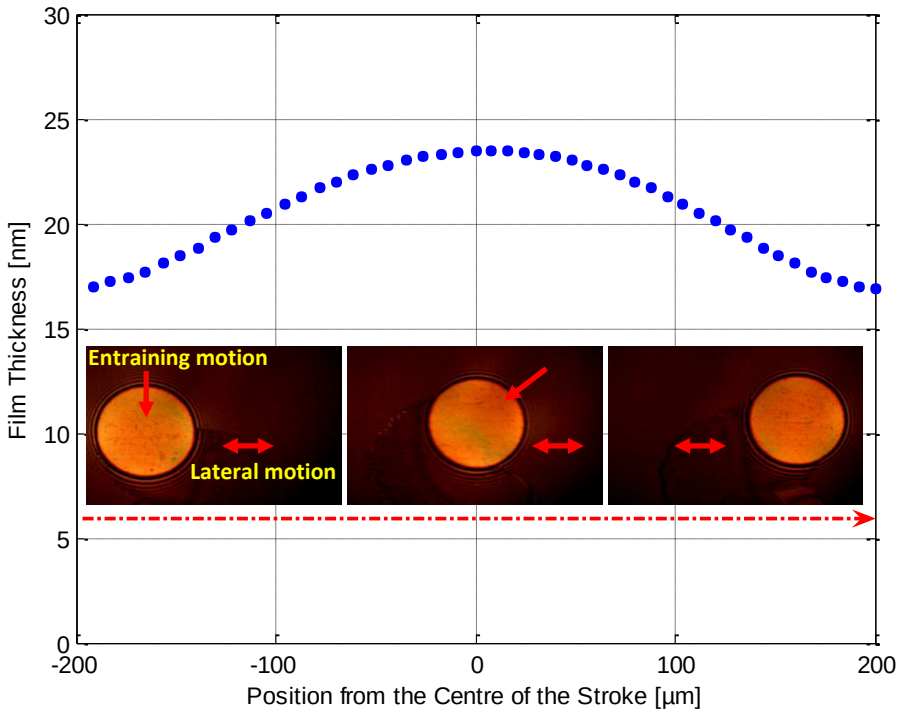

Figure 5.16: Theoretical Film Thickness variations along the stroke at a frequency of 100 Hz and at a main entrainment speed of 0.05 m/s

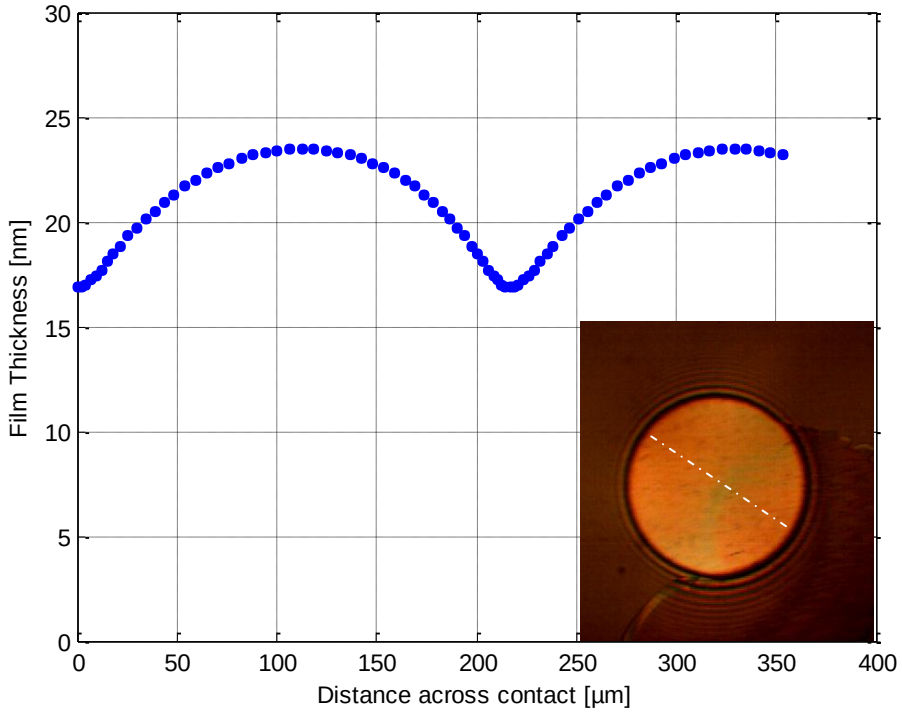

Figure 5.17: Theoretical Film Thickness variations across contact at a frequency of 100Hz

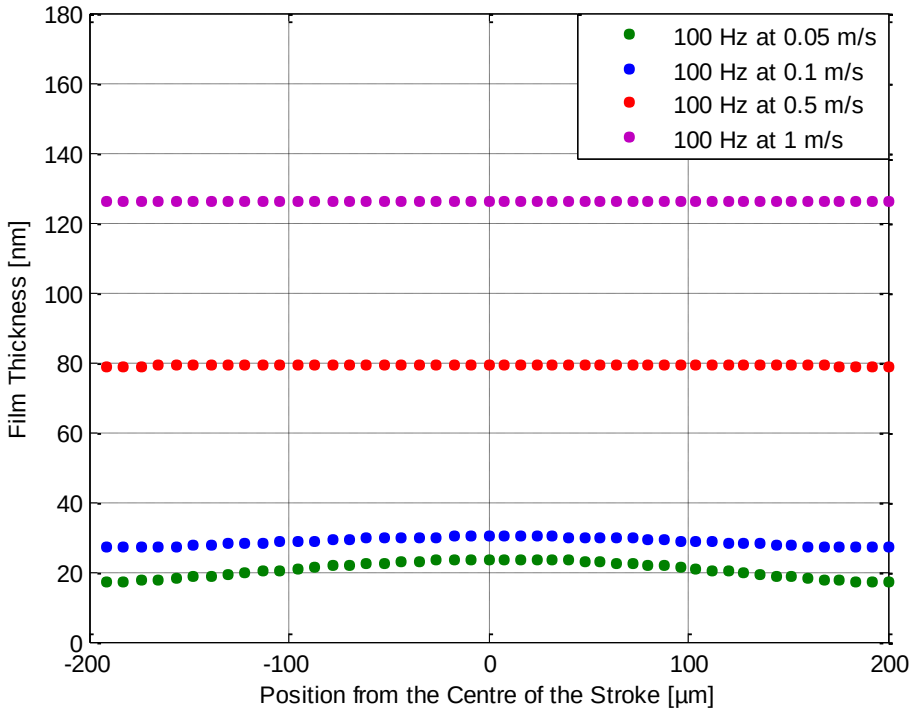

Figure 5.18: Theoretical Film Thickness variations along the stroke at different entrainment speeds

The variation of the averaged central film thickness during one period of oscillation at a wide range of main rolling speeds and at a constant frequency of 100 Hz is illustrated in Figure 5.18. From the plot, it can be seen that at low speeds the film thickness varies along the stroke and the larger value film can be detected at the centre stroke position. For larger speeds (0.5 m/s, 1 m/s) the central film thickness behaves quite steadily which in turn diminishes the squeeze effect. These phenomena were also detected during the experiments.

A summary of the experimental and theoretical film thickness is shown in table 5.1 which illustrates the results of both theoretical and experimental measurements under transient conditions. The dimensionless speed parameter, the lateral speed as well as the resultant speed were varied by changing the main entrainment speed.

Glass – Steel combination (100 Hz – Lateral Speed : 0.13 m/s)				Lubricant PAO 4
Central Film Thickness[nm]		V Resultant Speed [m/s]	U main rolling speed [m/s]	Dimensionless Speed Parameter $\overline{U}$
Theoretical	Experimental			
17 – 23.5	15 - 18	0.14	0.05	6.5×10^{-11}
27 - 30	18.5 - 22	0.16	0.1	9.4×10^{-11}
80	88	0.516	0.5	3.99×10^{-10}
126	155	1	1	7.94×10^{-10}
Dimensionless Load Parameter $\overline{W_L}$: 4.4×10^{-06}				
Dimensionless Material Parameter $\overline{G}$: 1.69×10^{03}				

Table 5.1: Theoretical and Experimental Measurements under transient conditions (Glass / Steel combination)

A relatively good agreement between the theoretical and experimental predictions can be found at entrainment speeds varying from 0.05 m/s and 0.5 m/s as seen in Table 5.1. Only at highest speeds the agreement was not quite good, with the measured predictions of film being larger than the theoretical values. This phenomenon may be attributed to the viscous heating in the inlet, as shown by Greenwood and Kauzlarich [122] or Moore [123].

5.3.2 Sapphire-Tungsten carbide combination

Additional comparisons were made between experimental findings and theoretical predictions using the other pair of test materials. The sapphire disc – tungsten carbide ball combination produced higher Hertzian pressure of 1.7 GPa than that obtained with steel on glass contact.

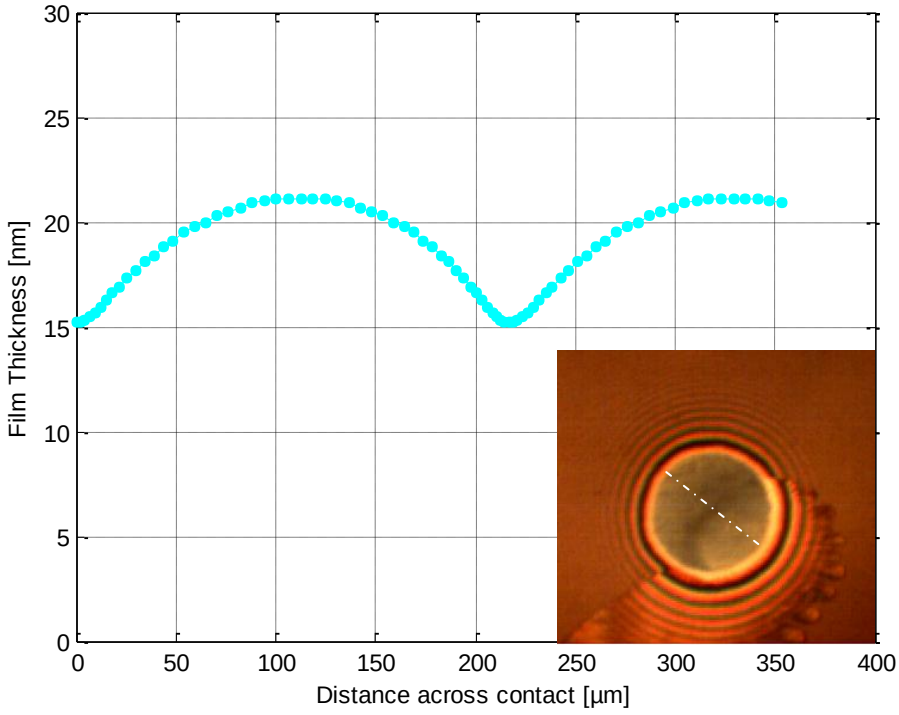

Figure 5.19: Theoretical Film Thickness variations across the contact at a frequency of 100 Hz (Sapphire / WC combination)

Figure 5.19 present the theoretical film thickness measured across the contact. The direction of flow is from left to right. It can be stated that, reduction in the film can be found even at larger Hertzian pressure. This plot corresponded to the theoretical study obtained at low main

rolling speed and at maximum lateral speed. In this case the film thickness was varied between 15 to 21 nm which was close with the experimental value (11 to 20 nm).

In Figure 5.20 it can be observed that, the central film thickness variation follow the same pattern as indicated earlier on glass – steel combination. As the main entrainment speed increases, the film also increases and no significant variation can be found along the stroke length.

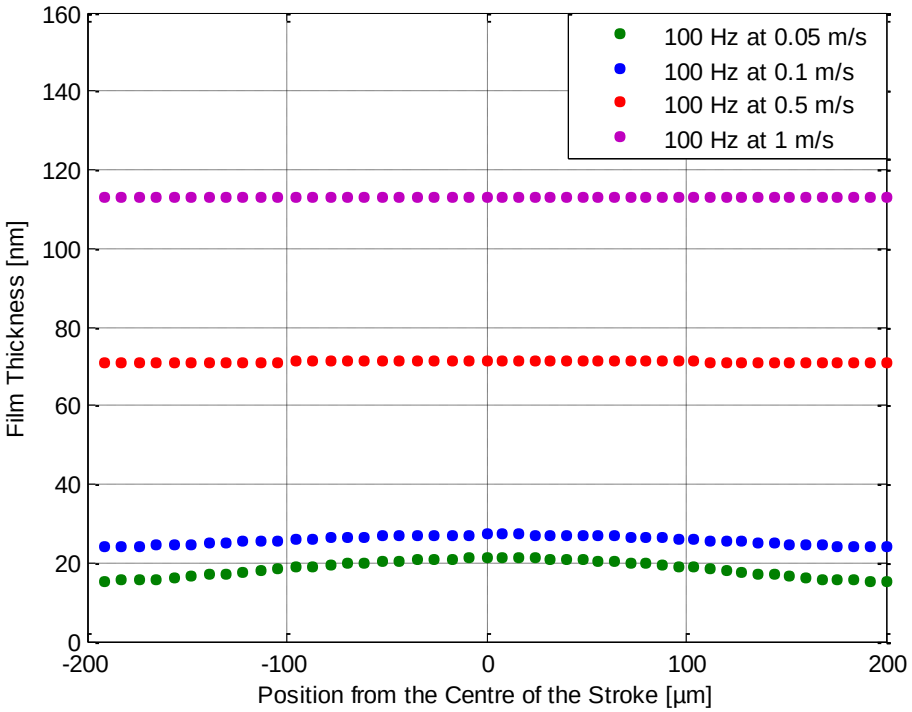

Figure 5.20: Theoretical Film Thickness variations along the stroke at different entrainment speeds (Sapphire / TC combination)

From the results in Table 5.2 it can be seen that, both theoretical and experimental measurements for sapphire – tungsten carbide combination have shown a relatively good

correlation at low main rolling speeds. In the case of 1 m/s the agreement between the experimental and the theoretical values was not so good, with the experimental values lagging behind the theoretical ones. Again thermal effects can be the main cause of this behaviour. Another cause may be the value of the phase shift in reflection, at the tungsten carbide ball surface, which was approximated with the value for steel ball, when constructing the calibration curves of film thickness versus RGB. It may be that this coefficient is different, which will account for some of the discrepancies between theoretical and measured values of film thickness.

Sapphire – TC combination (100 Hz – Lateral Speed : 0.13 m/s)				Lubricant PAO4
Central Film Thickness [m]		V Resultant Speed [m/s]	U main rolling speed [m/s]	Dimensionless Speed Parameter $\overline{U}$
Theoretical	Experimental			
15 - 21	11 - 20	0.14	0.05	1.5×10^{-11}
24 - 27	22 - 23.6	0.16	0.1	2.2×10^{-11}
71	65	0.516	0.5	9.3×10^{-11}
113	103	1	1	1.85×10^{-10}
Dimensionless Load Parameter $\overline{W_L}$: 1×10^{-04}				
Dimensionless Material Parameter $\overline{G}$: 1.07×10^{04}				

Table 5.2: Theoretical and Experimental Measurements under transient conditions (Sapphire / WC combination)

5.4 The Effect of Viscosity Index Improver Additive

The efficiency of lubricated machine elements including gears, transmissions, crankcase engines and hydraulic pumps depends strongly on the friction properties of the lubricant employed. For the design of modern, highly efficient lubricants it is thus crucial to understand the influence of the components of the lubricating fluid in terms of film formation and consequent friction [124]. ‘VIIs are polymeric compounds which become more soluble and thus adopt a more open molecular conformation in the solution as the temperature rises. In consequence they make a proportionately greater contribution to the viscosity of the blend at high rather than at low temperatures, thereby raising the viscosity index' [125].

In the current investigation, film thickness for a mixture of PAO 4 base oil and 10.7% weight polyalkylmethacrylate (PAMA) viscosity index improver polymer (supplied by Evonik - Romax) was measured at different rolling speeds varying from 0.05 m/s to 0.3 m/s, different frequencies and at a load of 45 N. The tests were conducted at temperatures of 30 ^{o}C and 80 ^{o} C.

Figure 5.21 presents coloured interferograms captured under steady state and transient conditions. The same procedure which was employed for base oil only, it has been used again; first, experiments have been conducted under steady state conditions over a wide speed range. Thereafter, lateral motion was introduced by setting the contact in motion, images were captured under non-steady state conditions. The figures in the left corner represent the main rolling speed. The vertical arrow shows the direction of the entraining motion while the horizontal arrow indicates the direction of lateral motion.

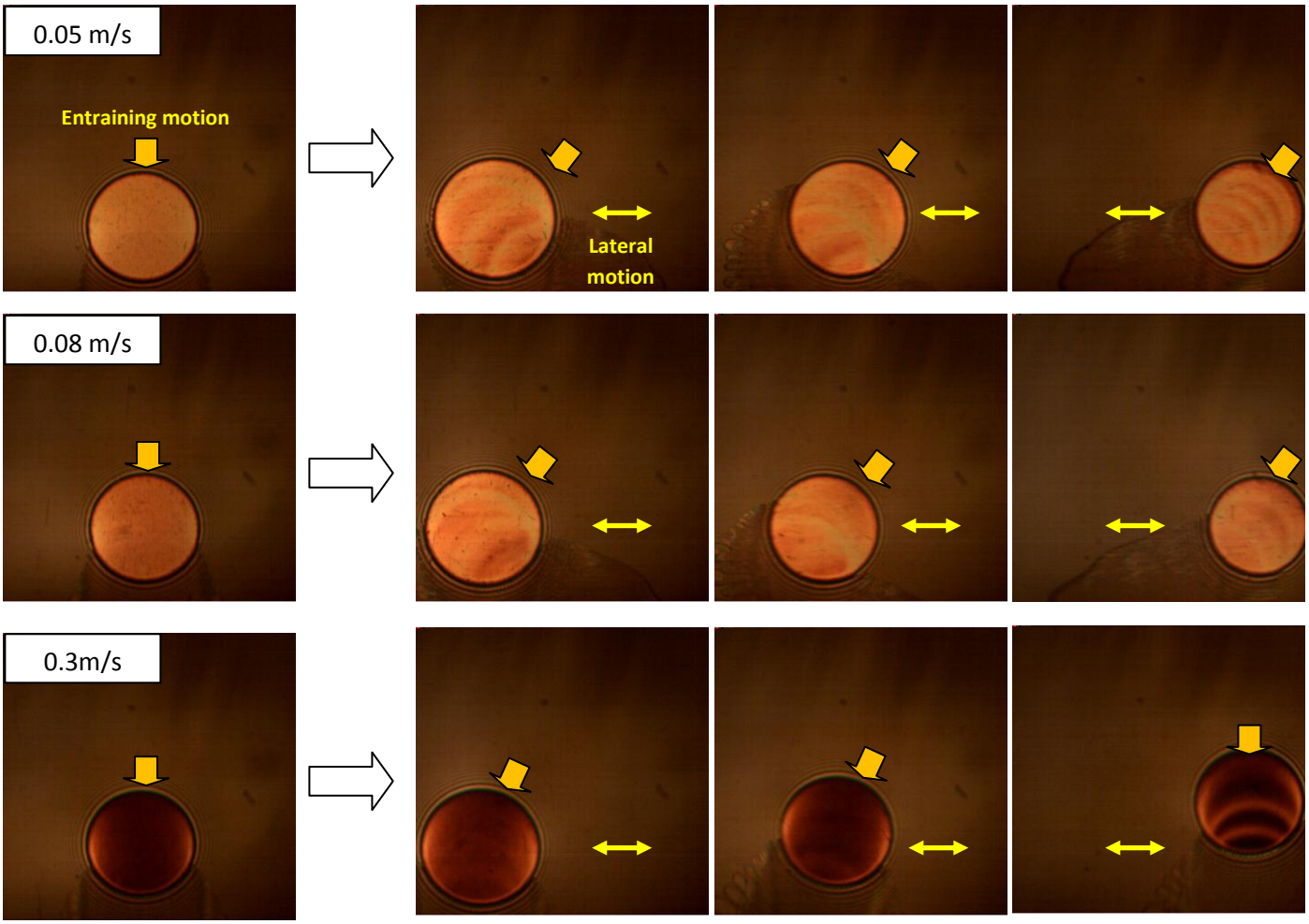

Figure 5.21: Coloured Interferograms under steady state and transient conditions with the addition of 10.7 % viscosity index improver

As seen in Figure 5.21 (a) the EHD contact is at the end of one stroke and the beginning of the left-to-right lateral motion. Film perturbations caused by the rapid decrease in lateral speed were formed in the same direction as the entraining motion (i.e. top left to bottom corners). When the contact starts to move from left to right, due to the increase of lateral speed a new series of waves of a thicker film are formed before the old ripples have travelled through the contact. The direction of the new ripples is now approximately from the top right to bottom left direction.

The coloured image and the corresponded film profile are illustrated in Figure 5.22, for 0.05 m/s and 100 Hz. The film thickness was taken diagonally (i.e. top left to bottom right). The horizontal arrows show the direction of lateral motion.

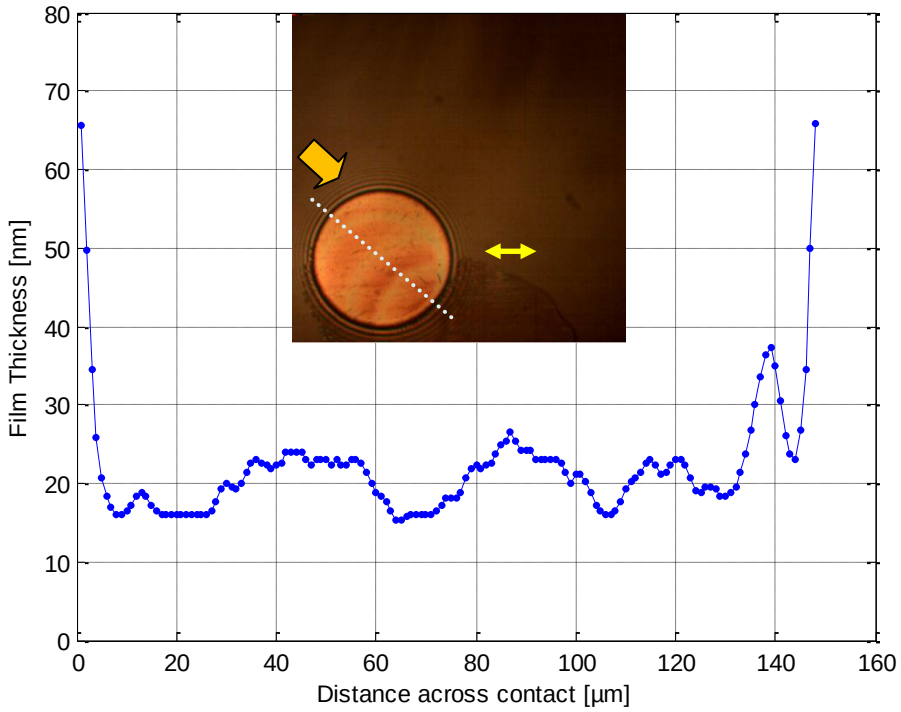

Figure 5.22: Coloured interferogram and Film Thickness profile for a PAO 4 blended with a 10.7 % viscosity index improver at 100 Hz for 0.05 m/s

A number of parameters including frequency variation, speed variation and temperature variation have also been studied. Figures 5.23 (a) to (c) illustrate snapshots and film profiles at a range of frequencies employ at the same rolling speed of 0.3 m/s and at same stroke position. The film thickness was calculated on a diameter perpendicular to the entraining

speed. The entraining motion is shown by the large arrow while the horizontal arrow indicates the direction of the lateral motion.

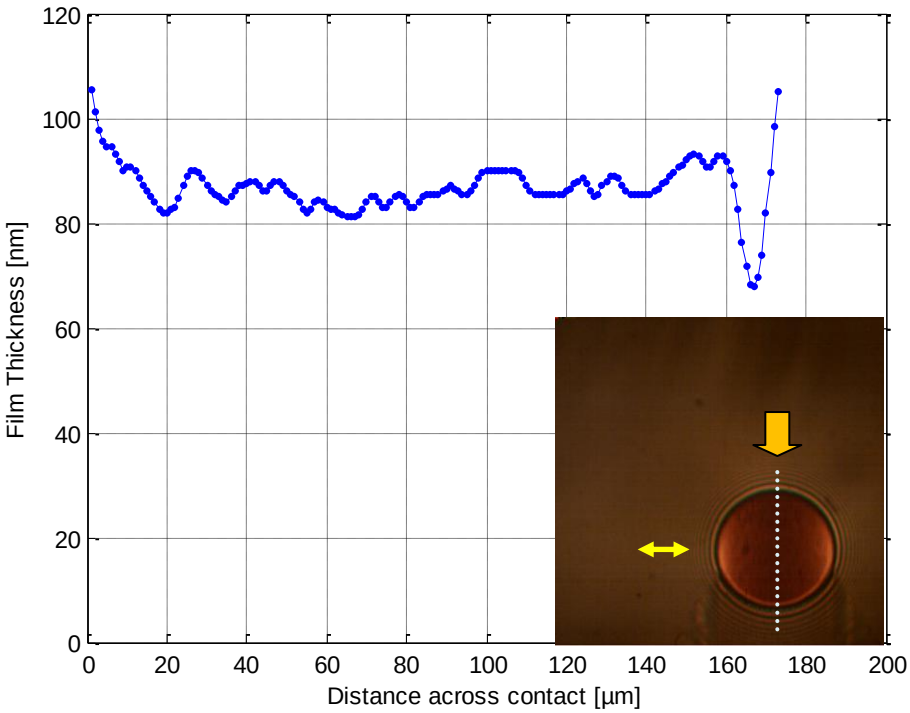

Figure 5.23(a): Coloured interferogram and Film Thickness profile for a PAO 4 blended with a 10.7 % viscosity index improver at 10 Hz for 0.3 m/s

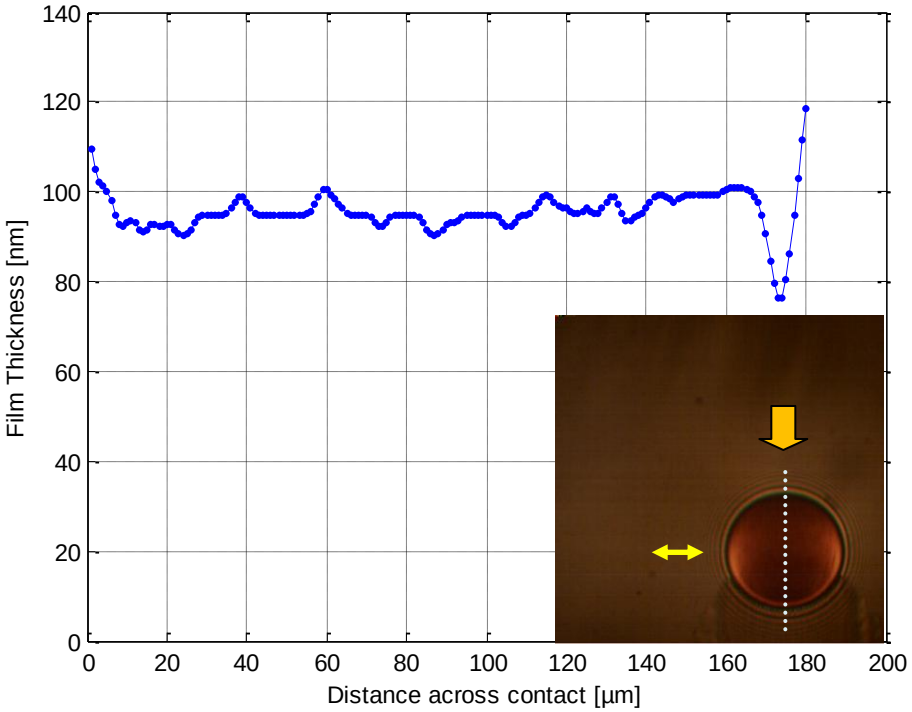

Figure 5.23(b): Coloured interferogram and Film Thickness profile for a PAO 4 blended with a 10.7 % viscosity index improver at 50 Hz for 0.3 m/s

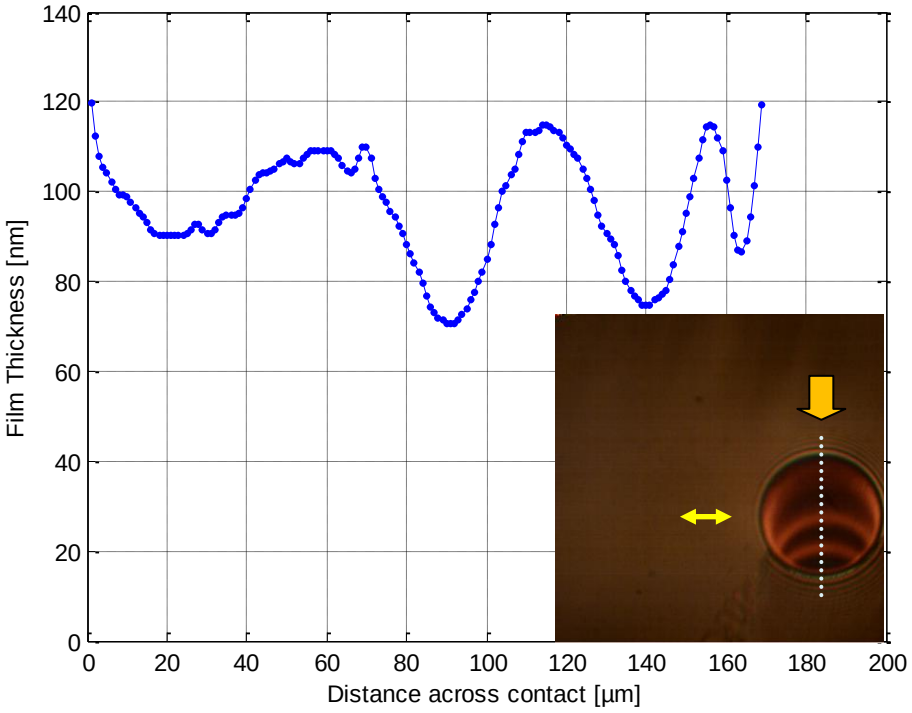

Figure 5.23(c): Coloured interferogram and Film Thickness profile for a PAO 4 blended with a 10.7 % viscosity index improver at 100 Hz for 0.3 m/s

As it can be observed from these plots, at the entrainment speed of 0.3 m/s, for which no film perturbations were detected for base oil only, strong perturbations can be seen at the largest frequency of 100 Hz. These perturbations are perpendicular to the entraining motion, as they are generated at the end of the lateral stroke. At that stroke position the entraining speed is more than twice larger than the lateral speed. The measured peak to valley variation was about 43 nm.

The influence of changing one of the parameters (entraining speed) is also studied. The corresponding optical interferometric images and film profiles measured at different rolling speeds and at a constant frequency of 100 Hz are shown in Figures 5.24 (a) to (c).

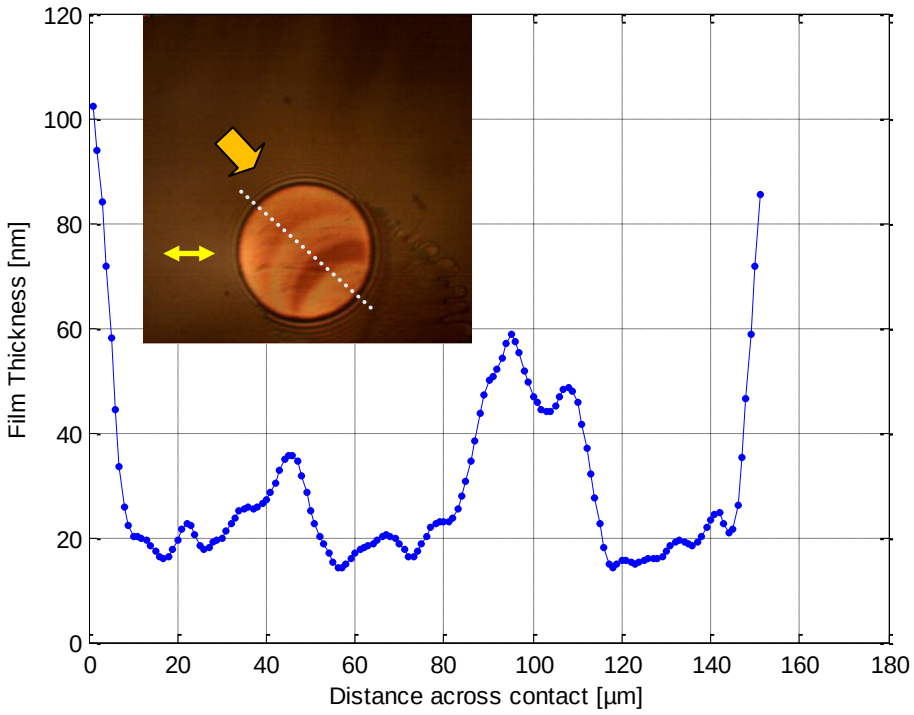

Figure 5.24(a): Coloured interferogram and Film Thickness profile for a PAO 4 blended with a 10.7 % viscosity index improver at 100 Hz for 0.05 m/s

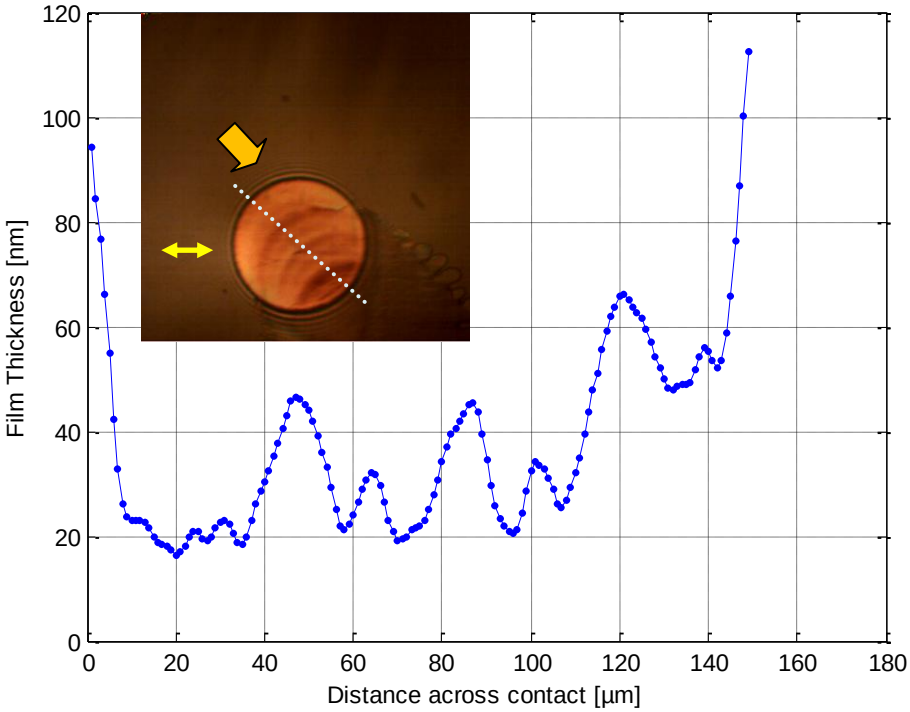

Figure 5.24(b): Coloured interferogram and Film Thickness profile for a PAO 4 blended with a 10.7 % viscosity index improver at 100 Hz for 0.08 m/s

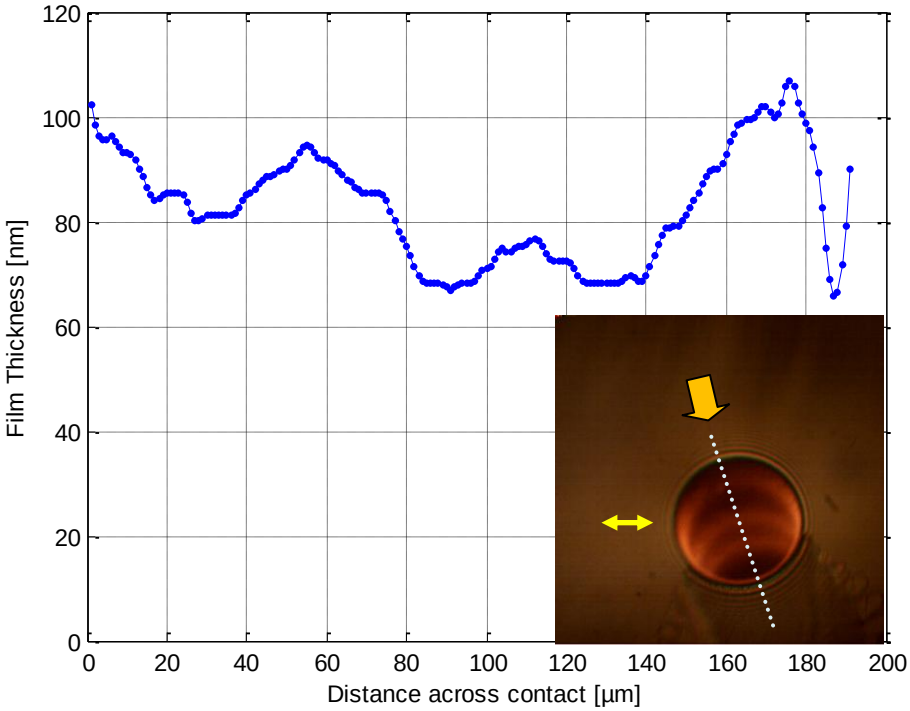

Figure 5.24(c): Coloured interferogram and Film Thickness profile for a PAO 4 blended with a 10.7 % viscosity index improver at 100 Hz for 0.3 m/s

Analyzing these results it was found that film perturbations which are revealed by crescent-shaped regions of different shades are clearly visible at all working speeds. At the lowest main entraining speed employed in this test the amplitude of the wave was about 45 nm while for the other two cases was between 30 nm and 35 nm (for the positions on the stroke shown).

5.4.1 Comparison between tests with and without VII at 30 ^{o}C

In this section, a comparison has been carried out between the results obtained at 30 ^{o}C for pure base oil and those performed with a mixture of PAO 4 and 10 percentage weight viscosity index improver polymer polyalkylmethacrylate (PAMA). Figures 5.25 (a) to (c) present coloured images and film thickness profiles measured at a range of frequencies (10 Hz, 50Hz, 100 Hz) and at a constant main rolling speed of 0.05 m/s. In the cases of 50 Hz and 100 Hz tests, the film thickness was calculated diagonally (top left to bottom corners) while at low frequencies the film thickness was taken along the main rolling direction.

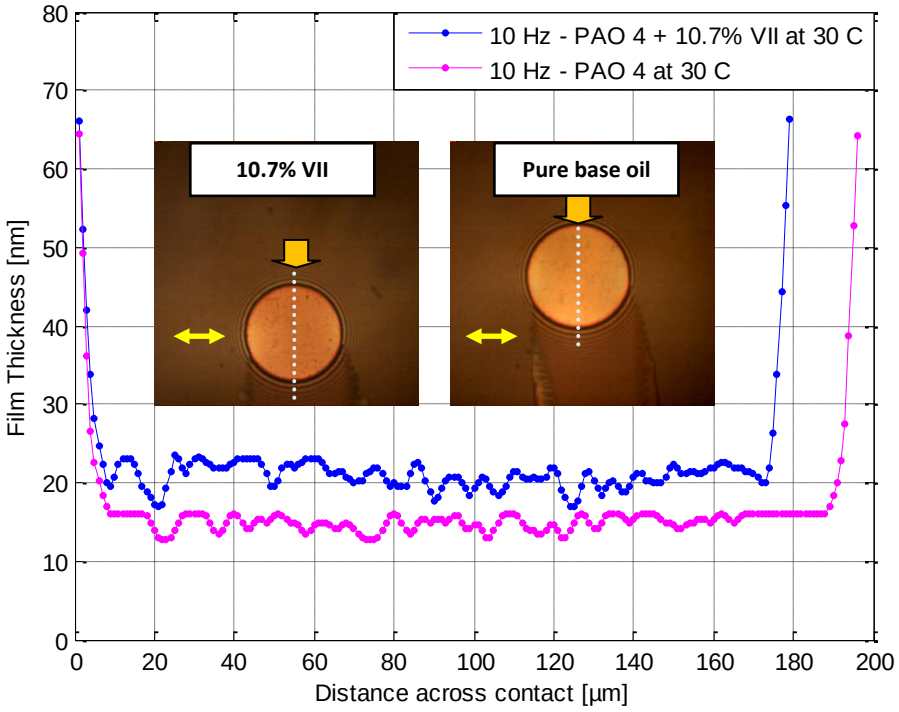

Figure 5.25(a): Coloured interferograms and Film Thickness profiles for a PAO 4 (30 ^{o}C) and an addition of 10.7% VII at 10 Hz for 0.05 m/s

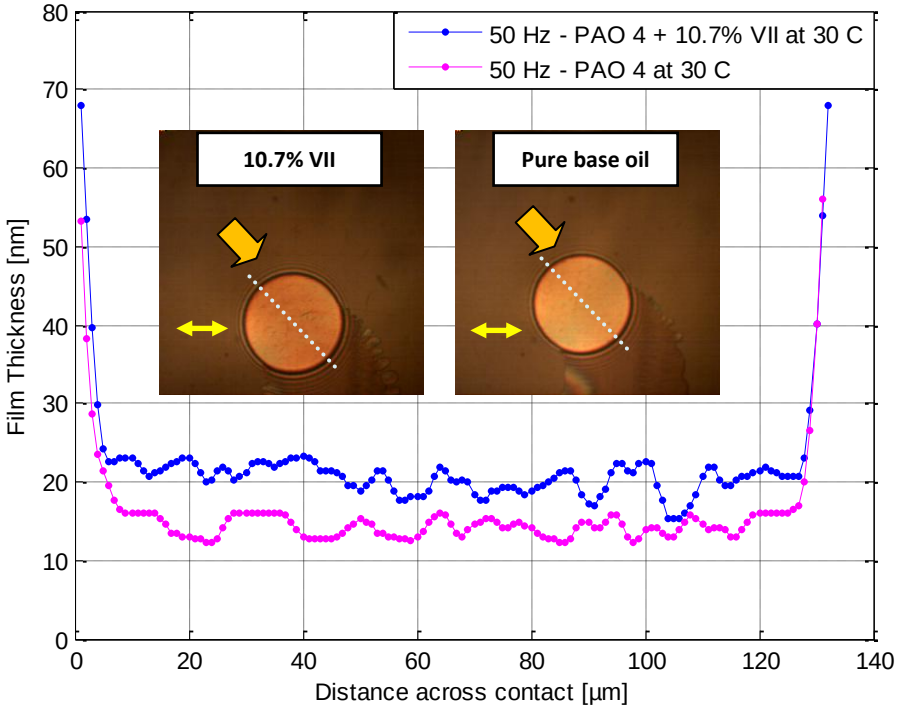

Figure 5.25(b): Coloured interferograms and Film Thickness profiles for a PAO 4 (30 ^{o}C) and an addition of 10.7% VII at 50 Hz for 0.05 m/s

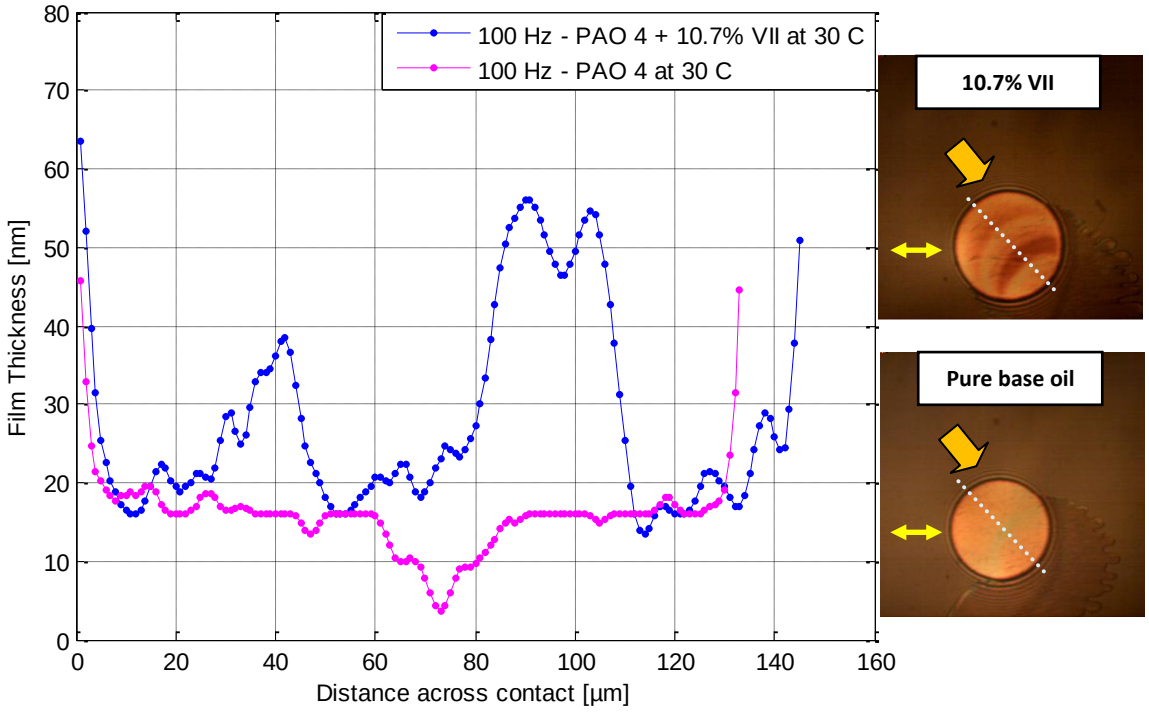

Figure 5.25(c): Coloured interferograms and Film Thickness profiles for a PAO 4 (30 ^{o} C) and an addition of 10.7% VII at 100 Hz for 0.05 m/s

Analysing the above plots, some aspects are immediately evident. As expected, the film thickness in the tests carried out with the viscosity added lubricant was slightly thicker than that measured in the tests performed with pure base oil, at all working frequencies. It has also to be mentioned that, when the largest frequency was employed, the shape of the film profile for the base oil was different from that of the VII added lubricant film profile. For instance, as seen in Figure 5.30(c), in the latter case, a series of waves of an enhanced film thickness which had different wavelength were formed in the inlet and travelled through the EHL conjunction while for the base oil tests a single ripple of a thinner film was found. The peak to valley variation for the VII added lubricant was about 40 nm while for the base oil only the perturbation was about 11-13 nm.

5.4.2 Comparison between tests with and without VII at 80 °C

The same comparison was done at 80 °C in order to evaluate the effect of VII.

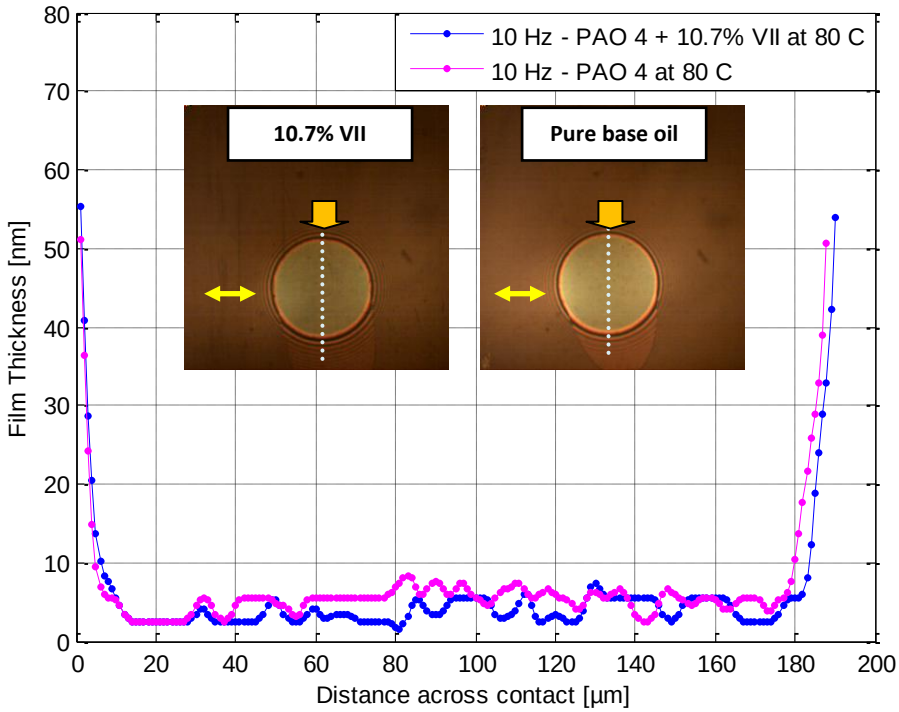

Figure 5.26(a): Coloured interferogram and Film Thickness profile for a PAO 4 (80 °C) and an addition of 10.7% VII at 10 Hz for 0.05 m/s

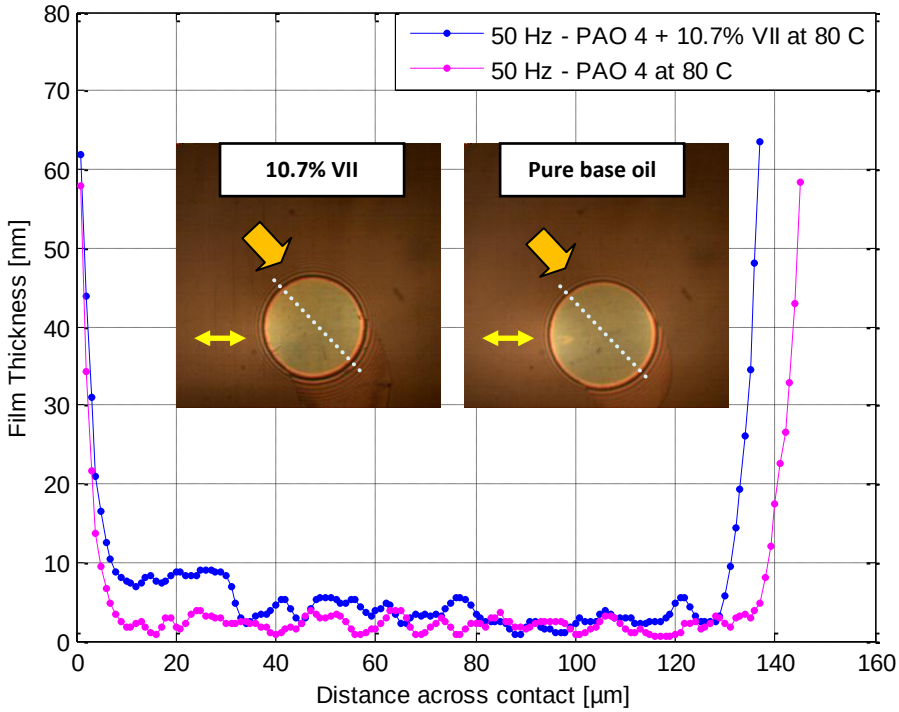

Figure 5.26(b): Coloured interferogram and Film Thickness profile for a PAO 4 (80 °C) and an addition of 10.7% VII at 50 Hz for 0.05 m/s

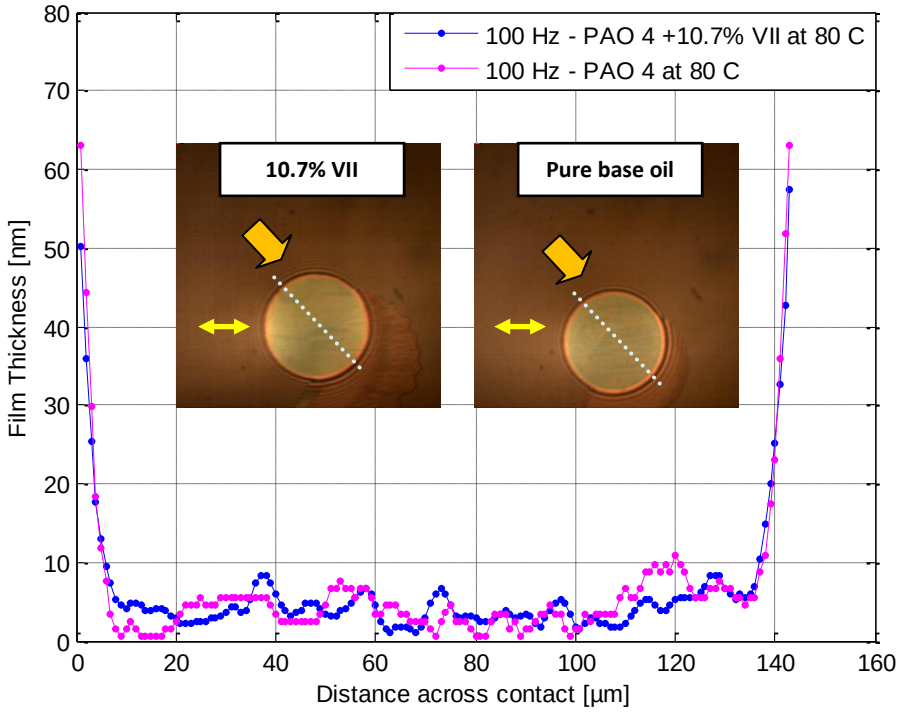

Figure 5.26(c): Coloured interferogram and Film Thickness profile for a PAO 4 (80 °C) and an addition of 10.7% VII at 100 Hz for 0.05 m/s

The film thickness has been measured at three different frequencies, constant rolling speed and the results are shown in Figures 5.26 (a) to (c). From the graphs obtained it is seen that, at all frequencies, the values of the film thickness is similar for the tests carried out with and without VII additive. Besides, the calculations in the film didn't reveal any significant fluctuations even at highest frequency thus at maximum lateral speed. This may be explained by the fact that at these very thin films, there not enough squeeze effect, because the solid surfaces are already too close to each other and the geometry in the converging inlet does not change significantly under variable lateral motion.

5.5 Behaviour of Grease Lubricants under lateral oscillations

Greases are the most common lubricants for rolling element bearings. The main advantages of using grease rather than lubricating oils are the ease manipulation, protection against corrosion and low friction. Grease is a complex two-phase lubricant consisting of base oil (about 90%) and a dispersed solid thickener. The lubricant properties of the grease depend on the shear rate as well as the duration of shearing. At low shear rates grease behaves as a plastic solid and does not flow until a critical yield stress has been reached. Thus, once the grease has been displaced from the track the contact will starve unless there is an external mechanism to flow back onto the track.

5.5.1 Track replenishment by lateral oscillations

The results shown in this section have been presented in reference [126] and are aimed at the evaluation of the effect of lateral oscillations upon the track replenishment in grease lubricated contacts. This study was carried out together with my colleague Yuichiro Nagata and the results have also been presented in his thesis [127]. My contribution to this part of the study was thirty percent.

In these, lateral motion has been applied onto the contact formed between a sapphire disc and a tungsten carbide ball, in order to get larger Hertzian pressures. The lateral frequency was 10 Hz which gave a maximum lateral speed of 13 mm/s. The main rolling speed was been kept constant through –out the tests at 0.5 m/s with a consistent load of 45 N.

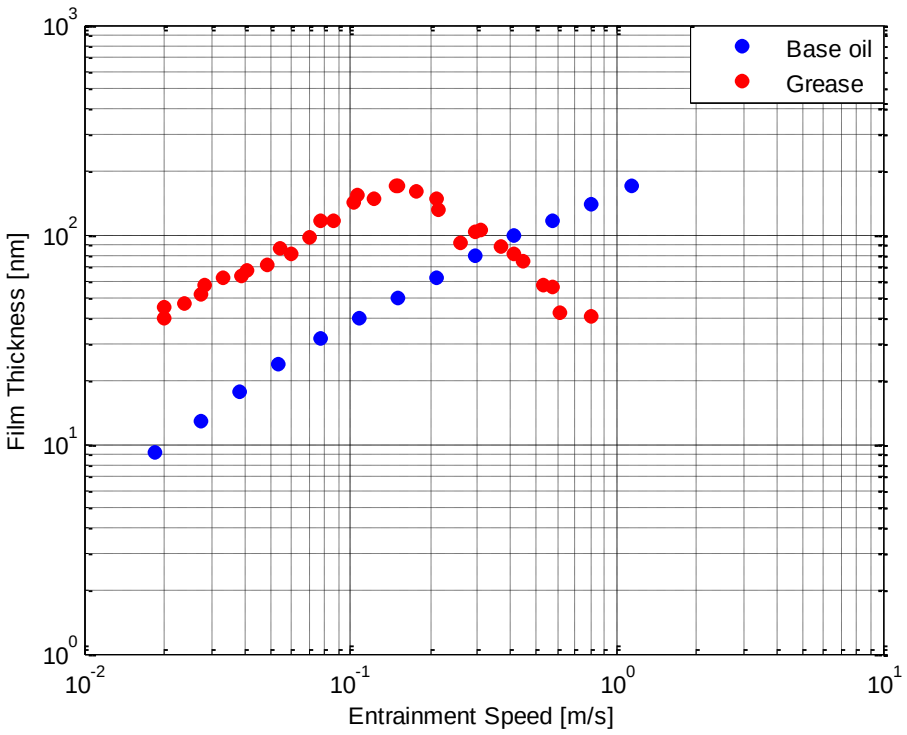

Figure 5.27: Film Thickness function of rolling speed for base oil and grease [126]

Before the beginning of study on the effect of lateral oscillations upon the film formation in grease lubricated contact, film thickness measurements of the base oil were performed under steady state conditions. Figure 5.27 illustrates a plot of the film thickness versus entrainment speed. As it can be observed from the graph, the film thickness of the base oil increases as the main entrainment speed increases and follows a power of law which can be presented as a straight line in log-log format. On the other hand, in the case of grease lubricated contact the film increases at low speeds and follows the same behaviour up to 0.15 m/s as the base oil. Then, at higher speeds (about 0.37 m/s), the film thickness starts to decrease with increasing the rolling speed as starvation starts to occur. This phenomenon has been shown before by many researchers [128, 129].

Another feature related to grease lubricated contact is that, the film thickness decreases significantly with time under steady state conditions. This can be seen in Figure 5.28, which illustrates the central film thickness variation over a period of 20 minutes under pure rolling conditions.

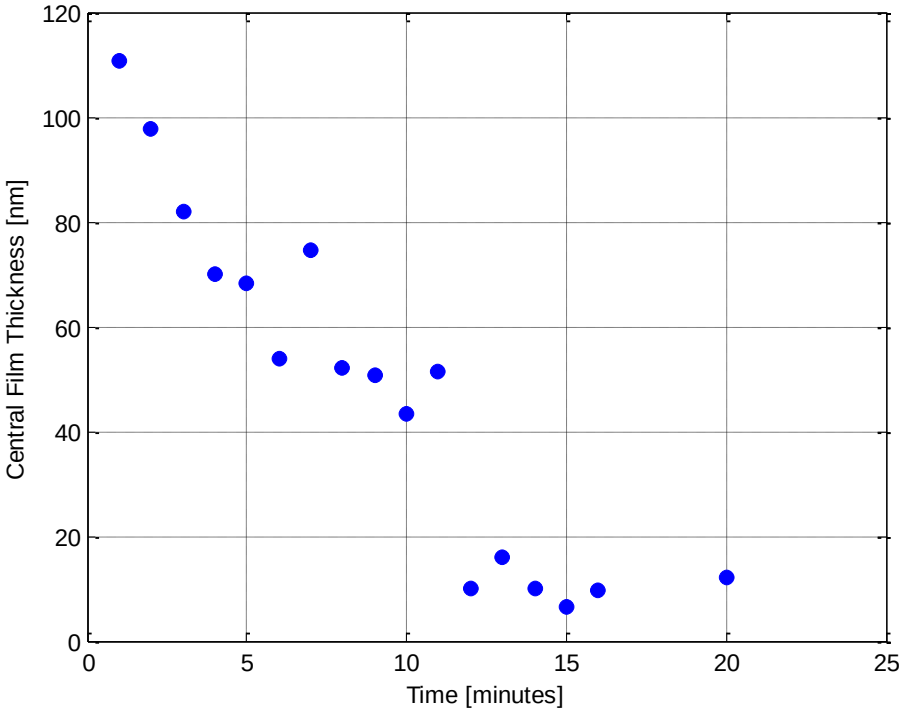

Figure 5.28: Grease Film Thickness evolution with time [126]

Initially, the film thickness measurements were taken under steady state condition for a period of 5 min at the constant main rolling speed of 0.5 m/s. Results showed that, when the contact was running under steady conditions after a period of time, it is clear that starvation occurs, as the track becomes depleted of grease and the interference image of the contact resembles a dry Hertzian contact.

After a five minutes period of running in steady state conditions the contact was subjected to lateral oscillatory motion. Figures 5.29(d) to (f) illustrate coloured interferograms taken at three stroke positions: extreme left, centre and extreme right, after the start of the lateral motion. The broken arrow indicates the direction of the lateral motion for this succession of images.

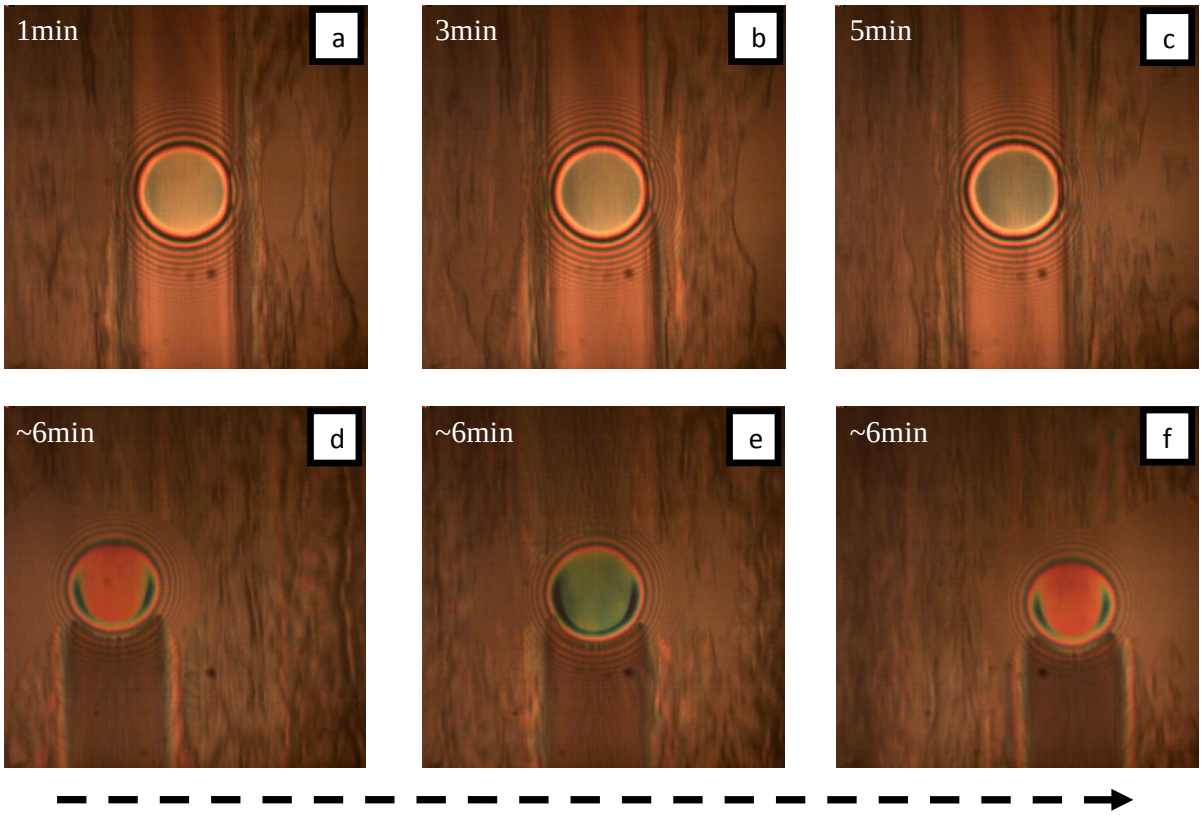

Figure 5.29: Grease Film Thickness decay and recovery under lateral oscillatory motion [126]

It can be observed that, as soon as the lateral motion starts, lubricant flows back to the track and fully flooded conditions occurred .Therefore , all the features of an EHD contact can be seen i.e. a typical horse-shoe-shaped film thickness distribution and the overall minimum value at the side lobes.

In addition, as seen in Figures 5.30(a) to (c), the averaged values of the central film thickness were extracted as a function of the position relative to the centre of the stroke. The film thickness values during the half cycle of lateral oscillating motion are shown.

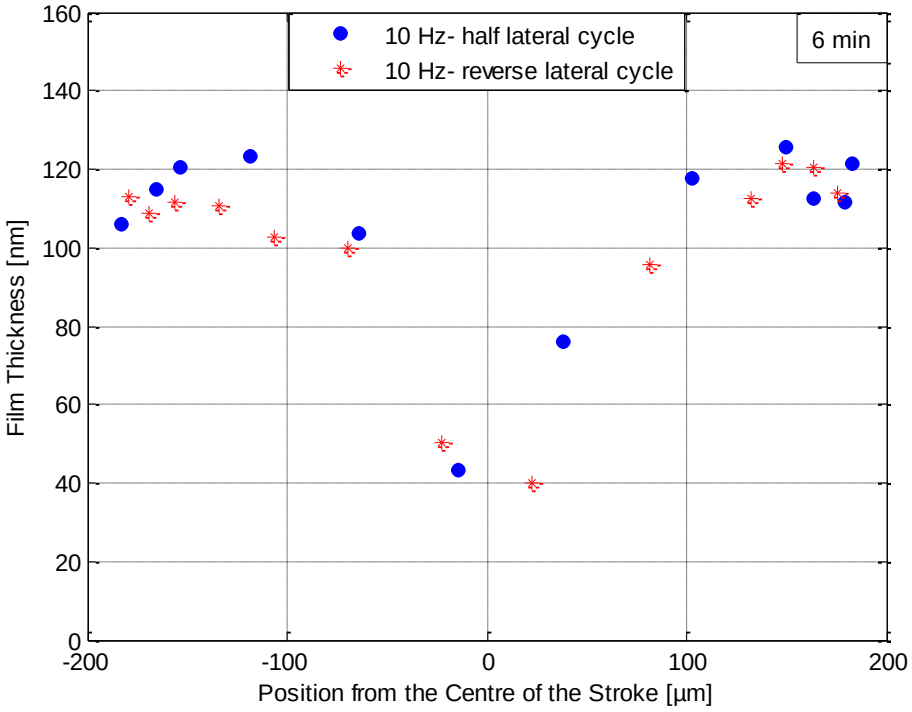

Figure 5.30(a): Central film thickness during a complete lateral cycle at 6 min [126]

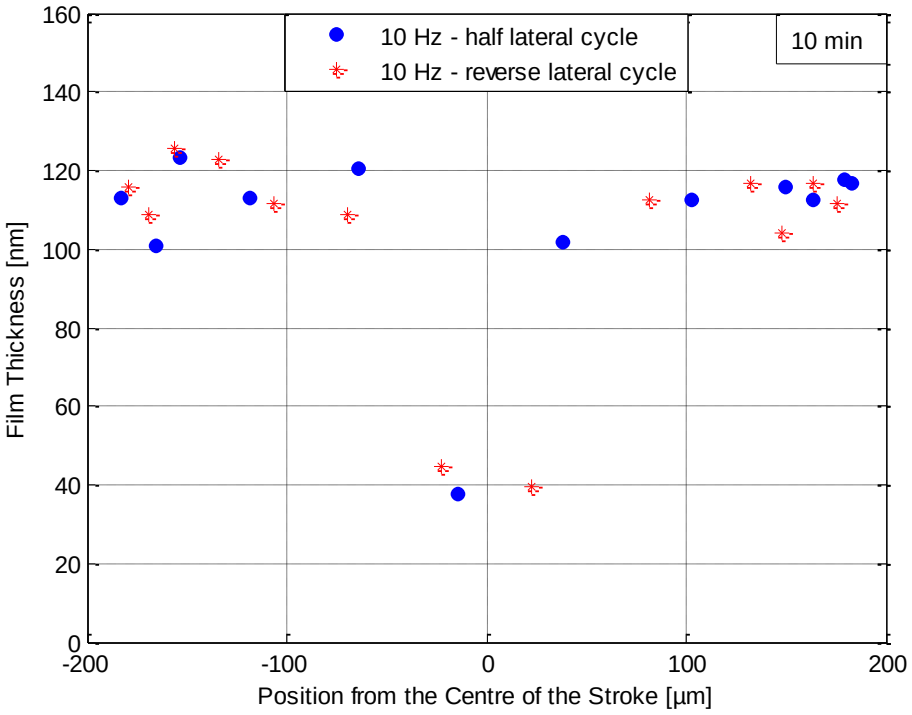

Figure 5.30(b): Central film thickness during a complete lateral cycle at 10 min [126]

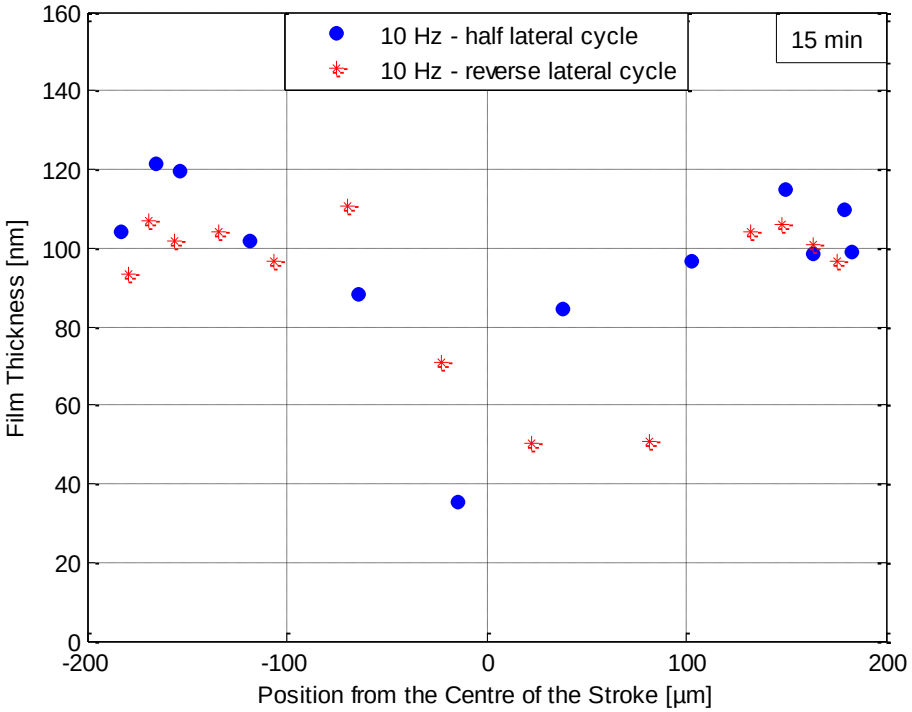

Figure 5.30(c): Central film thickness during a complete lateral cycle at 15 min [126]

It is observed from the graphs that, at the centre of the stroke the film thickness value was lower compared to those at the extreme positions. This could be explained by the fact that the rolled track area was depleted of oil during the first stage of the test which results a limited amount of lubricant in the inlet of the contact thus a minimum film thickness.

5.5.2 Analysis and Discussion of Results

Figures 5.30(d) to (f) revealed that the lateral oscillation is a replenishment mechanism which helps the lubricant flow back onto the rolled track preventing the starvation phenomena to settle in. Average values of the central film thickness function of time are shown in Figure

5.31. The averaged central film thickness values were extracted from the coloured interferograms as shown in Figure 5.30 (d) to (f) .In this graph, the film thickness was calculated as the averaged value during one period of lateral cycle. The central film for the base oil under pure steady state conditions is indicated with broken line.

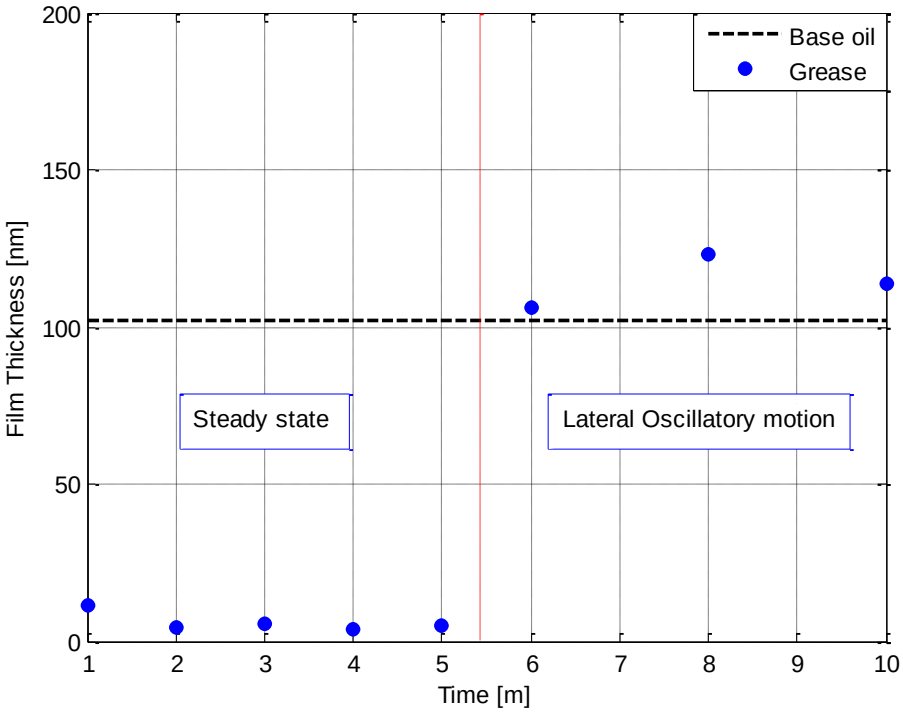

Figure 5.31: Central Film Thickness under steady state and transient conditions [126]

As seen in this plot, during steady state conditions, grease is squeezed out from the rolled track area and it takes some time to flow back onto the inlet; as a result the values of the film thickness are lower than that of the base oil. As soon as the lateral motion begins the film thickness increases to values above that of the base oil and remains relatively constant for periods of time far larger than 5 minutes shown in figure. It is obvious that lateral oscillatory motion is another mechanism which helps the lubricant to flow back to the contact area. Therefore, this leads to a much thicker film compared to the base oil values. However, this is

not the only mechanisms and there several factors which they can play an important role in the replenishment processes. These are:

- Surface tension
- Viscosity
- Quantity of lubricant
- Local surface properties

5.5.3 The effect of working parameters upon grease film behaviour under lateral oscillations

The results shown in the previous chapter were obtained for amplitude of the lateral motion much larger than the contact diameter. This is not always the case for rolling element bearings, where amplitudes of vibrations may be well smaller than the contact diameter. For this reason, tests were carried out in order to explore the effect of the working parameters, such as stroke length and frequency upon the behaviour of the grease film. These experiments were also carried out in common with my colleague Yuichiro Nagata, but have not been published in his thesis. My contribution to this part of the study was seventy percent.

In these experiments the contact was formed between a glass disc and steel ball at a load of 20 N. The contact diameter was about 270 μm.

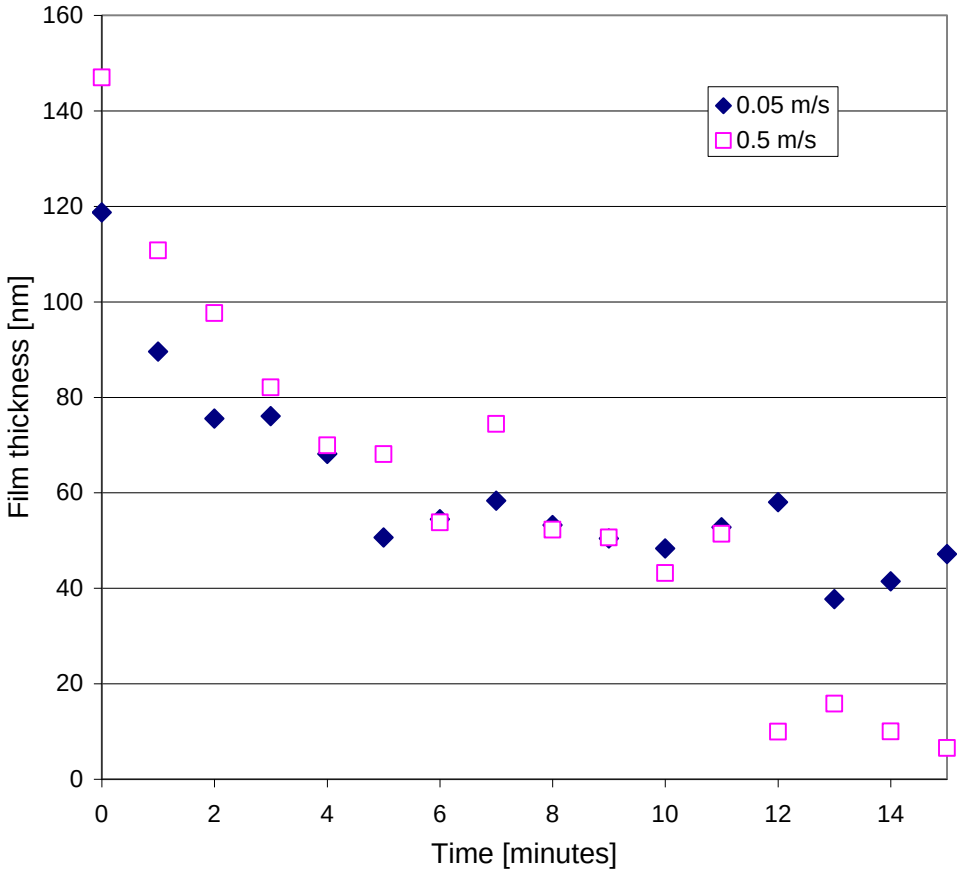

Figure 5.32: Variation of central film thickness with time at two different speeds

Steady state lubricant film thickness for two speeds is shown in Figure 5.32. It can be seen that at 0.05 m/s the film thickness stabilized at about 50 nanometres, 5 minutes after the start of the test, while at a speed ten times greater it stabilizes after about 11 seconds, but at a much lower film thickness of around 10 nanometres. For comparison to be noted that the central film thickness, for the base oil in these conditions is 108 nanometres at 0.05 m/s and 289 nanometres at 0.5 m/s. This implies that only partial replenishment of the track takes place. The replenishment time calculated according to reference [130] is given by:

$$t_r = \frac{\eta_0 a}{\sigma_s} \tag{5.1}$$

where η_0 is the viscosity of the base oil, at the temperature of the test, a is the width of the track and σ_s is the surface tension of the oil. Taking a viscosity of 0.073 Pa·s and a surface tension of 30 mN/m, for a track width of 270 nm the replenishment time becomes 0.6 ms. This is much smaller than the time between two passes over the same track location of the ball, which even for 0.5 m/s is about 0.5 seconds. It is possible that the soap structure of the grease does not release the oil at a rate which would allow complete replenishment of the track.

As it was shown in [126] once the lateral oscillations start, it is expected that the lubricant contained in the side ridges to be brought back onto the track and restore full film conditions. In order to evaluate the effect of the various parameters upon this process the present tests were carried out at stroke lengths that span a range from smaller than the contact radius to larger than contact diameter. Figure 5.33 (a), (b), and (c) show the variation of the central film thickness at a stroke length of 50 μm and three frequencies for 0.05 m/s, 0.1 m/s and 0.5 m/s main rolling speeds, respectively. The measurements were taken at the centre of the stroke, although calculations of the film thickness at the ends of the stroke showed nearly identical trend. For comparison, the steady state film thickness for the base oil and for the grease is also shown. Evidently the base oil film thickness is constant with time. As seen in Figure 5.33(a) the central film thickness for grease is larger than that of the base oil, at the beginning of the test, probably due to lumps of thickener passing through the contact. However, the film thickness, in steady state conditions decreases with time and eventually stabilizes at around 50 nm. The start of the lateral motion, at 5 minutes after the beginning of the test does not change significantly the behaviour of the film, although a slight increase of the average film thickness at the largest frequency of 100 Hz can be observed. This may not

be entirely due to replenishment of the track but also to the fact that at this frequency the lateral speed is maximum.

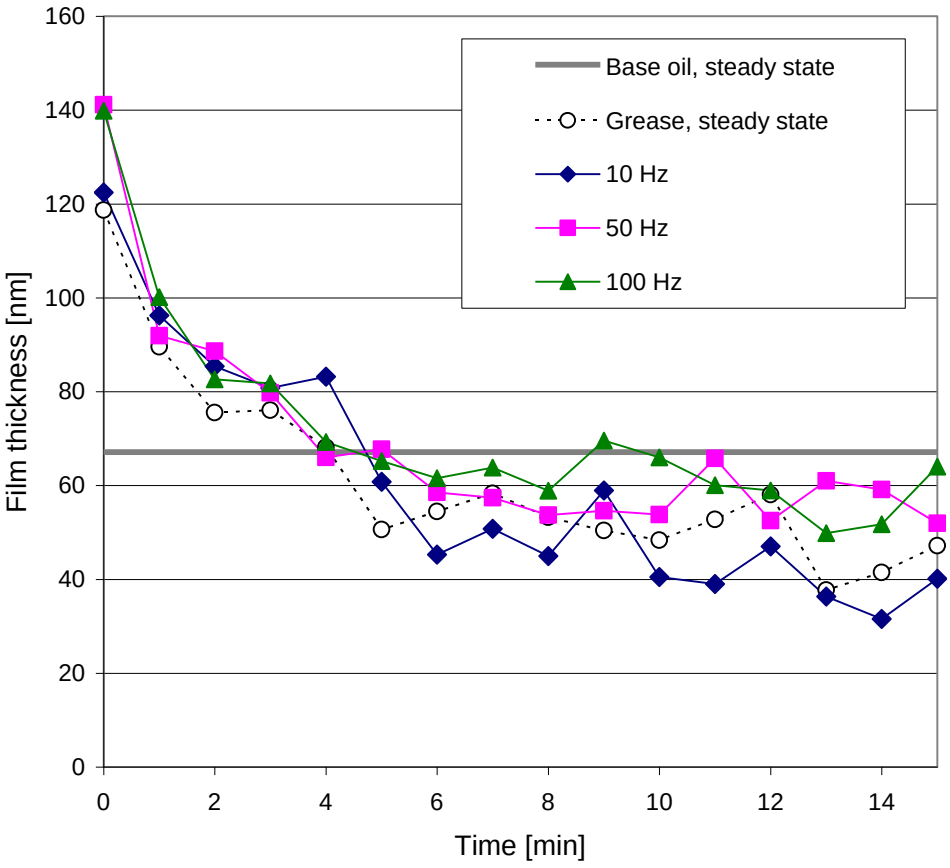

Figure 5.33(a): Film thickness variation for 0.05 m/s and 50 μm stroke length

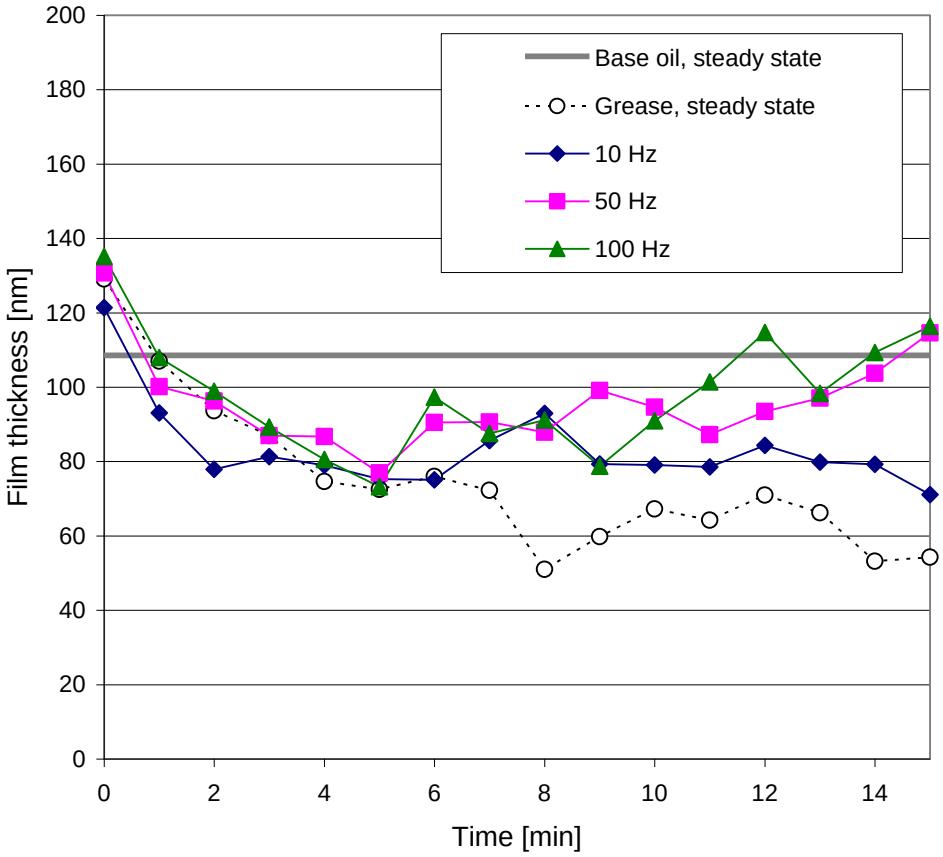

Figure 5.33(b): Film thickness variation for 0.1 m/s and 50 µm stroke length

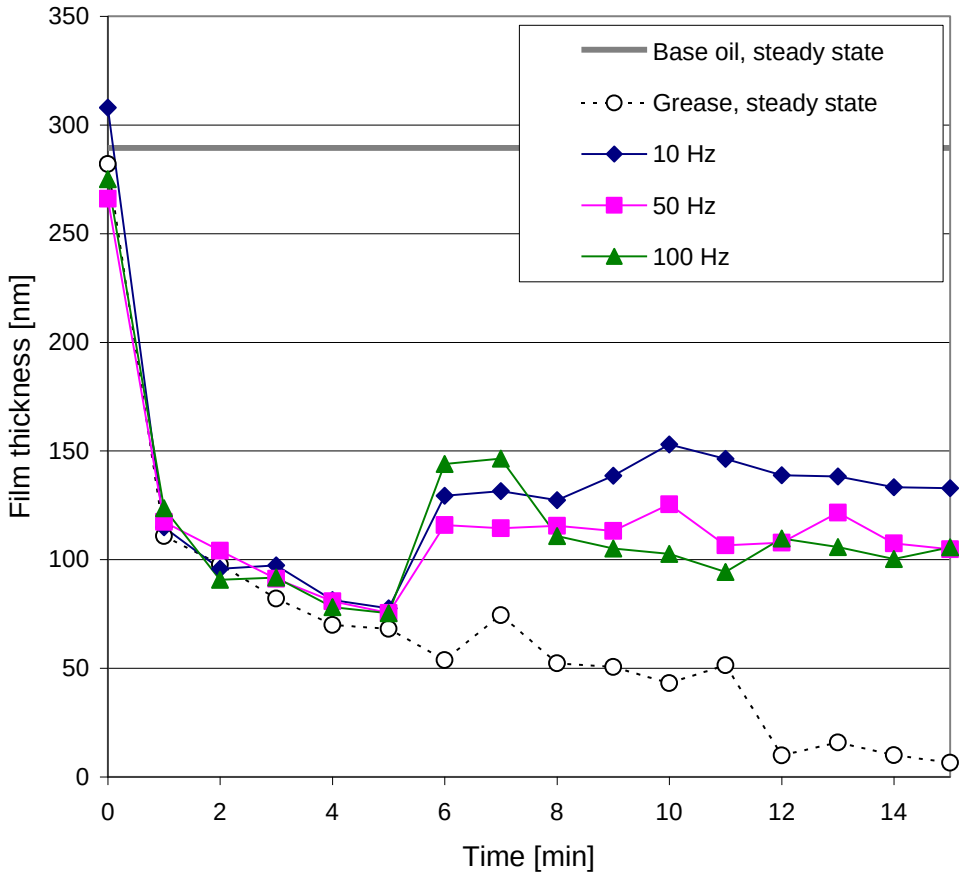

Figure 5.33(c): Film thickness variation for 0.5 m/s and 50 µm stroke length

As seen, although the film thickness does not approach the values of the base oil, there is still a marked increase once the oscillatory motion starts. It may be possible that at this speed centrifugal forces help spread the oil from the inside ridge back onto the track.

The tests with increasing stroke length, of 350 µm are shown in Figures 5.34(a), (b) and (c).

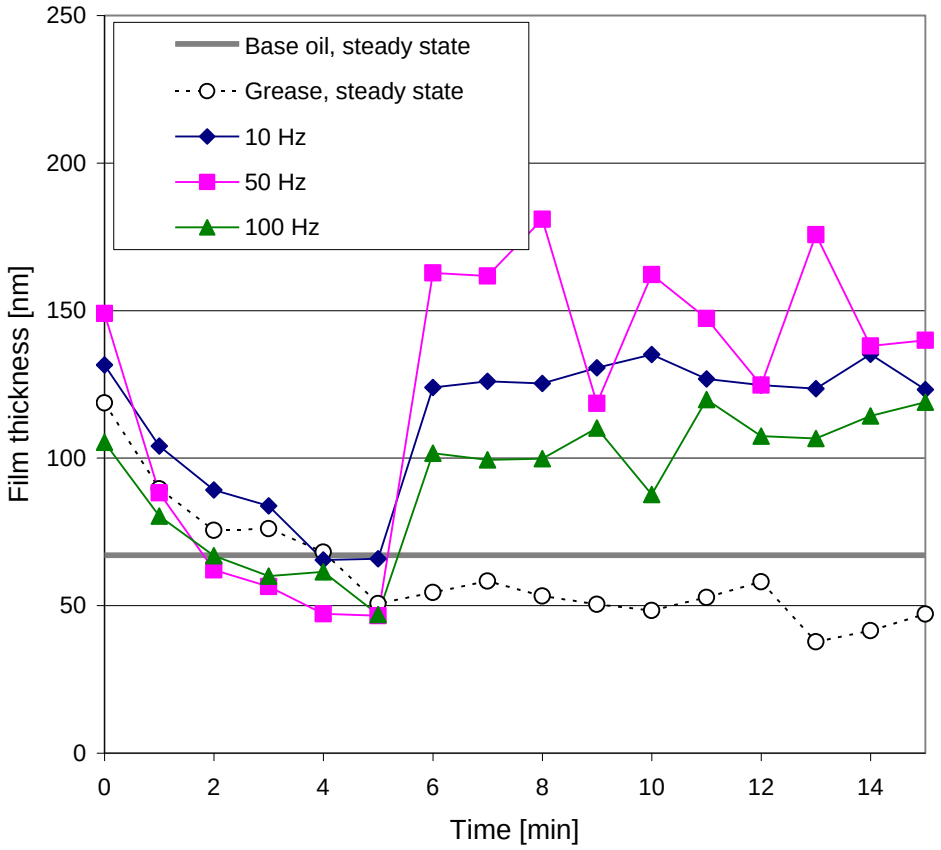

Figure 5.34(a): Film thickness variation for 0.05 m/s and 350 μm stroke length

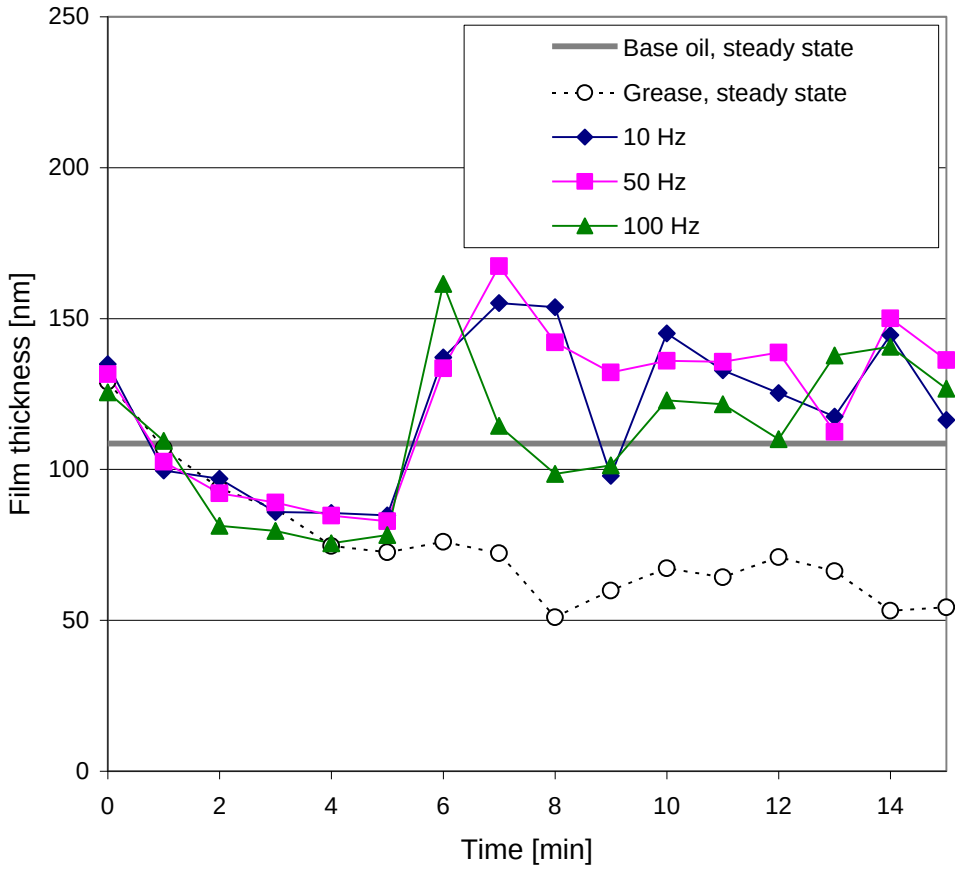

Figure 5.34(b): Film thickness variation for 0.1 m/s and 350 µm stroke length

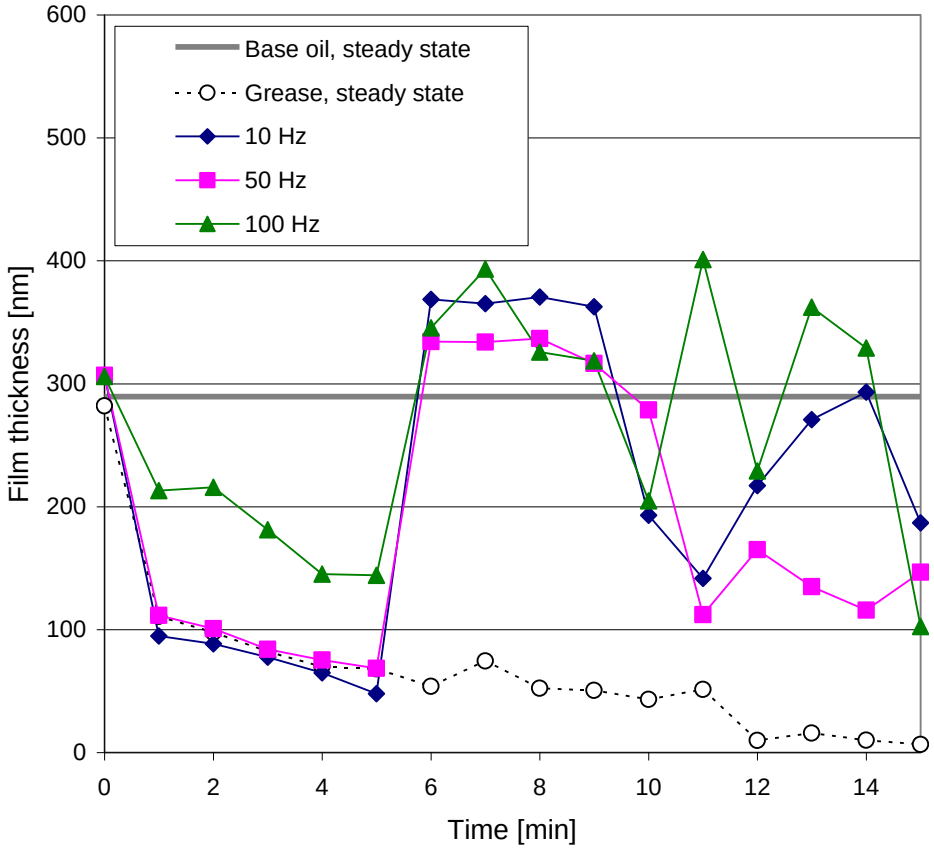

Figure 5.34(c): Film thickness variation for 0.5 m/s and 350 μm stroke length

If for the shorter stroke length the lateral oscillations diminish the severity of starvation, in case of a stroke length larger than the diameter of the contact the recovery of film thickness to values corresponding to those of the base oil is complete. Moreover rolling speed of 0.05 m/s and 0.1 m/s the film thickness under oscillations exceeds the base oil, steady state values. For 0.5 m/s, that is for entrainment speed much larger than the speed of the lateral oscillations, the film thickness recovers to values above those of the base oil for about 5 minutes then oscillates around a value lower than the base oil, but still at least twenty times larger than the pure rolling conditions, for grease. Variations of film thickness even in steady state conditions are typical to greases, due to their semi-solid consistency. It is possible that worked thickener adheres to the contacting surfaces, randomly and does not allow consistent

and constant flow of the base oil back onto the track, thus at some moments the contact is only partially flooded. Obviously, at larger rolling speed, there is less time between two successive passages of the ball over the same point on the disc, thus the more pronounced this effect is. Figure 5.35 shows an image of the contact which reveals the uneven distribution of the film thickness over the contact area.

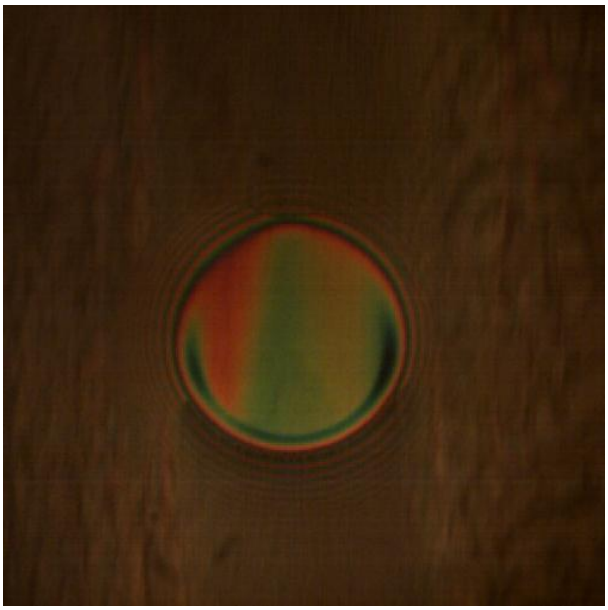

Figure 5.35: Uneven distribution of film thickness over the contact area

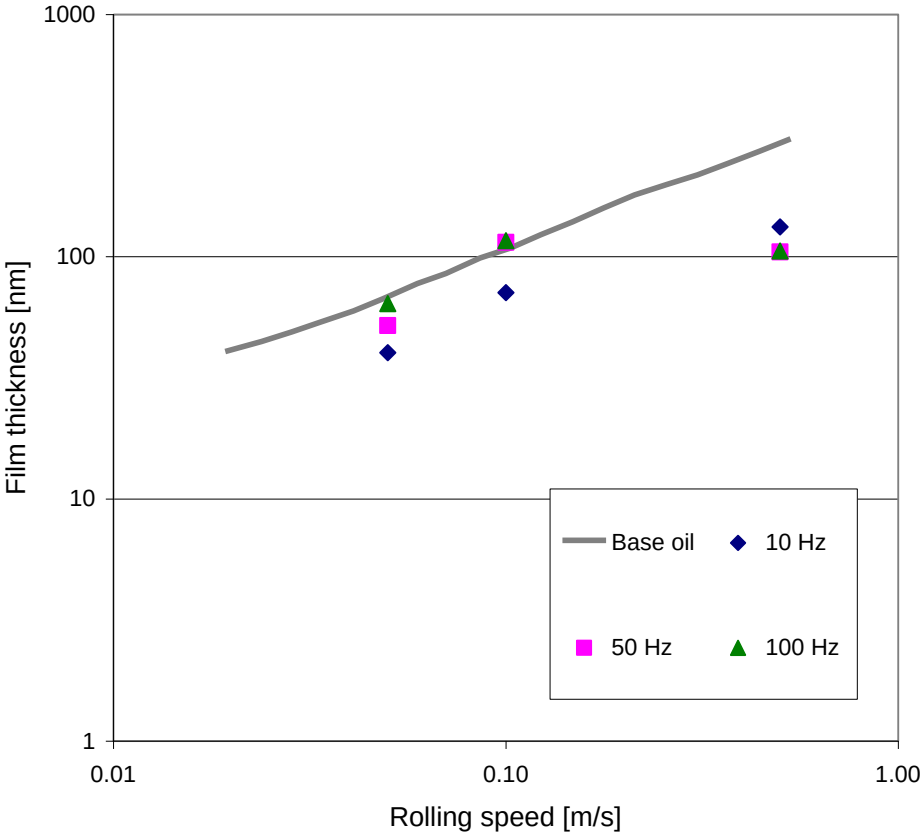

Figure 5.36(a): Effect of rolling speed upon film recovery at 50 µm stroke length

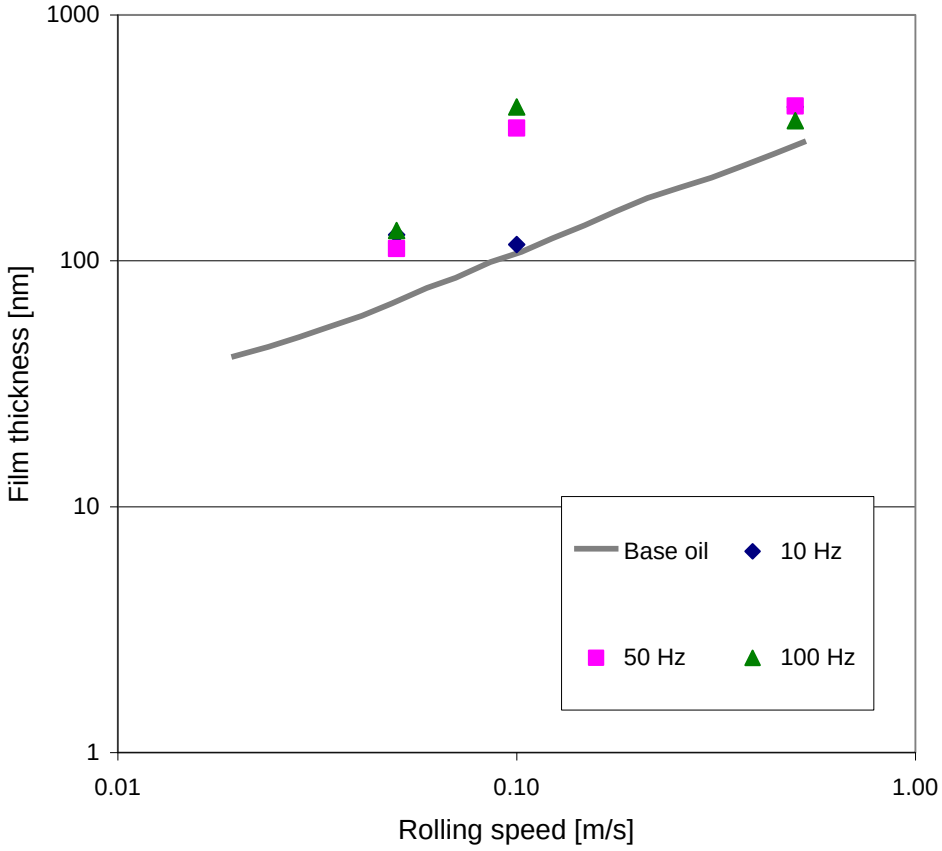

Figure 5.36(b): Effect of rolling speed upon film recovery at 350 μm stroke length

It is clear that the amplitude of the lateral oscillations play an important role on the replenishment mechanism, although a simple, unique mathematical function to describe this dependence is not possible to find, for all working conditions. By analyzing these figures it can also be seen that increasing the rolling speed increases the film thickness only at low values of this parameter; for 0.5 m/s rolling speed the film thickness under lateral oscillations is approximately equal to that obtained at 0.1 m/s. This is shown in Figures 5.36a and b. The base oil film thickness variation with entrainment speed appears as a straight line in the logarithmic representations in these figures.

The recovery of the grease EHD film thickness under lateral oscillations of the contact has an important practical application in rolling element bearings. These widely used machine elements are very often subjected to vibrations generated by the machine or mechanism they are part of, or transmitted from the surroundings. It is also know that most often the rolling bearings are packed with grease and sealed for the entire working life. It would be expected that in the absence of some replenishment mechanisms, the bearing's contacts to become starved after a few number of revolutions and thus the probability of bearing failure to be high. However, this does not normally happen and rolling bearings survive the designed life, which supports the idea that apart from surface tension there are other mechanisms which replenish the contact; vibrations can be one of those mechanisms.

CHAPTER 6: EHD Films subjected to Vertical Vibrations

In this chapter, the behaviour of EHD films subjected to vibrations taking place on a direction perpendicular to the contact has been examined. The EHD film studied was established under a constant load and thereafter this load was varied in a controlled, sinusoidal fashion, thus a forced vibration system was obtained.

6.1 Results of Film Thickness under vertical vibrations

6.1.1 The effect of frequency

The experiments have been performed at three working frequencies, 10 Hz, 20 Hz, and 50 Hz, in pure rolling conditions. The base oil studied was PAO4, with the properties shown in chapter 4. The temperature of the tests was 30 ˚C, and the speed in the range between 0.05 m/s to 2 m/s. Figures 6.1 presents a typical behaviour of the EHD contact subjected to vertical vibrations at a frequency of 10 Hz and at a lowest entraining speed of 0.05 m/s. In this case, 250 images were recorded corresponded to a complete loading –unloading process. Due to the clarity of images only 32 images are presented, taken at different period of oscillation. The complete period (loading-unloading period) where the EHD contact was subjected to vertical oscillations at that particular frequency was 100 ms. The loading period corresponds to frames from No.1 to No.20 and the unloading process from No.21 to No.32. The load varied between a maximum value of 40 N (P_H ~ 0.68 GPa) and a minimum load of 3 N (P_H ~ 0.28 GPa).

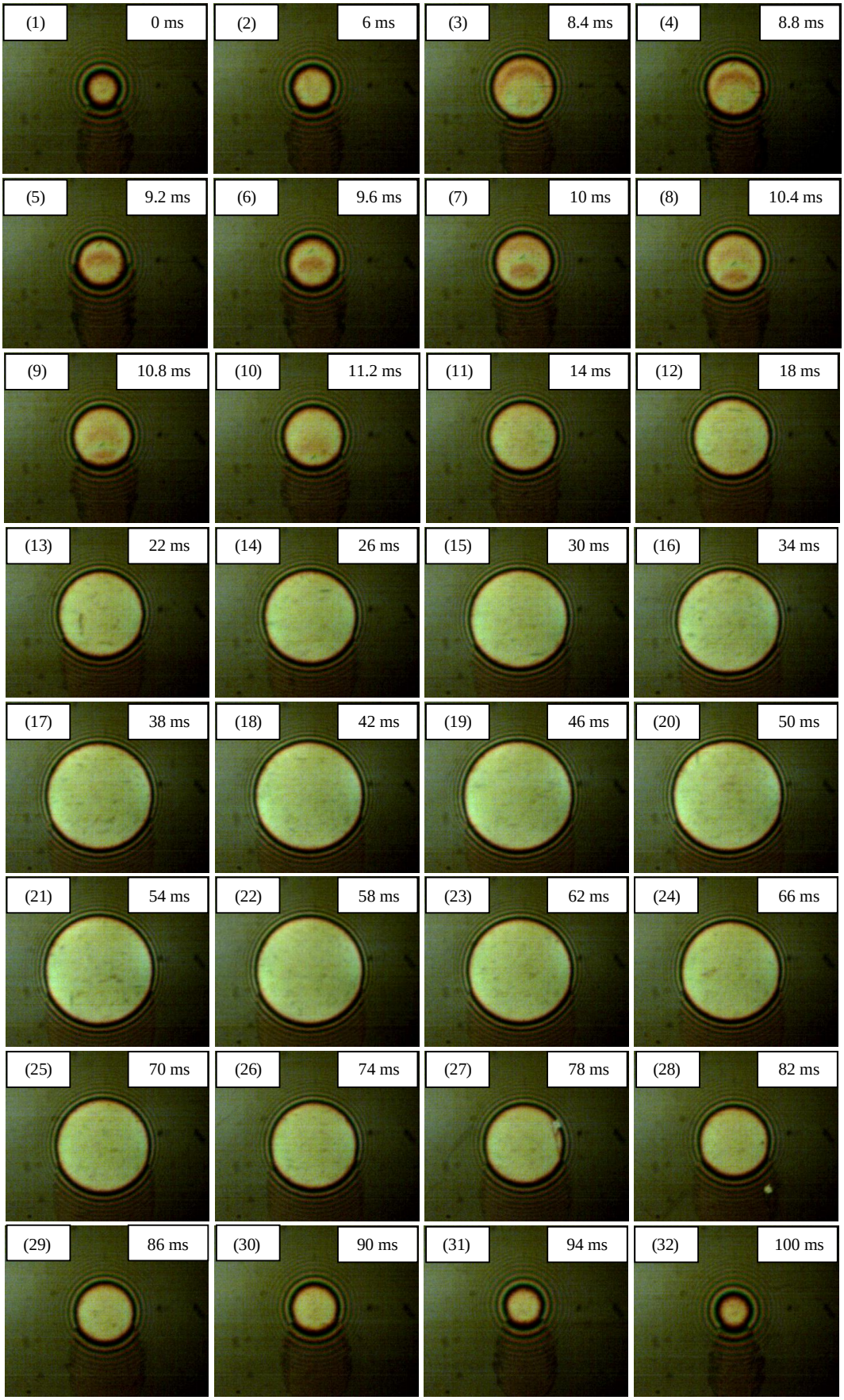

Figure 6.1: Typical Behaviour of an EHD contact subjected to vertical vibrations at 10 Hz

In the current investigation, in order to correlate the film thickness extracted from the images captured by the CCD camera with the values of the load, recorded by the oscilloscope, the two instruments were synchronised by the same triggering signal from the PC. This signal consisted of the transition from high (5 V) to low (0 V) of a TTL signal supplied by the digital section of a AD board in the PC. Figure 6.2 illustrates the dynamic load applied between the solid surfaces while the film thickness variation during a complete cycle of oscillation is shown in Figure 6.3.

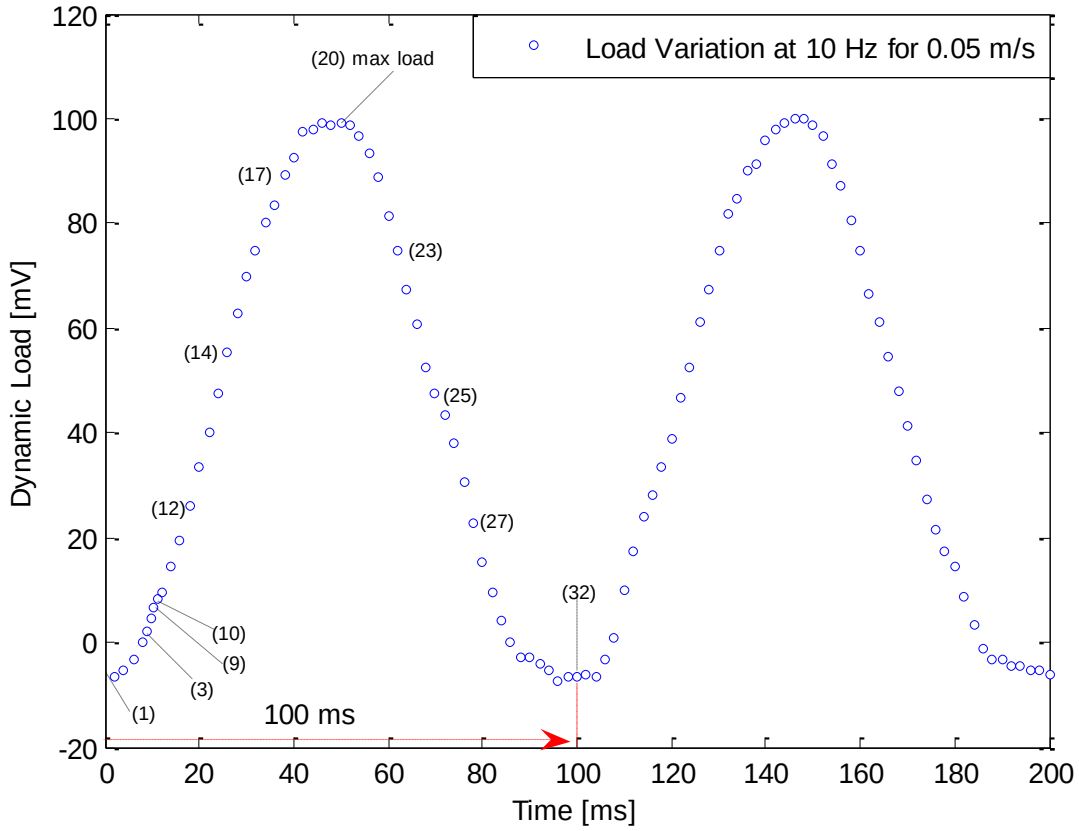

Figure 6.2: Load Variation at 10 Hz for 0.05 m/s

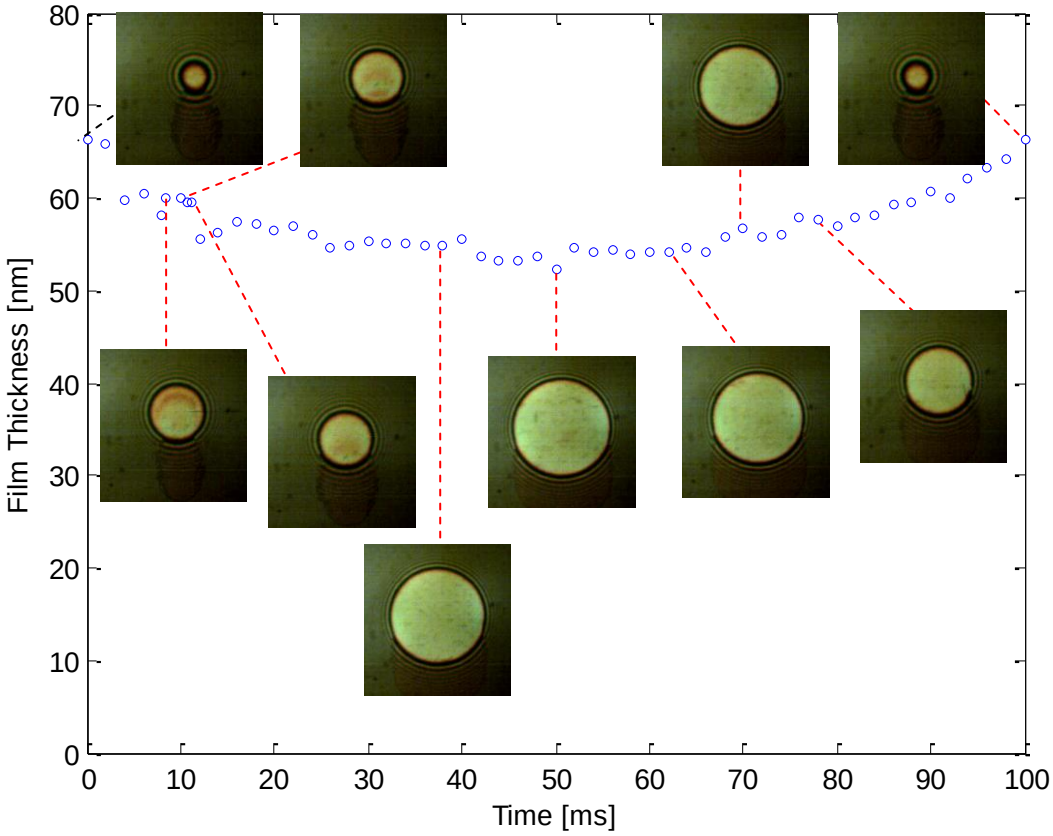

Figure 6.3: Film Thickness variation and coloured interferograms during loading-unloading phase at 10 Hz for 0.05 m/s

The central film thickness was extracted from the images (Figure 6.1) at different intervals during the loading and unloading phase. Fluctuations in the film, of a crescent shape, can be observed during the oscillation period from 0 ms to 10 ms. During this interval fluctuations of the applied load can also be detected by changes of the diameter of the contact, which does not increase continuously as expected. It is known that the EHD film thickness is established in the inlet of the contact. In the present case, due to load variation the film thickness will depend on a combination of squeeze effect and on the entraining speed. An increase of load as seen in Figure 6.3 at 8.4 ms has an effect of rapidly increasing the contact diameter and at the same time modifies the convergence in the inlet. Thus, in turn a thicker film is produced

at the inlet periphery of the initial contact zone. Once formed at the inlet the lubricant film travels unchanged through the contact as the condition of continuity of flow must be met. As in this case the contact diameter changes continuously, it is difficult to evaluate the exact speed at the perturbations travel across the contact, but in the absence of wall slip this speed is equal to the average speed of the surfaces. After this period of instability, the thickness of the film changes very little, as the load increases to its maximum value. The film thickness during the unloading phase increases again but without obvious perturbations. As the EHD film thickness depends only little of the load, it can be assumed that this increase is due to the fact that at very low loads, there is insignificant elastic deformation of the surfaces and the contact works rather in the hydrodynamic regime.

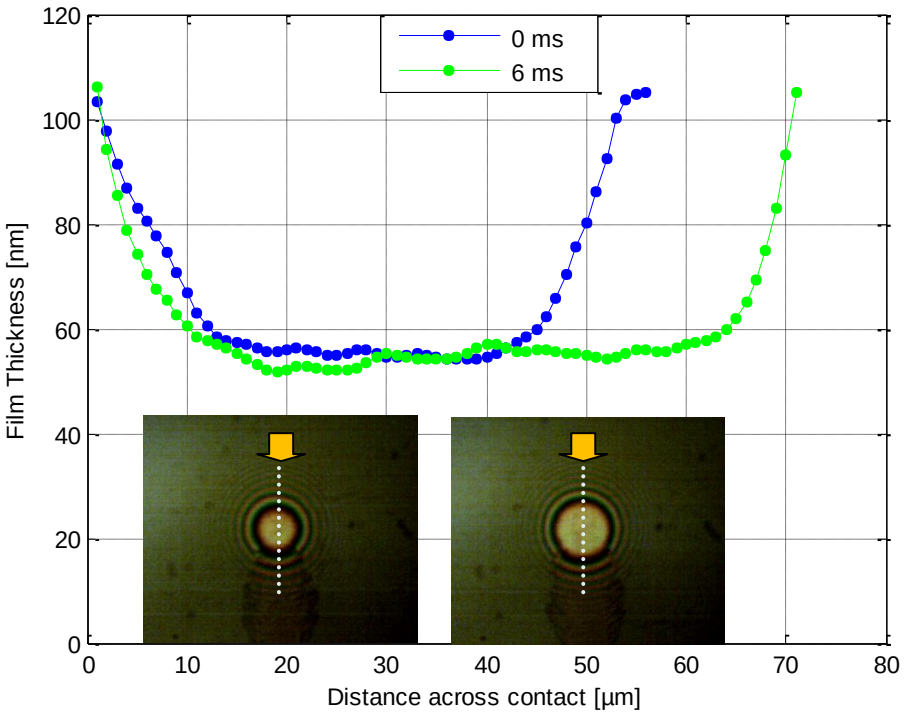

Figure 6.4(a): Coloured interferogram and Film Thickness profile at 10 Hz for 0.05 m/s (0 ms – 6ms)

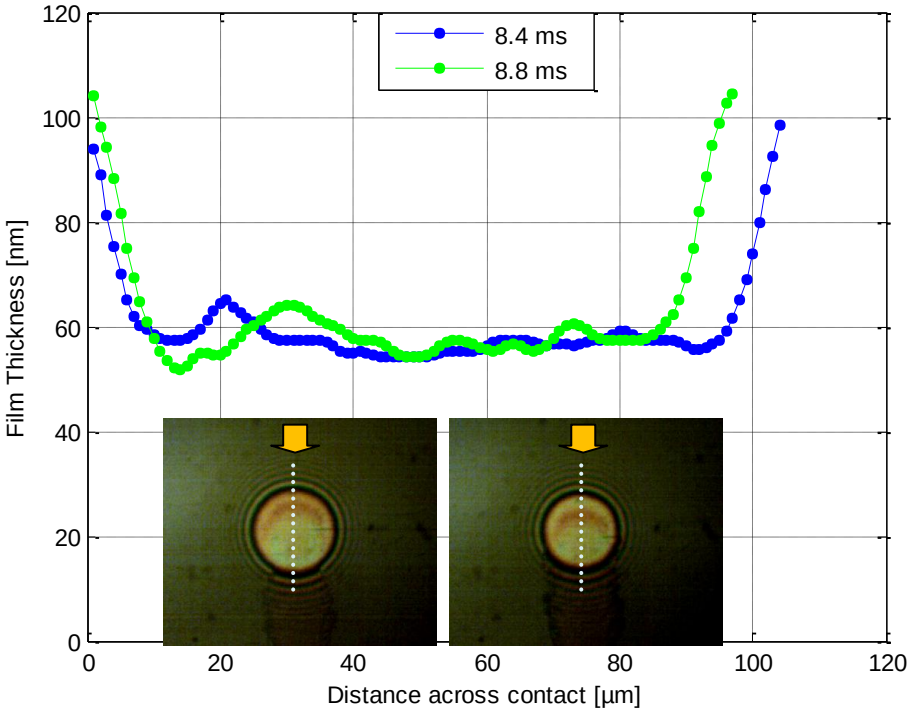

Figure 6.4(b): Coloured interferogram and Film Thickness profile at 10 Hz for 0.05 m/s (8.4 ms – 8.8 ms)

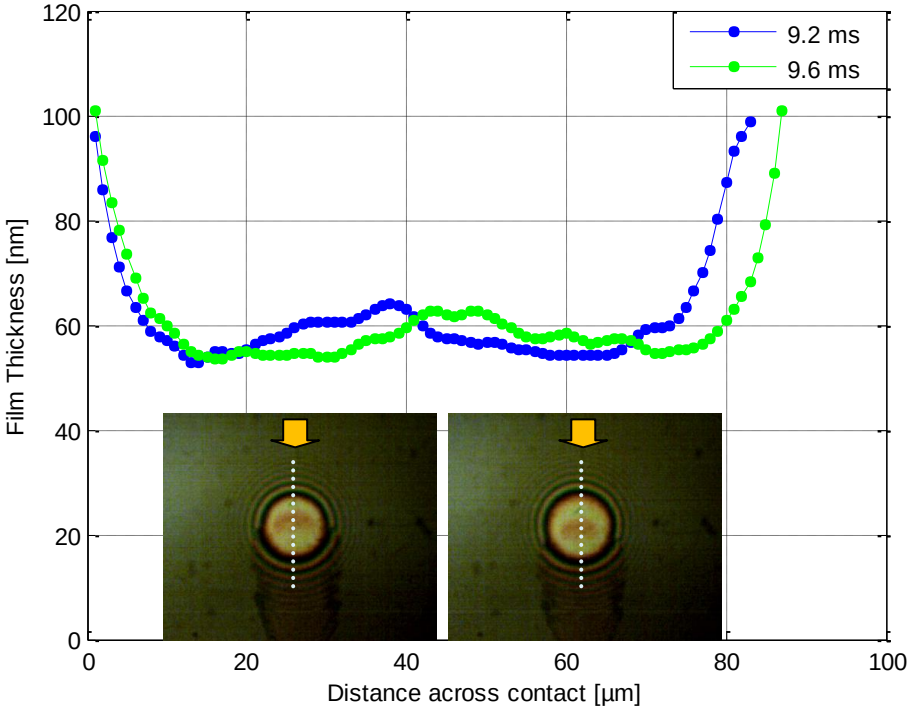

Figure 6.4(c): Coloured interferogram and Film Thickness profile at 10 Hz for 0.05 m/s (9.2 ms – 9.6 ms)

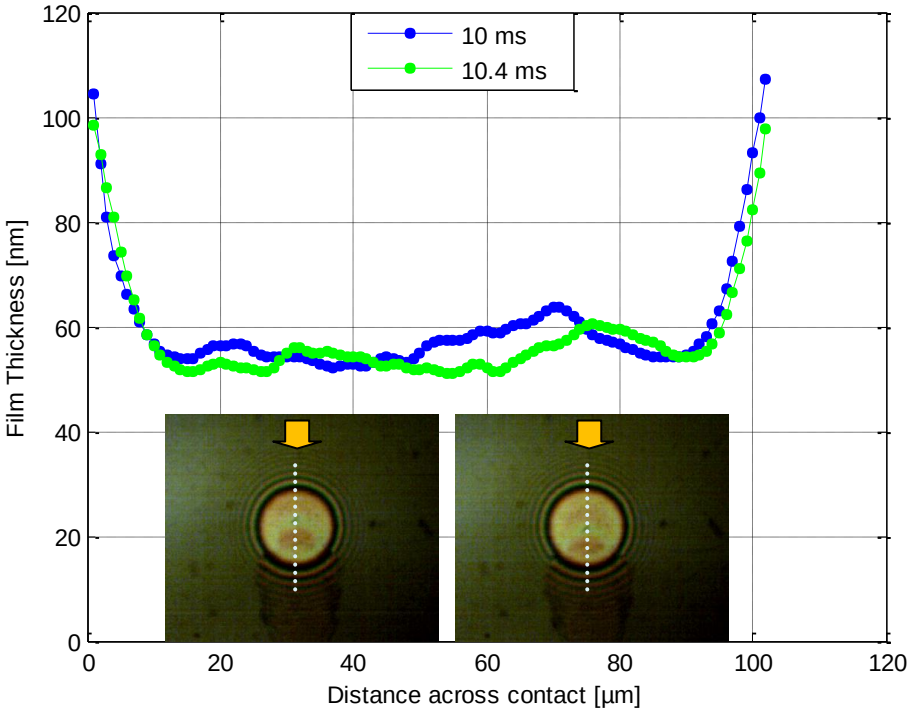

Figure 6.4(d): Coloured interferogram and Film Thickness profile at 10 Hz for 0.05 m/s (10 ms – 10.4ms)

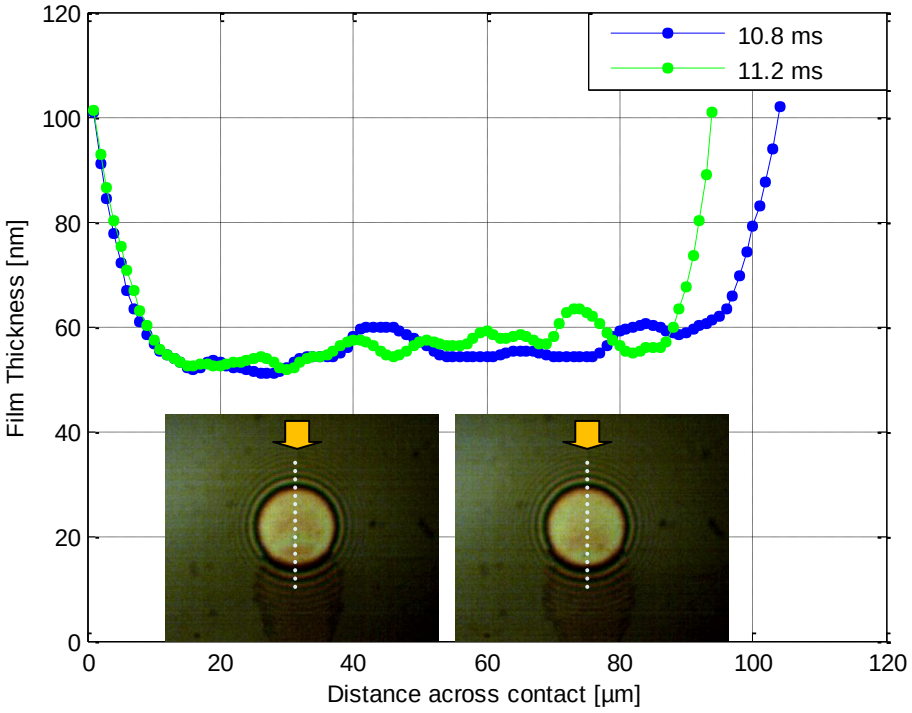

Figure 6.4(e): Coloured interferogram and Film Thickness profile at 10 Hz for 0.05 m/s (10.8 ms – 11.2 ms)

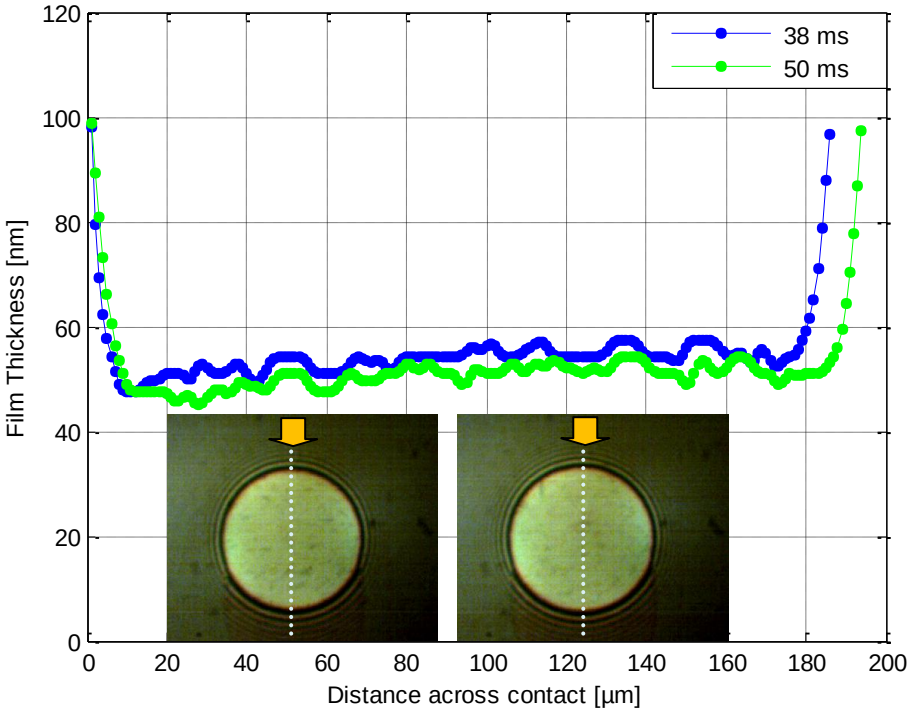

Figure 6.4(f): Coloured interferogram and Film Thickness profile at 10 Hz for 0.05 m/s (38 ms, 50 ms)

In order to better visualise the film behaviour, thickness profiles at different time locations during the cycle have been extracted from the interferograms. These are shown in Figures 6.4 (a) to (f). The entraining direction is shown by the large arrow while the broken line indicates the direction from which the film profile has been taken from. The fluctuations in the film thickness during the initial stage of the loading period i.e. 8.4 ms to 8.8 ms, was between 52 nm and 65 nm which is a variation of about 25 percent. It has to be mentioned that the amplitude of the wave of film perturbation decreased with time. This can be observed in the images recorded from 9.2 ms to 9.6 ms (Figure 6.4(c)). During that time, the film variation was about 9 nm to 11 nm. This slight decrease in the amplitude of the perturbation may be attributed to the side flow of the lubricant, which is enhanced as the load continues to increase. As seen in the next images taken at 10 ms to 10.8 ms a new increased film wave is

formed in the inlet, as illustrated in Figure 6.4(d). In this case, the peak to valley variation was roughly 5 to 12 nm. Thereafter as shown in Figure 6.4(e) at 11.2 ms the crescent shaped thick film passes through the EHL conjunction and moves towards the exit of the contact. For the rest of the loading period no significant fluctuations in the film have been detected.

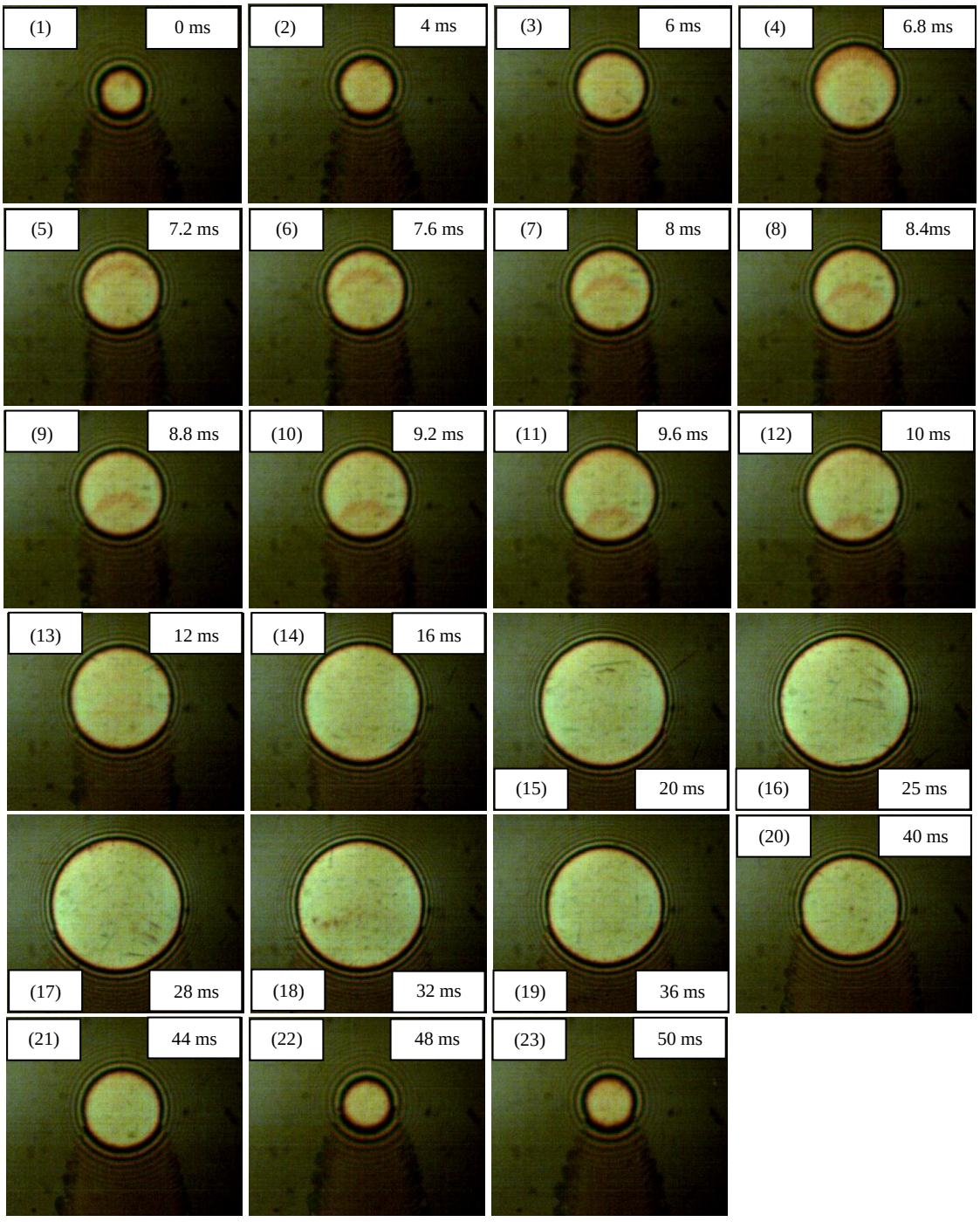

Figure 6.5: Typical Behaviour of an EHD contact subjected to vertical vibrations at 20 Hz

For 20 Hz tests, 128 images were captured for a complete period of the oscillatory motion. However, as illustrated in Figure 6.5 only 23 images are shown during the loading and unloading process.

In this case, periods of loading unloading were 25 ms. The first frame represents the initial load which is about 5 N (P_H ~ 0.33GPa) while the maximum load can be found at 25 ms corresponded to 51 N (P_H ~ 0.72GPa). It can be noted that the minimum load achievable was 5 N, which is larger than the value obtained at 10 Hz. This is a limitation of the loading system, which ultimately did not allow tests at frequencies larger than 50 Hz. The dynamic applied load for 20 Hz tests and the film thickness variation during the loading and unloading phases are shown in Figures 6.6 and 6.7.

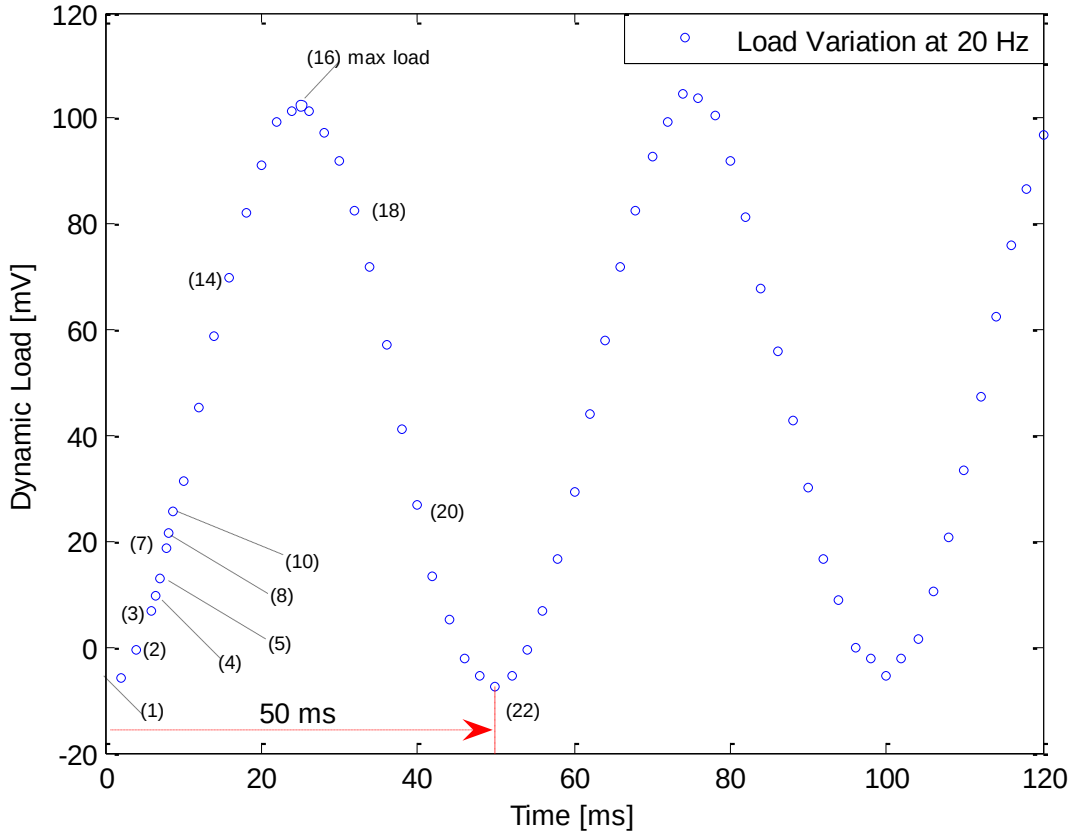

Figure 6.6: Load Variation at 20 Hz for 0.05 m/s

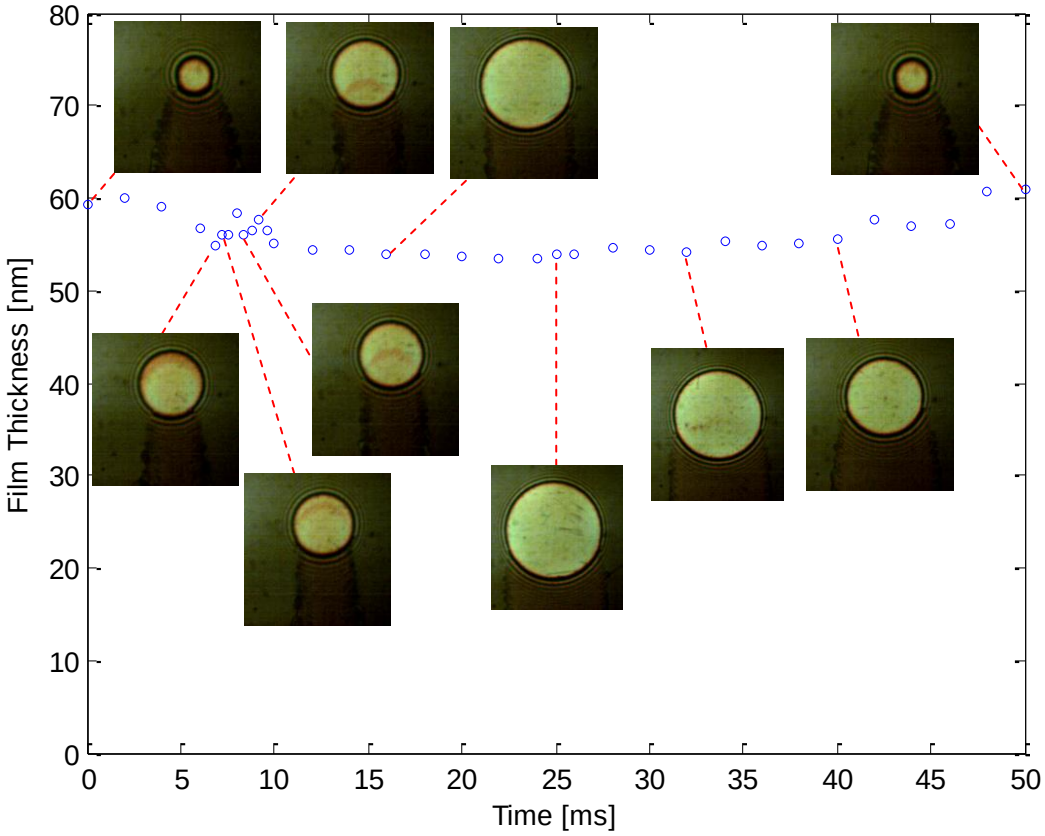

Figure 6.7: Film Thickness variation and coloured interferograms during loading-unloading phase at 20 Hz for 0.05 m/s

By comparing these results with those obtained at 10 Hz two main differences can be observed. Firstly the time instant when the crescent shaped enhanced film was earlier than in the lower frequency case, 6.8 ms in comparison to 8.4 ms. This is probably due to the larger rate of change of load 1.84 kN/s for 20 Hz and 0.74 kN/s for 10 Hz tests. The second feature is unexpected, as the film thickness fluctuation is no greater for the larger frequency. As seen in Figure 6.7 there is relatively little variation of the average film thickness in the contact, during one cycle of loading – unloading. It is suggested that, if local film fluctuations are ignored, the squeeze effect acts to cushion (dampen) the effect of load variation, affect which

is more pronounced at greater frequencies. One can also point at the fact that the contact was less unloaded in the case of larger frequency tests.

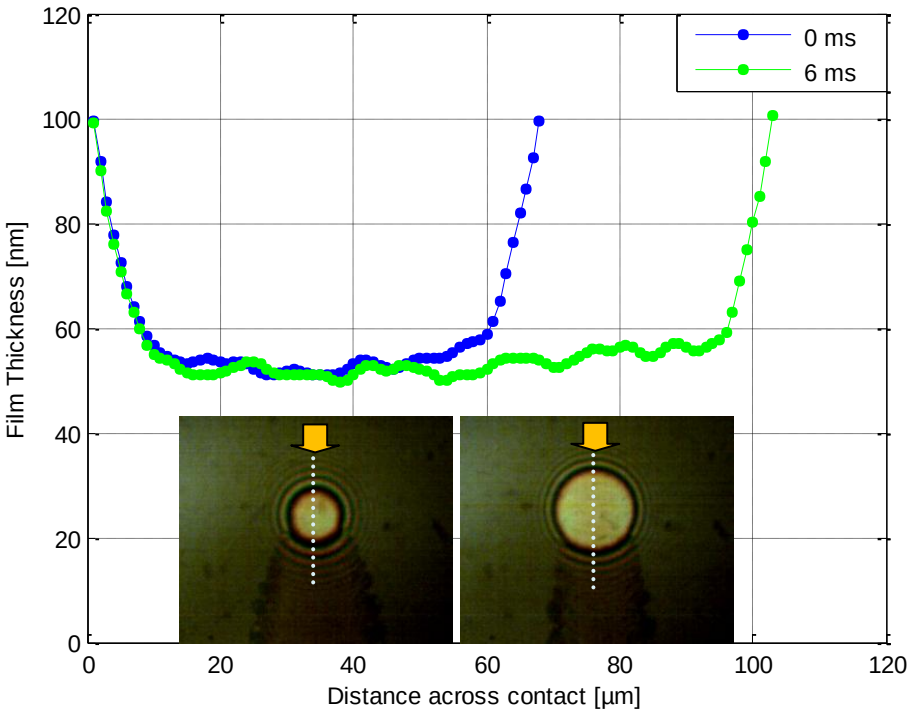

Figure 6.8(a): Coloured interferogram and Film Thickness profile at 20 Hz for 0.05 m/s (0 ms – 6 ms)

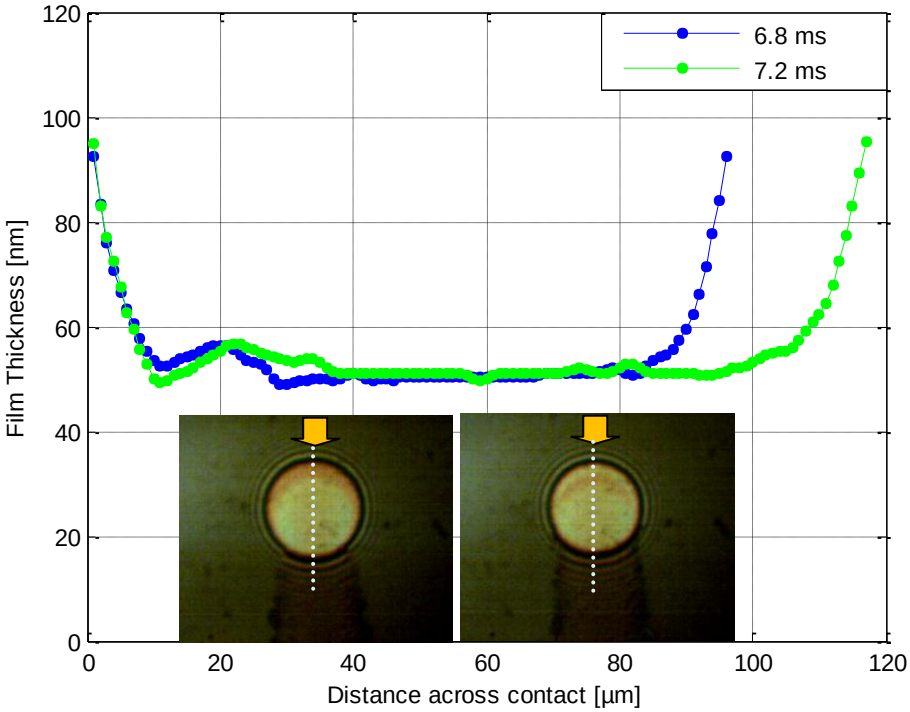

Figure 6.8(b): Coloured interferogram and Film Thickness profile at 20 Hz for 0.05 m/s (6.8 ms – 7.2 ms)

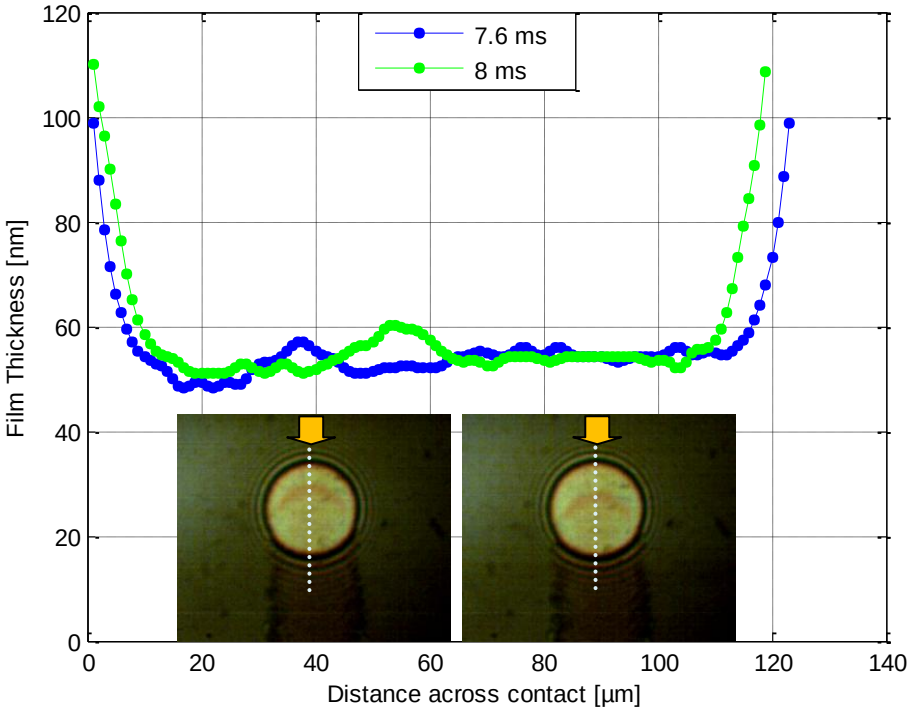

Figure 6.8(c): Coloured interferogram and Film Thickness profile at 20 Hz for 0.05 m/s (7.6 ms – 8 ms)

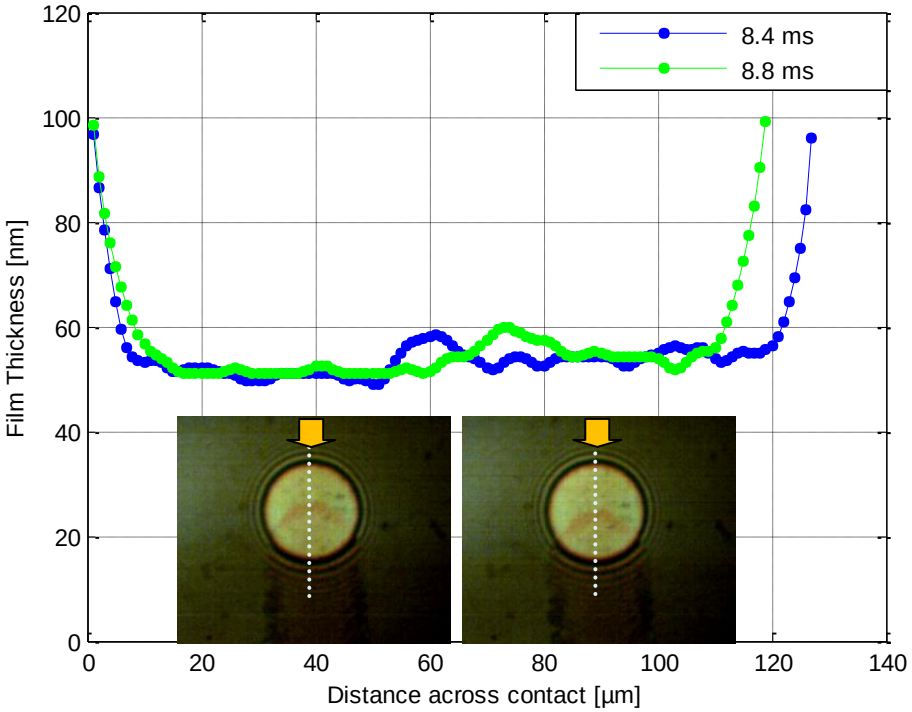

Figure 6.8(d): Coloured interferogram and Film Thickness profile at 20 Hz for 0.05 m/s (8.4 ms – 8.8 ms)

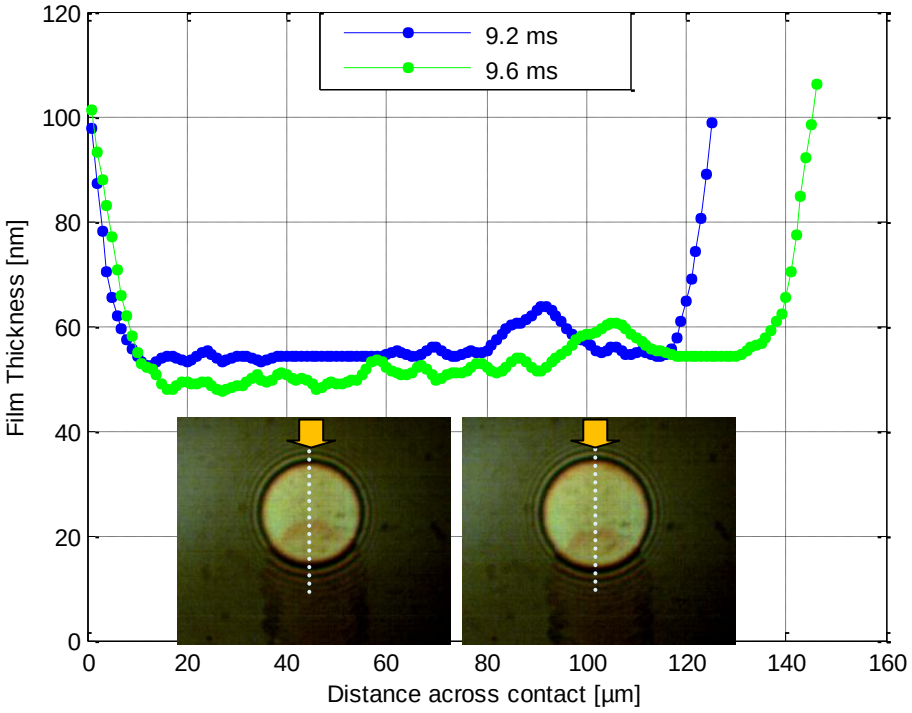

Figure 6.8(e): Coloured interferogram and Film Thickness profile at 20 Hz for 0.05 m/s (9.2 ms – 9.6 ms)

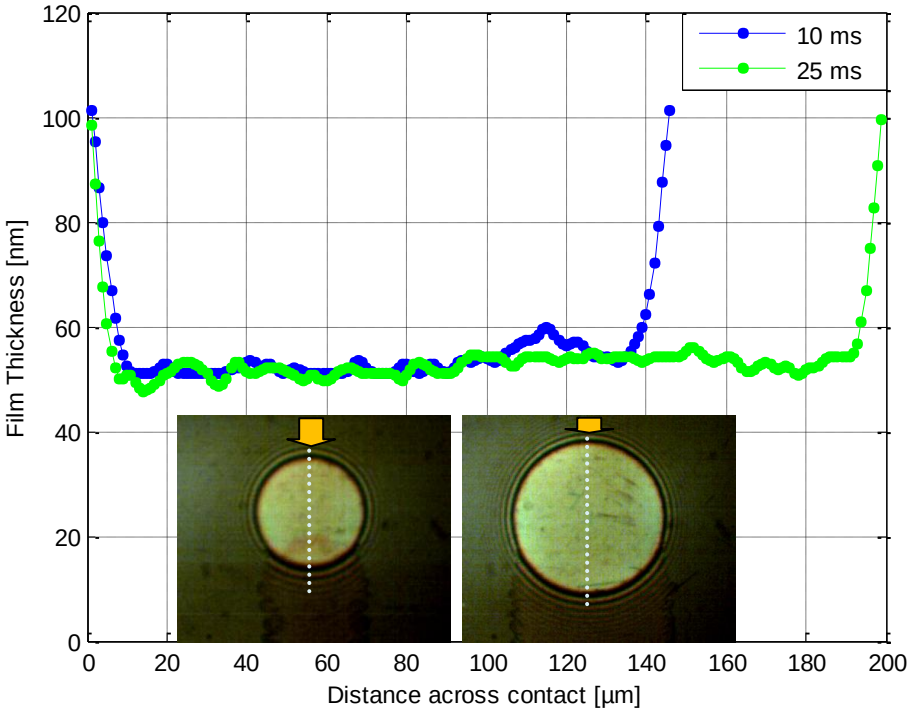

Figure 6.8(f): Coloured interferogram and Film Thickness profile at 20 Hz for 0.05 m/s (10 ms, 25 ms)

Figures 6.8(a) to (f) present the associated film thickness profiles and the coloured interferometric images taken during the loading phase. The analysis of the results show that, as illustrated in Figure 6.8(a), the maximum enhanced film throughout the loading – unloading cycle was about 9 nm to 12 nm, as observed in Figures 6.8(d) to (e).

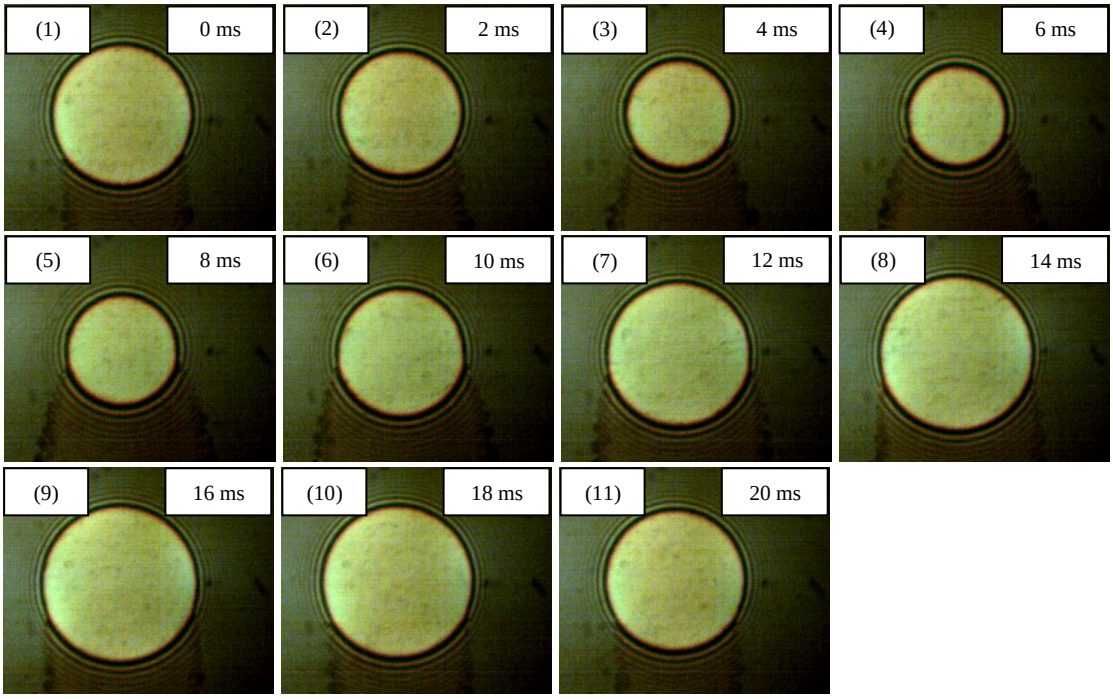

Figure 6.9: Typical Behaviour of an EHD contact subjected to vertical vibrations at 50Hz

For the 50 Hz tests 11 images were captured corresponded to a full vibration cycle as shown in Figure 6.9. The minimum load can be observed in the fourth frame at 6 ms which is roughly 16 N (P_H ~ 0.5 GPa)) while the maximum load is found in the ninth frame at 16 ms and corresponds to 54 N (P_H ~ 0.72 GPa).

As it can be observed from these images no significant film perturbations have been detected, despite the fact that the rate of change of load was maxim in this case at 3.8 kN/s. Analysing the behaviour of the film at all three frequencies it can be said that the variation of the pressure rather than the variation of the load is responsible for film thickness fluctuations. Indeed, in the 50 Hz test the Hertzian pressure varied only by 220 MPa in comparison to 390 MPa for 20 Hz and 400 MPa in the 10 Hz test. It is thus suggested that the lower variation of

the pressure caused a lesser change of the geometry in the inlet and thus less enhanced film was formed and subsequently travelled through the contact.

Figure 6.10 shows the load variation during a period of 20 ms while Figure 6.11 illustrates the averaged film thickness taken at different time intervals during a complete vibration cycle.

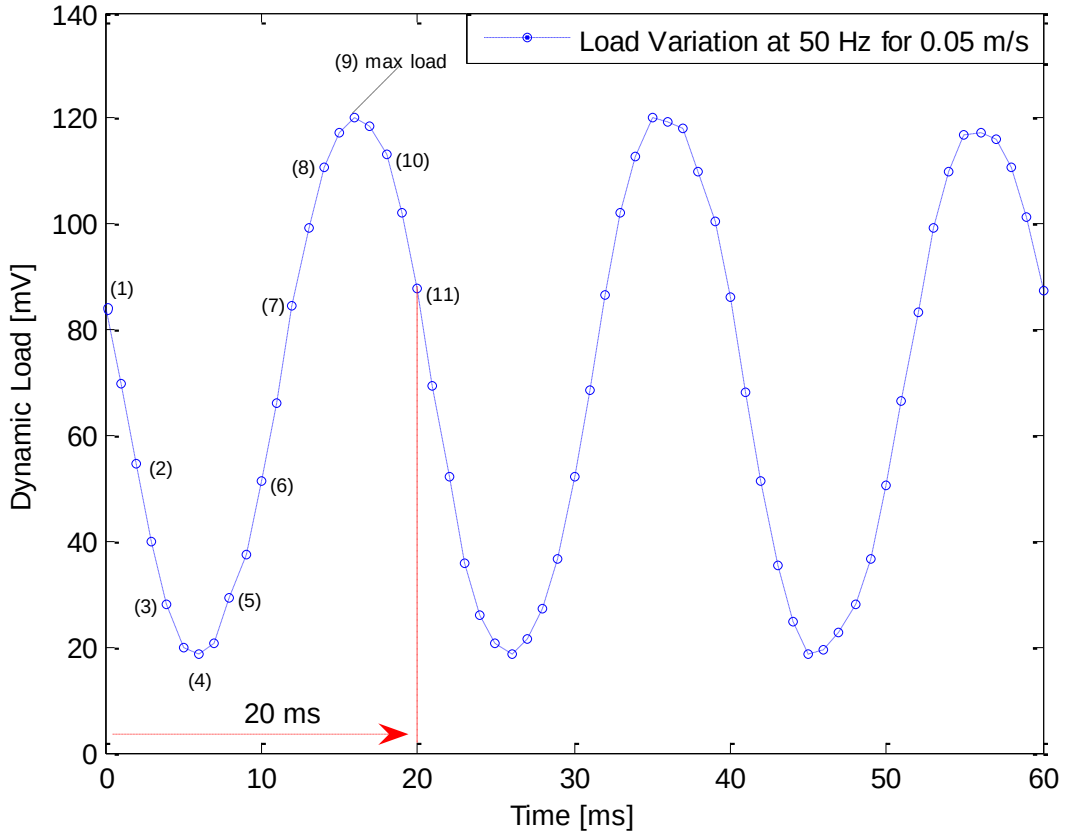

Figure 6.10: Load Variation at 50 Hz for 0.05 m/s

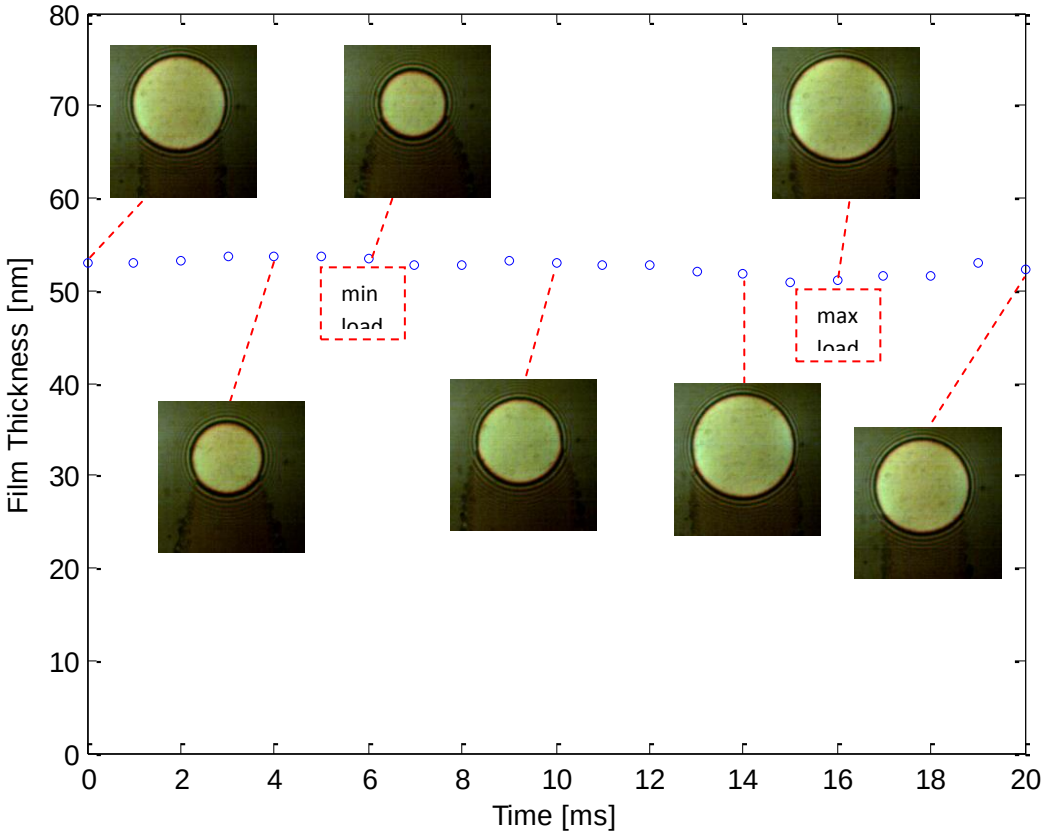

Figure 6.11: Film Thickness variation and coloured interferograms during loading-unloading phase at 50 Hz for 0.05 m/s

From the plot of the average film thickness over time it can be seen that the variation over one cycle is minimal, thus the trend observed for the 20 Hz case continued at 50 Hz.

6.1.2 The effect of entrainment speed

The effect of entrainment speed on the behaviour of EHD films subjected to rapid variations of load has also been examined. Film thickness has been measured at different entraining speeds ranging from 0.1 m/s to 2 m/s at frequencies of 10 Hz and 20 Hz.

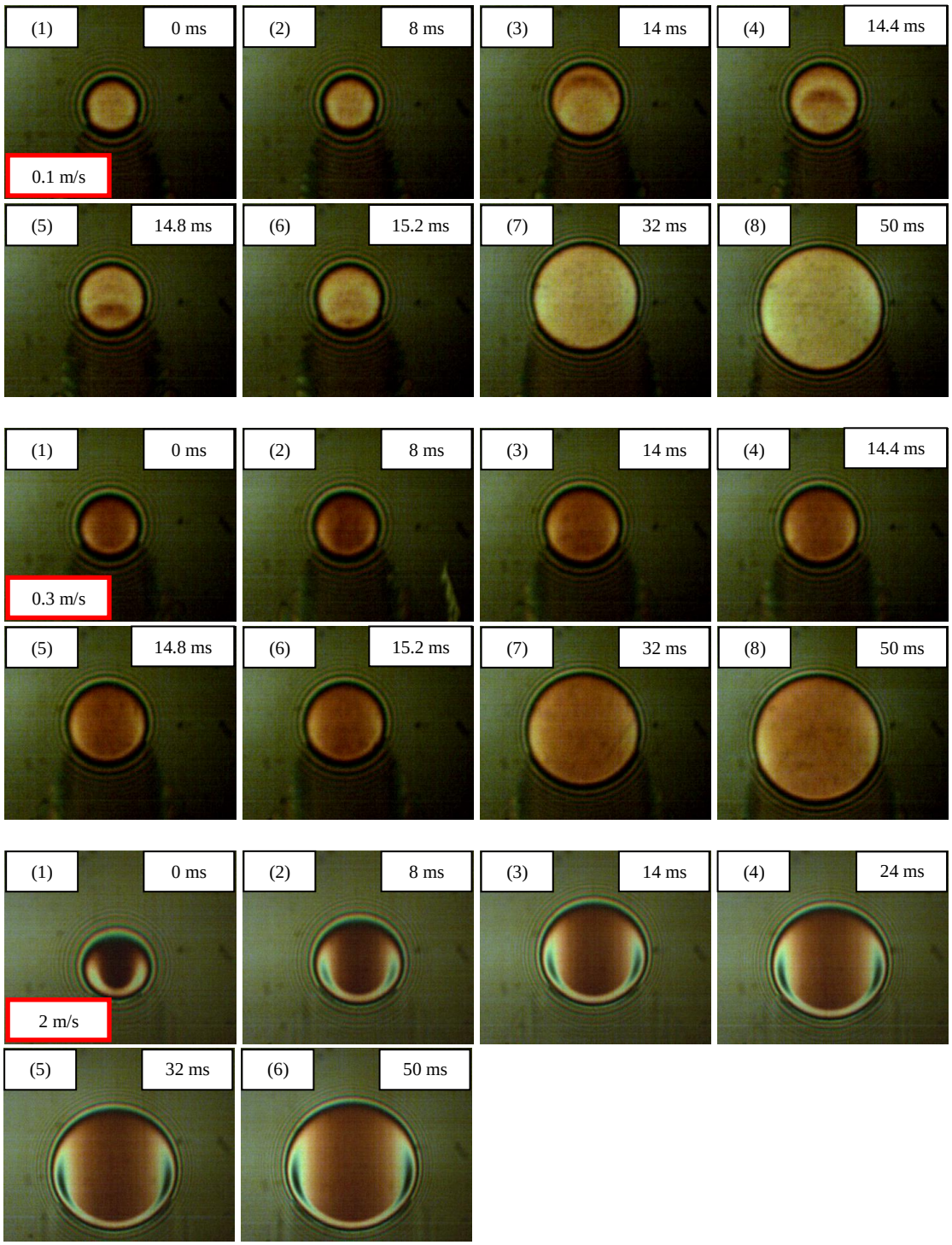

Figure 6.12: Typical Behaviour of an EHD contact subjected to vertical vibrations at 10 Hz over a wide speed range

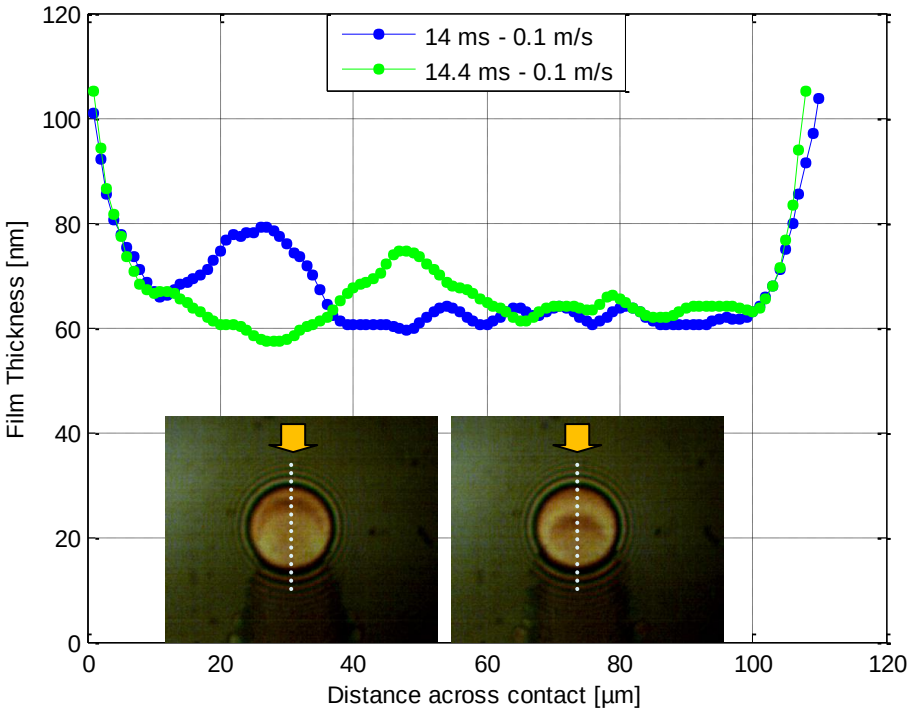

Figure 6.13(a): Coloured interferogram and Film Thickness profile at 10 Hz for 0.1 m/s (14 ms – 14.4 ms)

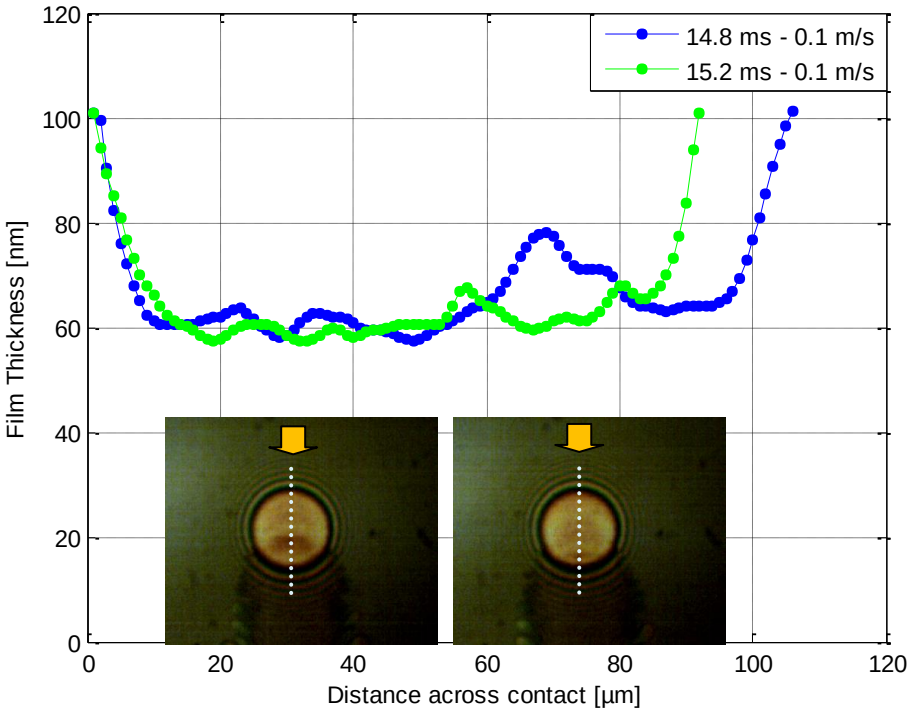

Figure 6.13(b): Coloured interferogram and Film Thickness profile at 10 Hz for 0.1 m/s (14.8 ms – 15.2 ms)

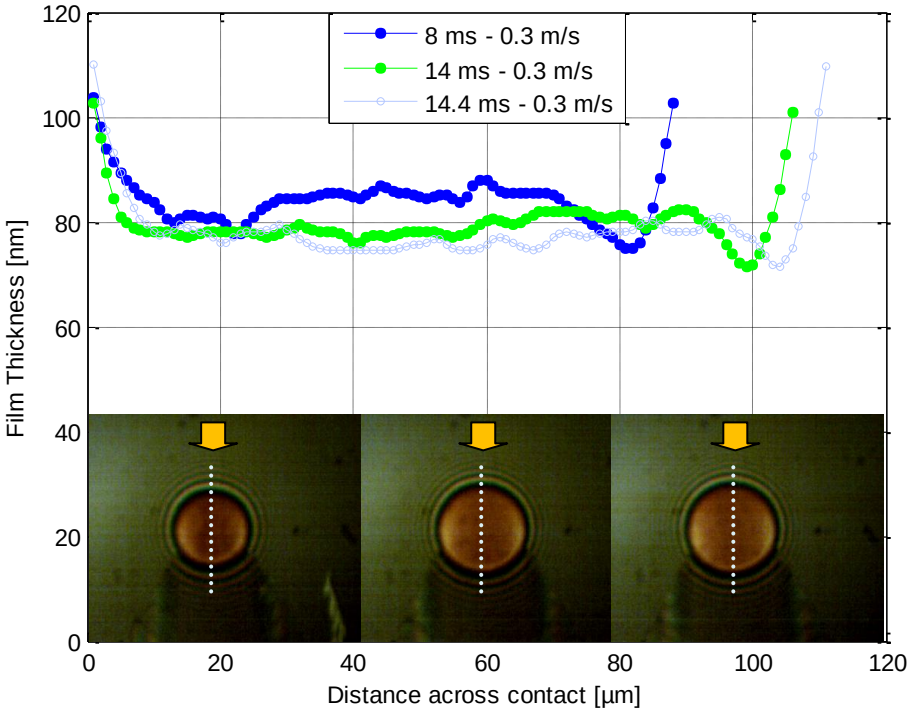

Figure 6.13(c): Coloured interferogram and Film Thickness profile at 10 Hz for 0.3 m/s (8 ms – 14.4 ms)

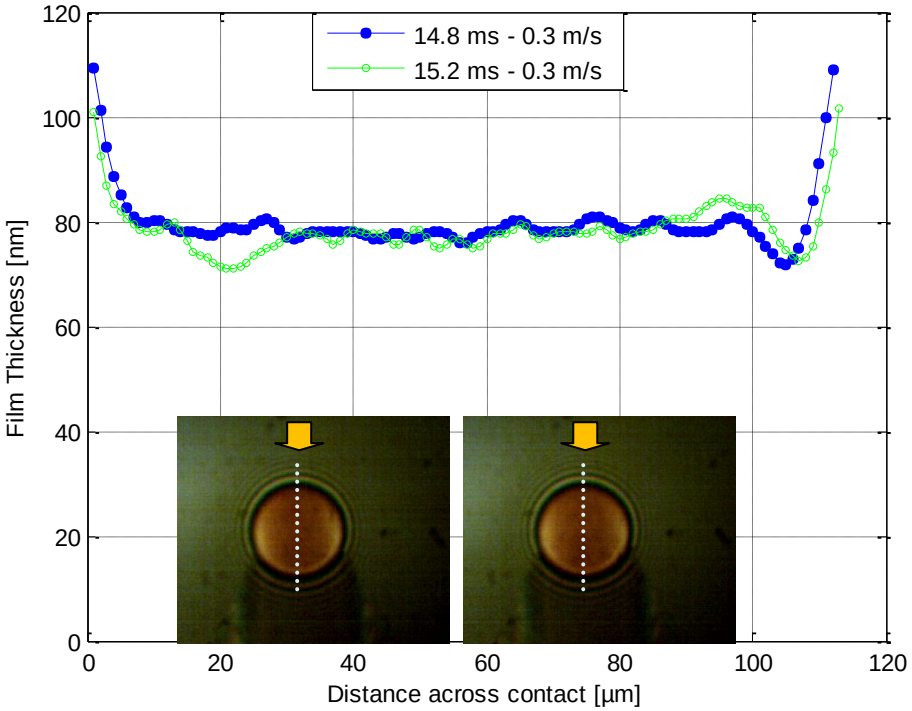

Figure 6.13(d): Coloured interferogram and Film Thickness profile at 10 Hz for 0.3 m/s (14.8 ms – 15.2 ms)

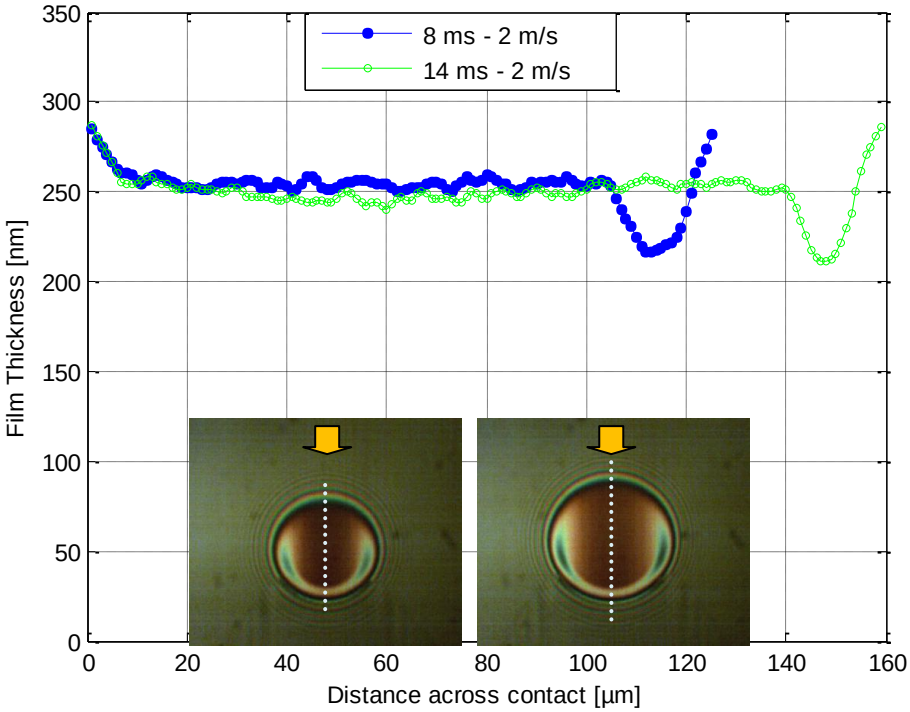

Figure 6.13(e): Coloured interferogram and Film Thickness profile at 10 Hz for 2 m/s (8 ms – 14 ms)

The analysis of the graphs obtained revealed that, perturbations large relative to the steady state film thickness can be observed at the lowest speed employed that is 0.05 m/s and 0.1 m/s. This can be seen in Figures 6.4 (b), (c) and 6.13(a), (b). The ratio between film perturbation to steady state film was about 25 percent for 0.05 m/s and about 30 percent for 0.1 m/s .This trend of increasing the perturbation in the film with the increase of the overall film thickness does not extend to the two large entrainment speeds employed in these experiments between the times of 14 ms to 15.2 ms. At 0.3 m/s has largest film fluctuations was about 13 nm, which represents 17 percent of the steady state film thickness. Finally at the highest entraining speed, i.e. 2 m/s no significant fluctuations have been identified. As it was shown previously fluctuations in the film occur during the first milliseconds after the

load has started to increase. A possible explanation may be the fact that the transit time of a particle of lubricant through the contact, at a speed, of 2 m/s is shorter than 100 μs while the capture rate of the camera was 399 µs. In this way the camera sensor acted as a integrator elements, overlapping light coming from four complete passages of the perturbations through the contact. In this way the images appear smooth. A reduction of the shutter speed did not work because there was not enough light and the images became too dark.

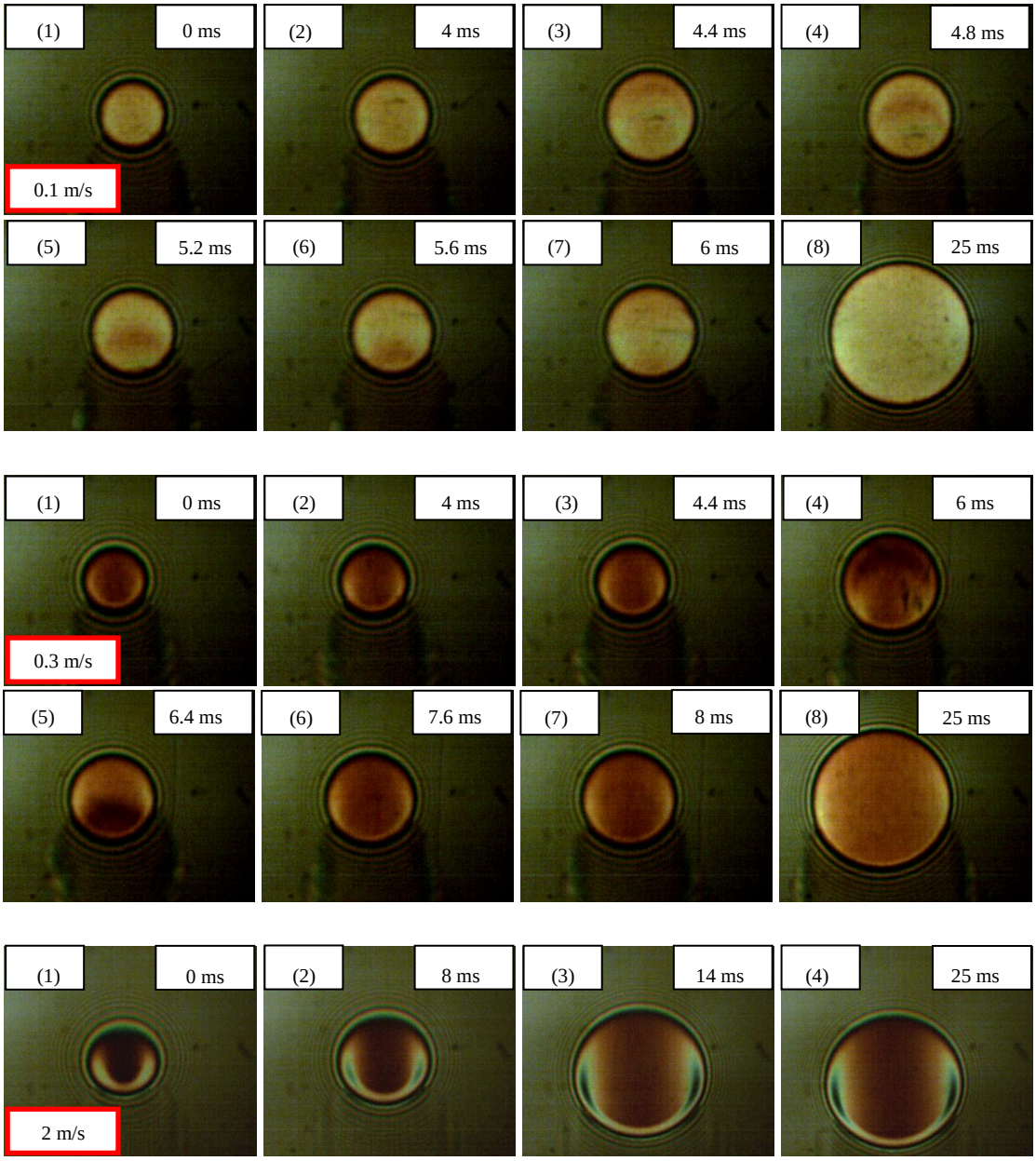

Figure 6.14: Typical Behaviour of an EHD contact subjected to vertical vibrations at 20 Hz over a wide speed range

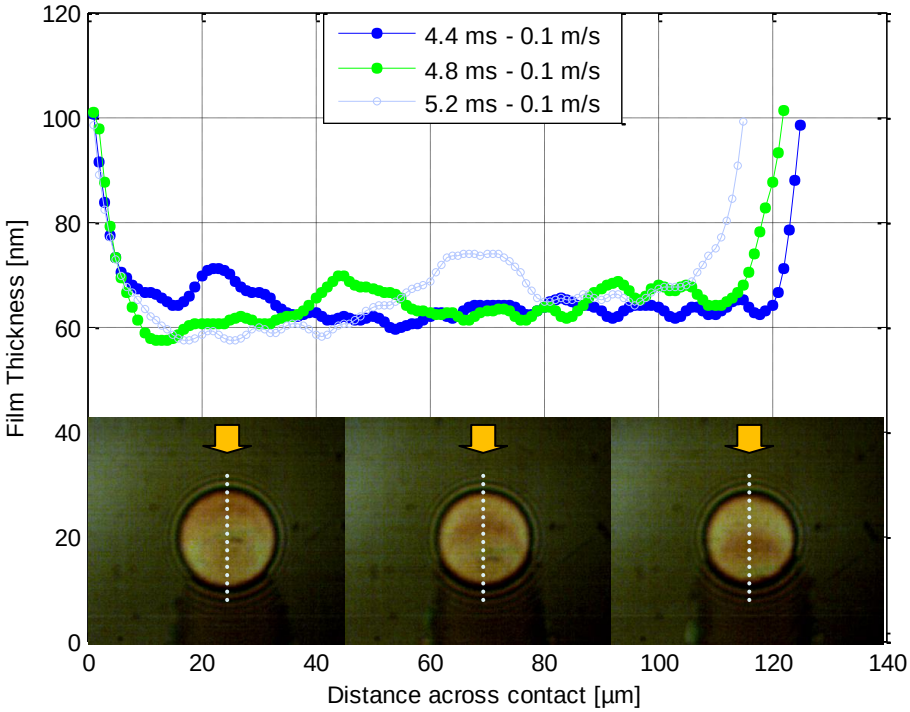

Figure 6.15(a): Coloured interferogram and Film Thickness profile at 20 Hz for 0.1 m/s (4.4 ms – 5.2 ms)

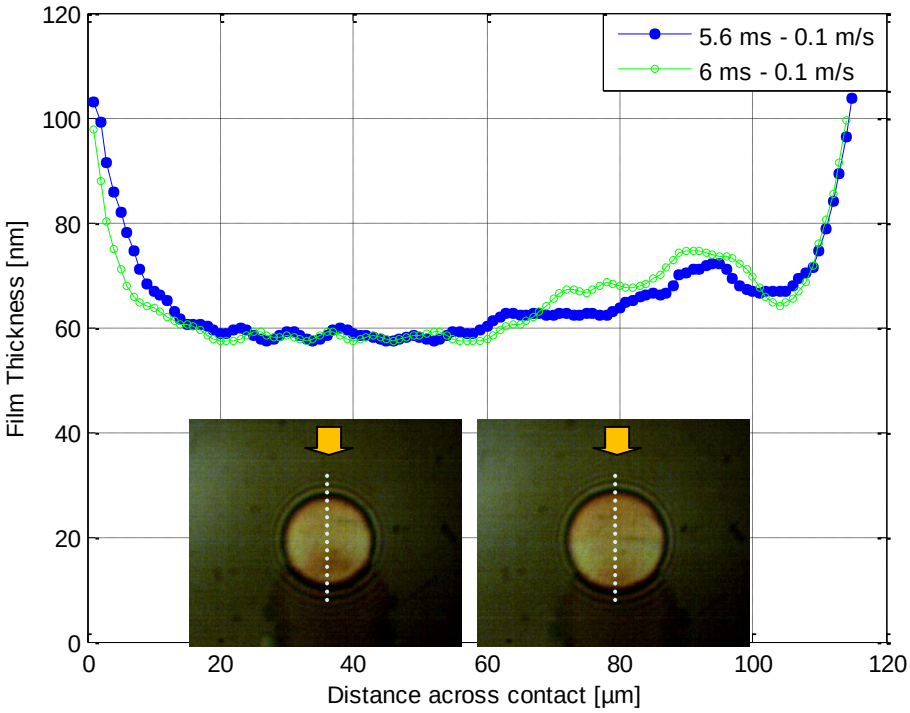

Figure 6.15(b): Coloured interferogram and Film Thickness profile at 20 Hz for 0.1 m/s (5.6 ms – 6 ms)

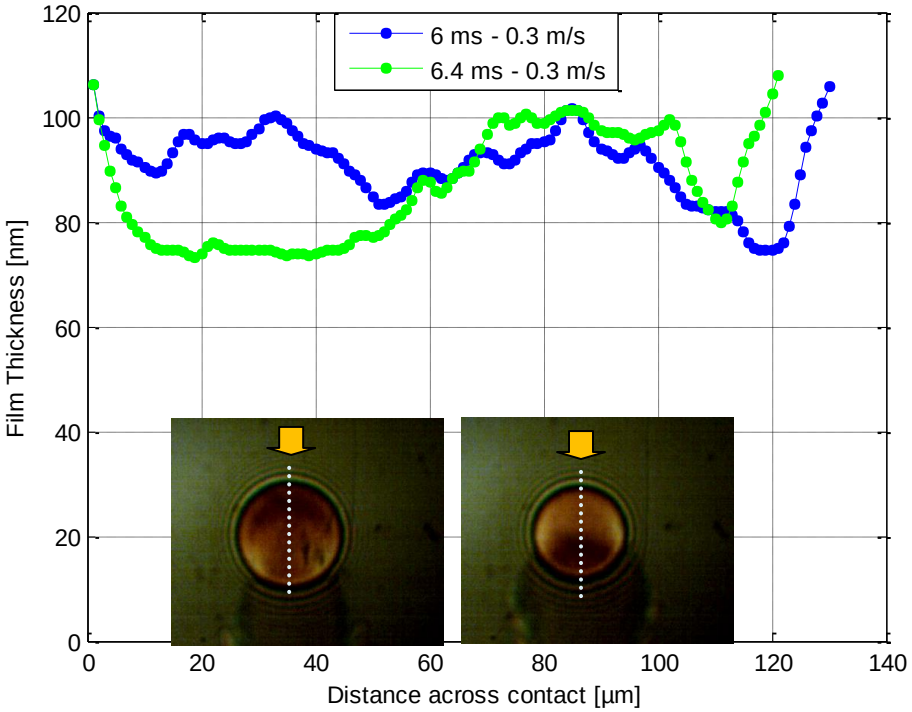

Figure 6.15(c): Coloured interferogram and Film Thickness profile at 20 Hz for 0.3 m/s (6 ms – 6.4 ms)

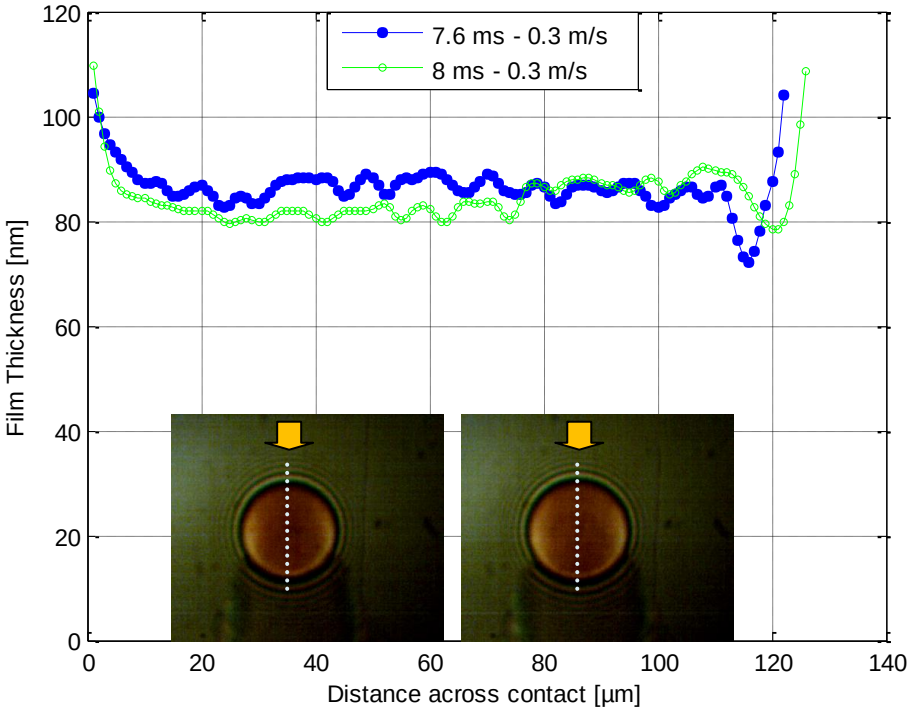

Figure 6.15(d): Coloured interferogram and Film Thickness profile at 20 Hz for 0.3 m/s (7.6ms – 8 ms)

Typical coloured interferograms together with the corresponded film midplane profiles over the same range of speeds at the frequency of 20 Hz are shown in Figures 6.14 and 6.15 (a) to (d). The analysis if these results show variations in the film thickness, similar to those obtained at 10 Hz. Film thickness perturbations were in the range of 17 nm for 0.1 m/s entrainment speed and 27 nm for 0.3 m/s .Again, at highest rolling speed no perturbations in the film can be seen.

CHAPTER 7: Conclusions and Recommendations for Future Research

During this PhD research an experimental optical test rig for the study of the dynamic behaviour of elastohydrodynamic lubricated contacts subjected to lateral and vertical vibrations have been successfully built and tested. The Spacer Layer Imaging method (based on optical interferometry) was adapted to this study for measuring the lubricant film thickness in transient conditions.

7.1 EHD Film Behaviour under Lateral Oscillations

In this part of the investigation, experiments were conducted in order to assess the effect of various parameters including the frequency of the lateral oscillations, Hertzian pressure, main rolling speed as well as the lubricant upon the behaviour of the EHD film subjected to lateral oscillatory motion. Initially, the experiments were conducted for glass on steel contact at different temperatures of 30 ^{o}C and 80 ^{o}C, three working frequencies i.e. 10 Hz, 20 Hz, 50 Hz and different entraining speeds. The lubricant initially tested was a synthetic base oil polyalfaolefin (PAO 4). The same experiments were repeated only at 30 ^{o}C using a different material combination (sapphire disc, tungsten carbide ball) producing larger Hertzian pressure. A comparison between experimental and theoretical predictions, using a simple model based on time of passage of the lubricant through the contact, was also carried out. Additional experiments have been conducted in order to evaluate the effect of lateral oscillatory motion upon the behaviour of EHD films formed by a Viscosity Index Improver additive. Film thickness for a mixture of PAO 4 base oil and 10.7 % weight polyalkylmethacrylate (PAMA) viscosity index improver polymer was measured at different working parameters. The tests have been performed with the glass steel combinations and at

temperatures of 30 ^{o} C and 80 ^{o} C. Given the fact that the majority of rolling bearings are lubricated with grease, experiments have also been carried out on a grease-lubricated contact. In that study both sapphire disc and a tungsten carbide ball and glass disc and steel ball combinations of materials have been used.

The main conclusions drawn from these experiments are summarised below.

1. For certain combinations of the values of the working parameters related to the lateral motion and to the steady state motion of the contact, perturbations in the film are generated at the inlet of the contact and subsequently travel through the contact, causing local variations in film thickness.
2. The perturbations in the film were only observed for the largest frequency of the lateral motion and lower main entrainment speeds; tests for two combinations of contacting materials, which gave different Hertzian pressures, glass – steel and sapphire – tungsten carbide, revealed that the pressure on the contact does not influence the behaviour of the EHD film subjected to lateral oscillations.
3. The parameter which influences the formation of the perturbations in the film is the ratio between the main entraining speed of the contact and the lateral speed. The smaller the ratio the larger the transient effects can be identified. In the case of base oil experiments film perturbations of 11-15 nanometres, peak to valley, were measured, at 0.05 m/s main rolling speed and 100 Hz frequency of lateral oscillations. Negligible perturbations in the film were observed at larger main entrainment speed.
4. The lateral oscillations influence the EHD film thickness only if it is able to create large squeeze effects due to rapid variation of the overall film thickness. For thick films, the variation of the combined entrainment speed due to lateral motion over imposed on the main entrainment, in not able to induce any transient effects in the film.

5. Comparison between the experimental results and film thickness predicted by a simple theoretical analysis based on the time of passage of the lubricant through the contact showed reasonable good agreement.
6. Tests carried out on a blend of base oil and a viscosity index improver polymer, at low temperatures have showed that film perturbations were formed in a range of main entrainment speed larger than that found for base oil alone. At thick film conditions obtained at. 0.3 m/s (a steady state film of about 80 nanometres), perturbations of amplitude three times larger than the largest perturbations obtained for base oil, were observed. 'This may be explained by a viscosity instability induced in the polymer film due to repeated shearing'.
7. Experiments with the viscosity index improver performed at a temperature of 80 ^{o}C, that is much lower overall film thickness did not reveal significant fluctuations even by at the maximum lateral speed. This proved again that at very thin films not enough squeeze effect can be generated in order to create perturbations in the film.
8. The results conducted for the viscosity index improver blend were compared with those obtained for base oil at both temperatures. As expected, in the case of low temperature the values of the film thickness for the addition of 10.7 % viscosity index improver polymer were larger compared with those measured with pure base oil at all working frequencies. The interesting phenomenon was observed at highest frequency of 100 Hz and at lowest entraining motion. The film formation was found to be different in the two cases. For example the VII blend formed a series of thick waves of different wavelength while in the case of the base oil only single wave of a thinner film was observed.
9. It is well documented that in steady state conditions grease-lubricated contact become starved after a small number of revolutions (passages of the rolling elements over the

same location), phenomenon characterised by an oil depleted track and a thinner then normal film thickness. Results of the tests on the effect of lateral oscillatory motion upon track replenishment in grease-lubricated contact have shown that lateral oscillations over-imposed on the main entraining motion help starved contacts recover their film thickness completely to values corresponding to fully flooded conditions. It can be concluded that, the lateral oscillations can be one of the mechanisms which helps the grease lubricated contacts recover to film thickness corresponding to fully flooded conditions. This can have important repercussion upon the lubrication of rolling elements bearings, which are most often grease lubricated.

10. These tests have also revealed that the stroke length (with other words the ratio between stroke length and the contact diameter) plays the most important role in the track replenishment mechanism.

7.2 EHD Film Behaviour under Vertical Vibrations

The effect of vibrations on a direction perpendicular to the area of contact upon EHD film thickness was the have also been investigated. In this study, a constant load was applied between a glass disc and a steel ball contact and a film was then established by rotating these elements. Thereafter a dynamic shaker was set in motion such that the load was varied in a controlled, sinusoidal fashion inducing forced vibrations on the lubricant film. The tests were performed under pure rolling conditions ranging from 0.05 m/s up to 2 m/s at three different frequencies of 10 Hz, 20 Hz and 50 Hz. It has to be mentioned that the experimental setup did not allow, at 50Hz, a variation of load with an amplitude comparable with that obtained at lower frequencies. This was also the reason for not trying even larger frequencies. The lubricant used in this investigation was PAO base oil and the temperature was set to 30 ^{o}C.

The main features of EHD film behaviour, revealed in this part of the study are:

1. Perturbations in the film thickness were observed during the unloading phase of the loading cycle. These perturbations had crescent-like shape and travelled unchanged through the contact, at the average speed of the surfaces.
2. An increase of load had an effect of increasing the contact diameter at the same time modifying the convergence geometry in the inlet. Therefore, an enhanced film thickness was produced at the inlet periphery of the initial contact zone. It is believed that during the loading phase the lubricant flows radially outwards and somehow cancels the effect of entrainment; this is why no film fluctuations were observed during the loading phase. During the unloading phase however the entrainment and inward flow due to squeeze sum up thus the perturbation formed in the inlet now travels through the contact.
3. Film perturbations were observable only at low frequencies (10Hz, 20Hz) and at entraining speeds of 0.05 m/s up to 0.3 m/s. At highest frequency employed no significant film variations were detected. This was due to the fact that the load variation was relatively small compared with the tests obtained at 10 Hz and 20 Hz.

7.3 Recommendations for Future Work

Overall, the present work has covered an experimental investigation into the effect of vibrations in EHD contacts. The film behaviour was evaluated during lateral and vertical vibrations in pure rolling conditions. However, is clear that further research is required for both types of vibrations. Changes and refinements to the existing experimental rig as well as different kind of experiments are recommended.

EHD Films under Lateral Oscillations

During this study three parameters were examined including, frequency of lateral oscillations, Hertzian pressure and the main rolling speed. Additional experiments are required for the study of the effect of different slide-to-ratios in EHD contacts under transient conditions using other material combinations.

Another topic can be to study the variation of the film thickness in an elastohydrodynamic point contact subjected to a combination of lateral and vertical oscillations. In that case the lateral oscillations will be perpendicular to the rolling direction while vertical vibrations will take place in a direction perpendicular to the plane of contact.

The results presented in this thesis and the research papers published were the first to report on the behaviour of EHD films under lateral oscillatory motion. Further improvements can envisage tests carried out at frequencies larger than 100 Hz, used in the present investigation, and on a wider range of amplitudes.

In addition, some modifications to the existing test rig are required; for instance the location and support of the microscope. Currently the microscope is held on a cantilever support, attached to the frame of the rig. This arrangement made the focusing of the lens difficult and thus the quality of the images sometimes suffered, which means many tests needed to be repeated. In order to overcome this problem it is suggested to mount the microscope away from the frame of the test rig.

It would also speed up and help the experiments if a ball track micrometer connected to the ball carriage thus allowing adjusting the track radius before or during the experiments is included.

EHD Films under Vertical Oscillations

In the current study experiments have been conducted in pure rolling conditions, three different frequencies using base oil at 30 ^{o} C. The results showed that film fluctuations are induced due to rapid variation of load. Unfortunately the trend was not possible to be followed at larger frequencies due to the inability of the testing rig to vary the load at large amplitudes, at greater frequencies. Thus the test rig must be modified, by replacing the existing (and rather old) electro-dynamic shaker with another system, for example an adjustable eccentric.

A number of tests have to be carried out to evaluate the effect of vertical oscillations in EHD films at different working conditions including temperature , contact pressure , higher frequencies i.e.100 Hz as well as at or around the resonance frequency of the system.

Another suggestion will be to study the effect of load variation in grease lubricated contacts. To do so, experiments have to be conducted in static and pure rolling conditions. In addition, the effect of slide-to-roll ratio at a wide range of speeds and frequencies it will be an interesting topic for investigation.

It is also essential to study the effect of damping. In the current investigation it was difficult to evaluate experimentally the damping coefficient due to the limitations of the dynamic shaker. This limitation didn't allow the author to use a sweep of frequencies from low to high in order to pass the resonant frequency of the system.

List of References

[1] Timosenko, S.P. and Goodier, J.M. (1951), ‘‘Theory of Elasticity’’, 2nd *Edition, McGraw Hill, N Y, USA, ISBN*

[2] Hertz, H. (1881), ‘‘Uber die Beruhrung Fester Elasticher Korper’’, *J. Reine und Angewandte Mathematik, Vol. 92,* pp. 156-171

[3] Hamrock, B.J., Jacobson, B. And Schmid, S.R. (1999), ‘‘Fundamentals of Machine Elements’’, *McGraw Hill , ISBN 0-256-19069-0*

[4] Reynolds, O. (1886), ‘‘On the Theory of Lubrication and its Application to Mr. Beauchamp Tower experiments including an experimental determination of the viscosity of olive oil’’, *Phil. Trans. R. Soc., London,* 177

[5] Gohar, C. (1988), ‘‘Elastohydrodynamics’’, *Ellis Horwood , ISBN 0-85312-820-0*

[6] Wijnant, Y.H. (1998), ‘‘Contact Dynamics in the Field of Elastohydrodynamic Lubrication’’, *PhD thesis, University of Twente , the Netherlands , ISBN 90-36512239*

[7] Wensing, J.A. (1998), ‘‘On the Dynamics of Ball Bearings’’, *PhD thesis, University of Twente, the Netherlands, ISBN* 90-36512298

[8] Barus, C. (1983), ‘‘Isothermals, Isopietics and Isometrics relative to Viscosity’’, *Am. J. of Science, 45,* pp. 87-96

[9] Dowson, D. And Ehret, P. (1999), ‘‘Past, Present and Future Studies in Elastohydrodynamics’’, *Proc. Instn Mech. Engrs, Part J, Journal of Engineering Tribology, Vol.213 (5),* pp.317-333

REFERENCES

[10] Roelands, C. (1996), ‘‘Correlational Aspects of the Viscosity-Temperature-Pressure Relationship of Lubricating Oils’’, *PhD thesis, Delft University, Delft, (VRB Groningen, The Netherlands).*

[11] Dowson, D. And Higginson, G.R. (1966), ‘‘Elastohydrodynamic Lubrication, *The Fundamentals of Roller and Gear Lubrication*’’, *Pergamon Press, Great Britain*

[12] Dowson, D. And Higginson, G.R. (1977), ‘‘Elastohydrodynamic Lubrication’’, *SI Edition, Pergamon Press*

[13] Hamrock, B.J. and Dowson, D. (1976), ‘‘Isothermal Elastohydrodynamic Lubrication of Point Contacts, Part III-Fully Flooded Results’’, NASA *TN D-8317*

[14] Hamrock, B.J. and Dowson, D. (1981), ‘‘Ball Bearing Lubrication- The Elastohydrodynamics of Elliptical Contacts’’, *Willey-Interscience, New York, ISBN: 9780471035534*

[15] Grubin, A.N. and Vinogradova, I.E. (1949), ‘‘Fundamentals of the Hydrodynamic Theory of Lubrication of Heavily Loaded Cylindrical Surfaces’’, *Central Scientific* Research Institute of Technology and Mechanical Engineering, Book No. 30 , *Moscow,* pp. 115–166

[16] Petrusevich, A.I. (1951), ‘‘Fundamental Conclusions from the Contact Hydrodynamic Theory of Lubrication’’, *Izu. Akad. Nauk SSR (OTN), 2,* pp. 209-223

[17] Hamrock, B.J. and Dowson, D. (1983), ‘‘Film Thickness for Different Regimes of Fluid-Film Lubrication’’, NASA *TM -81700*

[18] Johnson, K.L. (1970), ‘‘Regimes of Elastohydrodynamic Lubrication’’, *J. Mech. Eng. Sci., Vol. 12 (1),* pp.9-16

REFERENCES

[19] Esfahanian, M. and Hamrock, B.J. (1991), ‘‘Fluid Film Lubication Regimes’’, *Revisited, STLE Tribol. Trans., Vol. 34 (4),* pp.618-632

[20] Glovnea, R.P. (2010), “Transient Phenomena in Elastohydrodynamic Lubrication’’, Recent Developments in Wear Prevention, Friction and Lubrication, *Ed. G. Nikas, Research Signpost*, ISBN: 978-81-0377-7

[21] Christensen, H. (1962), “The Oil Film in a closing gap’’, *Proc. R. Soc. London, Ser. A, Vol. 226*, pp.312-328

[22] Vichard, J.P. (1971), “Transient Effects in the Lubrication of Hertzian Contacts’’, *J. Mech. Eng. Sci., Vol.13*, pp.173-189

[23] Wang, K.L and Cheng, H.S. (1981), ‘‘A Numerical Solution to the Dynamic Load, Film Thickness and Surface Temperatures in Spur Gears, Part I – Analysis’’, *ASME J. of Mech. Design, Vol. 103*, pp.177-187

[24] Hoglund, E. and Jacobson, B. (1986), ‘‘Experimental Investigation of the Shear Strength of Lubricants Subjected to High Pressure and Temperature’’, *ASME J. Tribology, Vol. 108,* pp.571-578

[25] Wada, S., and Tsukijihara, M. (1980), ‘‘Elastohydrodynamic Lubrication of Squeeze Films-Two Spherical Bodies Lubricated with Grease,’’ *Bull. JSME*, 23, pp. 766–772.

[26] Yang, P. R., and Wen, S. Z. (1991), ‘‘Pure Squeeze Action in an Isothermal Elastohydrodynamically Lubricated Spherical Conjunction,’’ *Wear, 142*, pp. 1–16.

[27] Wong, P. L., Lingard, S., and Cameron, A. (1992), “The High Pressure Impact Microviscometer,’’ *Tribol. Trans., 35*, pp. 500–508.

REFERENCES

[28] Ahrstrom, B.O. (2001), "Investigation of Frictional Properties of Lubricants at Transient EHD-Conditions", *Trib. Int., 34(12*), pp. 809-814

[29] Workel, M.F., Dowson, D., Ehret, P. and Taylor, C.M. (2001), "Design and Development of a Ball Impact Apparatus for Direct Measurement of Lubricant Friction under High Pressure and Shear Rates", *Proc. I.Mech.E., J. Eng. Trib., 215*, pp.211-222

[30] Chu, H.M, Lee, R.T and Chiou, Y.C. (2004), "Study of Pure Squeeze Elastohydrodynamic Lubrication Motion using Optical Interferometry and the Inverse Approach", *Proc. I.Mech.E., J. Eng. Trib., 218*, pp.503-512

[31] Kaneta, M., Ozaki, S., Nishikawa, H. and Guo, F. (2007), "Effects of Impact Loads on Point Contact Elastohydrodynamic Lubrication Films", *Proc. I.Mech.E., J. Eng. Trib., 221*, pp.271-278

[32] Larsson, R. and Lundberg, J. (1995), ''Study of Lubricated Impact using Optical Interferometry'', *Wear*, Vol.190 (2), pp.184-189

[33] Kaneta, M. (1999), "For the Establishment of a New EHL Theory", *Lubrication at the Frontier, Elsevier Science B.V*, pp.25-34

[34] Nishikawa, H., Handa, K., and Kaneta, M. (1995), ''Behaviour of EHL films in Reciprocating Motion,'' *JSME Int. J. Series C, 38*, pp. 558–567.

[35] Rutlin, H.C., Sayles, R.S. and Starkey, M.S. (1997), "An Optical EHD Study Using a Reciprocating Hertzian Contact Rig Designed to Simulate the Kinematics of Constant Velocity Joints," in *Proc. 23rd Leeds-Lyon Symp.*, Sept. 1996, Elsevier, pp 297-303.

REFERENCES

[36] Scales, L. E., Rycroft, J. E., Horswill, N. R., and Williamson, B. P. (1996), ‘‘Simulation and Observation of Transient Effects in Elastohydrodynamic Lubrication,’’ *SAE Tech. Paper,* 961143.

[37] Ohno, N., and Yamada, S. (2007), “Effect of High-Pressure Rheology of Lubricants upon Entrapped Oil Film Behaviour at Halting Elastohydrodynamic Lubrication”, *Proc. I.Mech.E., J. Eng. Trib., Vol.222,* pp.279-285

[38] Larsson, R. and Lundberg, J. (1994), ‘‘A Simplified Solution to the Combined Squeeze-Sliding Lubrication Problem’’, *Wear, Vol.173*, pp.85-94

[39] Sugimura, J., Okumura, T., Yamamoto, Y. and Spikes, H.A. (1999), ‘‘Simple Equation for Elastohydrodynamic Film Thickness under Acceleration,’’ *Tribol. Int., 32*, pp. 117–123.

[40] Zhao, J. and Sadeghi, F. (2003), “Analysis of EHL Circular Contact Shut Down”, *ASME Trans. J. Trib., 125 (1),* pp.76-90

[41] Holmes, M.J.A., Evans, H.P. and Snidle, R.W. (2003), “Comparison of Transient EHL Calculations with Shut-down Experiments”, *Tribology and Interface Engineering Series, Vol. 41*, pp.79-89

[42] Sugimura, J. and Spikes, H.A. (1997), ‘‘Technique for Measuring EHD Film Thickness in Non-Steady State Contact Conditions’’, *In: Dowson et al., editor, Elastohydrodynamics ’96, Amsterdam: Elsevier*, pp.91-100

[43] Sugimura, J., Jones, W.R. Jr. and Spikes, H.A. (1998), ‘‘EHD Film Thickness in Non-Steady State Contacts.” *ASME Trans J. of Tribology* 120, pp. 442-452

[44] Glovnea, R.P. and Spikes, H.A. (2001), ‘‘Elastohydrodynamic Film Formation at the Start-up of the Motion’’, *Proc. Instn Mech. Engrs, Vol. 215, Part J.*, pp. 125-138

REFERENCES

[45] Glovnea, R.P. and Spikes, H.A. (2001), ‘‘Elastohydrodynamic Film Collapse during Rapid Deceleration: Part I- Experimental Results’’, *ASME Trans., J. Trib., Vol.123*, pp. 254-261

[46] Glovnea, R.P. and Spikes, H.A. (2001), ‘‘Elastohydrodynamic Film Collapse during Rapid Deceleration: Part II- Theoretical Analysis and Comparison of Theory and Experiment’’, *ASME Trans., J. Trib., Vol.123*, pp. 262-267

[47] Glovnea, R.P., Spikes, H.A. and Jones, J.R. (2002), ‘‘Behaviour of Several Lubricants for Space Applications under Transient Speed Conditions’’, *J. Synthetic Lubrication, Vol.19,* pp.191-211, ISSN: 0265-6582

[48] Carson, R.M. and Johnson, K.L. (1971), ‘‘Surface Corrugations Spontaneously generated in a Rolling Contact Disc Machine’’, *Wear, Vol.17*, pp.59

[49] Gray, G.G and Johnson, K.L., (1972), “The Dynamic Response of Elastic Bodies in Rolling Contact to Random Roughness of their Surfaces, *J. Sound and Vibration, Vol. 22 (3),* pp. 323-342

[50] Sanborn, D.M. and Winer, W.O. (1973), ‘‘Fluid Rheological Effects in Sliding Elastohydrodynamic Point Contact, I: Film Thickness’’, *ASME Trans., J. Lubric. Technol., Vol.93,* pp.262-271

[51] Dareing, D.W. and Johnson, K.L. (1975), “Fluid Film Damping of Rolling Contact Vibrations’’, *J. Mech. Engng. Sci., Vol.17 (4),* pp.214-218

[52] Smith, A.G.D. and Cameron, A. (1983), “Scuffing under Cyclic Loading-Unexpected Effect of Frequency’’, *ASLE Trans., Vol.26 (2),* pp.236-242

REFERENCES

[53] Ren, N., Zhu, D. and Wen, S.Z. (1991), ‘‘Experimental Method for Quantitative Analysis of Transient EHL’’, *Tribology International, Vol.24,* pp.225-230

[54] Sabot, J., Krempf, P. and Janolin, C. (1998), “Non-Linear Vibrations of a Sphere-Plane Contact Excited by a Normal Load’’, *J. Sound Vibr., Vol.214 (2),* pp. 359-375

[55] Wijnant, Y.H., Wensing, J.A. and Nijen, G.C. (1999), “The Influence of Lubrication on the Dynamic Behaviour of Ball Bearings. *J. Sound Vibr., Vol.224 (4) ,* pp. 579-596

[56] Wijnant, Y.H., Venner, C.H., Larsson, R. and Eriksson, P., 1999, “Effects of Structural Vibrations on the Film Thickness in an EHL Circular Contact”, ASME Trans., J. Trib. 121, 259-264

[57] Rigaud, E. and Perret-Liaudet, J. (2003), “Experimental and Numerical Results on Non-Linear Vibrations of an Impacting Hertzian Contact, Part 1: Harmonic Excitation’’, *J. Sound Vibr., Vol.265 ,* pp. 289-307

[58] Sakamoto, M., Nishikawa, H. and Kaneta, M. (2004), “Behaviour of Point Contact EHL Films under Pulsating Loads”, *Trans. Proc. Trib., Elsevier,* pp.391-399

[59] Kaneta, M., Ozaki, S., Nishikawa, H. and Guo, F. (2007), “Effects of Impact Loads on Point Elastohydrodynamic Lubrication Films’’, *Proc. Instn Mech. Engrs, Vol. 221, Part J.,* pp. 271-278

[60] El Kilali, T., Perret-Liaudet, J. and Mazuyer, D. (2004), “Experimental Analysis of a High Pressure Lubricated Contact under Dynamic Normal Excitation Force’’, *Trans. Proc. Trib., Elsevier,* pp.409-417

REFERENCES

[61] Ciulli, E. and Bassani, R. (2006), “Influence of Vibrations and Noise on Experimental Results of Lubricated Non-Conformal Contacts”, *Proc. Instn Mech. Engrs, Vol.220, Part J.*, pp.319-331

[62] Glovnea, R.P. and Spikes, H.A. (2005), “EHD Contacts in Low-Amplitude Oscillatory Motion’’, Proc. WTC III, Washington DC, Sept. 12-16

[63] Kalogiannis, K., Glovnea, R.P. and Ioannides, S. (2009), “The Response of EHD Films to Lateral Oscillations’’, Proc. WTC IV, Kyoto, Sept.6-11

[64] Chapkov, A.D., Colin, F. and Lubrecht, A.A. (2006), “Influence of Harmonic Surfaces Roughness on the Fatigue Life of Elastohydrodynamic Lubricated Contacts’’, *Proc. Instn Mech. Engrs, Vol. 220, Part J.*, pp. 287-294

[65] MacConochie, I.O. and Cameron, A. (1960), “The Measurement of Oil-Film Thickness in Gear Teeth’’, *ASME Trans., J. Basic Eng., Vol.82 (D),* pp.29-34

[66] Dawson, P.H. (1962), “Effect of Metallic Contact on the Pitting of Lubricated Rolling Surfaces’’, *J. Mech. Eng. Sci., Vol.4 (1),* pp.16-21

[67] Tallian, T.E. and McCool, J.L. (1971), “An Engineering Model of Spalling Fatigue Failure in Rolling Contact, II. The Surface Model’’, *Wear, Vol.17,* pp.447-461

[68] Choo, J.W., Glovnea, R.P. and Spikes, H.A. (2003), “The Effects of Three-Dimensional Model Surface Roughness Features on Lubricant Film Thickness in EHL Contacts’’, *ASME Trans., J. Trib., Vol.125*, pp. 533-542

[69] Glovnea, R.P., Choo, J.W., Olver, A.V. and Spikes, H.A. (2003), “Compression of a Single Transverse Ridge in a Circular Elastohydrodynamic Contact’’, *ASME Trans., J. Trib., Vol.125*, pp. 275-282

REFERENCES

[70] Kaneta, M. and Nishikawa, H. (1999), "The Effects of a Transversely Oriented Bump on Point Contact EHL Films in Reciprocating Motion with a Short Length Stroke", *Lubrication at the Frontier Dowson* et al. Ed., Elsevier B.V., pp.185-192

[71] Kaneta, M. and Nishikawa, H. (1999), "Experimental Study on Micro-Elastohydrodynamic Lubrication", *Proc. I.Mech.E., J. Eng. Trib.,* 213, pp.371-381

[72] Venner, C.H., Kaneta, M., and Lubrecht, A.A. (2000), "Surface Roughness in Elastohydrodynamically Lubricated Contacts", Thinning Films and Tribological Interfaces, D. Dowson et al. *Ed., Elsevier B.V.*, pp.25-36

[73] Kaneta, M. Tani, N. and Nishikawa, H. (2003), "Optical Interferometric Observations of the Effect of Moving Transverse Asperities on Point Contact EHL Films", *Tribological Research and Design for Engineering Systems,* D. Dowson et al. Ed., Elsevier B.V., pp.101-109

[74] Guanteng, G., Cann, P.M., Spikes, H.A. and Olver, A.V. (1999), "Mapping of Surface Features in the Thin Film Lubrication Regime", *Proc. 1998 Leeds Lyon Trib. Symp. Elsevier Tribology Series 36,* Ed. D. Dowson, pp.175-183

[75] Guanteng, G., Cann, P.M., Olver, A.V. and Spikes, H.A. (2000), "Lubricant Film Thickness in Rough Surface, Mixed Elastohydrodynamic Contact", *ASME Trans. J. Trib. 122*, pp.65-76

[76] Felix-Quinonez, A., Ehret, P. and Summers, J.L. (2003), "New experimental results of a single ridge passing through an EHL conjunction", *ASME Trans., J. Trib., 125,* pp.275-282

[77] Felix-Quinonez, A., Ehret, P. and Summers, J.L. (2005), "On Three-Dimensional, Flat-Top Defects Passing Through an EHL Point Contact: A Comparison of Modelling and Experiment", *ASME Trans. J. Trib., 127*, pp.51-60

REFERENCES

[78] Ehret, P., Felix-Quinonez, A., Lord, J., Larsson, R. and Marklund, O. (2001), "Experimental analysis of micro-elastohydrodynamic lubrication conditions", *Proc. Int. Trib. Conf., Nagasaki, Japan,* pp.478-483

[79] Hartl, M., Krupka I. and Liska M. (2004), "Direct Observation of the Behaviour of Real Surface Roughness Passing through EHD Point Contact., *Trans. Proc. Trib., Elsevier*, pp.419-427

[80] Krupka, I. and Hartl, M. (2006), "The Effect of Surface Texturing on Thin EHD Lubrication Films", *Trib. Int., 40*, pp.1100-1110

[81] Krupka, I. and Hartl, M. (2007), "Experimental Study of Microtextured Surfaces Operating Under Thin-Film EHD Lubrication Conditions", *ASME Trans. J. Trib., 129*, pp.502-508

[82] Greenwood, J.A., and Johnson, K.L. (1992), "The Behaviour of Transverse Roughness in Sliding Elastohydrodynamically Lubricated Contacts", *Wear, 153*, pp.107-117

[83] Greenwood, J.A, and Morales-Espejel, G.E. (1994), "The Behaviour of Transverse Roughness in EHL Contacts", *Proc. Insts. Mech. Engrs., Part J, 208*, pp. 121-132

[84] Hooke, C.J. (1998), "Surface Roughness Modification in Elastohydrodynamic Line Contacts Operating in the Elastic Piezoviscous Regime," *Proc. Insts. Mech. Engrs., Part J, 212*, pp. 145-162

[85] Hooke, C.J. and Venner C.H. (2000), "Surface roughness attenuation in line and point contacts", *Proc. I.Mech.E., 214(J),* pp.439-444

[86] Hooke, C. J. (1998), ''Surface Roughness Modification in Elastohydrodynamic Line Contacts Operating in the Elastic Piezoviscous Regime'', *Proc. Inst. Mech. Eng., Part J: J. Eng. Tribol., 212*, pp. 145–162.

REFERENCES

[87] Venner, C. H., and Lubrecht, A. A. (1994), ‘‘Numerical Simulation of a Transverse Ridge in a Circular EHL Contact Under Rolling/Sliding,’’ *Trans. ASME J. Tribol., 116,* pp. 751–761.

[88] Venner, C. H., Couhier, F., Lubrecht, A. A., and Greenwood, J. A. (1996), ‘‘Amplitude Reduction of Waviness in Transient EHL Line Contacts’’, *Proc. Symp. Leeds-Lyon,* Elsevier, pp. 103–112.

[89] Lubrecht, A. A., Graille, D., Venner, C. H., and Greenwood, J. A. (1999), ‘‘Waviness Amplitude Reduction in Line Contacts Under Rolling-Sliding,’’ *ASME J. Tribol., 120,* pp. 705–709.

[90] Kweh, C. C., Evans, H. P., and Snidle, R. W. (1989), ‘‘Micro-Elastohydrodynamic Lubrication of an Elliptical Contact, With Transverse and Tri-Dimensional Roughness,’’ *ASME J. Tribol., 111,* pp. 577–583.

[91] Holmes, M.J.A., Qiao, H., Evans, H.P. and Snidle, R.W. (2004), “Transient Effects in EHL Point Contacts having Rough Trasverse Surface Finish’’, *Trans. Proc. Trib., Elsevier, Vol.43,* pp.201-212

[92] Almqvist, A. and Larsson, R. (2004), “The Effect of Two-Sided Roughness in Rolling/Sliding EHL Line Contacts’’, *Trans. Proc. Trib., Elsevier,* pp.243-250

[93] Wensing, J.A. (1998), ‘‘On the Dynamics of Ball Bearings’’, *PhD thesis, University of Twente, the Netherlands, ISBN* 90-36512298

[94] Upadhyay, S.H., Jain, S.C. and Harsha, S.P. (2010), ‘‘Chaotic Dynamics of High Speed Rotating Shaft supported by Ball Bearings due to Distributed Defects’’, *International Journal of Eng. Sci. and Tech., Vol.2 (10),* pp.5746 -5764, ISSN: 0975-5462

REFERENCES

[95] Steidel, R.F. (1971), ‘‘Introduction to Mechanical Vibrations’’, *John Wiley & Sons Inc., ISBN 0-471-820911*

[96] Zeillinger, R. and Köttritsch, R. (1996), ‘‘Damping in a Rolling Bearing Arrangement’’, *Evolution – The Business and Technology magazine from SKF*

[97] Crook, A.W. (1958), “Lubrication of Rollers”, *Phil. Trans. Roy. Soc. Lon. Series A, Vol. 250, 981*, pp.387-409

[98] Archard, J.F. and Kirk, M.T. (1960), “Lubrication of Point Contacts”, *Phil. Trans. Roy. Soc. Lon. Series A, Vol. 261, 1307*, pp. 532-550

[99] McCarthy, D.M.C., Glavatskih, S.B., and Sherrington, I. (2005), “Oil-Film Thickness and Temperature Measurements in PTFE and Babbit Faced Tilting-Pad Thrust Bearing”, *Proc. I.Mech.E., Vol. 219, Part J.*, pp. 179-185

[100] Furey, M.J. (1961), “Metallic Contact and Friction between Sliding Surfaces”, *ASLE Trans.***,** *4*, pp. 1-11

[101] Tallian, T.E., Chiu, Y.P., Huttenlocher, D.F., Kamenshine, J.A., Sibley, L.B. and Sindlinger, N.E. (1964), “Lubricant Films in Rolling Contact of Rough Surfaces”, *ASLE Trans.*, 7, pp.109-126

[102] Guanteng, G., Olver, A.V. and Spikes, H.A. (1999), “Contact Resistance Measurements in Mixed Lubrication”, *The Advancing Frontier of Engineering Tribology, STLE/ASME, editors: Q. Wang, J. Nethzel and F. Sadeghi*, pp. 64-71

[103] Cameron, A., and Gohar, R. (1966), “Theoretical and Experimental Studies of the Oil Film in Lubricated Point Contacts.” *Proc. Roy. Soc. London A291*, pp. 520-536.

REFERENCES

[104] Spikes, H.A. and Cann, P.M. (2001), "The Development and Application of the Spacer Layer Imaging Method for Measuring Lubricant Film Thickness", *Proc. Instn Mech. Engrs, Vol. 215, Part J.*, pp. 261-276

[105] Gohar, R. and Cameron, A. (1967), ''The Mapping of Elastohydrodynamic Contacts'', A*SLE Tribology Trans., Vol.10 (3),* pp.215-225

[106] Hamaguchi, H., Spikes, H.A. and Cameron, A. (1977), ''Elastohydrodynamic Properties of Water in Oil Emulsions'', *Wear, Vol.43,* pp.17-24

[107] Palacios, J.M., Arizmendi, L. and Cameron, A. (1980), ''Optical and Electrical Measurements in the Behaviour of Lubricating Greases'', *An. Fis. , Vol.76,* pp.285-288

[108] Wedeven, L. D., Evans, D. and Cameron, A. (1971), ''Optical Analysis of Ball Bearing Starvation'', *ASME Trans., J. Lubric. Technol., Vol.93,* pp.349-363

[109] Gledhill, R. H., Jackson, A. and Cameron, A. (1979), ''Interferometric Study of the EHL of Elliptical Contacts Aligned in the Direction of Rolling'', *In the Elastohydrodynamics and Related Topics, Proceedings of the 5th Leeds-Lyon Symposium on Tribology (Eds. D.Dowson et al.), Leeds,* pp.116-120

[110] Jackson, A. and Cameron, A. (1976), ''An Interferometric Study of the EHL of Rough Surfaces'', *ASLE Trans., Vol.19,* pp.50-60

[111] Pemberton, J.C. and Cameron, A. (1979), ''An Optical Study of the Lubrication of a 65mm Cylindrical Roller Bearing'', *ASME Trans., J. Lubric. Technol., Vol. 101*, pp.327-337

[112] Yung, K. M. And Cameron, A. (1979), ''Optical Analysis of Porous Metal Bearings'', *ASME Trans., J. Lubric. Technol., Vol. 101,* pp.99-104

REFERENCES

[113] Westlake, F.J. and Cameron, A. (1967-68), ‘‘A Study of Ultra-Thin Lubricant Films using an Optical Technique’’, *Proc. Instn Mech. Engrs, Vol.182, part 3G,* pp.75-78

[114] Johnston, G.J., Wayte, R. and Spikes, H.A. (1991), ‘‘The Measurement and Study of very Thin Lubricant Films in Concentrated Contacts’’, *Tribology Trans., Vol.34,* pp.187-194

[115] Sugimura, J. and Spikes, H.A. (1997), “Technique for Measuring EHD Film Thickness in Non-Steady State Contact Conditions”, *Proc. 23rd Leeds-Lyon Symposium, Elastohydrodynamics ’96, D.Dowson et al., ed., Elsevier, Amsterdam , Vol. 32* , pp.91-100

[116] Gustafson, L., Hoglund, E. and Marklund, O. (1994), ‘‘Measuring Lubricant Film Thickness with Image Analysis’’, *Proc. Instn Mech. Engrs, Vol. 208(J3), Part J.*, pp. 199-205

[117] Cann, P.M., Hutchinson, J. and Spikes, H.A. (1996), ‘‘The Development of a Spacer Layer Imaging Method (SLIM) for Mapping Elastohydrodynamic Contacts”, *Trib. Trans. 39,* pp. 915-921

[118] Luo, J., Wen, S and Huang, P. (1996), “Thin Film Lubrication. Part 1: Study on the Transition between EHL and Thin Film Lubrication using a Relative Optical Intensity Technique”, *Wear 194,* pp. 107-115

[119] Hartl, M., Krupka, I. and Liska, M. (1997), “Differential Colorimetry: Tools for Evaluation of Chromatic Interference Patterns”, *Opt. Eng. 36,* pp. 1-8

[120] Smeeth, M., Spikes, H.A., and Gunsel, S. (1996), “Boundary Film Formation by Viscosity Index Improvers”, *Trib. Trans. 39,* pp. 726-734

[121] Sakamoto, M., Nishikawa, H. and Kaneta, M. (2004), “Behaviour of Point Contact EHL Films under Pulsating Loads”, *Transient Processes in Tribology, Elsevier*, pp.391-399

REFERENCES

[122] Greenwood, J.A. and Kauzlarich, J.J. (1973), "Inlet Shear Heating in Elastohydrodynamic Lubrication'', *J. Lubr. Technol., Vol. 95, No. 4,* pp.417-426

[123] Moore, A.J. (1973), "Non-Newtonian Behaviour in Elastohydrodynamic Lubrication'', *Ph.D Thesis, University of Reading*

[124] Dardin, A., Hesdrich, K., Muller, M., Topolovec-Miklozic, K. and Spikes, H. (2003), "Influence of Polyalkylmethacrylate Viscosity Index Improvers on the Efficiency of Lubricants", *SAE Paper 2003-01-1967*

[125] Smeeth, M., Spikes, H.A. and Gunsel, S. (1996), "Boundary Film Formation by Viscosity Index Improvers", *Trib. Trans., Vol.39,* pp.726-734

[126] Nagata, Y., Kalogiannis, K. and Glovnea, R.P. (2012), "Track Replenishment by Lateral Vibrations in Grease-Lubricated EHD Contacts'', *Trib. Trans., Vol. 55, Issue 1,* pp. 91-98

[127] Nagata, Y., (2011), "Elastohydrodynamic Effects in Grease-Lubricated Contacts", D.Phil. Thesis, 2011, University of Sussex

[128] Cann, P.M. (1999), "Starved Grease Lubrication of Rolling Contacts'', *Trib. Trans., Vol.42, No.4,* pp.867-873

[129] Lubrecht, T., Mazuyer, D. and Cann, P. (2001), "Starved Elastohydrodynamic Lubrication Theory: Application to Emulsions and Grease'', *C.R. Acad. Sci. Phys., Vol.2, Series IV,* pp.717-728

[130] Cann, P.M., and Lubrecht, A.A. (2004) "The effect of transient loading on contact replenishment with lubricating greases" *Trans. Proc. Trib., Elsevier,* pp. 745-750